IMPERIAL COLLEGE OF SCIENCE AND TECHNOLOGY

(University of London)

RECONCILIATION OF PREDICTED AND MEASURED MODAL PROPERTIES OF STRUCTURES

by

Joga SIDHU

A thesis submitted to the University of London for the degree of Doctor of Philosophy, and for the Diploma of Imperial College.

Department of Mechanical Engineering
Imperial College, LONDON SW7 2BX

SEPTEMBER 1983

ABSTRACT

The subject of this thesis can be divided into two parts; (i) advanced modal testing methods and (ii) the utilization of modal properties to locate areas of discrepancy between theoretical and experimental models.

Theoretically generated data with known types and amounts of nonlinearity were analysed using a linear identification process, and a damping matrix was constructed for the data in the vicinity of resonance. The matrix showed a systematic change when examined on a 3-D diagram which could be used to identify the characteristics of the system. The technique was applied to a real structure and ways of obtaining 'best' values for the modal properties, even in the presence of nonlinear effects, have been discussed.

The response of nonlinear systems to nonsinusoidal excitation was investigated using an analogue computer and it was found that the presence of nonlinearities could not easily be detected from such measurements.

A new method was developed by which it is possible to locate areas of poor modelling using FE and incomplete experimental modal properties.

'Pseudo' inverse matrices can be calculated for both the experimental and the FE model properties, which, together with the full FE model spatial matrices, are then used to calculate approximate mass and stiffness error

matrices. The non-zero elements in the error matrices serve to locate the areas of disagreement, while their absolute values indicate the magnitude of the discrepancy between the two models.

The technique has been evaluated initially using two versions of a theoretical 8 DOF mass-spring system, the only difference between them being in the stiffness of one of the springs. In this case, only 4 modes were needed to locate the position where the spring stiffness was altered. The method has also been applied to a small welded beam and a practical structure.

ACKNOWLEDGEMENTS

The author is indebted to his supervisor Professor D J Ewins for his sustained help, guidance and encouragement before and throughout the duration of the project.

Thanks are also due to many friends and colleagues whose indirect contribution has been much appreciated. In this regard the author would like to mention in particular Dr H O Afolabi, Mr J J Amoah, Mr J Antonio, Dr P Cawley, Mr J Griffin, Professor P Grootenhuis, Dr B Hillary, Mr M Imregun, Mr D A Robb and a very special thank to G S Chaudhry. Mention must also be made of Mr R Gunn, laboratory technican, whom the author thanks for his help.

For their keen interest and time during many useful discussions the author would like to thank Mr D R Gaukroger and Mr M Nash, of the Royal Aircraft Establishment, Farnborough; Mr D Boon and Mr G M Venn, of the Westland Helicopters Plc, Yeovil; and Lieutenant Commander B J Dobson, of the Royal Naval Engineering College, Plymouth. The author acknowledges the interest shown in this work by the staff members of Rolls-Royce Ltd., Derby, and of the Admiralty Underwater Weapons Establishment, Portland and wishes to thank them sincerely.

Finally, the author is grateful for the award of a research studentship by the Science and Engineering Research Council and for the financial assistance towards the cost of equipment from the Royal Aircraft Establishment, Farnborough.

NOTATION

a	Amplitude of vibration.
e	Exponential constant (2.7182..).
$f(X,\dot{X})$	Displacement and velocity function.
i	$\sqrt{-1}$.
k	Spring constant.
k'	Equivalent spring constant.
m	Number of measured modes.
m_r	Modal mass of the r^{th} mode.
n	Number of measured coordinates.
r	Counter.
t	Time.
u_l	Displacement of coordinate l.
v_l	Rotation of coordinate l.
$_rA_{pq}$	Modal constant of the r^{th} mode corresponding to receptance α_{pq}.
F	Amplitude of force.
$F(t)$	Time dependent force.
N	Number of coordinates in an FE model.
R	Radius of modal circle.
R	Dry friction.
X_i	Amplitude of vibration of point i.
$X(t)$	Time dependent amplitude of vibration.
$Y_{p,q}$	Mobility corresponding to α_{pq}.
$\{F\}$	Forcing vector.
$\{V\}$	Displacement vector.
$[C]$	System damping matrix.
$[D_k]$	Difference of pseudo stiffness matrices.

$[D_m]$ Difference of pseudo mass matrices.

$[E_k]$ Stiffness error matrix.

$[E_m]$ Mass error matrix.

$[I]$ Identity matrix.

$[K]$ System stiffness matrix.

$[\overset{*}{K}]$ Pseudo stiffness matrix.

$[K_e]$ Element stiffness matrix.

$[K_e]$ Experimental stiffness matrix (assumed to be exact).

$[\overset{*}{K}_e]$ Experimental pseudo stiffness matrix.

$[K_p]$ Analytical (FE) stiffness matrix (assumed to be approximate).

$[\overset{*}{K}_p]$ Analytical (FE) pseudo stiffness matrix.

$[M]$ System mass matrix.

$[\overset{*}{M}]$ Pseudo mass matrix.

$[M_e]$ Element mass matrix.

$[\overset{*}{M}_e]$ Experimental pseudo mass matrix.

$[\overset{*}{M}_p]$ Analytical (FE) pseudo mass matrix.

α_{pq} Receptance (response at point p due to force input at q).

β Cubic stiffness coefficient.

γ_1 Constant.

γ_2 Constant.

ξ Viscous damping ratio ($C/C_{\emptyset}$)

η Loss factor.

η_r Loss factor of the r^{th} mode.

η_{ij} Loss factor calculated using frequency point i below and j above resonance.

$\overline{\eta}_{hk}$ Horizontal average loss factor of the k^{th} column (3-Ø3).

$\overline{\eta}_{vk}$ Vertical average loss factor of the k^{th} row (3-Ø4).

$\overline{\eta}_{dk}$ Average loss factor of a submatrix where k is the size of the submatrix (3-Ø5).

θ_r Phase angle of the r^{th} modal constant.

$\overline{\lambda}$ Equivalent damping coefficient.

σ Ratio of k'/k.

ω Excitation frequency.

ω_r Natural frequency of the r^{th} mode.

$\omega_Ø$ Undamped natural frequency.

ω_1 A frequency point such that $\omega_1 < \omega_Ø$.

ω_2 A frequency point such that $\omega_2 > \omega_Ø$.

$\overline{\omega}_Ø$ Equivalent resonance frequency.

Δ_A Modal constant confidence factor (4-Ø2).

$_r\Phi_p$ p^{th} element in the r^{th} mass-normalised eigenvector.

$_r\Psi_p$ p^{th} element in the r^{th} eigenvector.

Ω See figure 2-Ø3.

$\{\Phi\}$ Mass-normalised eigenvector.

$\{\Psi\}$ Arbitrary normalised eigenvector.

$[\Phi^R]$ Reduced mass-normalised eigenvectors matrix.

$[\lambda^2]$ Diagonal eigenvalues matrix.

$[\Phi_e^R]$ Experimental: reduced mass-normalised eigenvectors matrix.

$[\Phi_p^R]$ Analytical (FE): reduced mass-normalised eigenvectors matrix.

$[1/\lambda_{re}^2]$ Diagonal matrix containing the reciprocals of measured eigenvalues.

$[1/\lambda_{rp}^2]$ Diagonal matrix containing the reciprocals of analytical (FE) eigenvalues.

CONTENTS

CHAPTER

-1-

1. INTRODUCTION

1.1. GENERAL

The study of structural vibration, besides being important for its practical applications, is also useful as a link between the various branches of physics in which vibrations occur. The simplest natural vibrating systems have two attributes; inertia and stiffness about an equilibrium position. To a first approximation, the force tending to restore the system to equilibrium is often proportional to the displacement. Such systems are called 'linear systems' and can be represented by linear differential equations which in turn can easily be solved to obtain the characteristics of the systems. This kind of analysis is now a relatively straightforward task, and has been greatly aided in the recent past by the advent of minicomputers.

Parallel to the analytical methods, inertance measurement techniques together with modal analysis have become a very popular means of studying the dynamic behaviour of complex structures. This process reveals the basic modal properties of a structure under test (natural frequency, damping, modal constants etc.) and these may be further processed to display the mode shapes or to construct a mathematical model which can be used for a wide range of further applications.

For most of the modal testing currently being

performed the basic assumption is made that the structure under test is either linear or can be approximated as linear over a certain frequency range. Often, analytical models are constructed and correlated with the test results, again assuming a linear system. In most cases, the linear assumption is adequate but there are many instances where this is not the case, resulting in poor correlation and incorrect conclusions.

Many complex structures need system analysis and system identification for the investigation and qualification of their dynamic behaviour. System analysis according to construction drawing leads to approximate results based on several assumptions and simplifications. Most aerospace structures are so complex that even when considered in small components, they defy accurate modelling by purely theoretical methods and thus prevent a complete system model from being formed.

In practice, we often have two models; an experimental model which is incomplete but a true representation of the structure and an analytical model, such as a finite element (FE) model which completely defines the structure (in a given frequency range and at points of interest on the structure) but is not always accurate. The modal properties of such models are often compared by displaying the mode shape vectors and a visual comparison of the natural frequencies is carried out. This simple technique sometimes reveals large discrepancies between the two models, but gives very little or no information about the location and

the amount of discrepancies between the two models. It does not inform the analyst why the analytical model is inaccurate (assuming that the experimental model is more accurate) or what action to take in order to improve the correlation. In the two sets of modal data - analytical (FE) and experimental - there should be enough information about the two models to be able to locate the areas and to quantify the extent of the discrepancies between the two models.

One objective of this study is to discuss the problems faced in integrating and correlating experimental and analytical modal properties in order to locate the areas of discrepancies. The current techniques available will also be examined to see if there is any indication in the comparison of these data about the size and location of the areas that are inaccurately modelled.

1.2. MODAL TESTING

The remarkable advances made in theoretical dynamics have not diminished the importance of experimental dynamic analysis, instead it has become more popular. The development of mini and digital computers means that many of the processes in modal testing can be automated, thus reducing the amount of time spent on experiments. Most of the methods for analysis of the measured data are based on curve-fitting routines, whether in the frequency or the time domain.

Modal testing can be divided into two major parts; measurement and analysis.

1.2.1. MEASUREMENT METHODS

The testing method used to acquire frequency response data from a structure depends on several factors, such as the availability of hardware, the size of the structure, testing environment, allowable testing time etc. Nevertheless, measurement techniques can be divided into two categories; multi point and single point excitation.

Multipoint excitation was the main technique used for modal testing in the 196Øs. This method was mainly confined to the aerospace industry because of the high cost of the hardware required to carry out such tests, and only large companies had the resources to be able to afford the necessary equipment. Not only the cost was high but the usage of such equipment requires skilled operators. However, those people who have mastered the art of the multipoint technique obtained very good results with it [1,2,3,4].

In the multipoint excitation method, the structure is excited at several points simultaneously using shakers which are tuned to vibrate the structure at a mode of interest of vibration. The main advantage of this method is that it can be used to determine the modal properties of a structure with high modal density i.e. close modes [5]. Once a mode of vibration is excited, very little further analysis is

required to extract the modal properties.

Despite the ability of the multipoint excitation method to analyse close modes, it is very rarely used nowadays and the only people who are using this technique are the ones who have invested large sums of money in the equipment and the software to automate the tuning process.

On the other hand, single-point excitation has become very popular since the early 197Øs and has been the main technique which has been used for most of the modal testing these days. Relative to multi point excitation the hardware for this type of testing is inexpensive and the setting up time for tests is short.

In the single-point excitation method the structure is excited at a point and the response measured at all the points of interest on the structure. The modal consistency can be checked by moving the point of excitation and repeating the measurements. The disadvantage of the technique is that certain modes of vibration might not be excited, but this can be overcome if the point of excitation is moved to another location on the structure. However, if the point of input happens to be close to a node for a particular mode of vibration then the structure will not be adequately excited.

1.2.2. ANALYSIS OF MEASURED DATA

The data acquired from a test structure are usually in the form of frequency response plots at discrete frequency points and further analysis is required to reveal the modal properties. There are several methods that can be used to extract modal properties and all of them are based on one or other form of curve fitting process, ranging from the single degree-of-freedom (SDOF) to the 'global' curve fit.

Now we shall briefly describe some of the common and the latest methods used to extract modal properties from measured data.

(i) Single degree-of-freedom (SDOF) curve fitting. As the name suggests, each resonance of a multidegree-of-freedom system is assumed to behave as a SDOF system in the immediate vicinity of the resonance. Thus a multidegree-of-freedom system can be treated as several SDOF systems by considering one mode at a time. The properties of this mode are usually extracted from the Nyquist plot using a development of the Kennedy and Pancu method [6]. This offers a very simple yet reasonably accurate way of analysing a 'well behaved' structure. However, this technique does not always produce a consistent set of modal properties especially for structures with high modal density (close modes).

(ii) Multidegree-of-freedom (MDOF) curve fitting. This is an extension of the SDOF method. One plot of frequency response data from a whole set of measured

transfer functions are treated as a $MDOF_{\wedge}^{system}$ and simultaneous curve fit to all the modes reveals the modal properties of the structure. The contribution of the modes outside the frequency range of measurement can also be estimated [7]. This technique is especially useful for analysis of structures with high modal density. To increase the efficiency of the computational process, an initial estimate of modal parameters can be used as starting values (i.e. from $SDOF_{\wedge}^{system}$ analysis) and these, together with the measured data and subsequent iterations, converge to the 'correct' values. However, the process does not always converge to the desired values especially if the data are polluted with noise or by nonlinearities.

(iii) Global curve fitting. This curve fitting routine, unlike the previous ones, fits simultaneous curves to <u>all</u> the measured frequency response functions hence ensuring modal consistency i.e. only one value of natural frequency and modal damping is estimated for each mode, while the SDOF and MDOF give one estimate for each mode of each transfer function and these are usually slightly different for each transfer function. This may be considered to be a disadvantage because from just one estimate it is not possible to check the quality of the identified parameters whereas with SDOF and MDOF one has many estimates and the variation of these can be used as a measure of the consistency. Also, the mode shape vectors extracted using global curve fitting are automatically orthogonal. The disadvantage of this approach is that

errors in the measured data, such as those due to noise and nonlinearities, make the curve-fitting process very unstable and also it can only be used on machines with a large memory because of the large amount of data that has to be used simultaneously. Although the latter disadvantage can be overcome and may be less of a problem in the near future because of inexpensive computer memory; the former is a serious drawback.

(iv) Ibrahim time domain (ITD). This is one of the latest techniques used to identify modal properties and the main difference between this and the previously described routines is that this uses the data in the time domain whereas the others use the data in the frequency domain. A curve fit to the free-decay response gives the modal properties of structures. Because it is less costly and faster to measure free-decay rather than frequency response function hence this technique can be very fast in identifying modal properties. Although this method is based on the free-decays, it can be applied to the data in other forms providing that free-decay response can be computed from these. The method can easily be automated and hence requires very little input from the operator. However, it is known to be very sensitive to small nonlinearities and can sometimes extract modal properties of a mode which is not present [8,9].

1.3. IDENTIFICATION OF NONLINEARITIES

Structural nonlinearities must be taken into account when constructing a model from identified modal parameters. Failure to do so may lead to an incorrect model being formed which might have very little resemblance to the actual testpiece. Many of the trouble-shooting problems in modal analysis are associated with small structural nonlinearities. Although the apparent effect of these pollutants may be small on the measured frequency response data, they can result in very large errors in the extracted modal properties which in turn may lead to incorrect conclusions.

Theoretically generated data with known types and amounts of nonlinearity can contribute a great deal to the understanding of nonlinearities in real structures. For example, the effect of cubic stiffness on frequency response data was examined by Ulm and Morse [10] who showed that this type of nonlinearity has a large effect on the spacing of the frequency points. No attempt was made to investigate the effect of this type of nonlinearity on the extracted modal properties. However, there are other types of nonlinearity, such as frictional (dry friction), which do not distort the spacing and hence will be difficult to detect. The Ulm and Morse method is not very useful in practice because most structural nonlinearities are small and hence the distortion of the frequency response functions is small and visual examination in general will not be adequate to detect small deviations.

The Hilbert transform [11,12,13] offers a method by which the measured frequency response function can be checked for contamination by nonlinearities or other pollutants. The complex transfer function can be split in to its real and imaginary parts and it is possible to calculate one from the other using the Hilbert transform e.g. the real part of frequency response function may be computed from the measured imaginary part and vice versa. The transformation is carried out assuming that the structure is linear and hence in the cases where the data are polluted with nonlinearities the transformation will not yield identical components of the transfer function to the measured ones. Hence, comparison of the measured and calculated constituents will show any discrepancy between the actual and the computed parts and a systematic shift in the two versions of, say the real part, can be attributed to nonlinearities. However, it must be stressed that the difference between the measured and calculated constituent is generally very small and so a close examination of the two sets of data must be carried out. Because of this small deviation, it will be difficult in practice to say whether the change is due to nonlinearities or to other pollutants in the data. Nevertheless, this technique offers a very useful way of assessing the quality of measured data.

1.4. CORRELATION OF MODELS

Experimental modal testing serves two basic purposes; first, in the absence of any analytical model, an experimental approach is the only way of understanding the dynamic behaviour of a complex structure; secondly, if an analytical model, such as one using the finite element method, exists it is usually necessary to verify it using the experimental data which are assumed to be a true representation of the structure. There are very few papers that deal with the subject of verifying an FE model in a systematic manner using experimental data. Any comparison between two such sets of data has generally been indirect, inconvenient and slow. For most cases, this comparison has consisted of manually interfacing the results and perhaps some arbitrary modification of one model in an attempt to improve the correlation. This 'trial-and-error' process is costly and seldom yield the optimum modification.

Methods based on the sensitivity of the modal parameters are sometimes used (i.e. derivatives of eigenvalues and eigenvectors with respect to a given parameter, such as the stiffness or the mass of an element). The determination of eigenvalue derivative is shown to be a straightforward and simple calculation [14,15,16,17], but the calculation of eigenvector derivatives is found to be much more complicated [18]. With the aid of the sensitivity method it is possible to determine the minimum alteration that must be carried out in order to achieve a given shift in the natural frequency of the structure. Unfortunately,

there are cases when the derivative method predicts changes that are impossible to carry out in practice (negative mass etc.) and have no physical meaning. Incorporating these unrealistic changes will give the desired results numerically but the model might not be a true representation of the actual structure. Another reason why the sensitivity method is not widely used is the high cost of computing the eigenvector derivatives.

Other techniques on the subject of correlating the analytical and experimental models rely on the assumption that either the mass or the stiffness matrix in the analytical model is correct and only one of these needs modifying [19,20]. It is most likely that if an error exists between the two models then it would be expected to be in both the mass and the stiffness matrices. Despite the above-mentioned assumption, this technique is very involved mathematically, and that is perhaps why most engineers are reluctant to use it.

The perturbation method [21] is very useful in predicting the effect of changes but before such a change can be made it is necessary to know where it should be made. Gaukroger [22] recently proposed a method by which it is possible to obtain specified natural frequencies by modifying given structural stiffnesses. Again, the choice of area to be modified is left to the analyst's judgement.

Clearly, there is a need to develop new techniques to aid the analyst to locate the areas that should be altered

in an FE model in order to reduce the discrepancies between the experimental and the FE models. The 'trial-and-error' methods are no longer acceptable as they are slow, costly and seldom give the optimum region to be modified.

In the light of the problems that need investigating, the following presentation has been adopted.

Basic principles of Finite Element modelling and experimental modal analysis are given in chapter 2. Chapter 3 opens with a discussion of the difficulities faced in the modal analysis of real structures which exhibit small nonlinearities and to highlight the problems, the results from a special structure - the NASTRAN testpiece - are presented. The major part of chapter 3 is devoted to a study of theoretical nonlinear SDOF and linear 2DOF systems in investigating the effects of small nonlinearity on the identified modal properties. Chapter 4 contains the results of a detailed study carried out on the NASTRAN structure. The response of nonlinear SDOF systems to sinusoidal, random and transient inputs was studied using an analogue computer and the results, together with the necessary theory, are given in chapter 5.

The comparison of modal properties are dealt with in chapters 6 and 7. In chapter 6 a new method is developed by which it is possible to compare modal properties of two models in order to locate the areas of discrepancy between them. The technique has been applied to synthesised data from an 8DOF system while chapter 7 concentrates on the application of this method to real structures the SAMM II B beam and the NASTRAN structure.

CHAPTER

-2-

2. FINITE ELEMENT MODELLING AND MODAL IDENTIFICATION PRINCIPLES

2.1. INTRODUCTION

Two techniques which are widely used to develop models that describe dynamic characteristics of structures are experimental modal analysis and finite element (FE) methods. The technique of characterizing a structure's dynamic behaviour from experiment has the advantage of providing the engineer with a model of the actual structure rather than an idealisation of it. This can often provide a more representative description of the dynamics than do the results of an analytical model such as would be provided by a finite element analysis. On the other hand, the analytical approach has the advantage that it can be used to evaluate the structural modal properties without carrying out any experiments and, consequently, the test hardware equipment is not required.

Both experimental and the FE modelling techniques have their own advantages and both are frequently used in the study of structural vibration. In this chapter we shall outline the basic concepts of these methods. Only the very fundamental topics will be mentioned because the aim is to use the existing techniques with little modification to obtain the necessary information (accurate modal properties) about the structure.

2.2. BASIC FINITE ELEMENT METHODOLOGY

2.2.1. GENERAL CONCEPTS

Most structures are so complex that their behaviour cannot easily be predicted with accuracy. However, small parts of the structure may often be assumed to behave in a relatively simple manner. For example, it may be assumed that the stress over a small part of a long beam is constant, or that the temperature over a small area of a plate is constant etc. In finite element analysis these small parts of the structure are referred to as finite elements.

Any structure, large or small, complex or simple, can be represented by a set of finite elements which are assumed to interact at particular points. The number of variables (unknown displacements and rotations) at each point is called the number of 'degrees-of-freedom' (DOF). Theoretically, a continuous structure has an infinite number of degrees-of-freedom, but in finite element analysis, such a structure is approximated by selecting a finite number of elements and hence a finite number of degrees-of-freedom.

The geometry of the element used depends on the size of the structure. There exist many types of elements e.g. bar, beam, plate, cylindrical etc. The choice of elements depends to some extent on the geometry of the structure but to a great extent on the individual's choice, as there is more than one element that may be used to represent the

structure. For most complex problems a combination of several types of element is necessary for an efficient and accurate analysis.

In structural dynamics, an FE analysis requires the formulation of mass [M], stiffness [K] and damping [C] matrices. Often, damping is not included in the analysis; this is justified if the damping is small, but even in heavily damped structures, the presence of damping is ignored because it cannot easily be modelled. Consequently, the analysis is usually reduced to one of undamped vibration.

2.2.2. FORMULATION OF MASS AND STIFFNESS MATRICES

There are two types of element that are frequently used in the study of structural vibration; namely, beam elements and plate elements. Most engineering structures can be analysed using one or both of these types of element. In this study, we shall only consider beam elements, although the theories for beam and plate elements are very similar. The beam element is assumed to be a straight bar of uniform cross-sectional area (figure 2-Ø1).

Using stress analysis, it is possible to relate forces to the displacements via the properties of the material and the geometry of the element [23].

$$\{F\} = [K_e]\{V\} \qquad (2\text{-}Ø1)$$

where

$$\{F\} = \begin{Bmatrix} F_{x_1} \\ F_{y_1} \\ \vdots \\ M_{y_2} \\ M_{z_2} \end{Bmatrix} \qquad \{V\} = \begin{Bmatrix} X_1 \\ Y_1 \\ \vdots \\ \theta_{y_2} \\ \theta_{z_2} \end{Bmatrix}$$

The square matrix $[K_e]$, which is 12x12 in this case, is known as the 'element stiffness matrix'. By considering the dynamics of the element, it is also possible to relate the forces to the accelerations.

$$\{F\} = [M_e]\{\ddot{V}\} \qquad (2\text{-}\emptyset2)$$

where $\{\ddot{V}\}$ is the second time derivative of the displacement vector and matrix $[M_e]$ is the 'element mass matrix'.

The mass and stiffness matrices for beam and plate elements have been derived by many authors [23,24]. The bar element is perhaps one of the simplest and its mass and stiffness matrices are to be found in the majority of books and papers dealing with the basics of finite element analysis [25,26,27]. The mass and stiffness matrices for beam, rectangular plate, triangular plate and many other types of elements, have also been constructed by Prezemieniecki [23] and Szilard [24]. The mass and stiffness matrices for the beam element in figure 2-Ø1 are given in appendix 1Ø.1.

In a finite element analysis, mass and stiffness matrices are constructed for all the elements of the structure and these are then joined to form the overall mass [M] and stiffness [K] matrices of the complete model. This

process is called 'assembling the element matrices'. There is no general method for assembling these matrices and each problem has to be tackled individually. As an example, the overall stiffness matrix for a straight beam, with three elements, shown in figure 2-Ø2, is given in table 2-Ø1, where the matrix $[K_e]^n$ is the n^{th} element's stiffness matrix. More examples on assembling element matrices can be found in reference 28.

Once the overall mass and stiffness matrices are assembled for the structure, then the problem reduces to that of an eigenvalue solution i.e. solving equation 2-Ø3.

$$\left[[K]-\omega^2[M]\right]\{X\} = \{0\} \qquad (2\text{-}Ø3)$$

There are many standard subroutines that are capable of solving equation 2-Ø3 to produce eigenvalues $[\lambda_r^2]$ and the corresponding eigenvectors $[\Psi]$. The eigenvectors may be mass normalised;

$$[\Phi]^T[M][\Phi] = [I]$$

$$[\Phi]^T[K][\Phi] = \left[\lambda_r^2\right] \qquad (2\text{-}Ø4)$$

where $[\Phi]$ is the mass normalised eigenvector matrix. These two matrices, $[\lambda_r^2]$ and $[\Phi]$, completely characterize the undamped behaviour of the structure.

2.3. MODAL TESTING

2.3.1. GENERAL CONCEPTS

Modal analysis, via the experimental route, has become a very popular means of analysing the dynamic behaviour of an existing structure, especially since the recent reduction in the cost of minicomputers. During the 1940s, modal analysis was applied exclusively in the aerospace industry, largely due to the high cost of the hardware which was required for the tests. Nowadays, it is quite common for small companies to have the necessary equipment to carry out the tests and to analyse the test data.

There are two main techniques that are currently used to obtain modal data from a test structure. Probably the easiest and the most popular, is the single point excitation technique. As the name suggests, the structure is excited at a single point and its response is measured at points of interest.

The other technique, which is not so widely used these days, is the multi-shaker (or multi point) excitation method. In this method several shakers are attached to the structure. The magnitudes of displacement and phase of each shaker are varied until a pure mode is excited. The advantage of this technique is that once a mode of vibration is excited, very little further analysis is needed to derive the modal properties. The main drawback of this method is that it is very cumbersome to tune the shakers so as to excite the mode of interest and to do this one needs to have

a reasonably good knowledge about the nature of the mode which is to be excited.

Just as there are several techniques available for measuring data, there are also several different types of inputs that may be used to excite the structure under test e.g. stepped or discrete sine, swept sine, random, impact etc. The choice of input depends on a number of factors, such as the hardware, the length of time available to carry out the test and so on. For a broad band frequency measurement, step sinusoidal excited tests take longer than the nonsinusoidal tests but the quality of data generated by discrete sinewave excitation is superior to that generated by other types of inputs. Regardless of the type of input used, the end result is in the form of frequency response data at discrete frequency points. For each coordinate that is measured on the structure, one set of frequency response data is obtained. These data can take one of three forms, now commonly used, inertance ($\ddot{X}/F$), mobility ($\dot{X}/F$) or receptance (X/F). It is possible to construct a matrix of test data as shown in table 2-Ø2, where symbol α denotes receptance and α_{pq} is defined as the complex ratio of response (X) at point p due to a force (F) at point q.

$$\alpha_{pq} = \frac{X_p}{F_q} \qquad (2\text{-}Ø5)$$

Only one row or column of the matrix in table 2-Ø2 is required to characterize the dynamic behaviour of the structure. Normally, more than one row or column is

measured, so as to provide a check on the quality of the measured data and the derived modal properties [29].

2.3.2. SINGLE-DEGREE-OF-FREEDOM MODAL TESTING THEORY

There are several types of linear curve fitting routines that may be used to extract modal properties from the measured data i.e. single-degree-of-freedom (SDOF), multi-degree-of-freedom (MDOF), poly curve fitting (taking more than one set of measured data and fitting a simultaneous curves to these), curve fitting in the time domain, which is often called the 'Ibrahim Time Domain' (ITD) etc. The simplest of these is the SDOF routine and is sometimes known as the 'circle fitting' method. This technique was developed by Kennedy and Pancu [6].

In this section we shall consider only the Kennedy and Pancu method because one of the aims of this study is to see how we can use the simplest of techniques to identify nonlinearities and to extract 'accurate' modal properties without using nonlinear curve fitting routines.

The dynamic behaviour of a structure, in terms of its modal properties, is given by [31,32,33];

$$\alpha_{pq}(\omega) = \sum_{r=1}^{m} \frac{({}_r\Psi_p)({}_r\Psi_q)}{m_r\omega_r^2(1-(\omega/\omega_r)^2 + i\eta_r)} \qquad (2\text{-}\emptyset 6)$$

where m - number of modes;

ω_r - natural frequency of the r^{th} mode;

η_r - loss factor of the r^{th} mode;

m_r - modal mass of the r^{th} mode;

${}_r\Psi_p$ - p^{th} element in the r^{th} mode shape vector $\{\Psi\}$;

${}_r\Psi_q$ - q^{th} element in the r^{th} mode shape vector $\{\Psi\}$.

Equation 2-Ø6 can also be written in the form;

$$\alpha_{pq}(\omega) = \sum_{r=1}^{m} \frac{({}_r\Phi_p)({}_r\Phi_q)}{\omega_r^2(1-(\omega/\omega_r)^2 + i\eta_r)} \qquad (2\text{-}Ø7)$$

$$\begin{aligned} {}_r\Phi_p &= \frac{{}_r\Psi_p}{\sqrt{m_r}} \\ {}_r\Phi_q &= \frac{{}_r\Psi_q}{\sqrt{m_r}} \end{aligned} \qquad (2\text{-}Ø8)$$

The vector $\{\Phi\}$ is the r^{th} 'mass normalized' mode shape corresponding to the vector $\{\Psi\}$.

The modal constant (${}_rA_{pq}$) for the r^{th} mode is defined as;

$${}_rA_{pq} = ({}_r\Phi_p)({}_r\Phi_q) \qquad (2\text{-}Ø9)$$

Since ${}_r\Psi_p$, ${}_r\Psi_q$, ${}_r\Phi_p$ and ${}_r\Phi_q$ are all complex quantities, the modal constant is also a complex number. In terms of the modal constants, equation 2-Ø7 becomes;

$$\alpha_{pq}(\omega) = \sum_{r=1}^{m} \frac{|{}_rA_{pq}|e^{i\theta_r}}{\omega_r^2(1-(\omega/\omega_r)^2 + i\eta_r)} \qquad (2\text{-}1Ø)$$

where θ_r is the phase associated with the r^{th} modal constant (figure 2-Ø3). The receptance equation for a single mode of

a structure is;

$$\alpha_{pq}(\omega) = \frac{|A_{pq}|e^{i\theta}}{\omega_0^2(1-(\omega/\omega_0)^2+i\eta)} \qquad (2\text{-}11)$$

The above equation may easily be separated into its real and imaginary parts.

$$Real_{\alpha_{pq}} = \frac{|A_{pq}|}{\omega_0^2}\left(\frac{(1-(\omega/\omega_0)^2)\cos\theta+\eta\sin\theta}{(1-(\omega/\omega_0)^2)^2+\eta^2}\right)$$

$$Imag_{\alpha_{pq}} = \frac{|A_{pq}|}{\omega_0^2}\left(\frac{(1-(\omega/\omega_0)^2)\sin\theta-\eta\cos\theta}{(1-(\omega/\omega_0)^2)^2+\eta^2}\right) \qquad (2\text{-}12)$$

Eliminating the excitation frequency (ω) from equations 2-12;

$$\left(Real_{\alpha_{pq}} - \frac{|A_{pq}|\sin\theta}{\omega_0^2\eta}\right)^2 + \left(Imag_{\alpha_{pq}} + \frac{|A_{pq}|\cos\theta}{\omega_0^2\eta}\right)^2 = \left(\frac{|A_{pq}|}{2\omega_0^2\eta}\right)^2 \qquad (2\text{-}13)$$

Clearly, the above expression is the equation of a circle, with centre at coordinates $\left(\frac{|A_{pq}|\sin\theta}{\omega_0^2\eta}, \frac{-|A_{pq}|\cos\theta}{\omega_0^2\eta}\right)$ and radius $\left(\frac{|A_{pq}|}{2\omega_0^2\eta}\right)$, as shown in figure 2-Ø3.

The natural frequency ($\omega_Ø$) is given when the rate of change of the angle Ω, with respect to the excitation frequency (ω), is maximum, i.e.

$$\text{when } \frac{\partial \Omega}{\partial \omega} \text{ is maximum}$$

$$\text{or } \frac{\partial^2 \Omega}{\partial \omega^2} = 0 \tag{2-14}$$

The above equation gives the natural frequency of a SDOF system. Once $\omega_{\emptyset}$ is known, the complexity (θ) of the modal constant (A) can easily be calculated. From this and the geometry of the circle, it is possible to show [3Ø], that the modal damping (η) is given by;

$$\eta = \frac{\omega_2^2 - \omega_1^2}{\omega_0^2}\left(\frac{1}{\tan\phi_1 + \tan\phi_2}\right) \tag{2-15}$$

where ω_2 - a frequency point such that $\omega_2 > \omega_{\emptyset}$;

ω_1 - a frequency point such that $\omega_1 < \omega_{\emptyset}$;

ϕ_1, ϕ_2 - are the angles subtended by the modal diameter of the circle passing through the point $\omega_{\emptyset}$ and the arcs joining the displaced origin to the points of ω_1 and ω_2 respectively (see figure 2-Ø4).

The radius (R) of the circle is related to the modal properties by;

$$R = \frac{|A_{pq}|}{2\omega_0^2\eta}$$

$$|A_{pq}| = 2R\omega_0^2\eta \tag{2-16}$$

The four quantities, natural frequency ($\omega_{\emptyset}$), loss factor (η), modulus of the modal constant (A_{pq}) and the

modal phase (θ), define completely the mode under consideration. A multi-degree-of-freedom system can be analysed by considering frequency points in the vicinity of each resonance to behave locally as a SDOF system. Thus a MDOF system may be broken down into several SDOF systems. The error introduced by this process can be calculated [30].

More rigorous theory on MDOF systems can be found in references 7 and 31.

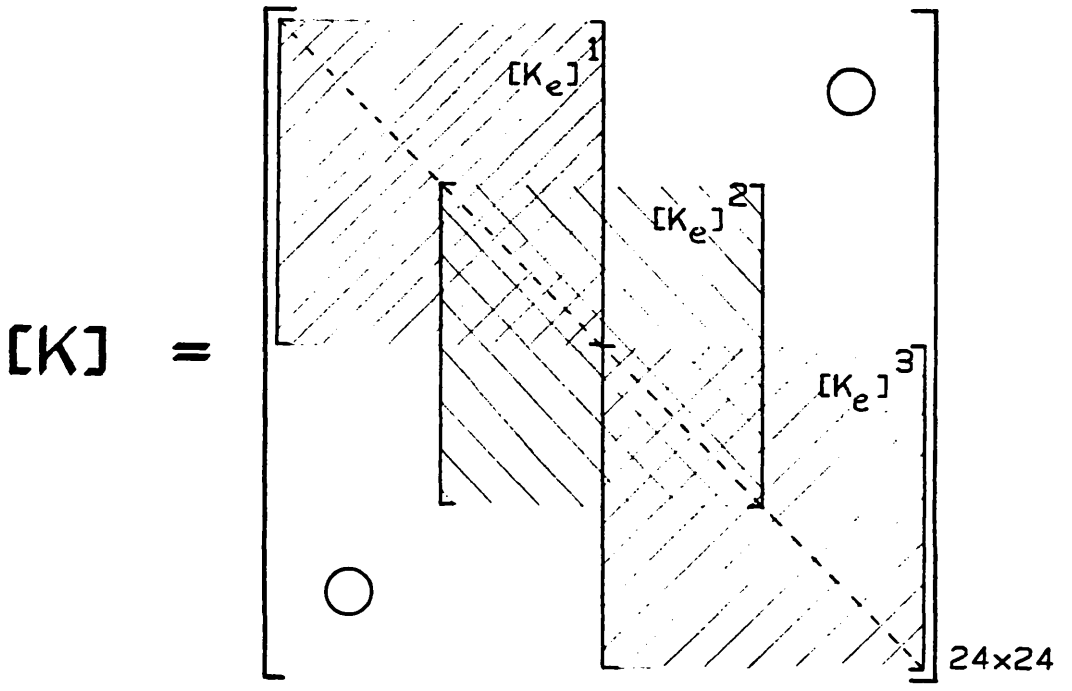

TABLE 2-01 : Overall stiffness matrix for a three element beam.

$$\begin{bmatrix} \alpha_{11} & \alpha_{12} & \cdots & \alpha_{1n} \\ \alpha_{21} & \alpha_{22} & \cdots & \alpha_{2n} \\ \vdots & \vdots & & \vdots \\ \alpha_{n1} & \alpha_{n2} & \cdots & \alpha_{nn} \end{bmatrix}$$

TABLE 2-02 : Receptance table.

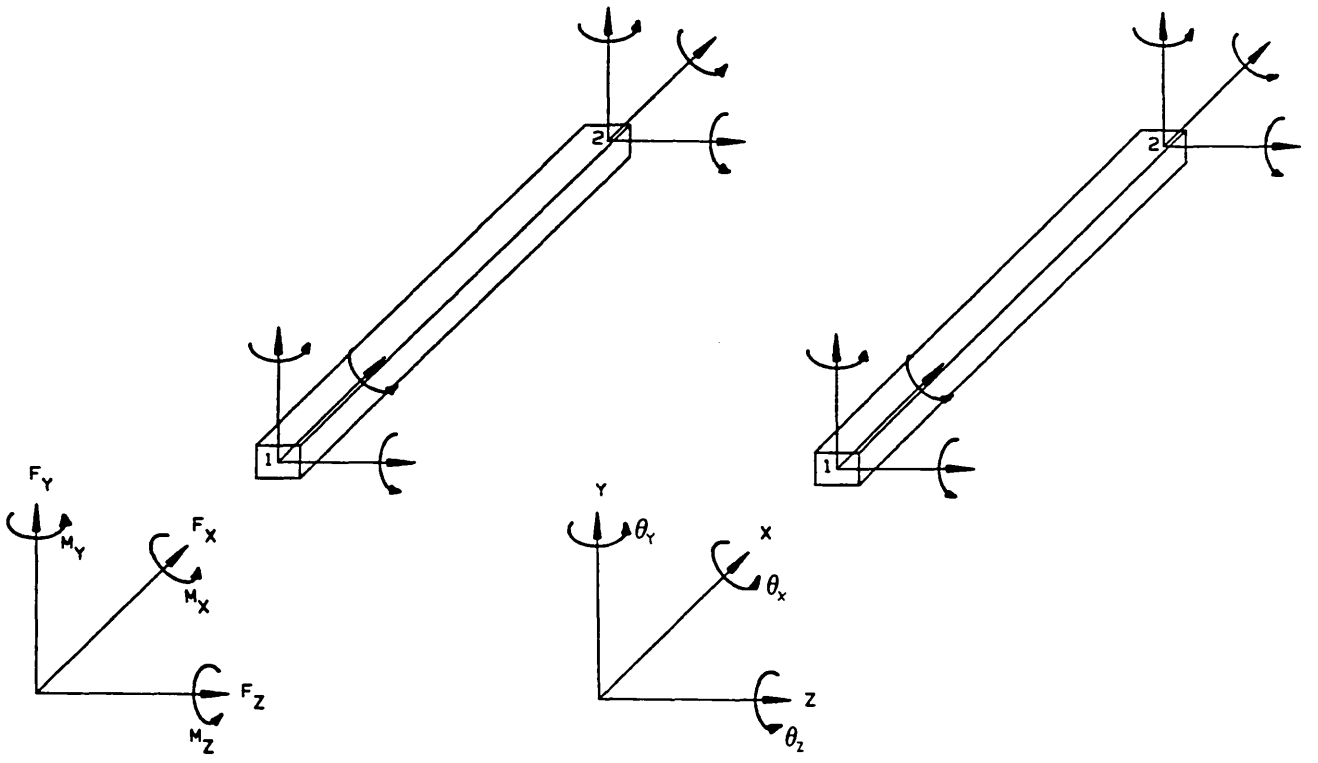

FIGURE 2-01 : Beam element.

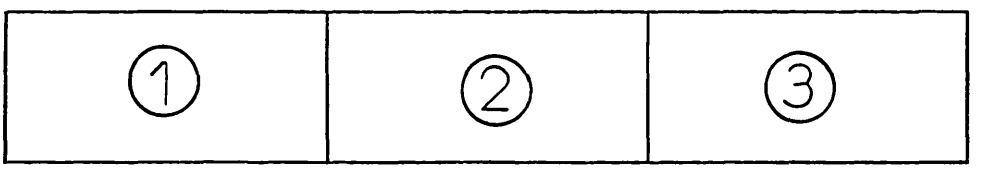

FIGURE 2-02 : Straight beam: three elements.

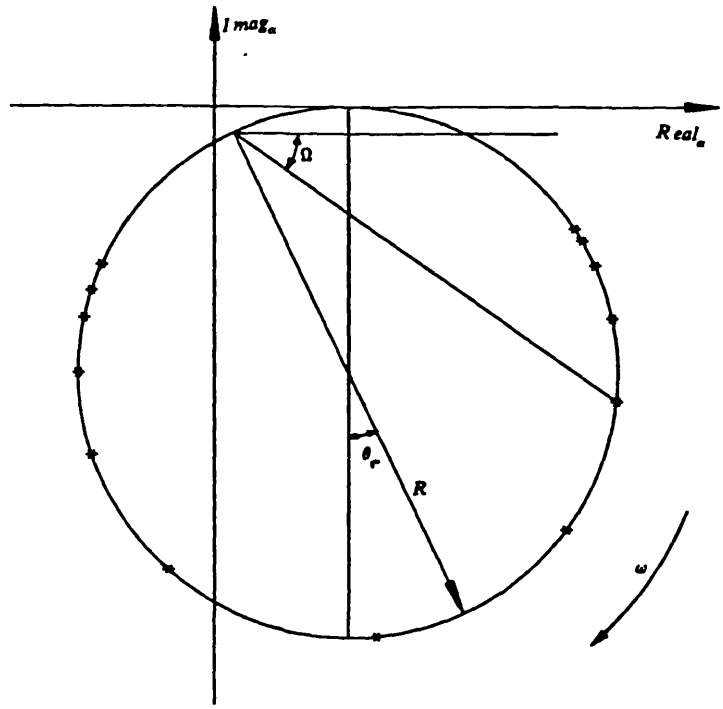

FIGURE 2-03 : Displaced modal circle.

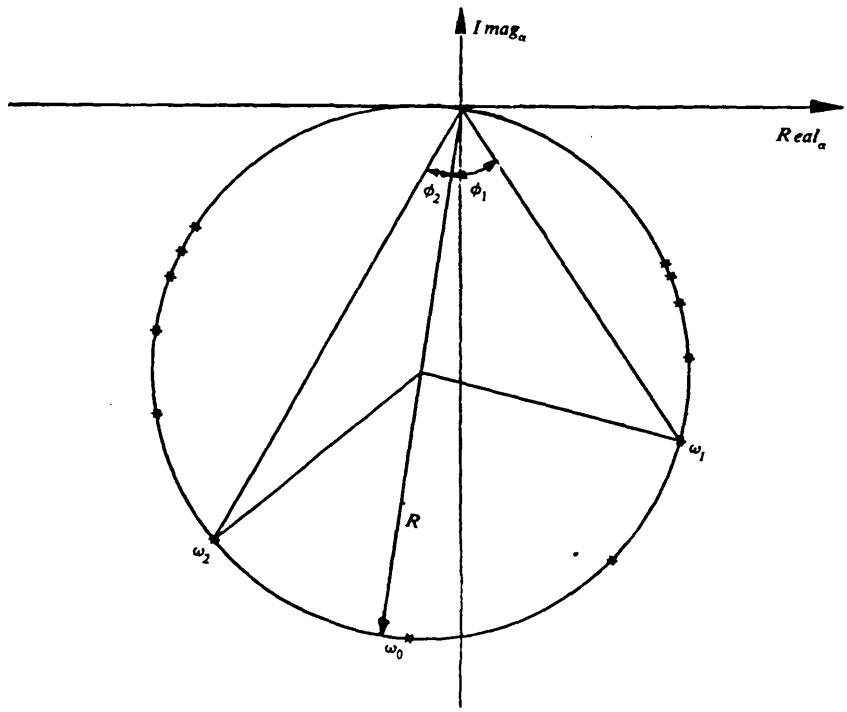

FIGURE 2-04 : Modal circle.

CHAPTER

-3-

3. IDENTIFICATION OF NONLINEARITIES FROM FREQUENCY - RESPONSE DATA

3.1. INTRODUCTION

The measurement of frequency-response data does not present any great difficulties, whether it be in the frequency domain or in the time domain. It is possible to obtain good measured data with the aid of reasonably priced equipment. The main difficulty arises in the analysis of these data. Perhaps the main cause of error in the analysis is due to structural nonlinearities because the algorithms used to extract modal properties are based on a assumptions of linearity. The errors due to these unwanted effects can be reduced and in some cases eliminated, by using a nonlinear modal identification algorithm. Unfortunately, the various types of nonlinearity present in the data are not known until some analysis is completed. Hence the exact form of the nonlinearity to be incorporated in the identification process is not known at the analysis stage.

Since most of the modal identification algorithms are based on linear relation between the applied force and the measured response, it is necessary to check whether the structure under test behaves as a linear system or, at least, is approximately linear within a certain frequency range. This requires some consideration of the measured data and the type of excitation method used [34,35,10].

It is frequently found that an actual structure, and even a simple one, does not satisfy the linearity criteria. For this reason, it is advisable for the user of experimental modal analysis to judge by visual examination of the measured data (as a first step) whether the structure under test is linear. This judgement can be a turning point in the process of obtaining 'good' modal properties. Unfortunately, it is impossible to detect slight nonlinearities by visual examination of the measured data. Apparently linear data can produce modal properties which are not truly representative of the structure's behaviour. Modal constants derived from such data, using a linear algorithm, may well be so complex (large phase angle) that no reasonable explanation can be given for this complexity. Modal constants may defy the basic law of reciprocity and modes of vibration are seldom orthogonal to each other. To make matters worse, repeatability is often found to be inadequate. All these unwanted effects can be attributed to small structural nonlinearities which increase the uncertainty in the quality of the modal parameters extracted.

The key to 'accurate' modal properties is the early detection of nonlinear behaviour. One of the tasks of any modal analyst should be to check whether the structure is linear. If nonlinearities are detected at the measurement stage then the experiment should be carried out in such a way as to reduce the effect of nonlinearities [36]. Unfortunately, this check is usually overlooked and it is

only at or after the analysis stage, when the results are not what they should be, that one starts to look for possible explanations of these unexpected and unacceptable results.

It is possible to use very basic knowledge in the processing of measured frequency response data to detect nonlinearities. There is no need to use complex multidegree-of-freedom curve fitting routines or, even worse, nonlinear curve fitting routines. The simplest modal identification process (linear single-degree-of-freedom identification routine in the immediate vicinity of resonance) can yield the necessary information for the detection of nonlinearities in a structure.

3.2. CRITICAL ASSESSMENT OF THE SINGLE-DEGREE-OF-FREEDOM MODAL IDENTIFICATION METHOD

This study commenced by the investigation of the modal properties of the 'NASTRAN' structure: a special testpiece consisting of a stiffened base plate, supporting a square-sectioned plated tower with various diaphragms positioned inside. One side of the tower consists of a lightweight honeycomb sandwich panel. On top of the tower is a mounting arrangement for a heavy mass which is connected to the structure via three pin supports. The structure is connected to the ground in eight positions around the base plate. The structure was designed to contain many of the features common in aircraft construction which give rise to problems and uncertainties in the

theoretical modelling stage, such as rivetted joints, stiffened plates, honeycomb sandwich panels, heavy masses on relatively flexible components etc. (figure 3-Ø1).

The structure has four modes of vibration in the frequency range from 3Ø to 120 Hz. Discrete sinusoidal excitation was used to vibrate the structure and the response was measured using accelerometers. The value of mobility was computed, using a Solartron 1172 frequency response analyser, for each frequency point. A typical mobility modulus plot ($Y_{Ø7,12}$) of the NASTRAN structure is shown in figure 3-Ø2. Modal parameters for each mode were extracted from polar plots (in the immediate vicinity of each mode) in the Nyquist plane as described in the last chapter. These modal properties (table 3-Ø1) can, in turn, be used to regenerate a theoretical model of the measured mobility data. Both measured and regenerated data were plotted on the same axis (figure 3-Ø2). These curves indicate a reasonable agreement between the measured and generated data and hence the derived modal properties can be taken as an accurate representation of the structure.

However there is a large scatter on the measured data around 5Ø Hz, as a consequence of which the quality of the curve fit in this area is not so good. The reason for the poor quality of data around 5Ø Hz is that the response of the structure in this frequency range is very small and hence the actual signal to noise ratio is low (due to mains interference).

The quality of the measured data may be improved by increasing the input force (by increasing the gain of the power amplifier) because the higher the input force, the higher the response (for a linear system). This will improve the signal to noise ratio and, these data with a high level of excitation are displayed in figure 3-Ø3.

The region around 5Ø Hz has now been 'cleaned up' and once again modal parameters were extracted using a linear algorithm (table 3-Ø2). This frequency response plot resists attempts to perform a satisfactory modal analysis on it; the best results obtained being shown in figure 3-Ø3 together with the measured data. This peculiarity is very puzzling because it is usually assumed that the better the quality of measured data, the better will be the curve fit, but in this case the reverse is the case. To understand this strange phenomenon it is necessary to consider nonlinearities.

3.2.1. NONLINEARITY CHECK ON THE 'NASTRAN' STRUCTURE

For a linear system, or structure, the ratio of response to input force is constant at a given frequency. However, for a nonlinear system this ratio is no longer constant but is a function of the applied force. Perhaps the simplest way of detecting nonlinearities would be to verify this law, and this can be accomplished by carrying out the measurement at several different forcing levels. Figures 3-Ø4 and 3-Ø5 show some results ($Y_{12,12}$) from such tests on the NASTRAN structure for modes 3 and 4 respectively. It is clearly seen that the ratio of response to force is not constant as the force changes for a given frequency. This demonstrates the structure's nonlinear behaviour and any 'blind' attempt to extract modal properties from the measured data, using a linear algorithm, will generally yield unsatisfactory results.

The modal properties derived from these sets of curves using a linear algorithm are listed in tables 3-Ø3 and 3-Ø4 for modes 3 and 4 respectively. The force is given in terms of volts (output of charge amplifier) rather than Newtons because over a narrow frequency range, as in this case the force applied to the structure is proportional to the voltage output of the charge amplifier.

Tables 3-Ø3 and 3-Ø4, together with figures 3-Ø4 and 3-Ø5, indicate that in this case, the modal properties are very much dependent on the forcing level and it is difficult to say what the true value of the modal parameters should be

because the variation in the natural frequencies (for the two modes considered) are about 3% while the change in the estimates of damping and modal constant is of the order of 30%. Clearly, the modal parameters are force dependent and, hence the structure under test must be nonlinear.

3.3. IDENTIFICATION OF NONLINEARITIES FROM A SINGLE FREQUENCY-RESPONSE CURVE

Most modal analysts, especially in industry, are not fortunate enough to have the time to carry out tests at several different forcing levels in order to check for nonlinearities. In most cases there is only one set of data and no comparison can be carried out as described above. Consequently, the technique of last section cannot be applied.

Structural nonlinearities can effect the frequency response data in many ways; the spacing of the frequency points might be distorted; the level of response may be altered for a given frequency; the natural frequency might be shifted from its true position etc. [37,38,39,40]. Thus, it is conceivable that the nonlinearities might be detected by making use of one or more of the features mentioned above, and we shall now explore this possibility.

The modal damping of a linear system may be determined using equation 3-01 and is independent of the choice of frequency points (ω_1 and ω_2) used for the calculation (figure 3-06).

$$\eta = \frac{\omega_2^2 - \omega_1^2}{\omega_0^2}\left(\frac{1}{\tan\phi_1 + \tan\phi_2}\right) \qquad (3\text{-}\emptyset 1)$$

In fact, many estimates of damping (η) can be computed using equation 3-Ø1 by choosing different frequency points ω_1 and ω_2; below and above the natural frequency ($\omega_\emptyset$). In theory, for a linear system, with well separated modes, all these estimates of damping will be identical. In practice, however, typical experimental data yields small variations in these damping estimates, due to small random errors in the measured data. Usually, an average value of these estimates is taken to be a good indication of the damping in that mode. The standard deviation of the estimates serves as a check on the quality of the results; the lower the standard deviation, the higher the confidence in the identified modal properties. Normally, the percentage variation is small - of the order of 2 or 3 % - but there are cases when the variation is very large and this indicates a significant scatter in the damping estimates which often cannot be accounted for by small random errors in the measured data. In such cases, before an average value is assumed to be a good representation, it is necessary to look for any recognizable pattern or any unusual trend in the derived estimates of damping. This is conveniently done by displaying the computed estimates in a matrix form [41] as shown in table 3-Ø5, where η_{ij} is the damping estimate calculated using frequency point i below resonance ($\omega_i = \Omega_i < \omega_\emptyset$) and j above ($\omega_j = \Omega_j > \omega_\emptyset$)

$$\eta_{ij} = \frac{\omega_j^2 - \omega_i^2}{\omega_0^2}\left(\frac{1}{\tan\phi_i + \tan\phi_j}\right) \qquad (3\text{-}\emptyset 2)$$

In general, the loss factor matrix thus obtained will be rectangular and a typical result obtained from experimental data is given in table 3-Ø6.

As well as for damping, matrices of estimates for the angle PHI (figure 3-Ø6) and the modal constant can also be constructed in a similar manner.

Table 3-Ø6 exhibits small random variations in the damping values for different combinations of points, but requires careful scrutiny to see any trends. Such a matrix may more easily be examined by displaying its values in an isometric three-axis plot. Two base axis are the two frequency axis; one for the points below resonance and the other for those above resonance, while the third axis represents the magnitude of the elements in the matrix (figure 3-Ø7). When plotted on such a diagram, the loss factor values of table 3-Ø6 produce the shape shown in figure 3-Ø8.

For a linear system with well separated modes, the surface of such a plot should be flat and any systematic deviation from this will probably indicate the presence of nonlinearities and/or that of closely-coupled modes.

The average value of the elements in the loss factor matrix is the one that is normally used for further analysis but if the plot is not flat then this average value is very

much dependent upon which points are chosen for its calculation from the matrix. We shall now examine the three types of average that will be useful in the next section but before this, it is necessary to renumber the elements of the matrix in table 3-Ø5 using normal matrix convention, (i.e. the first element in the matrix (top left hand side) is numbered 1,1 and, the second element in the top row is 1,2 and so on.)

Three types of average that may be useful are;

(i) Horizontal : this is the average of the elements in a row and is given by;

$$\overline{\eta}_{hk} = \frac{1}{n}\sum_{i=1}^{n}\eta_{ik} \qquad (3\text{-}Ø3)$$

where n - the number of damping estimates in the k^{th} row;

$\overline{\eta}_{hk}$ - horizontal average loss factor of the k^{th} row.

(ii) Vertical : this is the average of the elements in a column and is given by;

$$\overline{\eta}_{vk} = \frac{1}{n}\sum_{i=1}^{n}\eta_{ki} \qquad (3\text{-}Ø4)$$

where n - the number of damping estimates in the k^{th} column;

$\overline{\eta}_{vk}$ - vertical average loss factor of the k^{th} column.

(iii) Diagonal : this is the average of the elements in a square submatrix of the loss factor matrix. The submatrix is taken from the top left hand side of the loss

factor matrix.

$$\bar{\eta}_{dk} = \frac{1}{k^2} \sum_{i=1}^{k} \sum_{j=1}^{k} \eta_{ij} \qquad (3\text{-}\emptyset5)$$

where k - the size of the submatrix;

$\bar{\eta}_{dk}$ - diagonal averages loss factor of submatrix.

3.4. NUMERICAL STUDY

It is customary to demonstrate and to evaluate new techniques using theoretically generated data with known parameters. In dynamics this means solving differential equations of motion to obtain an analytical solution. The advantage of a numerical study is that the effect of varying any parameter can easily be investigated by keeping the values of all other parameters constant. The solution of the equations of motion can be obtained in the time or the frequency domains.

Because of the low cost of digital computers, numerical techniques for solving differential equations have become very popular. The computing cost is not the only factor in favour of numerical solutions; perhaps the main reason for using this technique is the fact that most nonlinear differential equations have no known analytical solutions.

Approximate numerical methods for solving complicated nonlinear differential equations can be employed under certain constraints. An approximate method which is

frequently used in the solution of such equations is the 'perturbation' method. This requires an initial estimate of the unknown parameter and then provides an update of this value via the governing differential equation, leading to the 'correct' value. Unfortunately, this technique does not always converge to the desired value or does not converge at all.

Another method which can be used for solving equations with small nonlinearities is the 'equivalent linearization' method. In this method, a nonlinear equation is replaced by an equivalent linear equation which in turn can easily be solved using numerical methods. This technique will be employed to solve all the nonlinear equations described in this section.

The following study is confined to the analysis of four systems;

(i) Linear single-degree-of-freedom (SDOF) system with viscous damping. This provides a datum case against which all other cases will be compared.

(ii) Single-degree-of-freedom system with viscous damping and softening cubic stiffness spring.

(iii) Single-degree-of-freedom system with viscous damping and Coulomb friction (Dry friction).

(iv) Linear two-degree-of-freedom system with hysteretic damping. This system will be used to investigate the effect of close modes on the modal properties derived

using the SDOF analysis method and, in particular, on the isometric loss factor plots.

3.4.1. LINEAR SINGLE-DEGREE-OF-FREEDOM SYSTEM WITH VISCOUS DAMPING

The equation of motion of a linear SDOF system with viscous damping is;

$$\ddot{X} + 2\xi\omega_0\dot{X} + \omega_0^2 X = F(t) \qquad (3\text{-}\emptyset 6)$$

where ξ - viscous damping ratio ($C/C_{\emptyset}$);

$\omega_{\emptyset}$ - natural frequency of the system (rad/sec);

F(t) - forcing function.

If the forcing function F(t) is sinusoidal then equation 3-Ø6 becomes;

$$\ddot{X} + 2\xi\omega_0\dot{X} + \omega_0^2 X = F e^{i\omega t} \qquad (3\text{-}\emptyset 7)$$

where ω - the excitation frequency (rad/sec);

F - amplitude of force (N/Kg).

An equation of the form 3-Ø7 describe Damped Forced Harmonic Vibrations, and it's steady state solution is given by the Particular Integral of the equation. Thus the solution is;

$$a = \left(\frac{(\omega_0^2 - \omega^2) - (2\xi\omega_0\omega)i}{(\omega_0^2 - \omega^2)^2 + (2\xi\omega_0\omega)^2}\right)F \qquad (3\text{-}\emptyset 8)$$

where a - the amplitude of vibration which is given by;

$$X(t) = ae^{i\omega t} \tag{3-09}$$

In the receptance (α=a/F) form;

$$\alpha(\omega) = \frac{(\omega_0^2 - \omega^2) - 2\xi\omega_0\omega i}{(\omega_0^2 - \omega^2)^2 + (2\xi\omega_0\omega)^2} \tag{3-10}$$

Separating real and imaginary parts;

$$Real(\alpha) = \frac{\omega_0^2 - \omega^2}{(\omega_0^2 - \omega^2)^2 + (2\xi\omega_0\omega)^2}$$

$$Imag(\alpha) = \frac{-2\xi\omega_0\omega}{(\omega_0^2 - \omega^2)^2 + (2\xi\omega_0\omega)^2} \tag{3-11}$$

For different values of damping coefficient (ξ), equations 3-11 can be used to generate data in the form of real and imaginary receptance as a function of excitation frequency (ω).

Frequency response data generated for the following conditions;

$\omega_{\emptyset}$ = 4Øπ rad/sec (2Ø Hz)

F = 1.Ø N/Kg

ξ = Ø.ØØ3, Ø.ØØ5, Ø.Ø1 and Ø.Ø2

are plotted on mobility modulus, mobility phase and Nyquist diagrams (figure 3-Ø9). These plots indicate that for a given frequency both the response and the diameter of the modal circle decrease but the natural frequency appears to be unaffected by the amount of viscous damping in the

system. The real against imaginary receptance (Nyquist) plots for viscous damping are not true circles but for systems with small damping these may be assumed to be almost circles.

These data were analysed using a linear SDOF algorithm to extract modal properties from each set of data (table 3-Ø7). The angle PHI, loss factor and modal constant matrices were compiled and are given in table 3-Ø8 for viscous damping coefficient (ξ) = Ø.ØØ5. These matrices are best examined on 3-D isometric and conventional (averages) plots (figures 3-1Ø through 3-12). For a SDOF system, linear or otherwise, the angle PHI always increases as the frequency points, taken in the calculation of this angle, move away from the natural frequency.

3.4.2. EQUATION OF MOTION FOR NONLINEAR SINGLE-DEGREE-OF-FREEDOM SYSTEMS

In general, the equation of motion of a forced nonlinear system is;

$$\ddot{X} + \omega_0^2 X + \mu f(X,\dot{X}) = F(t) \qquad (3\text{-}12)$$

where μ - is a constant;

$f(X,\dot{X})$ - function of displacement (X) and velocity ($\dot{X}$);

F(t) - forcing function.

For small nonlinearities, i.e. $\mu << 1$, the above equation may be written in an approximate equivalent linear form [42,45];

$$\ddot{X} + \bar{\lambda}\dot{X} + \bar{\omega}_0^2 X = F(t) \tag{3-13}$$

where $\bar{\lambda}$ - is the equivalent damping coefficient;

$\bar{\omega}_{\emptyset}$ - is the equivalent natural frequency.

Both $\bar{\lambda}$ and $\bar{\omega}_{\emptyset}$ are amplitude dependent and are given by;

$$\bar{\lambda} = \frac{-\mu}{\pi a \omega_0} \int_0^{2\pi} f(a\cos\phi, -a\omega_0 \sin\phi) \sin\phi \, d\phi$$

$$\bar{\omega}_0^2 = \omega_0^2 + \frac{\mu}{\pi a} \int_0^{2\pi} f(a\cos\phi, -a\omega_0 \sin\phi) \cos\phi \, d\phi \tag{3-14}$$

where a - is the amplitude of vibration;

$\omega_{\emptyset}$ - is the natural frequency of the linear system.

If the forcing function of equation 3-13 is sinusoidal, i.e. $F(t) = Fe^{i\omega t}$, then the steady state solution is obtained by;

$$X(t) = \left(\frac{\bar{\omega}_0^2 - \omega^2 - \omega\bar{\lambda} i}{(\bar{\omega}_0^2 - \omega^2)^2 + (\bar{\lambda}\omega)^2} \right) F e^{i\omega t}$$

$$a = \frac{F}{\sqrt{(\bar{\omega}_0^2 - \omega^2)^2 + (\bar{\lambda}\omega)^2}} \tag{3-15}$$

In the real and imaginary receptance form;

$$Real(\alpha) = \frac{\bar{\omega}_0^2 - \omega^2}{(\bar{\omega}_0^2 - \omega^2)^2 + (\bar{\lambda}\omega)^2}$$

$$Imag(\alpha) = \frac{-\omega\bar{\lambda}}{(\bar{\omega}_0^2 - \omega^2)^2 + (\bar{\lambda}\omega)^2} \tag{3-16}$$

$$\tan\theta = \frac{\bar{\lambda}\omega}{\omega^2 - \bar{\omega}_0^2} \tag{3-17}$$

where θ is the phase difference between the applied force and the response vector.

3.4.2.1. SINGLE-DEGREE-OF-FREEDOM SYSTEM WITH VISCOUS DAMPING AND SOFTENING-CUBIC-STIFFNESS

The equation of motion of a SDOF system with viscous damping and softening cubic stiffness is;

$$\ddot{X} + 2\xi\omega_0\dot{X} + \omega_0^2(X - \beta X^3) = F(t) \qquad (3\text{-}18)$$

where β - is the cubic stiffness coefficient (m^{-2}).

The above equation can be written in the same form as equation 3-12 with;

$$F(t) = F e^{i\omega t} \qquad (3\text{-}19)$$

$$\mu f(X,\dot{X}) = 2\xi\omega_0\dot{X} - \omega_0^2\beta X^3 \qquad (3\text{-}20)$$

Using equations 3-14 to obtain the equivalent damping ($\bar{\lambda}$) and the natural frequency ($\bar{\omega}_{\emptyset}$);

$$\bar{\lambda} = \frac{-1}{\pi a\omega_0}\int_0^{2\pi}(2\xi\omega_0(-a\omega_0\sin\phi) - \beta\omega_0^2 a^3\cos^3\phi)\sin\phi\, d\phi$$

$$\bar{\lambda} = 2\xi\omega_0 \qquad (3\text{-}21)$$

$$\bar{\omega}_0^2 = \omega_0^2 + \frac{1}{\pi a}\int_0^{2\pi}(2\xi\omega_0(-a\omega_0\sin\phi) - \beta\omega_0^2 a^3\cos^3\phi)\cos\phi\, d\phi$$

$$\overline{\omega_0^2} = \omega_0^2(1 - 3\beta a^2/4) \qquad (3\text{-}22)$$

Equation 3-21 indicates that the equivalent damping of a softening cubic stiffness system is identical to that of a linear system (i.e. cubic stiffness does not directly effect the damping of the system). The equivalent resonance frequency (equation 3-22) has now been reduced by a factor of $\sqrt{1 - 3\beta a^2/4}$. The natural frequency of a softening cubic stiffness system, will always be lower than the natural frequency ($\omega_{\emptyset}$) of the linear system because both 'β' and 'a' are positive quantities and hence the expression in the brackets of equation 3-22 is less than unity.

The system becomes unstable when;

$$1 - 3\beta a^2/4 < 0$$

$$\beta a^2 > 4/3 \qquad (3\text{-}23)$$

Substituting equations 3-21 and 3-22 into equation 3-15 gives;

$$a = \frac{F}{\sqrt{\omega_0^4(1 - 3\beta a^2/4)^2 + (2\xi\omega_0\omega)^2}}$$

Simplifying, we obtain;

$$(3/4\beta\omega_0^2)^2 a^6 - 3/2(\omega_0^2 - \omega^2)\beta\omega_0^2 a^4 + ((\omega_0^2 - \omega^2)^2 + (2\xi\omega_0\omega)^2)a^2 - F^2 = 0 \qquad (3\text{-}24)$$

The above equation is a cubic polynomial with amplitude squared (a^2) as the unknown variable and its values are given by the roots of the equation 3-24.

Depending on the values of the parameters, equation 3-24 can either have one real and two complex roots or three real roots. In the latter case, the well - known jump phenomenon occurs as shown in figure 3-13 [43,44,45]. For real structures, nonlinearities are usually small and in such cases the jump phenomenon does not occur (i.e. equation 3-24 has only one real root for different values of the excitation frequency). In this study we shall only consider the case of one real root.

Equation 3-24 has an exact solution which allows the value of the amplitude of vibration (a) to be calculated as a function of the excitation frequency. Once the amplitude is known, the equivalent damping ($\bar{\lambda}$) and the equivalent natural frequency ($\bar{\omega}_{\emptyset}$) can be computed using equations 3-21 and 3-22 and hence the real and imaginary parts of receptance can be calculated (equation 3-15).

Frequency response data were generated for different levels of softening cubic stiffness. Mobility modulus, mobility phase and Nyquist plots were constructed for the following input values;

$$\omega_{\emptyset} = 40\pi \quad \text{rad/sec (20 Hz)}$$

$$\xi = 0.005$$

$$F = 1.0 \text{ N/Kg.}$$

$$\beta = 50,\ 200,\ 400 \text{ and } 600 \text{ m}^{-2}.$$

and these plots are shown in figure 3-14.

The mobility modulus diagram 'leans back' but its

maximum response (or mobility because force is constant) appears to be unaffected by the amount of cubic stiffness. However, the frequency at which this maximum response occurs is dependent on it. For high levels of nonlinearity the frequency spacing, especially near resonance, is distorted and the mobility modulus plots are no longer symmetrical about the frequency of maximum response. Nyquist plots also show the distortion of frequency spacing although the diameters of the modal circles are virtually independent of the amount of cubic stiffness.

Modal parameters extracted from these data, using a linear SDOF algorithm, are given in table 3-Ø9. Again, 3-D isometric plots, together with the different types of averages, are constructed and figures 3-15 and 3-16 show the plots for β = 5Ø and 2ØØ m^{-2} respectively. The value of loss factor that one would obtain (input value), in the absence of softening cubic stiffness (β = Ø m^{-2}) are marked on the 3-D plots with asterisks.

For the frequency points below resonance the loss factor increases as the point for the calculation of this value move away from the resonance (ω_2, frequency point above resonance being fixed). However, for points above resonance the loss factor decreases with increasing frequency (figures 3-15 and 3-16) and the 'tilt' of the 3-D diagrams increases with increasing nonlinearity.

It is interesting to note that the graph for the vertical averages is a straight line, the slope of which is

a function of the nonlinearity and increases with it. However, there is no simple relation between the slope and the amount of nonlinearity.

The diagonal-average diagram exhibits a maximum, the value of which is very close to the input or true value of the loss factor (table 3-10).

Unlike in the theoretical study, the amount of nonlinearity in the real structure cannot be changed easily. The only function that can be readily altered is the input force and this is equivalent to keeping the nonlinearity constant and carrying out tests at several different but constant levels of excitation, as in section, 3.1.1. To study the effect of keeping nonlinearity constant and changing the force, the following input data were used;

$$\omega_{\emptyset} = 40\pi \quad \text{rad/sec (20 Hz)}$$
$$\xi = \emptyset.\emptyset\emptyset5$$
$$\beta = 2\emptyset\emptyset \ m^{-2}$$
$$F = \emptyset.5,\ 1.\emptyset,\ 1.5 \text{ and } 2.\emptyset \ (N/Kg)$$

The mobility modulus, mobility phase and Nyquist diagrams are displayed in figure 3-17. The effect of increasing the force is the same as that of increasing the softening cubic stiffness. Again, modal parameters were extracted from these data using a linear SDOF algorithm (table 3-11). The isometric loss factor plots for this case are shown in figure 3-18. The graphs of the averages are omitted because they are similar to those obtained for varying levels of cubic stiffness (figures 3-15 and 3-16).

The isometric loss factor diagrams indicate that the effect of increasing the force is the same as increasing the amount of nonlinearity.

Also constructed are the graphs of mobility modulus, mobility phase and Nyquist plots (figure 3-19) as a function of softening cubic stiffness for several values of the excitation frequency. These diagrams indicate how the response varies as a function of the nonlinearity. The locus of real against imaginary receptance is a circle and the effect of cubic stiffness is to distort the Nyquist plot clockwise. As the nonlinearity increases the amount by which the modal circle is distorted also increases.

3.4.2.2. SINGLE-DEGREE-OF-FREEDOM SYSTEM WITH VISCOUS DAMPING AND COULOMB FRICTION

The equation of motion of a SDOF system with viscous damping and coulomb (or dry) friction is;

$$\ddot{X} + 2\xi\omega_0\dot{X} + \omega_0^2 X + R\frac{\dot{X}}{|\dot{X}|} = F(t) \qquad (3\text{-}25)$$

where R - is the dry friction coefficient (N/Kg).

Comparing equations 3-25 and 3-12 yields;

$$F(t) = Fe^{i\omega t} \qquad (3\text{-}26)$$

and

$$\mu f(X,\dot{X}) = 2\xi\omega_0\dot{X} + R\frac{\dot{X}}{|\dot{X}|} \qquad (3\text{-}27)$$

The equivalent damping and natural frequency can be

calculated using equations 3-14;

$$\bar{\lambda} = \frac{-1}{\pi a \omega_0}\left(\int_0^{2\pi} 2\xi\omega_0(-a\omega_0 \sin\phi)\sin\phi\, d\phi + 2R\int_0^{\pi}(-\sin\phi)\, d\phi\right)$$

$$\bar{\lambda} = 2\xi\omega_0 + \frac{4R}{\pi a \omega_0} \qquad (3\text{-}28)$$

$$\overline{\omega_0^2} = \omega_0^2 + \frac{1}{\pi a}\left(\int_0^{2\pi} 2\xi\omega_0(-a\omega_0 \sin\phi)\cos\phi\, d\phi + 2R\int_0^{\pi}(-\cos\phi)\, d\phi\right)$$

$$\overline{\omega_0^2} = \omega_0^2 \qquad (3\text{-}29)$$

Equations 3-28 indicate that the damping of the equivalent linear system has increased by an amount of $\frac{4R}{\pi a \omega_0}$ but the natural frequency remains unaffected (equation 3-29).

Substituting equations 3-28 and 3-29 into the equivalent linear equation 3-15 gives;

$$a = \frac{F}{\sqrt{(\omega_0^2 - \omega^2)^2 + (2\xi\omega_0\omega + \frac{4R\omega}{\pi a\omega_0})^2}}$$

$$(\omega_0^2 - \omega^2)^2 a^2 + (2\xi\omega_0\omega + \frac{4R\omega}{\pi a\omega_0})^2 a^2 = F^2$$

Simplifying yields;

$$\left((\omega_0^2 - \omega^2)^2 + (2\xi\omega_0\omega)^2\right)a^2 + \frac{8\xi\omega^2 R}{\pi}a + \left((\frac{4R\omega}{\pi\omega_0})^2 - F^2\right) = 0 \qquad (3\text{-}3\emptyset)$$

The above equation is a quadratic polynomial, with amplitude (a) as the variable, which can be calculated from the roots of this equation for different values of the excitation frequency. Hence, the equivalent damping and the natural frequency can also be computed from equations 3-28 and 3-29 respectively. Knowing this, the real and imaginary parts of receptance can be obtained from equations 3-16.

The stability of the system, represented by equation 3-3Ø depends on the form of the roots of this equation. If the roots are real then the system defined by the equation is stable otherwise it becomes unstable i.e. the equation of stability is;

$$\left(\frac{8\xi\omega^2 R}{\pi}\right)^2 - 4\left(\left(\frac{4R\omega}{\pi\omega_0}\right)^2 - F^2\right)\left((\omega_0^2 - \omega^2) + (2\xi\omega_0\omega)^2\right) > 0 \qquad (3\text{-}31)$$

Frequency response data calculated for different values of dry friction are displayed in the form of mobility modulus, mobility phase and Nyquist plots (figure 3-2Ø) for the following input values;

$\omega_{Ø}$ = 4Øπ rad/sec (2Ø Hz)

ξ = Ø.ØØ5

F = 1.Ø N/Kg

R = Ø.1Ø, Ø.25, Ø.4Ø and Ø.55 N/Kg

As the dry friction increases, the mobility decreases thus indicating an increase in damping as shown by the equation 3-28. The natural frequency does not appear to change with dry friction. At low levels of dry friction (R = Ø.1Ø and Ø.25 N/Kg), the Nyquist plots appear to be circles (almost) but of different diameters and as the nonlinearity increases, the modal diameter decreases distorting the circle into an 'egg' shaped plot (R = Ø.55 N/Kg).

The identified modal properties derived using a linear SDOF curve fitting process are shown in table 3-12. In the

case of dry friction, the conventional plots of different types of average give no useful information and so only the isometric (3-D) diagrams are displayed (figure 3-21). These plots indicate that the damping decreases as the frequency points used in the calculation of loss factor move away from the resonance below and above. The maximum estimated value of the damping occurs around the resonance i.e. maximum damping is given by the two adjacent points around resonance, one below and one above the natural frequency. Data polluted with dry friction nonlinearity give damping estimates that are much higher than those that would be obtained in the absence of any nonlinearity.

As in the case of cubic stiffness, here we shall also examine the effect of altering the force while the amount of dry friction remains constant. For this the following input data were used;

$$\omega_{\emptyset} = 40\pi \quad \text{rad/sec (20 Hz)}$$

$$\xi = \emptyset.\emptyset\emptyset5$$

$$R = \emptyset.25 \text{ N/Kg}$$

$$F = \emptyset.5,\ 1.\emptyset,\ 2.\emptyset \text{ and } 5.\emptyset \text{ (N/Kg)}$$

The mobility modulus, mobility phase and Nyquist plots are exhibited in figure 3-22. The effect of increasing the force appears to be the same as that of reducing the dry friction. At high levels of force, the Nyquist plots are circular but as the force decreases these circles degenerate into 'egg' shaped plots. The modal properties extracted from these data using a linear SDOF algorithm are shown in

table 3-13. The loss factor isometric plots (figure 3-23) indicate a reduction in the effect of the dry friction as the force is increased and at low levels of excitation, the dry friction has large influence on the estimated values of loss factor.

The effect of varying dry friction on the response, for a given excitation frequency was also investigated (figure 3-24). The Nyquist plot shows that as the dry friction increases the modal diameter decreases.

3.4.3. LINEAR TWO-DEGREE-OF-FREEDOM SYSTEM WITH HYSTERETIC DAMPING

In the analysis of SDOF systems, it is often assumed that the modes of vibration are well separated from each other so that the effect of all the modes except the one under consideration is assumed to be constant over a narrow frequency range. With this assumption, a multi-degree-of-freedom system can be analysed as several SDOF systems by considering the frequency points in the immediate vicinity of each mode separately. Tnis leads to a simple method for extracting modal properties from the frequency response data. However, there are many cases when the modes are too close for this assumption to be valid. Analysis of data from such cases using a SDOF circle-fitting routine will lead to inaccurate results and to a badly identified curve.

In this section we shall investigate how close coupled

modes effect the modal properties identified using a SDOF algorithm. Again, the loss factor values around resonance will be examined together with the angle PHI plots.

The equation governing a multidegree of freedom system is;

$$\alpha_{pq}(\omega) = \sum_{r=1}^{m} \frac{|_rA_{pq}|e^{i\theta_r}}{\omega_r^2(1-(\omega/\omega_r)^2 + i\eta_r)} \qquad (3\text{-}32)$$

where p,q - coordinates of response and excitation;

ω_r - natural frequency of the r^{th} mode;

η_r - loss factor of r^{th} mode;

$_rA_{pq}$ - modal constant of the r^{th} mode;

θ_r - modal phase of the r^{th} mode;

m - number of modes.

In the case of two modes only;

$$\alpha_{pq}(\omega) = \frac{|_1A_{pq}|e^{i\theta_1}}{\omega_1^2(1-(\omega/\omega_1)^2 + i\eta_1)} + \frac{|_2A_{pq}|e^{i\theta_2}}{\omega_2^2(1-(\omega/\omega_2)^2+i\eta_2)} \qquad (3\text{-}33)$$

The above equation can be solved to obtain the real and imaginary parts of receptance.

The effect of close coupled modes can be investigated by altering the natural frequencies of one or both of the modes (ω_2 and ω_1) so that they converge towards a single frequency value. The natural frequency of mode 1 (ω_1) was kept constant at 20 Hz while that of mode 2 (ω_2) was decreased from 21 to 20 Hz. The input data for

equation 3-33 were as follows;

MODE 1

$$\omega_1 = 40\pi \text{ rad/sec (20 Hz)}$$
$$\eta_1 = 0.01$$
$$_1A_{pq} = 1.0 \text{ 1/Kg}$$
$$\theta_1 = 0 \text{ deg}$$

MODE 2

$$\omega_2 = 21.0,\ 20.6,\ 20.4\ 20.2,\ 20.1 \text{ and } 20.0 \text{ Hz}$$
$$\eta_2 = 0.01$$
$$_2A_{pq} = 1.0 \text{ 1/Kg}$$
$$\theta_2 = 0 \text{ deg}$$

The mobility modulus and mobility phase plots are displayed in figure 3-25 and the corresponding Nyquist plots in figure 3-26. Table 3-14 shows the derived modal properties from these data using the SDOF identification process.

Some of the 3-D loss factor and angle PHI plots for modes 1 and 2 are shown in figures 3-27 and 3-28 respectively.

The damping plot for mode 1 (ω_2 = 20.6 Hz; figure 3-27) indicates a large variation in the loss factor estimates. The maximum value occurs at exactly the same frequency as that of the second mode. The angle PHI diagram also shows a large change at the point where a peak is detected on the loss factor plot. As mentioned earlier, the angle PHI always increases as the frequency points used in the calculation of this angle move away from resonance and the only time the angle PHI does not increase is when the

effect of a neighbouring mode is not negligible.

The angle PHI is increasing for the frequency points below resonance but above resonance there is a sudden change. Since this change (in the PHI matrix) occurs at the frequency points above natural frequency this indicates the presence of at least one mode in the neighbourhood of the mode under consideration, its natural frequency being higher than the mode being analysed. Similarly, plots for mode 2 (figure 3-28) reveal the presence of at least one mode below the second mode.

3.5. CONCLUSIONS

For any linear SDOF system the modal parameters are independent of the choice of frequency points for their derivation, but for close modes and for nonlinear systems, the choice of points can greatly influence the results. In the case of close modes, an error of the order of 100% is not unusual if a simple average is taken for the modal parameters for all the combinations of points. Large errors may also occur due to the nonlinearities.

From the study of theoretical data, we have been able to calibrate the 3-D plots so that diagrams from the data of real structures may be compared with these to identify the the type of pollutant and hence to determine what steps should be taken in order to reduce its effect in the final data e.g. to reduce the effects of cubic stiffness, a low

level of excitation should be used and to reduce the effect of dry friction, a high input force is necessary.

Isometric plots of loss factor estimates are more sensitive to cubic stiffness and close modes than to dry friction. A large amount of dry friction produces a relatively small change in the shape of the loss factor plot. Consequently, dry friction will be more difficult to detect from these plots than will cubic stiffness or close modes.

In applying the above criteria, one must be very careful because the results, in this thesis, relate to only two types of nonlinearity and it is inevitable that in real structures other types of nonlinearities will exist and could produce similar effects. Further, it is possible that the combination of two or more types of nonlinearity together with close modes may also produce similar changes in the isometric loss factor plots as illustrated above for each type of nonlinearity individually. Nevertheless, the above technique provides a useful diagnostic when the data are not ideal and care must be taken when interpreting the results.

MODE NUMBER	NATURAL FREQUENCY (Hz)	LOSS FACTOR x1000	RMS ERROR (%)	MODAL CONSTANT x1000 (1/Kg)	MODAL PHASE (Deg)
1	33.135Ø	14.47	1.13	3.4293	Ø.65
2	34.985Ø	11.5Ø	3.Ø1	4.5876	-17Ø.95
3	79.756Ø	6.79	Ø.71	5.ØØ89	-2.55
4	1Ø4.47ØØ	13.72	Ø.89	2.1217	-178.19

TABLE 3-01 : Identified modal parameters of $Y_{07,12}$
(Low level of excitation).

MODE NUMBER	NATURAL FREQUENCY (Hz)	LOSS FACTOR x1000	RMS ERROR (%)	MODAL CONSTANT x1000 (1/Kg)	MODAL PHASE (Deg)
1	32.9625	15.Ø6	1.62	3.1891	-Ø.39
2	34.715Ø	14.2Ø	1.76	4.6423	-157.95
3	79.4Ø6Ø	7.51	Ø.35	4.8883	-2.18
4	1Ø4.2ØØØ	12.91	Ø.57	1.9Ø59	176.73

TABLE 3-02 : Identified modal parameters of $Y_{07,12}$
(High level of excitation).

EXCITATION LEVEL (volts)*	NATURAL FREQUENCY (Hz)	LOSS FACTOR x1000	RMS ERROR (%)	MODAL CONSTANT x1000 (1/Kg)	MODAL PHASE (Deg)
Ø.Ø5	79.165Ø	6.89	1.56	5.1543	-148.36
Ø.1Ø	78.91ØØ	6.87	1.93	4.5386	-134.Ø5
Ø.2Ø	78.665Ø	6.31	5.99	3.82Ø5	-13Ø.65
Ø.3Ø	78.49ØØ	6.25	4.83	3.5742	-132.33
Ø.4Ø	78.335Ø	5.66	8.93	3.1355	-122.31
Ø.6Ø	78.11ØØ	5.57	13.27	2.9322	-129.79
Ø.8Ø	77.86ØØ	5.28	17.27	2.6Ø92	-121.65
1.ØØ	77.615Ø	7.18	9.65	3.2Ø74	-12Ø.16

TABLE 3-03 : Identified modal parameters of mode 3 for point mobility $Y_{12,12}$ as function of excitation level.

EXCITATION LEVEL (volts)*	NATURAL FREQUENCY (Hz)	LOSS FACTOR x1000	RMS ERROR (%)	MODAL CONSTANT x1000 (1/Kg)	MODAL PHASE (Deg)
Ø.Ø5	1Ø3.98ØØ	13.74	Ø.46	2.8771	1Ø.73
Ø.1Ø	1Ø3.89ØØ	14.11	Ø.27	2.8235	12.14
Ø.2Ø	1Ø3.635Ø	14.6Ø	2.22	2.78Ø6	21.69
Ø.3Ø	1Ø3.49ØØ	14.68	1.2Ø	2.6765	28.37
Ø.4Ø	1Ø3.27ØØ	12.89	2.16	2.2755	33.58
Ø.6Ø	1Ø2.92ØØ	12.Ø1	3.47	2.ØØ1Ø	4Ø.6Ø
Ø.8Ø	1Ø2.71ØØ	11.64	6.64	1.9677	3Ø.79
1.ØØ	1Ø2.42ØØ	12.3Ø	4.87	2.Ø216	38.ØØ

TABLE 3-04 : Identified modal parameters of mode 4 for point mobility $Y_{12,12}$ as function of excitation level.

* 1 volt ≙ 22 N

		frequency points below resonance					
		Ω_6	Ω_5	Ω_4	Ω_3	Ω_2	Ω_1
frequency points above resonance	Ω_7	η_{67}	η_{57}	η_{47}	. . . . .		η_{17}
	Ω_8	η_{68}	η_{58}	η_{48}	. . . . .		η_{18}
	Ω_9	η_{69}	η_{59}	η_{49}	. . . . .		η_{19}
	Ω_{10}	.	.	.			$\eta_{1\ 10}$
	Ω_{11}	.	.	.			$\eta_{1\ 11}$
	Ω_{12}	.	.	.			$\eta_{1\ 12}$
	Ω_{13}	$\eta_{6\ 13}$	$\eta_{5\ 13}$	$\eta_{4\ 13}$	$\eta_{3\ 13}$	$\eta_{2\ 13}$	$\eta_{1\ 13}$

TABLE 3-05 : Matrixof damping estimates around resonance.

TABLE OF LOSS FACTORS x1000

	9	8	7	6	5	4	3	2	1
10	14.81	14.29	13.69	12.60	12.55	13.30	12.31	12.90	12.95
11	12.58	12.96	12.88	12.23	12.25	12.90	12.12	12.65	12.71
12	14.79	14.53	14.11	13.25	13.12	13.64	12.78	13.24	13.25
13	13.17	13.29	13.18	12.64	12.61	13.09	12.42	12.84	12.86
14	14.16	14.10	13.87	13.27	13.16	13.58	12.88	13.25	13.26
15	13.63	13.65	13.52	13.04	12.97	13.35	12.75	13.09	13.11
16	13.07	13.16	13.10	12.73	12.70	13.06	12.54	12.87	12.90
17	13.62	13.64	13.53	13.14	13.07	13.39	12.86	13.16	13.17
18	13.36	13.40	13.33	13.00	12.95	13.24	12.77	13.05	13.07
19	13.78	13.79	13.68	13.33	13.26	13.53	13.05	13.30	13.31

TABLE 3-06 : Experimental loss factor matrix.

VISCOUS DAMPING	NATURAL FREQUENCY (Hz)	LOSS FACTOR x1000	RMS ERROR (%)	MODAL CONSTANT x1000 (1/Kg)	MODAL PHASE (Deg)
0.003	20.0000	5.97	13.01	995.77	8.50
0.005	20.0000	10.05	4.75	1004.71	5.31
0.010	20.0000	20.03	0.83	1001.45	2.29
0.020	20.0000	39.99	0.21	1000.24	0.29

TABLE 3-07 : Identified modal properties as a function of viscous damping.

TABLE OF ANGLE PHI(DEG)

	21	20	19	18	17	16	15	14	13
22	53.3	106.1	142.8	165.4	179.6	189.1	195.9	200.9	204.7
23	90.3	143.0	179.8	202.3	216.6	226.1	232.8	237.8	241.6
24	112.9	165.7	202.4	225.0	239.2	248.8	255.5	260.5	264.3
25	127.2	180.0	216.7	239.3	253.5	263.1	269.8	274.8	278.6
26	136.8	189.5	226.3	248.9	263.1	272.6	279.4	284.3	288.2
27	143.6	196.3	233.1	255.6	269.9	279.4	286.1	291.1	294.9
28	148.6	201.3	238.0	260.6	274.9	284.4	291.1	296.1	299.9
29	152.4	205.1	241.9	264.4	278.7	288.2	294.9	299.9	303.7
30	155.4	208.2	244.9	267.5	281.7	291.2	298.0	302.9	306.8
31	157.9	210.6	247.3	269.9	284.2	293.7	300.4	305.4	309.2

TABLE OF LOSS FACTORS x1000

	21	20	19	18	17	16	15	14	13
22	9.98	10.02	10.02	10.02	10.02	10.02	10.02	10.02	10.02
23	10.00	10.02	10.02	10.02	10.02	10.02	10.02	10.02	10.02
24	10.01	10.02	10.02	10.02	10.02	10.02	10.02	10.02	10.02
25	10.01	10.02	10.02	10.02	10.02	10.02	10.02	10.02	10.02
26	10.01	10.02	10.02	10.02	10.02	10.02	10.02	10.02	10.02
27	10.01	10.02	10.02	10.02	10.02	10.02	10.02	10.02	10.02
28	10.02	10.02	10.02	10.02	10.02	10.02	10.02	10.02	10.02
29	10.02	10.02	10.02	10.02	10.02	10.02	10.02	10.02	10.02
30	10.02	10.02	10.02	10.02	10.02	10.02	10.02	10.02	10.02
31	10.02	10.02	10.02	10.02	10.02	10.02	10.02	10.02	10.02

TABLE OF MODAL CONSTANTS (1/Kg)

	21	20	19	18	17	16	15	14	13
22	1.00	1.00	1.00	1.00	1.00	1.00	1.00	1.00	1.00
23	1.00	1.00	1.00	1.00	1.00	1.00	1.00	1.00	1.00
24	1.00	1.00	1.00	1.00	1.00	1.00	1.00	1.00	1.00
25	1.00	1.00	1.00	1.00	1.00	1.00	1.00	1.00	1.00
26	1.00	1.00	1.00	1.00	1.00	1.00	1.00	1.00	1.00
27	1.00	1.00	1.00	1.00	1.00	1.00	1.00	1.00	1.00
28	1.00	1.00	1.00	1.00	1.00	1.00	1.00	1.00	1.00
29	1.00	1.00	1.00	1.00	1.00	1.00	1.00	1.00	1.00
30	1.00	1.00	1.00	1.00	1.00	1.00	1.00	1.00	1.00
31	1.00	1.00	1.00	1.00	1.00	1.00	1.00	1.00	1.00

TABLE 3-08 : Angle PHI, loss factor and modal constant matrices for viscous damping (ξ = 0.005).

SOFTENING CUBIC STIFFNESS (m^{-2})	NATURAL FREQUENCY (Hz)	LOSS FACTOR x1000	RMS ERROR (%)	MODAL CONSTANT x1000 (1/Kg)	MODAL PHASE (Deg)
50	19.9775	9.76	8.95	973.97	-168.42
200	19.9225	9.25	19.64	919.65	-151.97
400	19.8675	8.89	20.90	881.02	-143.55
600	19.8275	8.65	23.08	855.10	-140.06
EXACT VALUE	20	10	0	1000	-180

TABLE 3-09 : Identified modal properties as a function of softening cubic stiffness (F = 1.0 N/Kg).

SOFTENING CUBIC STIFFNESS (m^{-2})	SLOPE OF VERTICAL AVERAGE (m^{-2})	MAXIMUM VALUE OF DIAGONAL AVERAGES LOSS FACTOR
50	3.64E-04	0.0100
200	6.12E-04	0.0098
400	7.35E-04	0.0094
600	8.15E-04	0.0093
EXACT VALUE	------	0.01

TABLE 3-10 : Slope of vertical averages and maximum value of the diagonal plot as a function of softening cubic stiffness.

EXCITATION FORCE (N/Kg)	NATURAL FREQUENCY (Hz)	LOSS FACTOR x1000	RMS ERROR (%)	MODAL CONSTANT x1000 (1/Kg)	MODAL PHASE (Deg)
Ø.5	19.9775	9.76	8.95	973.97	-168.42
1.Ø	19.9225	9.25	19.64	919.65	-151.97
1.5	19.8325	8.59	42.8Ø	849.15	-121.62
2.Ø	19.7775	8.24	26.43	813.25	-131.73
EXACT VALUE	2Ø	1Ø	Ø	1ØØØ	-18Ø

TABLE 3-11 : Identified modal properties as function of excitation force (β = 200 m^{-2}).

DRY FRICTION (N/Kg)	NATURAL FREQUENCY (Hz)	LOSS FACTOR x1000	RMS ERROR (%)	MODAL CONSTANT x1000 (1/Kg)	MODAL PHASE (Deg)
Ø.1Ø	19.9975	11.12	3.51	923.92	4.7Ø
Ø.25	19.9975	12.6Ø	1.83	739.19	3.83
Ø.4Ø	19.9975	14.67	3.55	529.82	2.27
Ø.55	2Ø.ØØ5Ø	16.71	8.47	274.99	-2.61
EXACT VALUE	2Ø	1Ø	Ø	1ØØØ	-18Ø

TABLE 3-12 : Identified modal properties as function of dry friction (F = 1.0 N/Kg).

EXCITATION FORCE (N/Kg)	NATURAL FREQUENCY (Hz)	LOSS FACTOR x1000	RMS ERROR (%)	MODAL CONSTANT x1000 (1/Kg)	MODAL PHASE (Deg)
Ø.5	2Ø.ØØ5Ø	16.74	5.98	4Ø1.55	-3.11
1.Ø	19.9975	12.6Ø	2.94	739.17	3.83
2.Ø	19.9975	11.1Ø	3.72	865.19	4.7Ø
5.Ø	19.9975	1Ø.47	4.38	953.28	5.Ø8
EXACT VALUE	2Ø	1Ø	Ø	1ØØØ	Ø

TABLE 3-13 : Identified modal properties as function of excitation force (R = 0.25 N/Kg).

MODE1

INPUT NATURAL FREQUENCY OF MODE 2 (Hz)	NATURAL FREQUENCY (Hz)	LOSS FACTOR x1000	RMS ERROR (%)	MODAL CONSTANT x1000 (1/Kg)	MODAL PHASE (Deg)
21.Ø	19.995Ø	9.5Ø	13.Ø2	93Ø.97	9.36
2Ø.6	2Ø.Ø1ØØ	8.73	11.78	87Ø.93	-2.46
2Ø.4	19.985Ø	1Ø.37	8.22	987.Ø8	18.9Ø
2Ø.2	19.985Ø	19.69	12.89	2982.87	51.13
2Ø.1	2Ø.Ø55Ø	12.66	4.54	2178.98	Ø.6Ø
2Ø.Ø	2Ø.ØØ5Ø	1Ø.ØØ	Ø.Ø1	2ØØØ.1Ø	-Ø.Ø1
EXACT VALUE	2Ø	1Ø	Ø	1ØØØ	Ø

MODE2

INPUT NATURAL FREQUENCY OF MODE 2 (Hz)	NATURAL FREQUENCY (Hz)	LOSS FACTOR x1000	RMS ERROR (%)	MODAL CONSTANT x1000 (1/Kg)	MODAL PHASE (Deg)
21.Ø	21.ØØ5Ø	9.16	3.78	891.77	Ø.97
2Ø.6	2Ø.58ØØ	6.96	29.79	783.66	17.37
2Ø.4	2Ø.36ØØ	6.54	4Ø.74	81Ø.31	33.11
2Ø.2	2Ø.225Ø	18.5Ø	7.88	2835.69	-51.91
2Ø.1	-------	-----	-----	-------	------
2Ø.Ø	-------	-----	-----	-------	------
EXACT VALUE	INPUT VALUE	1Ø	Ø	1ØØØ	Ø

TABLE 3-14 : Identified modal properties of modes 1 and 2.

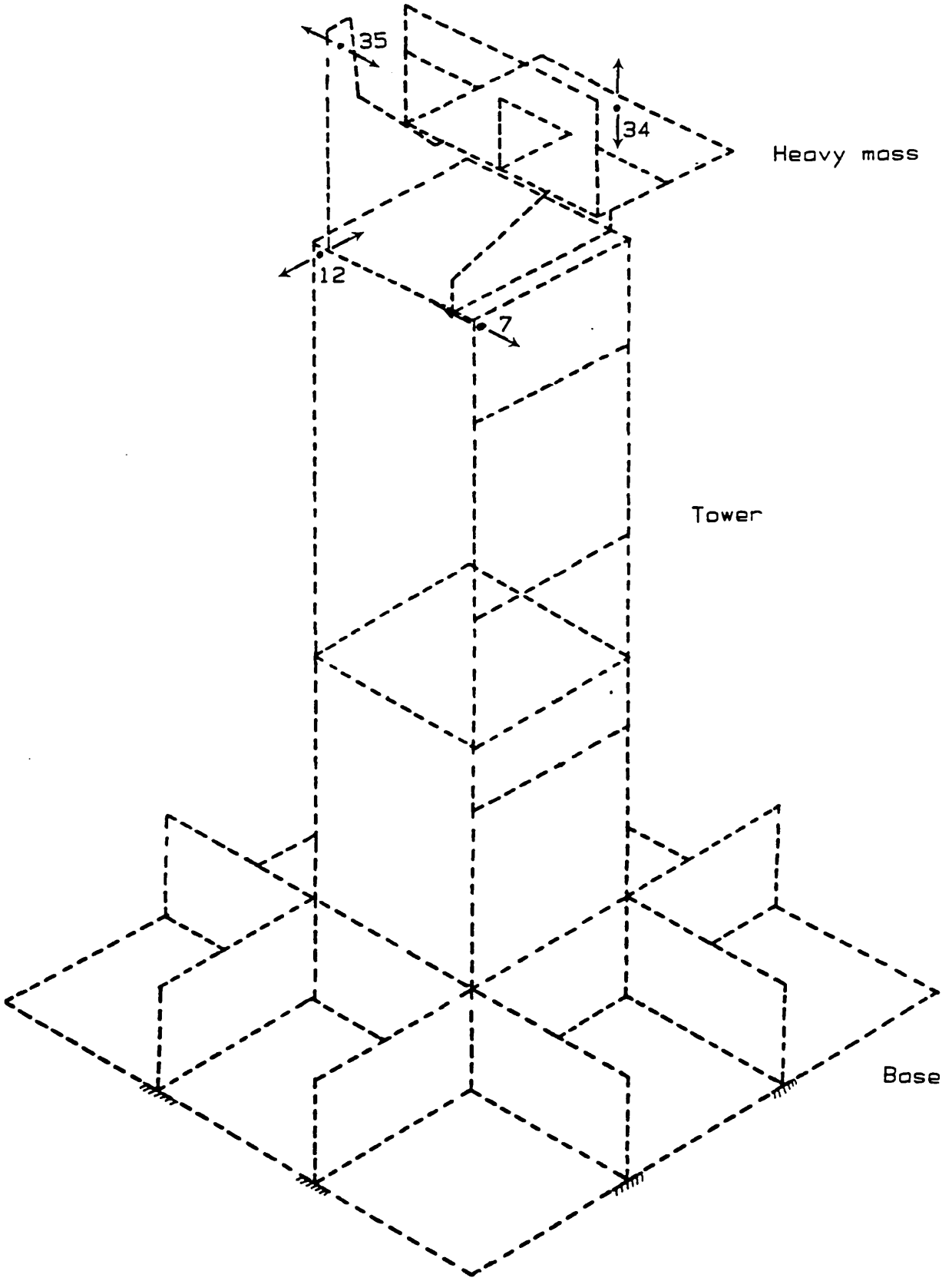

FIGURE 3-01 : The general view of the NASTRAN test structure.

$Y_{07,12}$ (Low level of excitation)

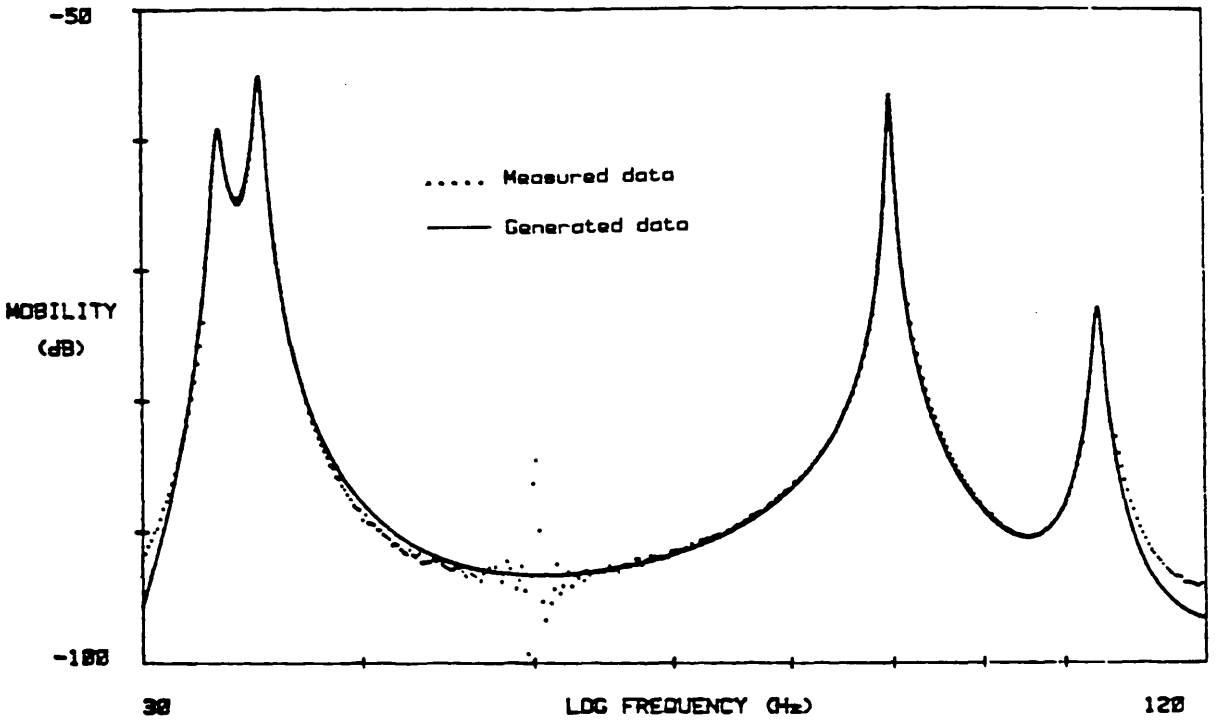

FIGURE 3-02 : Mobility modulus plot of measured and generated data of $Y_{07,12}$ (Low level of excitation).

Mobility (dB) is with ref. to 1 m/sec/N throughout the thesis.

$Y_{07,12}$ (High level of excitation)

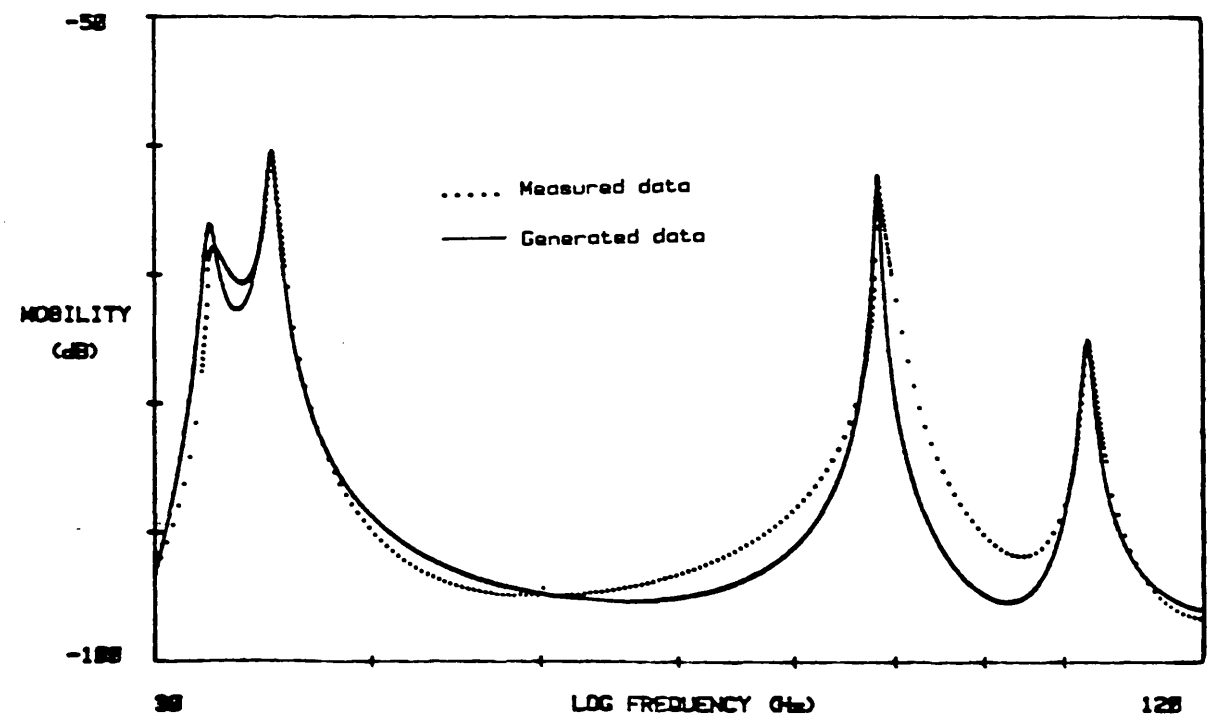

FIGURE 3-03 : Mobility modulus plot of measured and generated data of $Y_{07,12}$ (High level of excitation).

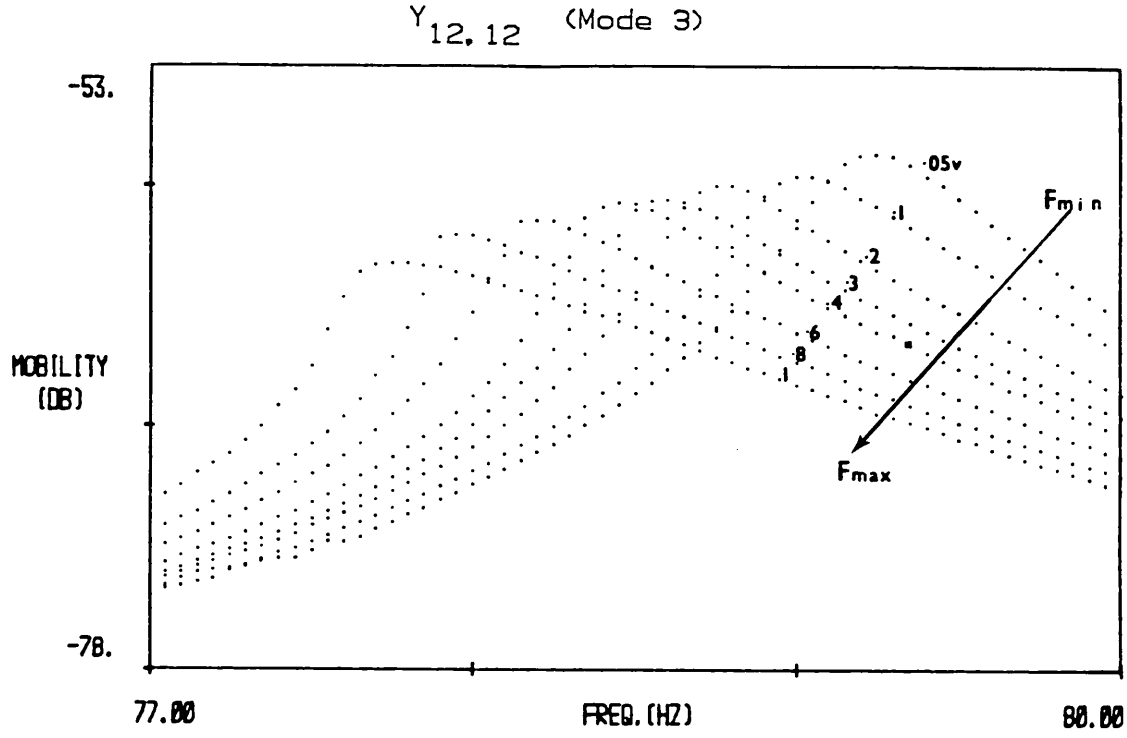

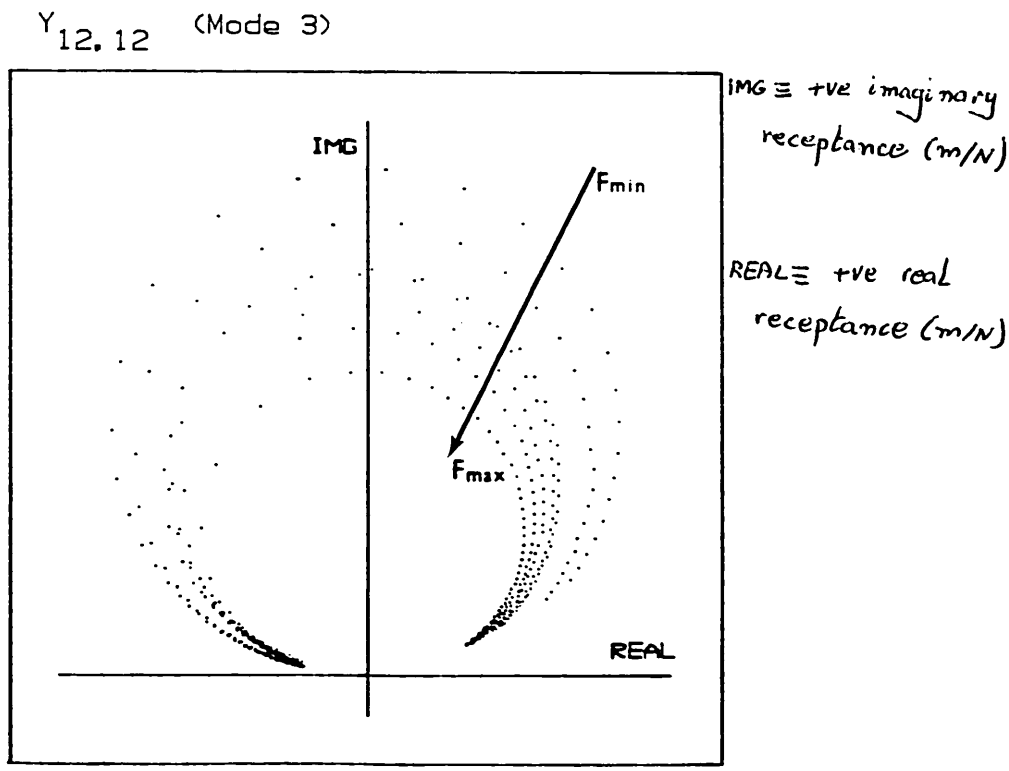

FIGURE 3-04 : Mobility modulus and Nyquist plots for point measurement $Y_{12,12}$ under constant levels of excitation (mode 3).

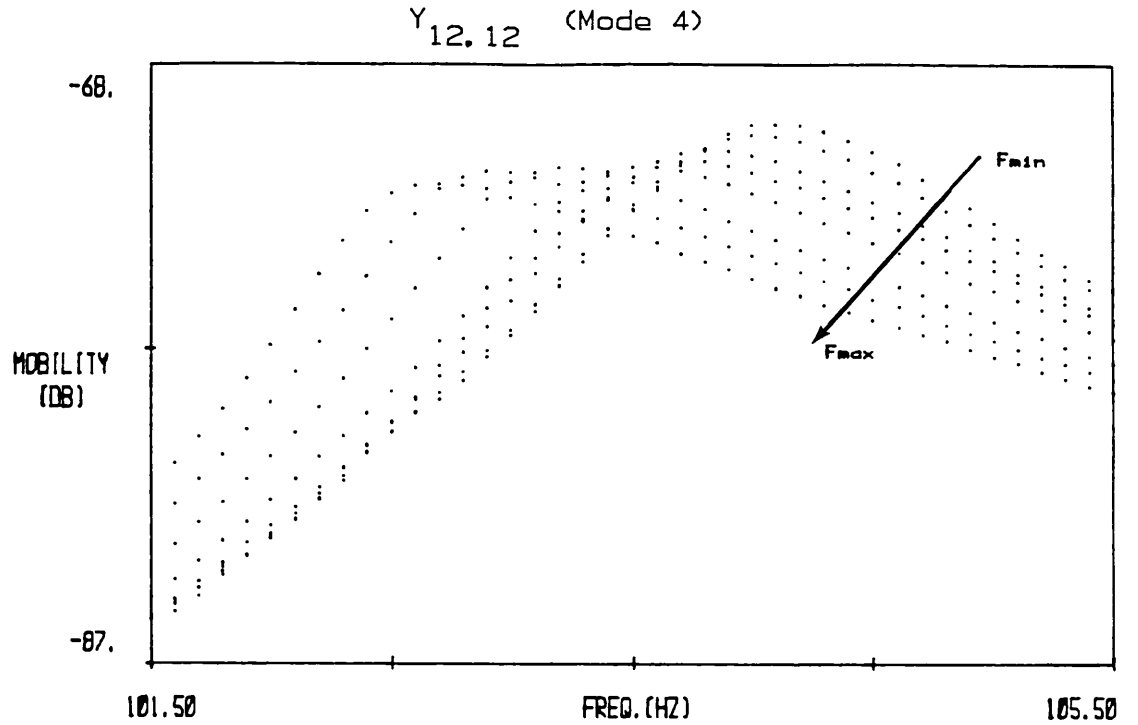

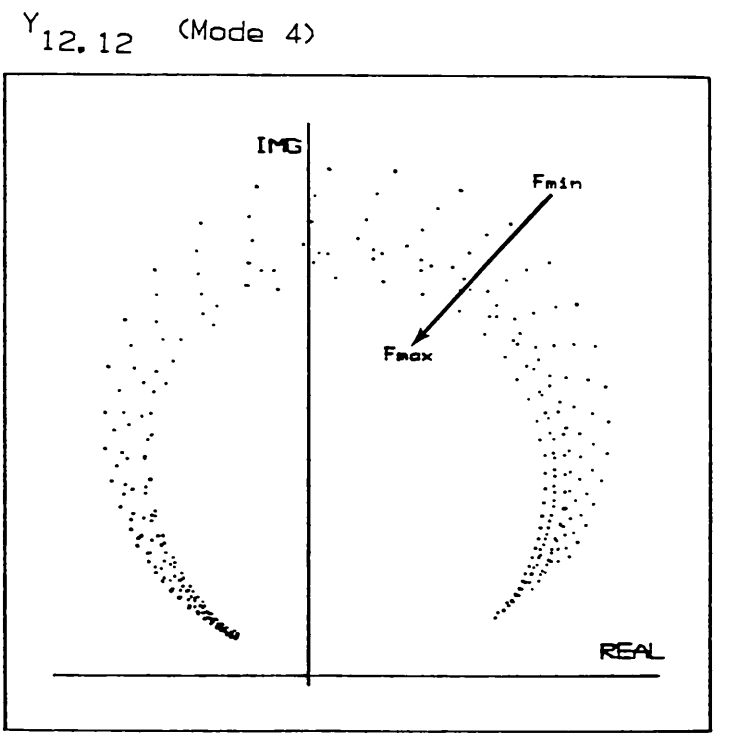

FIGURE 3-05 : Mobility modulus and Nyquist plots for point measurement $Y_{12,12}$ under constant levels of excitation (mode 4).

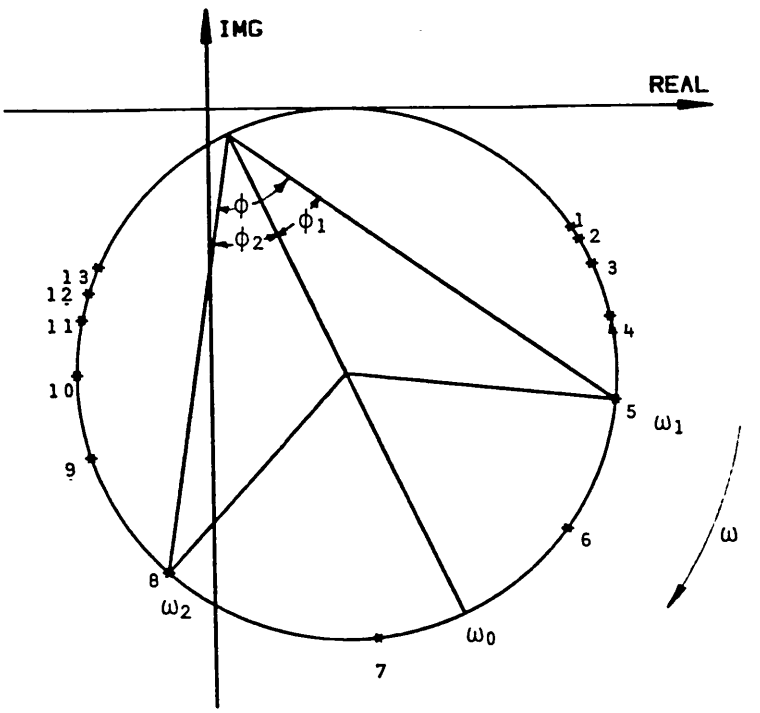

FIGURE 3-06 : Circle fit in the Nyquist plane.

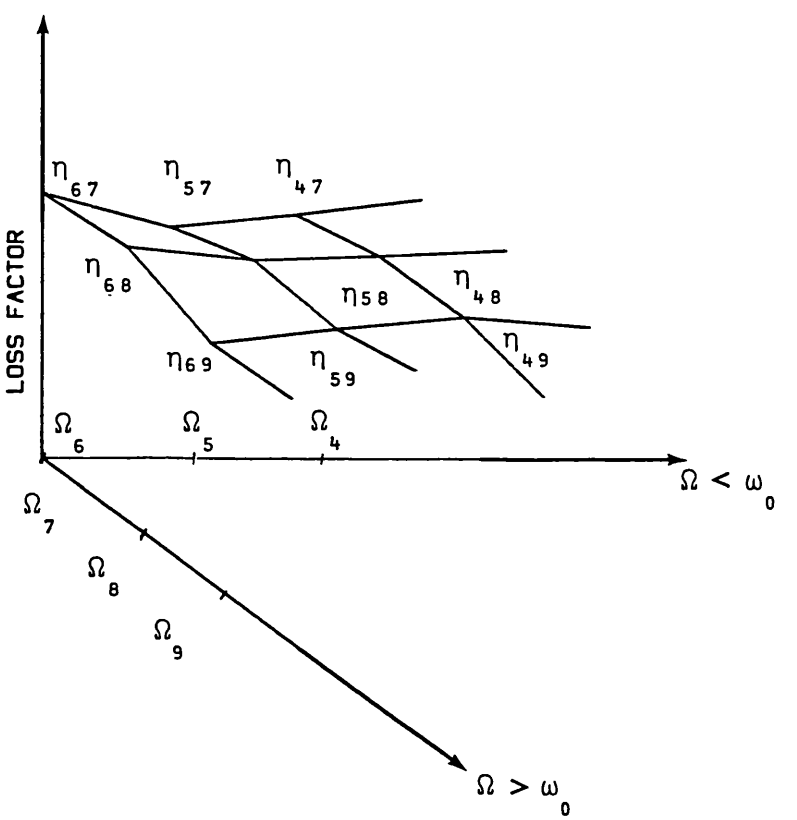

FIGURE 3-07 : An isometric representation of table 3-05.

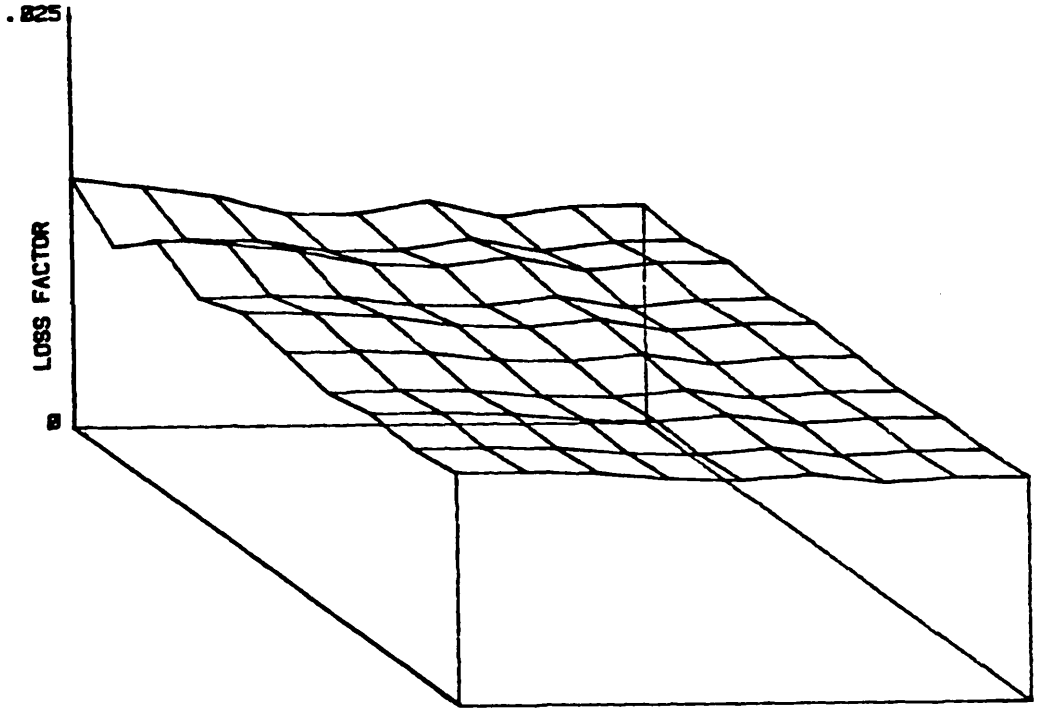

FIGURE 3-08 : An isometric plot of experimental loss factor matrix.

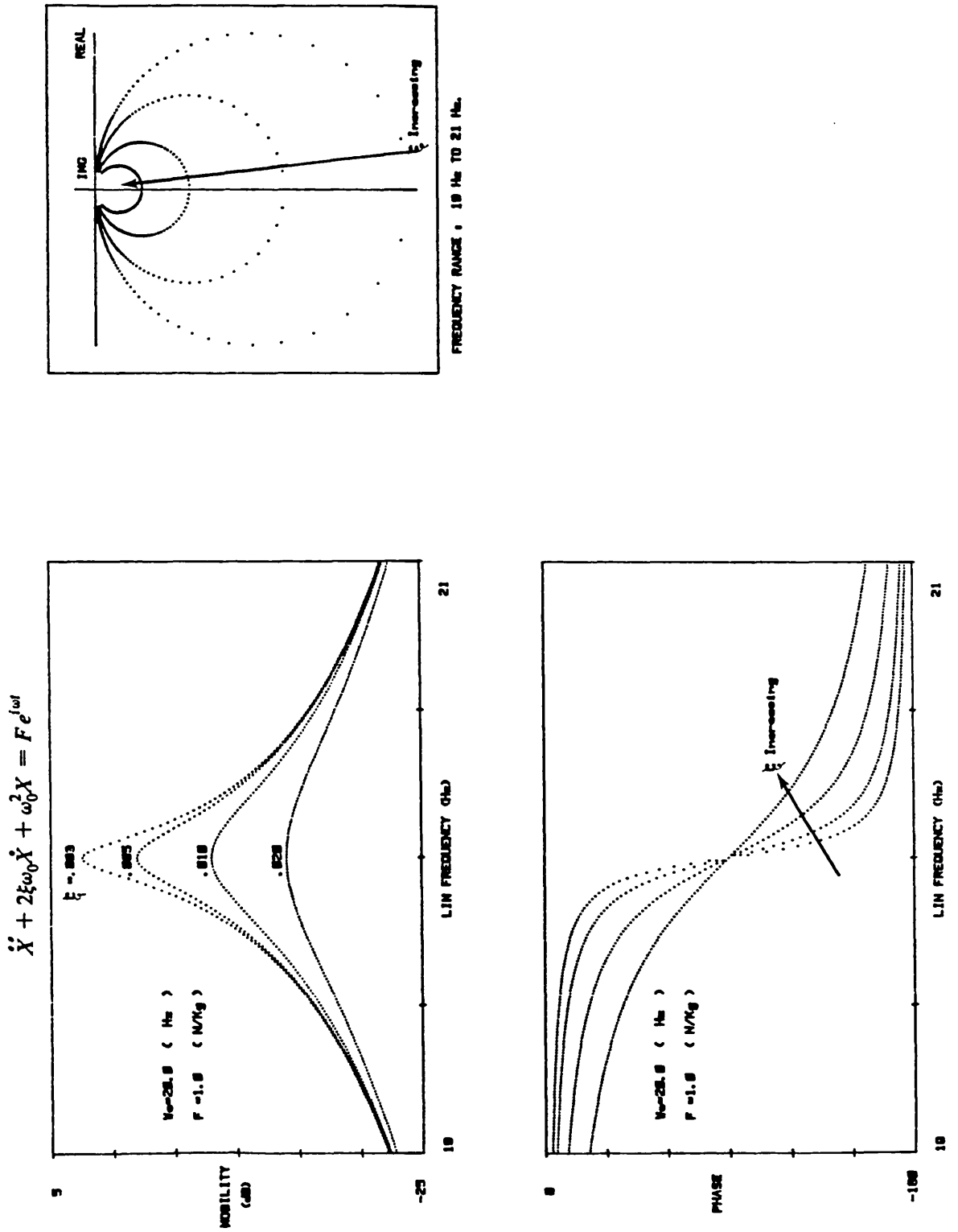

FIGURE 3-09 : Mobility modulus, mobility phase and Nyquist plots for varying levels of viscous damping.

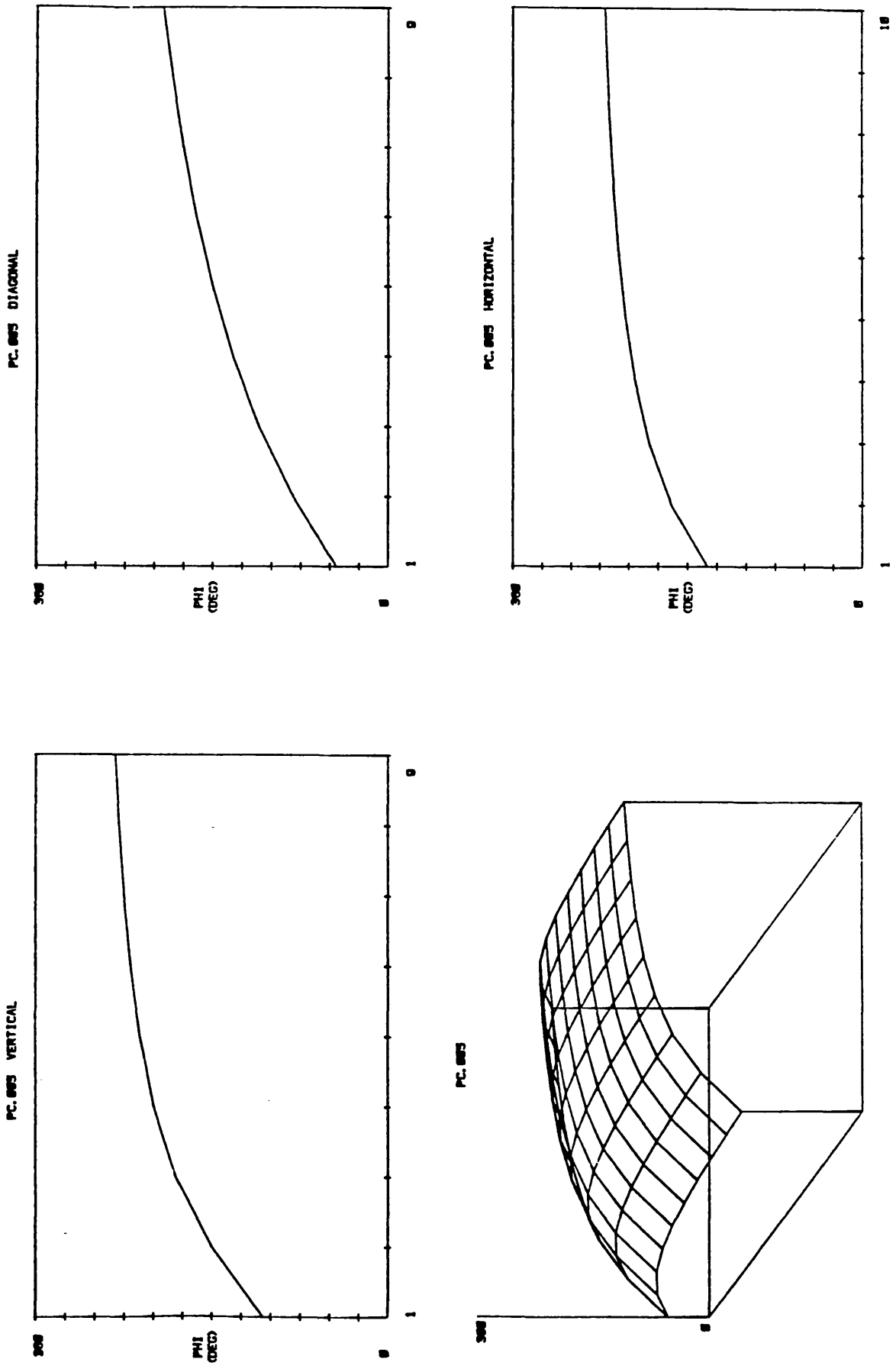

FIGURE 3-10 : Isometric and conventional plots of angle PHI for viscous damping (ξ = 0005).

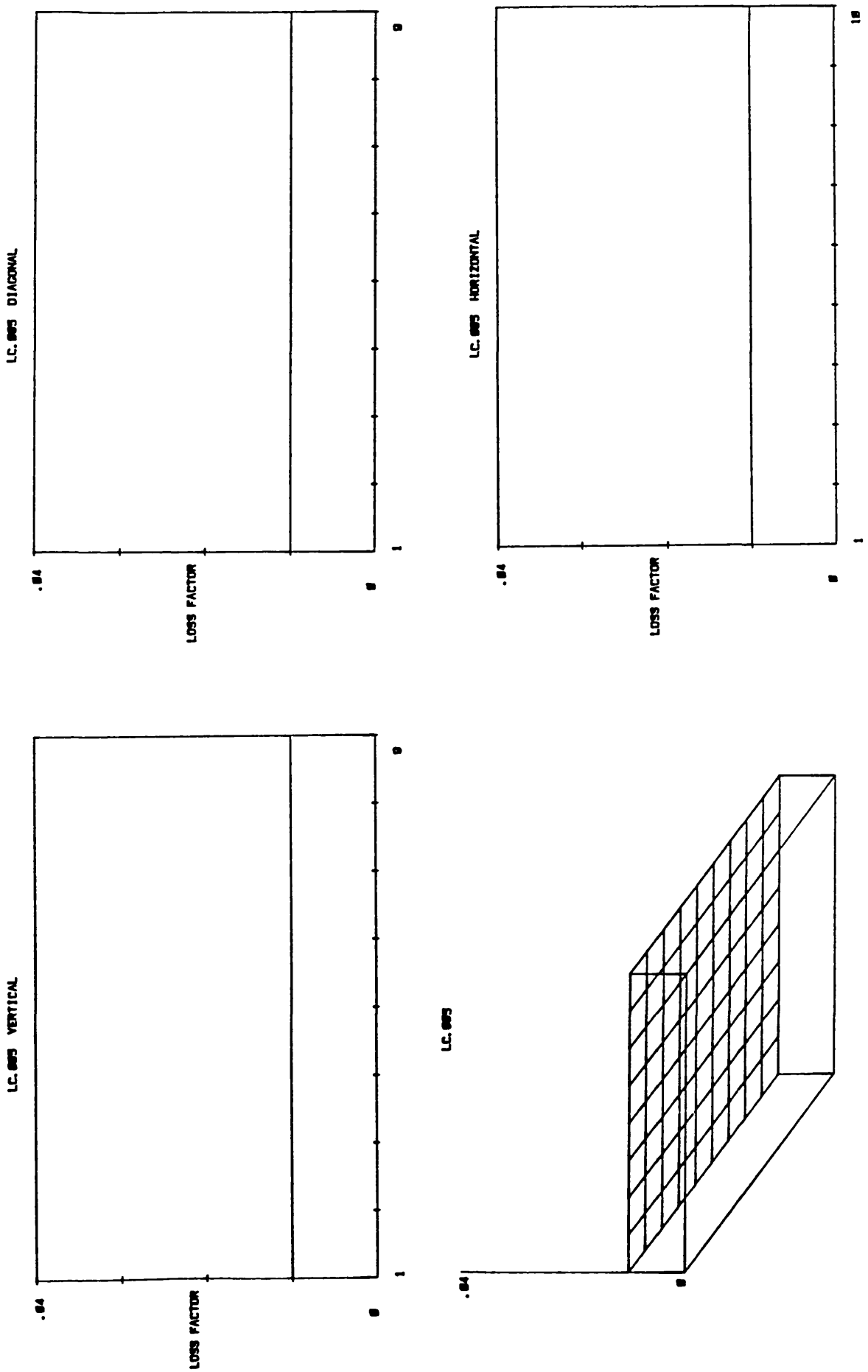

FIGURE 3-11 : Isometric and conventional plots of loss factor for viscous damping (ξ = 0005).

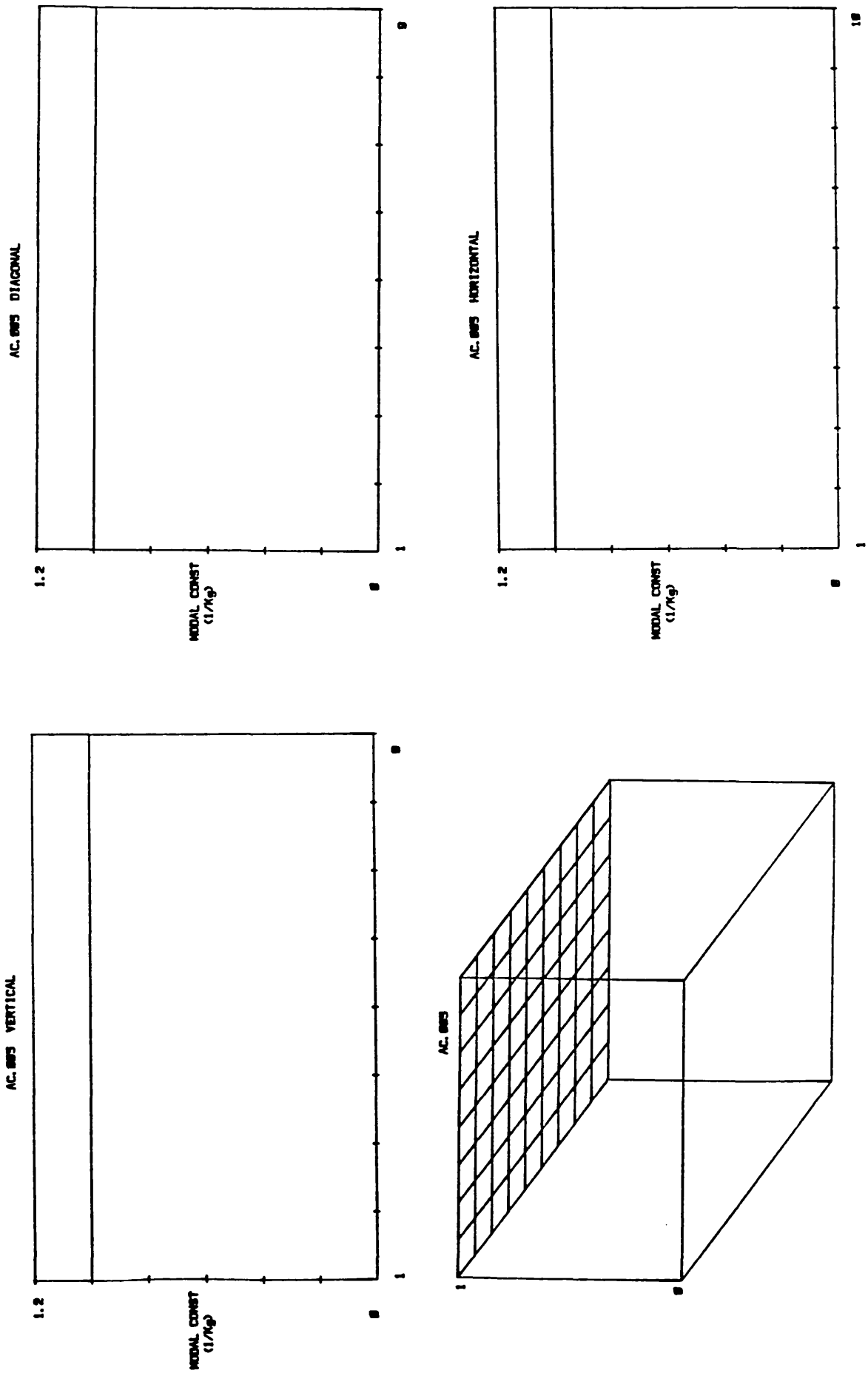

FIGURE 3-12 : Isometric and conventional plots of modal constant for viscous damping (ξ = 0005).

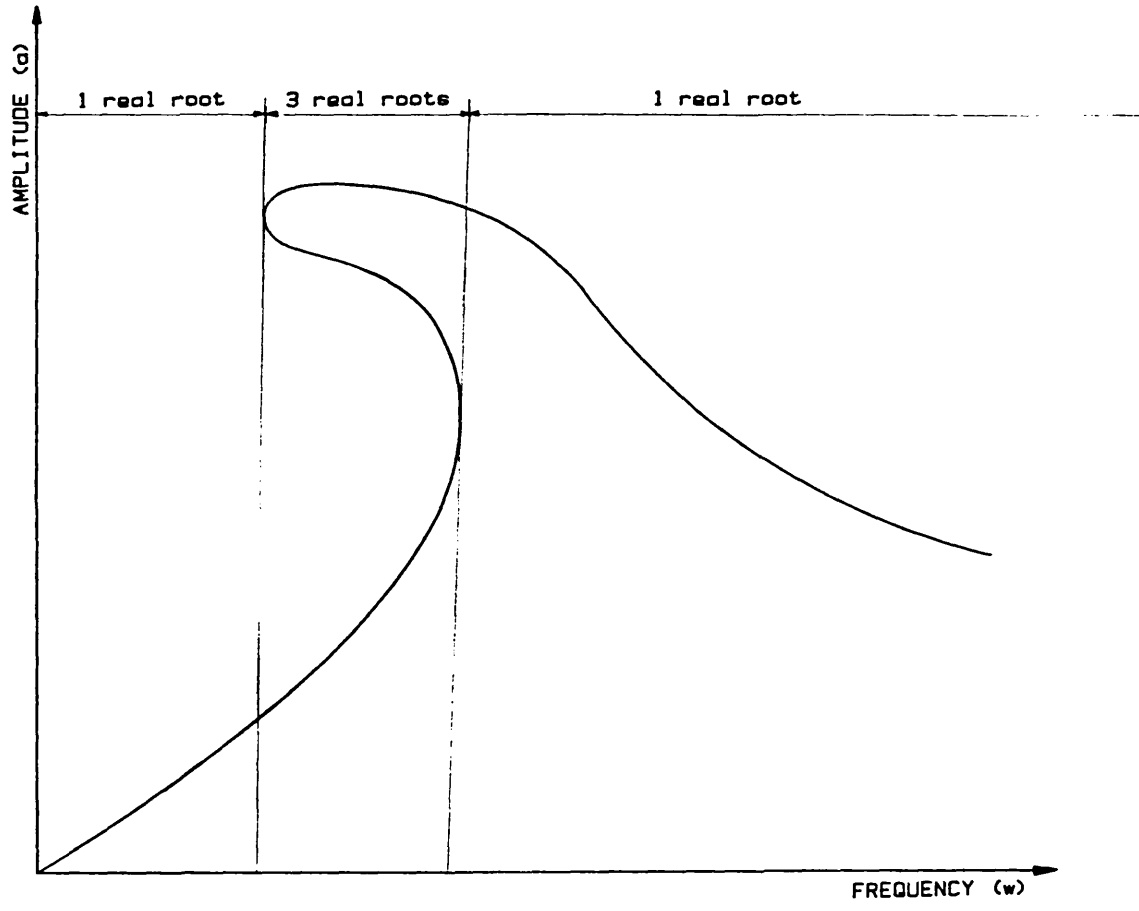

FIGURE 3-13 : The jump phenomenon for the softening spring.

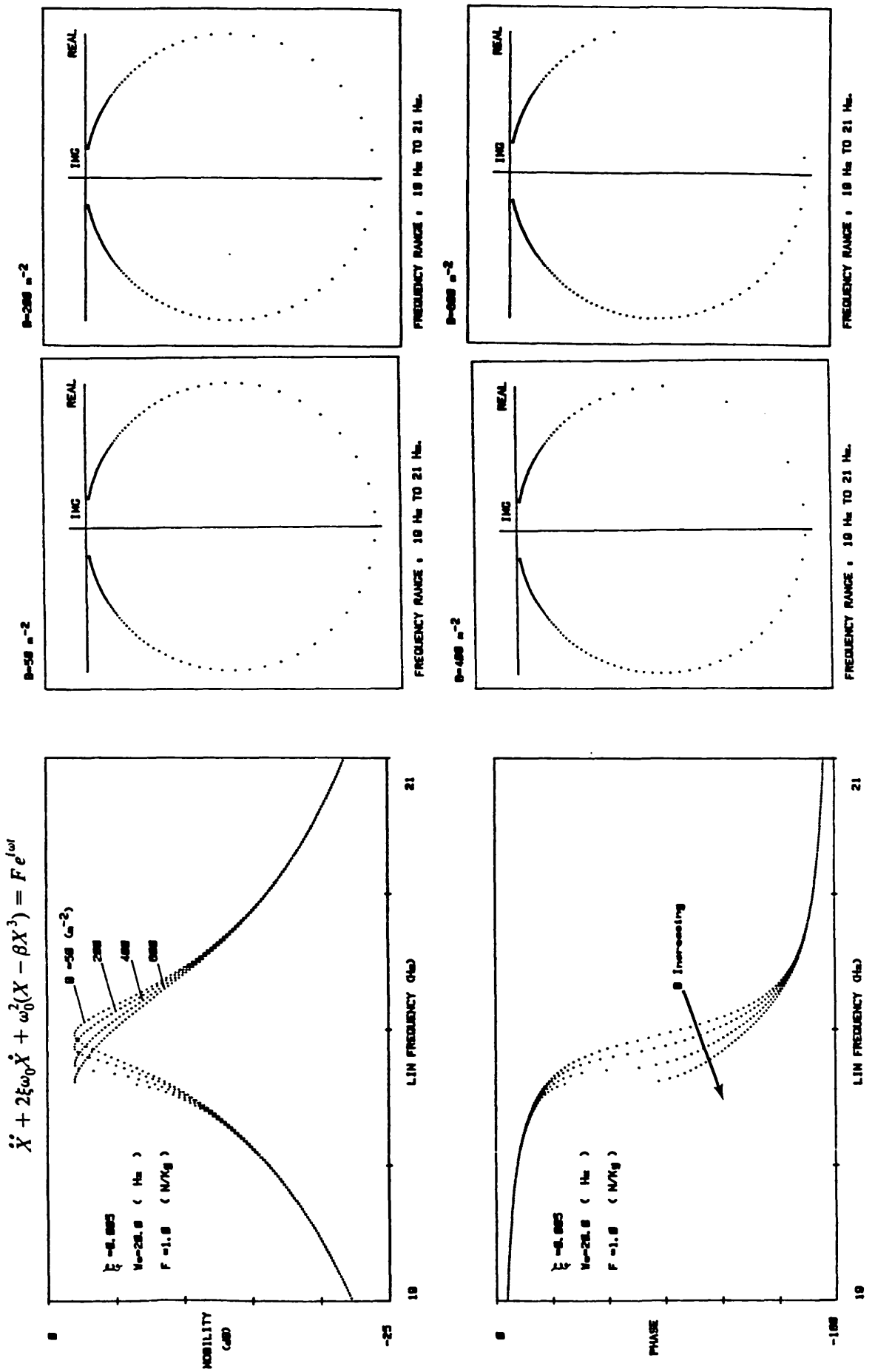

FIGURE 3-14 : Mobility modulus, mobility phase and Nyquist plots for varying levels of softening-cubic stiffness.

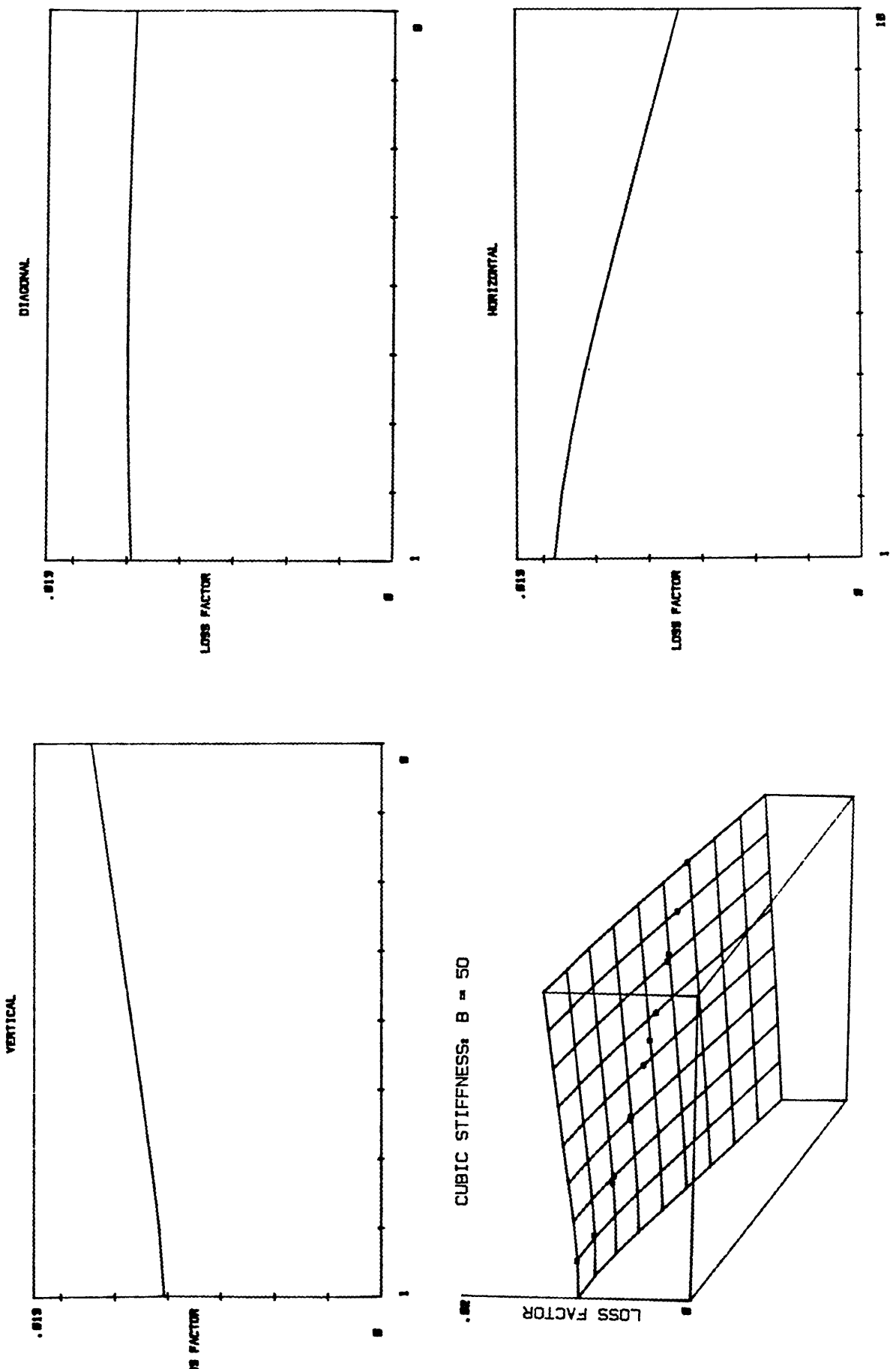

FIGURE 3-15 : Isometric and conventional plots of loss factor for softening cubic stiffness ($\beta = 50\ m^{-2}$).

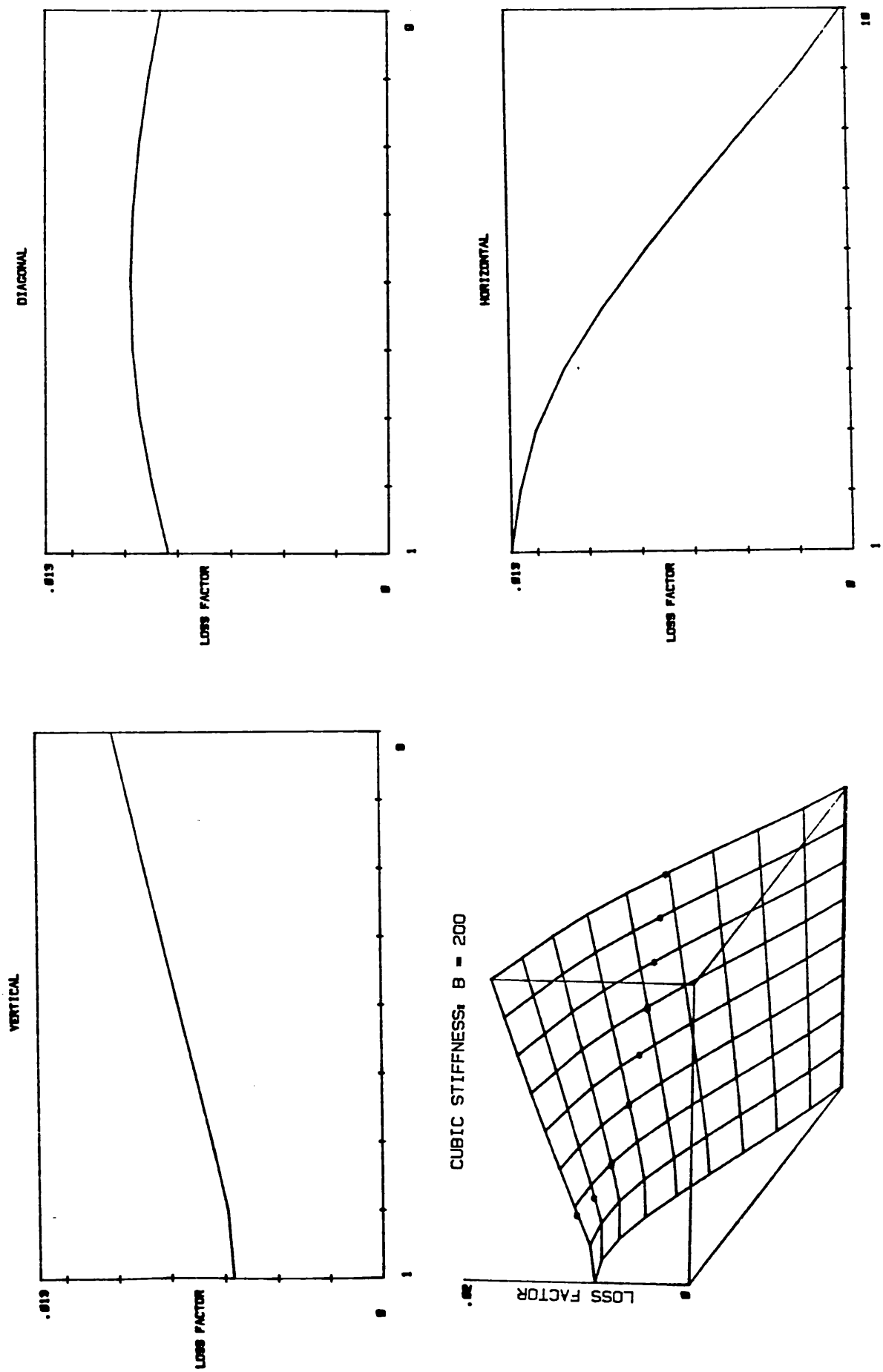

FIGURE 3-16 : Isometric and conventional plots of loss factor for softening cubic stiffness (β = 200 m^{-2}).

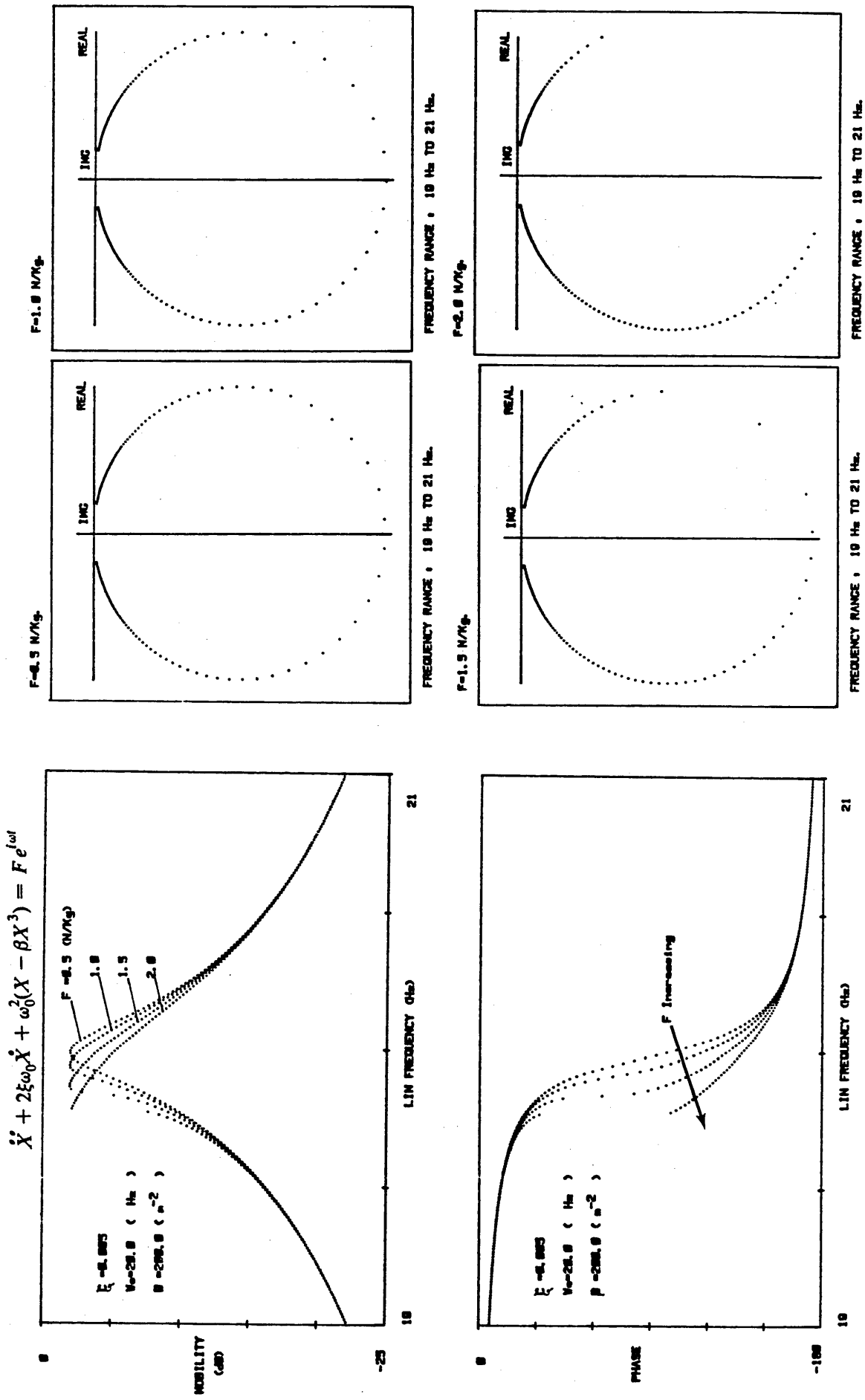

FIGURE 3-17 : Mobility modulus, mobility phase and Nyquist plots of softening cubic stiffness for varying levels of excitation force.

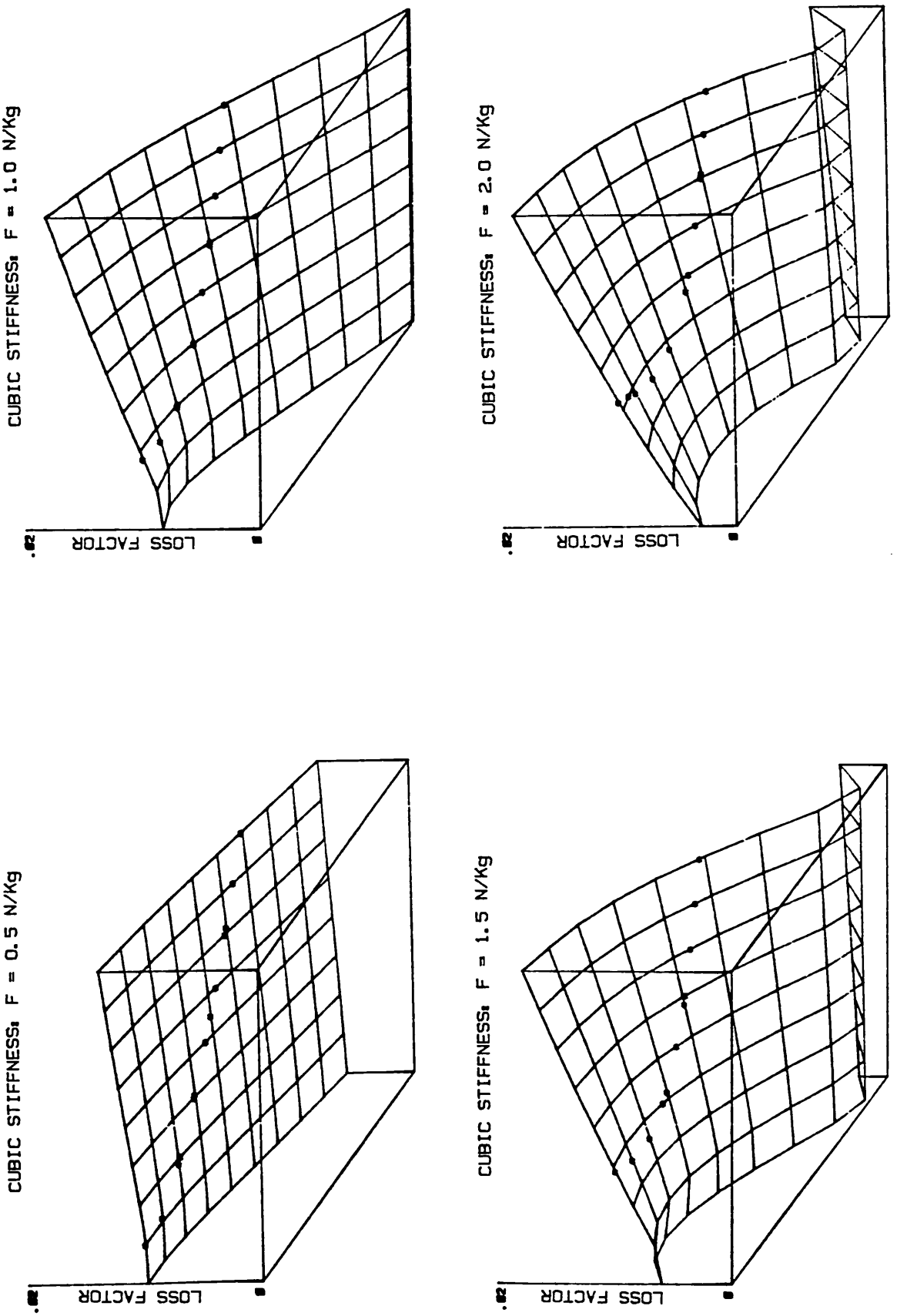

FIGURE 3-18 : Isometric loss factor plots of softening cubic stiffness for varying levels of excitation force.

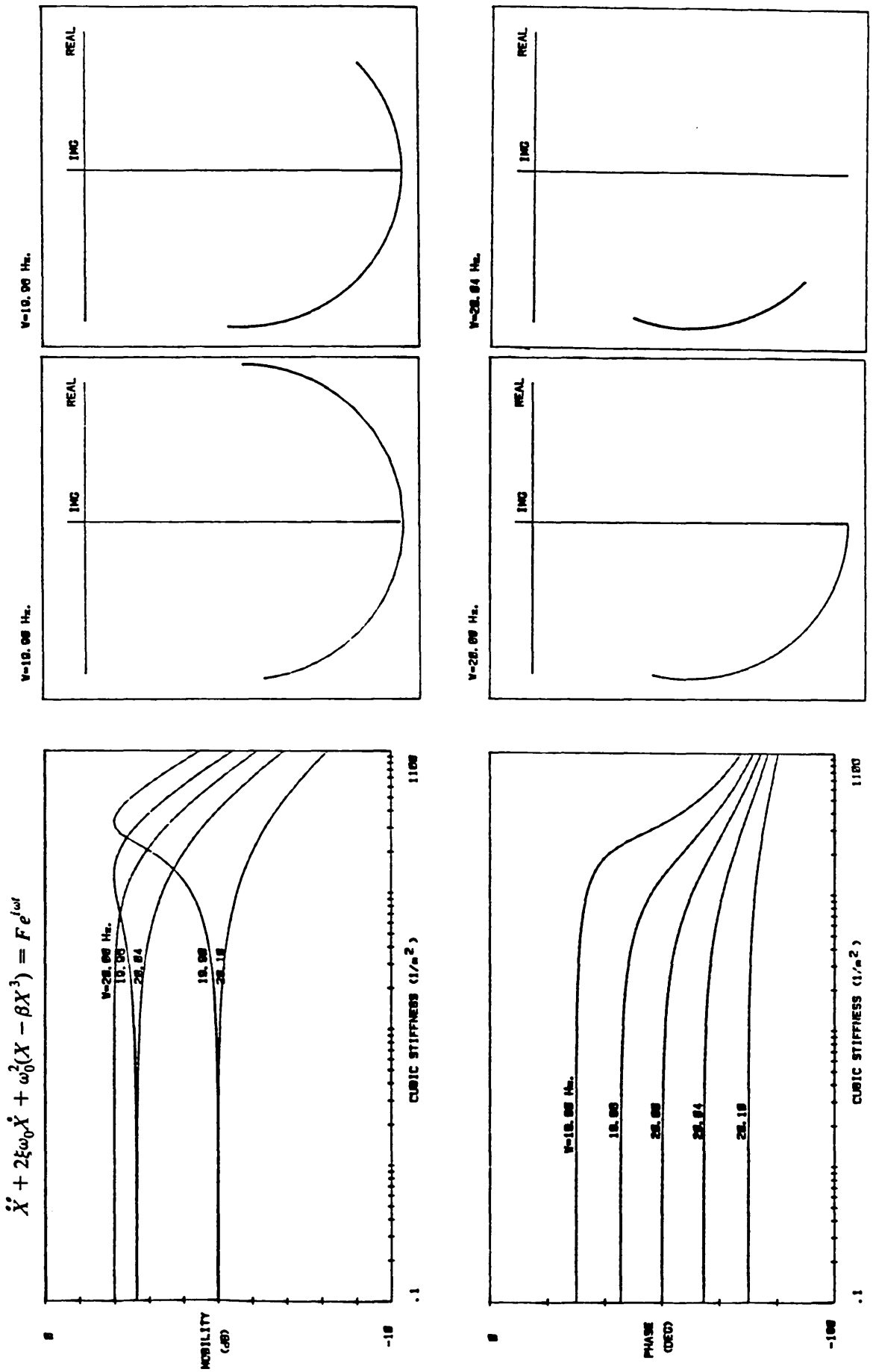

FIGURE 3-19 : Mobility modulus, mobility phase and Nyquist plots as function of softening cubic stiffness for various excitation frequencies.

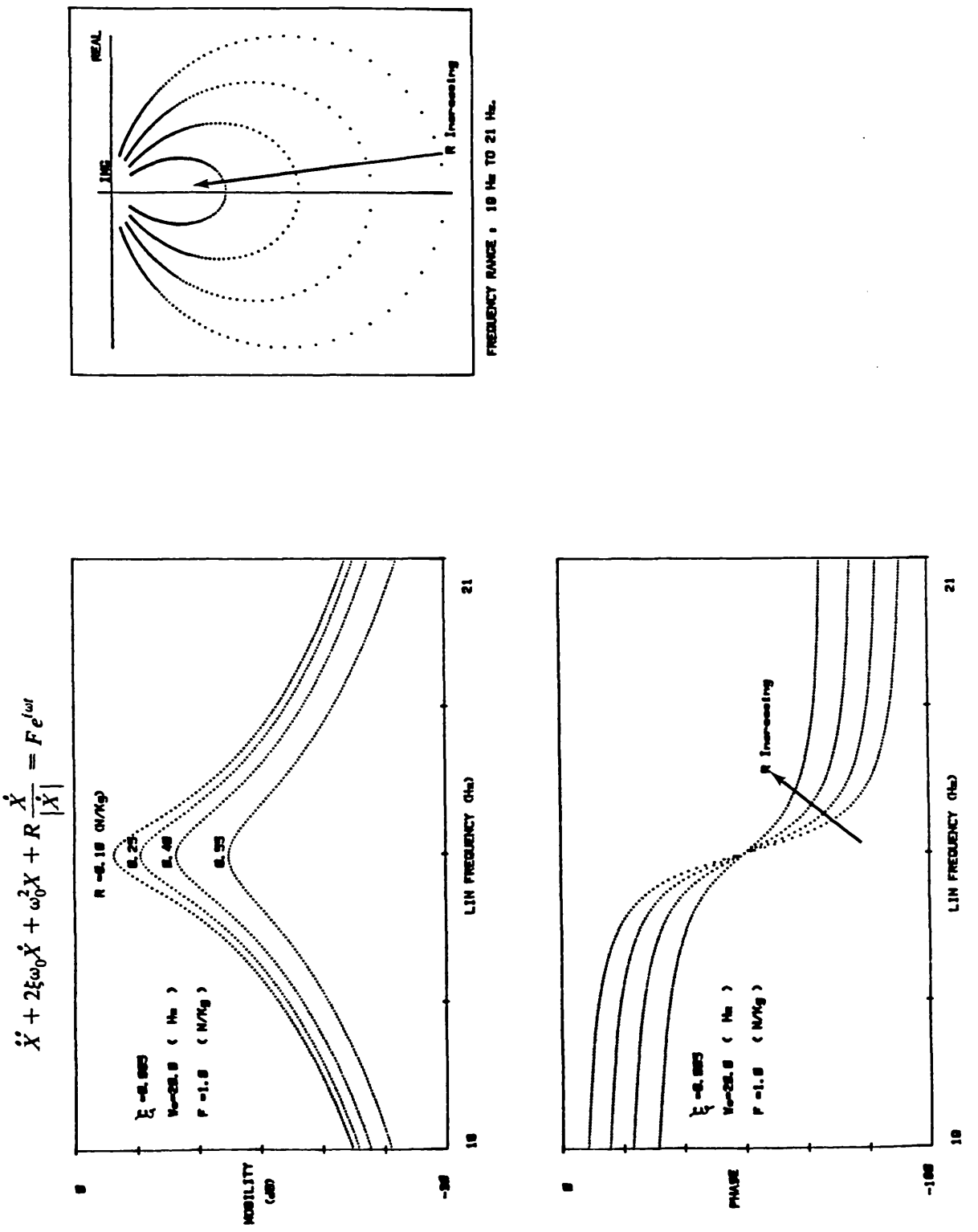

FIGURE 3-20 : Mobility modulus, mobility phase and Nyquist plots for varying levels of dry friction.

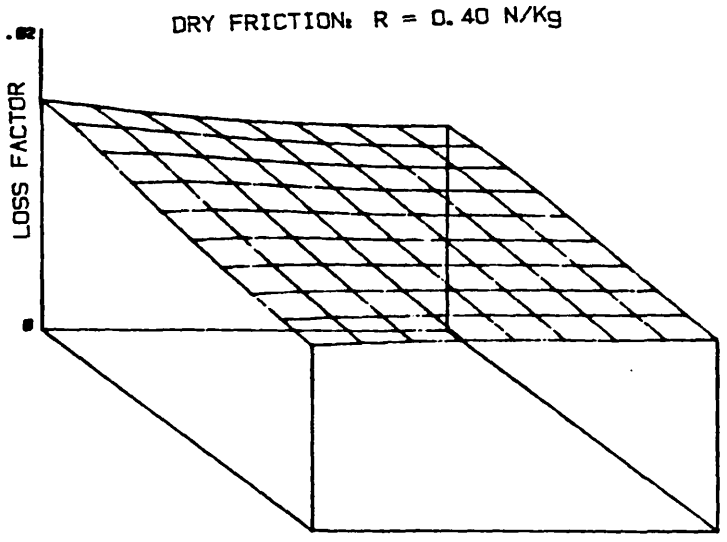

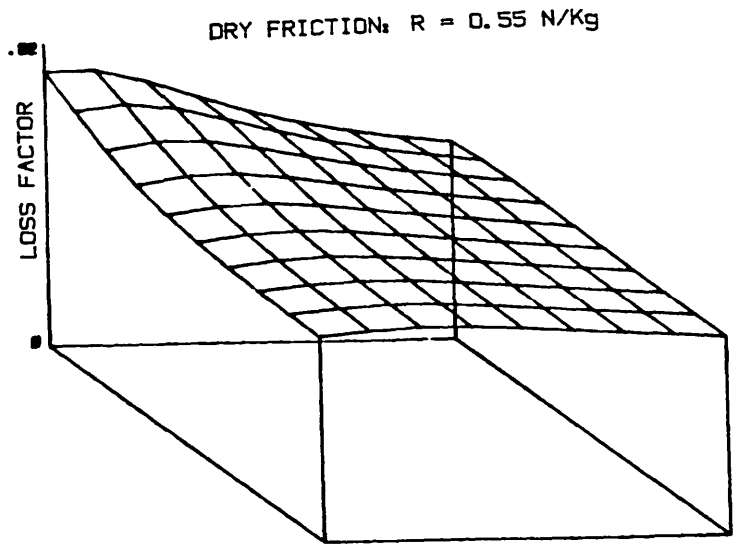

FIGURE 3-21 : Isometric loss factor plots for dry friction.

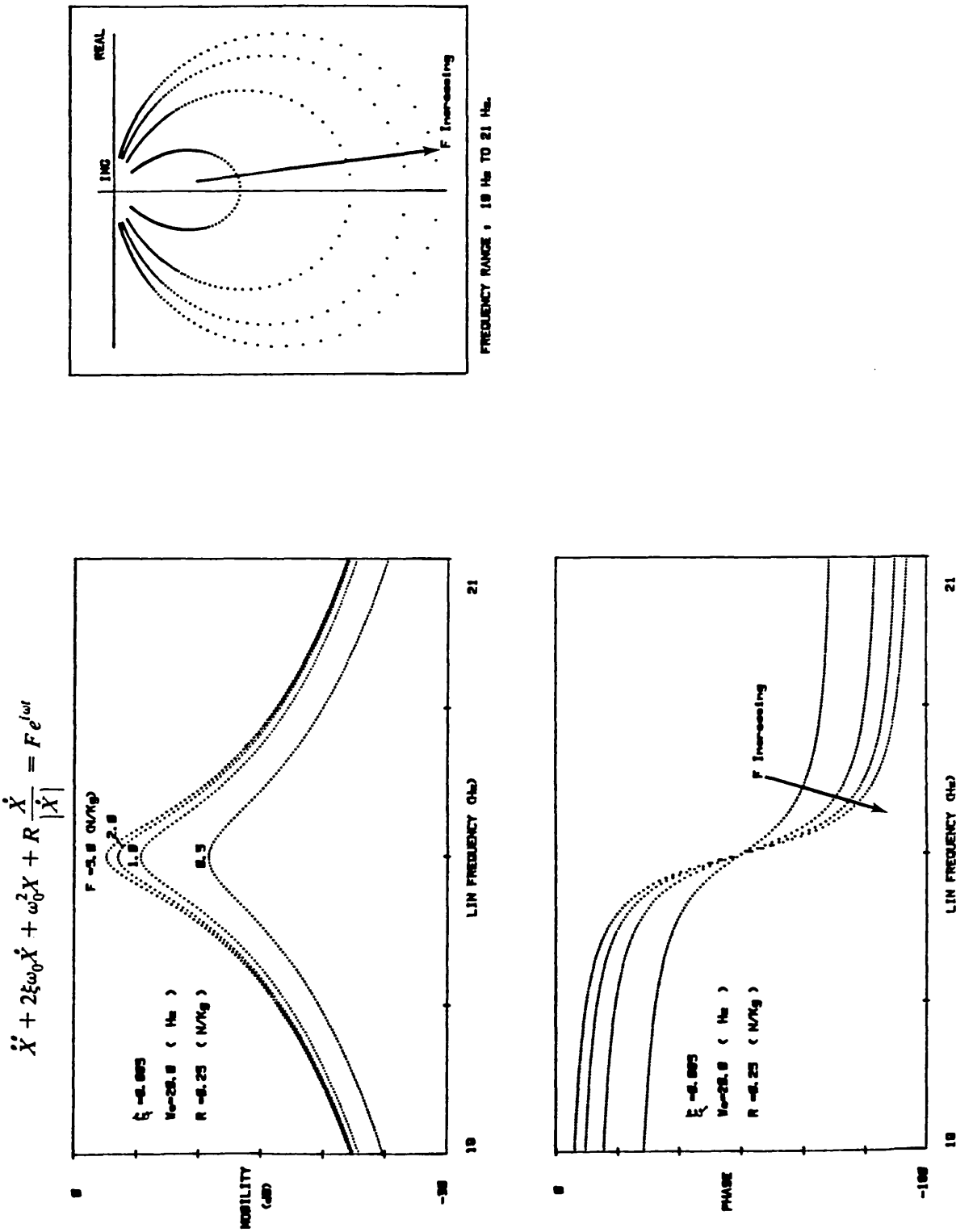

FIGURE 3-22 : Mobility modulus, mobility phase and Nyquist plots of dry friction for varying levels of excitation force.

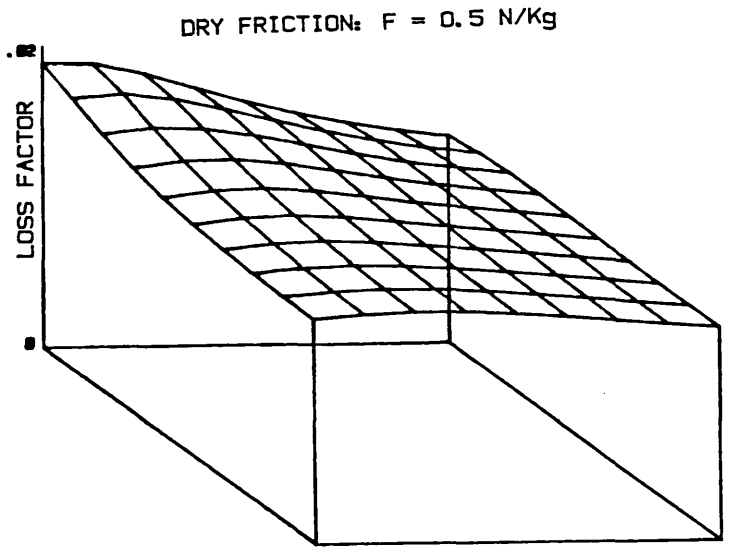

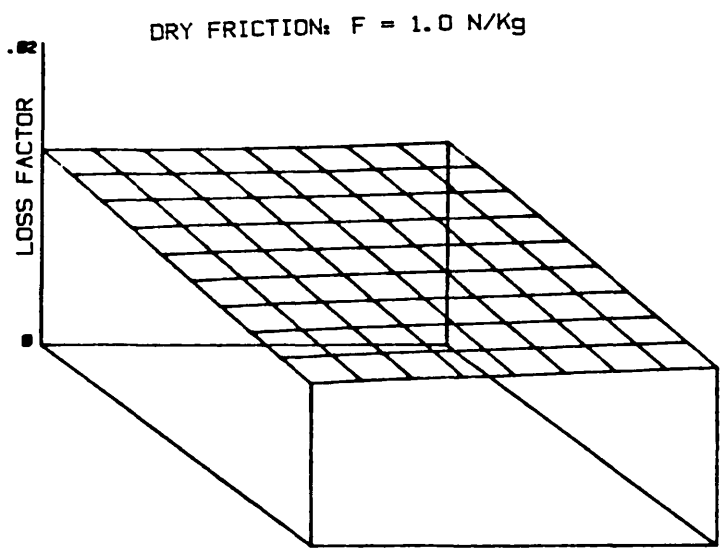

FIGURE 3-23 : Isometric loss factor plots of dry friction for varying levels of excitation force.

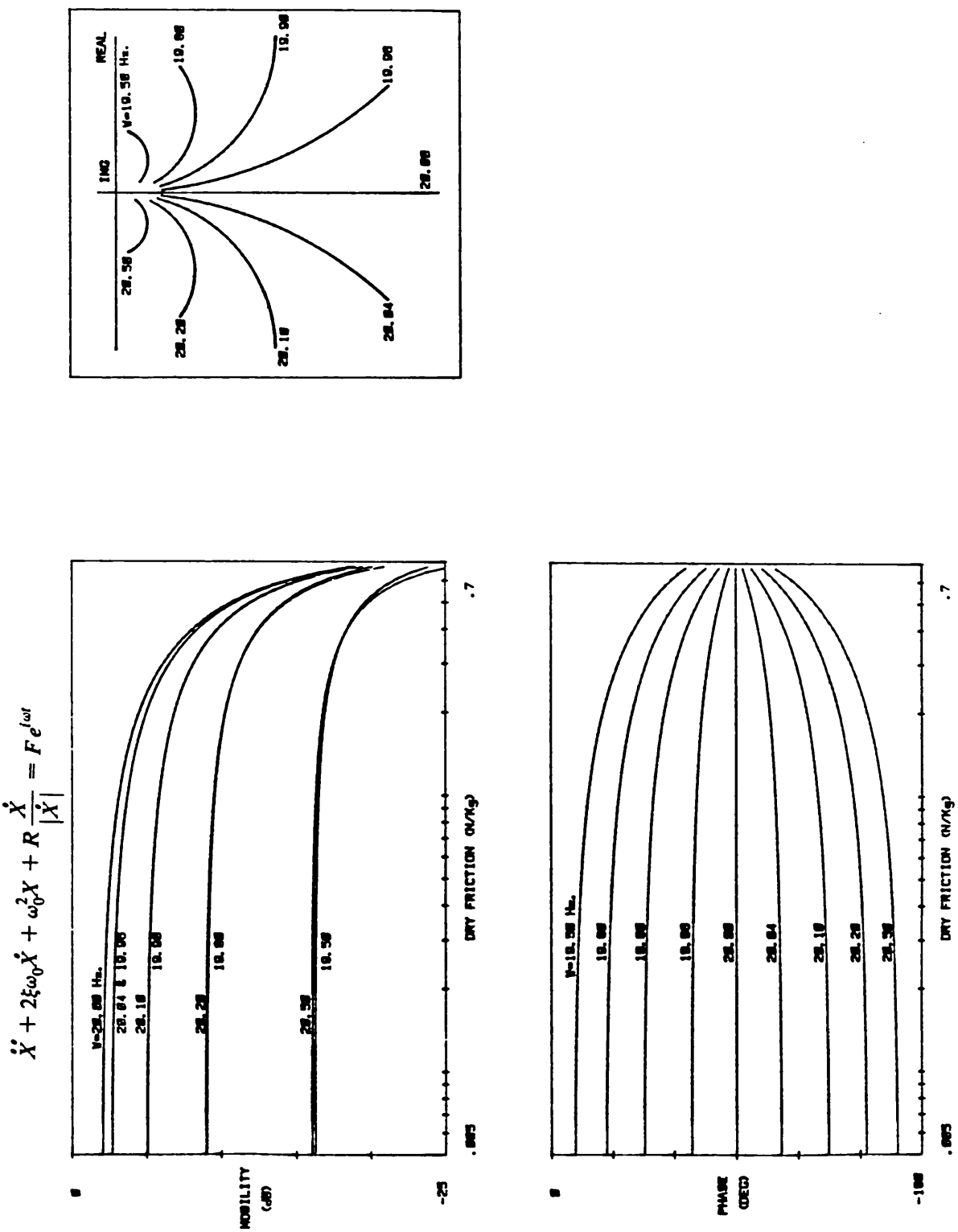

FIGURE 3-24 : Mobility modulus, mobility phase and Nyquist plots as function of dry friction for various excitation frequencies.

$$\alpha_{pq}(\omega) = \frac{|_1A_{pq}|e^{i\theta_1}}{\omega_1^2(1-(\omega/\omega_1)^2+i\eta_1)} + \frac{|_2A_{pq}|e^{i\theta_2}}{\omega_2^2(1-(\omega/\omega_2)^2+i\eta_2)}$$

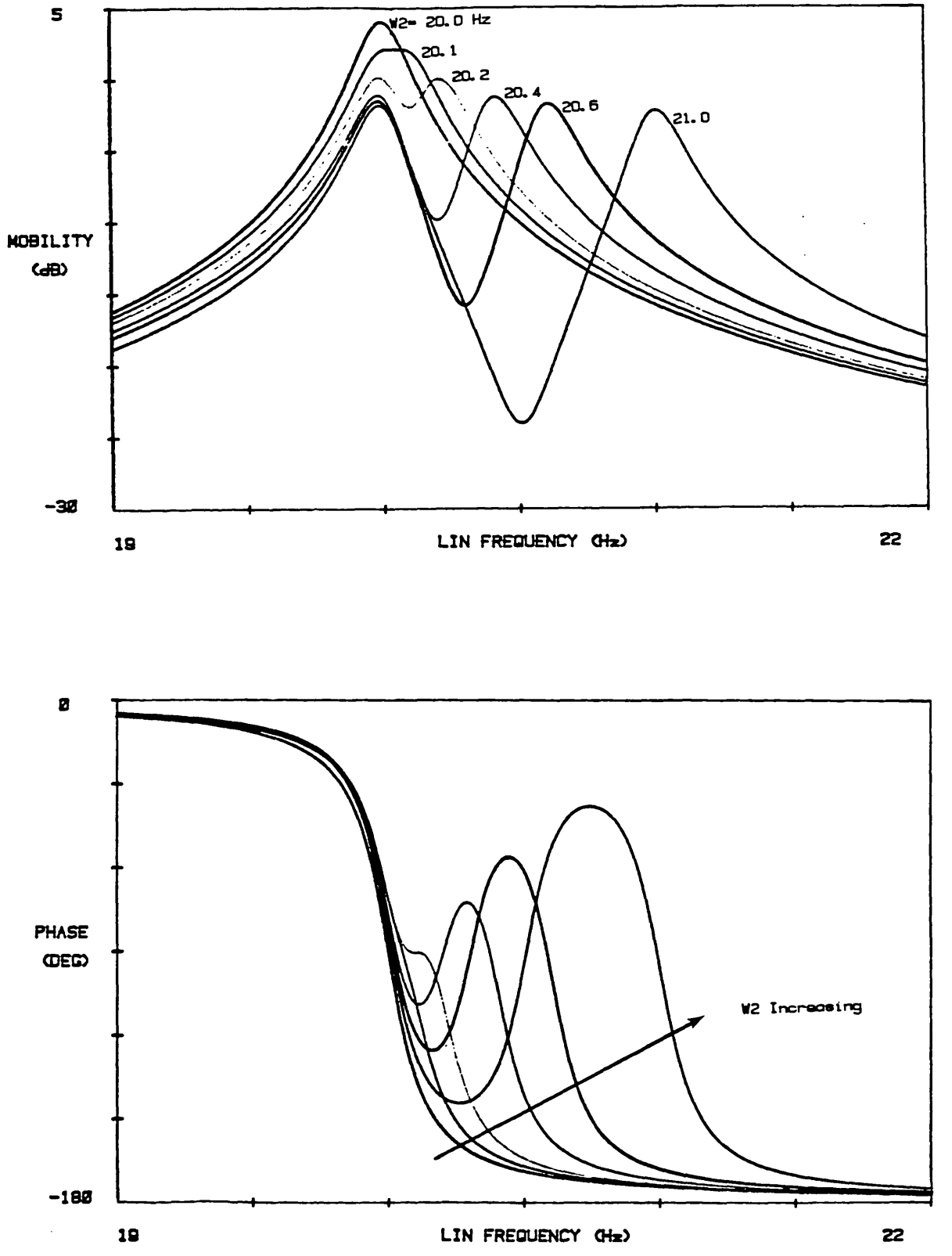

FIGURE 3-25 : Mobility modulus and mobility phase plots for linear two-degree-of-freedom system for varying resonance frequencies of mode 2.

$$\alpha_{pq}(\omega) = \frac{|_1A_{pq}|e^{i\theta_1}}{\omega_1^2(1-(\omega/\omega_1)^2+i\eta_1)} + \frac{|_2A_{pq}|e^{i\theta_2}}{\omega_2^2(1-(\omega/\omega_2)^2+i\eta_2)}$$

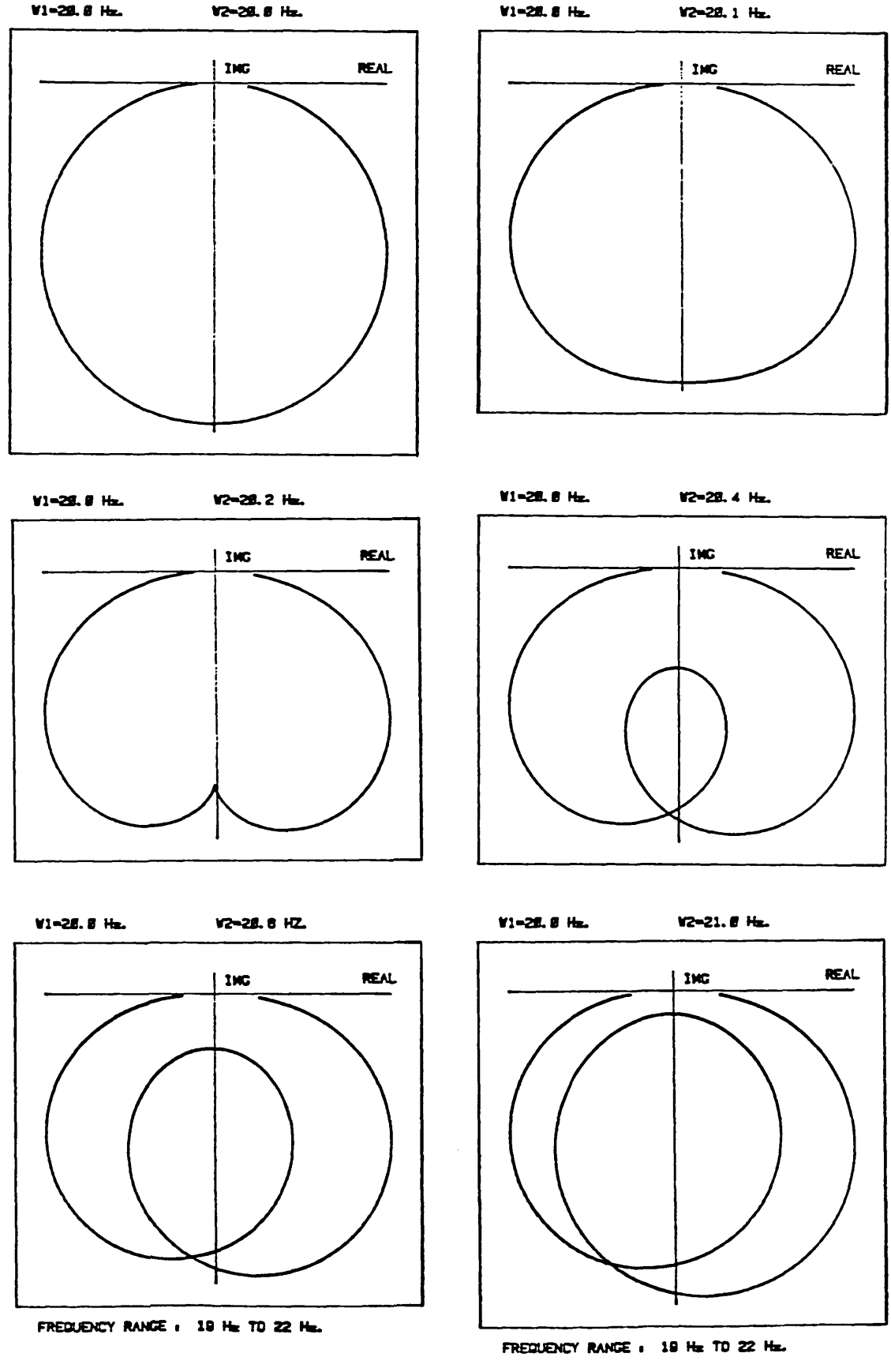

FIGURE 3-26 : Nyquist plots for linear two-degree-of-freedom system for varying resonance frequencies of mode 2.

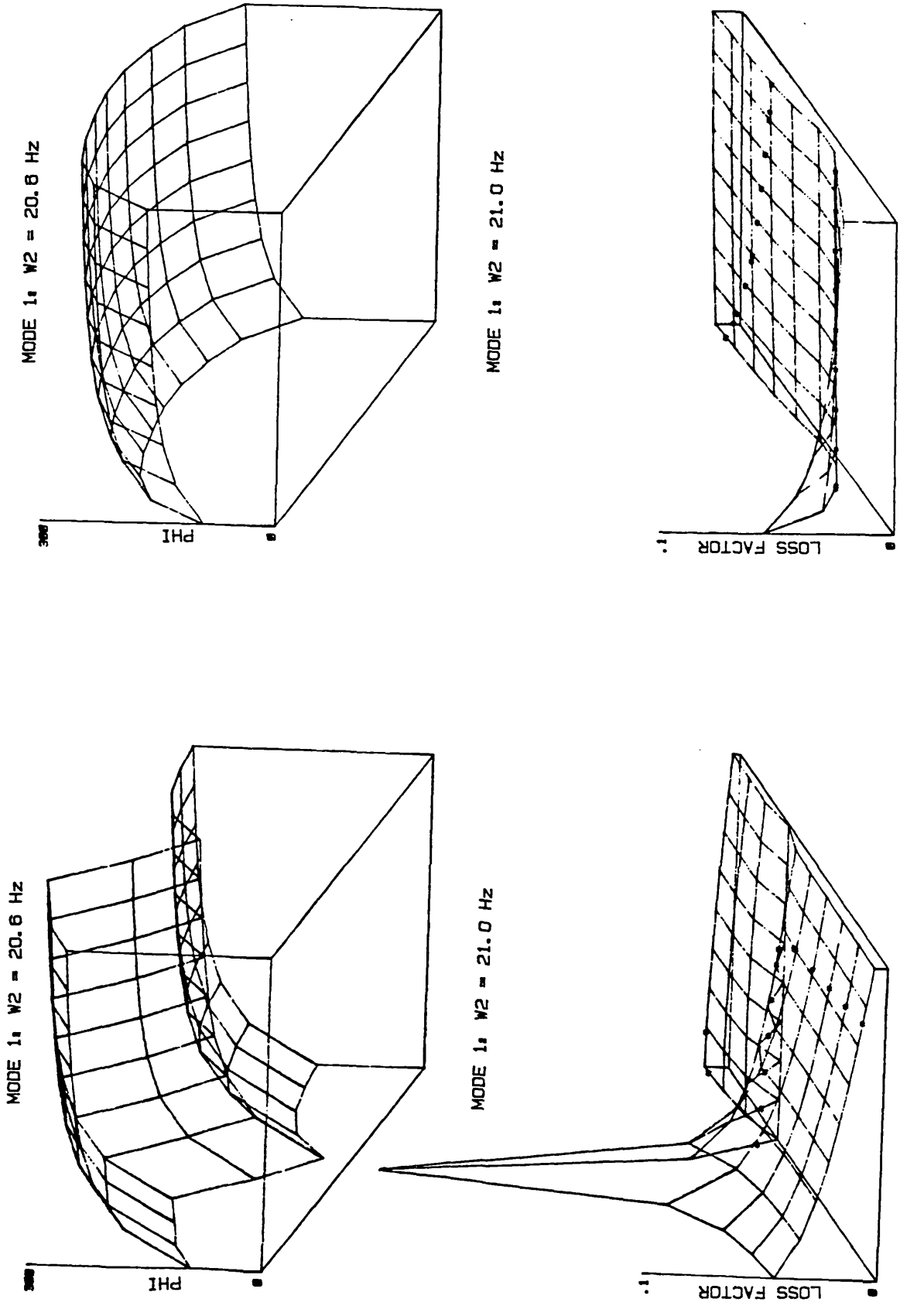

FIGURE 3-27 : Isometric plots of angle PHI and loss factor of mode 1 for ω_2 = 20.6 and 21.0 Hz.

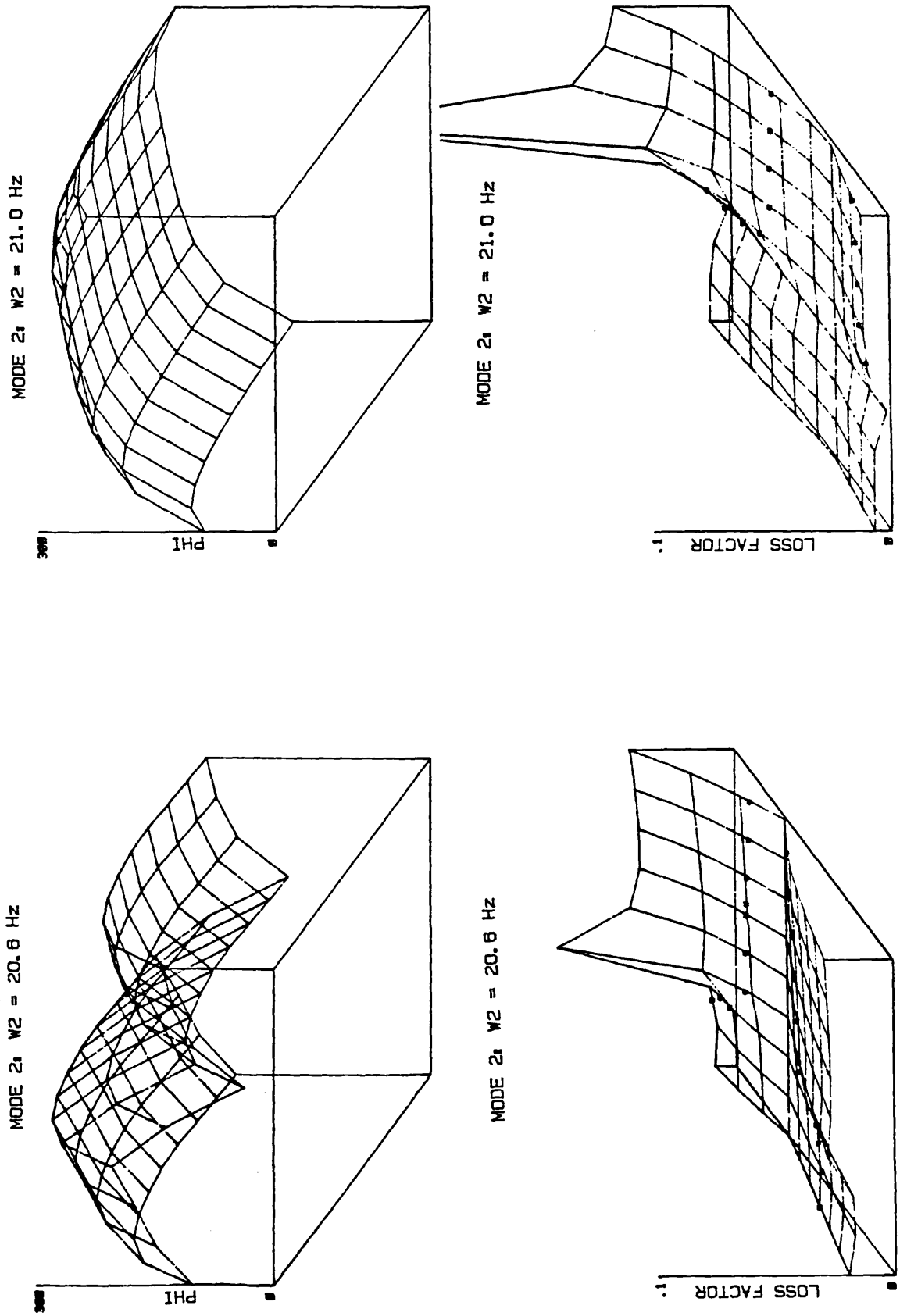

FIGURE 3-28 : Isometric plots of angle PHI and loss factor of mode 2 for ω_2 = 20.6 and 21.0 Hz.

CHAPTER

-4-

4. A DETAILED STUDY OF SOME MODAL PROPERTIES OF THE 'NASTRAN' STRUCTURE

4.1. INTRODUCTION

In section 3.2.1 it was noted that the 'NASTRAN' structure (figure 3-Ø1) is nonlinear. This was shown by testing the structure at several different but constant levels of excitation. Since the mobility modulus and Nyquist plots were found to be force dependent, the structure must be nonlinear.

In this chapter we shall try to identify the nonlinearities and, if possible, see how 'accurate' modal properties may be obtained even in the presence of these pollutants. But before this, it is necessary to outline the criterion to be used to check the quality of the identified modal properties.

4.2. ASSESSMENT OF THE QUALITY OF IDENTIFIED MODAL PROPERTIES

The first step in checking the measured modal properties is to see how large is the variation in the different estimates of loss factor around resonance. This is easily done by noting the RMS error: the smaller the error, the better the results. A second check that can give some indication of the reliability of the data is the degree of complexity of the modal constant (value of modal phase): the closer the modal phase is to Ø or 18Ø degrees, the

greater the confidence in the identified value. Sometimes the second check can give misleading information because close modes and nonproportionally damped structures can also produce large values of modal phase. Nevertheless, this serves as a first check and warns the analyst.

Another method of assessing the reliability of measured modal data is by examining the consistency of the various parameters measured at different points on the structure. All the frequency response functions should yield identical results for the natural frequencies and damping values for each mode analysed. Any discrepancies encountered must be justifiable in terms of the accuracy of the various measured quantities but close inspection of this feature often reveals wider scatter than can be attributed to 'measurement errors'. A more discriminating check can be obtained from the other parameters - the modal constants. The nature of this check is to make measurements with the excitation at various points on the structure so that we obtain a set of modal constants;

$$ {}_rA_{jp},\ {}_rA_{jq} \text{ etc. } r = 1,m;\ j = 1,n. $$

where p,q are the points of excitation.

In a simple example, we shall consider two series of measurements, first with the exciter at point p and secondly at point q. Amongst the many frequency responses measured will be α_{pp}, α_{qp} in the first series and α_{pq}, α_{qq} in the second. For each mode of the structure we shall thus find;

$r^A_{pp'}$ $r^A_{qp'}$ $r^A_{pq'}$ r^A_{qq}

and it may be seen from the definition of modal constant (equation 2-Ø9) that these four values should be inter-related so that;

$$r^A_{pp}\ r^A_{qq} - r^A_{pq}\ r^A_{qp} = 0 \qquad (4\text{-}Ø1)$$

If we define;

$$\Delta_A = 1 - \frac{r^A_{pp}\ r^A_{qq}}{r^A_{pq}\ r^A_{qp}} \qquad (4\text{-}Ø2)$$

then the closeness of Δ_A to zero will provide an assessment of the reliability of the results obtained for that mode.

Two alternative versions of the same concept are (i) the measurement and comparison of a reciprocal pair of frequency responses, α_{pq} and α_{qp} and (ii) the use of two measured (and analysed) functions - such as α_{pp} and α_{qp} - to predict or synthesize the respective third - α_{qq}. While the first of these checks is useful, the second can sometimes give a falsely negative results because of limitations to the amount of data used [5Ø].

4.3. CONSTANT FORCE TESTS ON THE 'NASTRAN' STRUCTURE

4.3.1. IDENTIFICATION OF NONLINEARITIES

For this study we shall examine the response of the 'NASTRAN' structure (figure 3-Ø1) at two points - 7 and 12 - due to sinusoidal excitation at these points, exciting one point at a time. First the structure was tested to check for nonlinearities by the simple procedure of constant forcing levels. Results from similar tests were shown in chapter 3 but it was necessary to repeat these tests as there was a gap of about 9 months between the first tests and this more detailed study. Mode 3 was considered to be a good specimen for the purpose of detecting nonlinearities because it is well separated from other modes (figure 4-Ø1) and any variation in the loss factor plot could reasonably be attributed to nonlinearities rather than to close modes.

Exciting one point at a time - 7 or 12 - and measuring the response at points 7 and 12, produces a 2x2 mobility matrix: shown in table 4-Ø1. Some of the measured data for $Y_{12,12}$ and $Y_{Ø7,12}$ at several constant forcing levels are shown in figures 4-Ø2 and 4-Ø3 respectively. These plots show a slight drop in the mobility modulus and a large decrease in the natural frequency as the forcing level is increased. As in the last chapter, these data were analysed using a SDOF algorithm and the modal properties thus extracted are shown in tables 4-Ø2 and 4-Ø3 for $Y_{12,12}$ and $Y_{Ø7,12}$ respectively. The modal properties for $Y_{12,Ø7}$ and $Y_{Ø7,Ø7}$ were also identified and are given in reference 36.

The following conclusions are drawn from the extracted modal properties of tables 4-Ø2 and 4-Ø3;

As the excitation force increases:

(i) the resonance frequency decreases;

(ii) the loss factor decreases;

(iii) in general, the modal constant decreases;

(iv) the complexity of the modal constant increases;

(v) the RMS error increases, indicating a large scatter in the damping estimates at high levels of excitation.

Isometric loss factor plots were constructed and are displayed in figures 4-Ø4 and 4-Ø5 for $Y_{12,12}$ and $Y_{Ø7,12}$ respectively. These plots indicate a systematic change, rather than a random one, in the estimated damping values around resonance. The plots for a low level of excitation (F = Ø.Ø5 v) show a reasonably flat surface, except near the origin (two adjacent points around resonance) where the value of damping is largest compared with the rest of the values and may be due to some type of frictional nonlinearity - perhaps dry friction (compare this plot with those with dry friction given in chapter 3).

As the forcing level increases, the plots lose their flatness and become tilted, somewhat similar to cubic stiffness plots, and this suggests a stiffness type of nonlinearity (cubic stiffness). For a high level of excitation (F = 1.Ø v), there is a larger variation in estimates of loss factor for different points around the

resonance frequency. The first indication of this is given by the large RMS error in the modal properties of tables 4-Ø2 and 4-Ø3.

The isometric plots, together with the mobility modulus and Nyquist diagrams, indicate the presence of two types of nonlinearity, a frictional type (dry friction) - the effect of which is maximum at low levels of excitation - and a softening stiffness type nonlinearity (softening cubic stiffness) - the effect of which increases with increasing force. The softening cubic stiffness nonlinearity is the dominant of the two. The effect of dry friction is very small; and it may be ignored, hence we shall not consider it in subsequent analysis of the NASTRAN structure.

4.3.2. ASSESSMENT OF IDENTIFIED MODAL PROPERTIES

Next we shall employ the criterion outlined in section 4.2 to examine the quality of the identified modal properties.

Tables 4-Ø2 and 4-Ø3 show an increase in both the modal phase and the RMS error as the excitation force increases and hence an indication of a drop in the quality of the identified modal parameters. For a given excitation force, we have four estimates of the natural frequencies for each mode, one for each of the measured mobility plots listed in table 4-Ø1. Figure 4-Ø6 shows these four estimates plotted as a function of the excitation level. At low forcing levels, the calculated values of the natural

frequencies are reasonably close to each other (as indeed they should be because the natural frequency is a property of the structure and in theory is independent of the points of excitation and response), but at high levels (F = Ø.8 and 1.Ø v) there is a large spread. Consequently, at high levels of excitation the confidence in the calculated natural frequency is low.

Figure 4-Ø7 shows the variation of Δ_A as a function of the excitation force. At low levels of excitation, values of Δ_A are close to the zero line (Δ_A < 5%) but as the force increases so does Δ_A. The value of Δ_A being close to zero does not necessarily mean that the identified modal constants are accurate, as two or more errors in these parameters can cancel out and give misleading results. However, if Δ_A is not close to the zero line, then certainly the modal parameters cannot be accurate. A deviation of 1Ø% from the zero line is considered to be acceptable for most practical applications. In this case the values of Δ_A for high levels of excitation are greater than 1Ø% - one being close to 35% - hence using these identified modal parameters in further analysis may lead to inaccurate predictions or inaccurate model of the structure.

4.4. CONSTANT AMPLITUDE OF VIBRATION TESTS ON THE 'NASTRAN' STRUCTURE

4.4.1. WHY USE CONSTANT AMPLITUDE OF VIBRATION ?

All the evidence from the measurements point to a particular type of nonlinearity - softening stiffness - as being dominant. Nonlinearities of this kind can be represented analytically by;

$$F = kX\{1-(\gamma_1 X + \gamma_2 X^2 \gamma_3 X^3 + ...)\} \qquad (4\text{-}\emptyset 3)$$

where F - the force;

k - stiffness coefficient;

X - displacement of spring;

$\gamma_1, \gamma_2, ..$ - constants.

If the vibration displacement amplitude is kept constant as the frequency of excitation (ω) varies, then the expression in the curly brackets of equation 4-Ø3 is a constant (say σ), thus;

$$F = kX\sigma$$

$$= k'X \qquad (4\text{-}\emptyset 4)$$

where $k' = k\sigma$

Equation 4-Ø4 is of the same form as a linear spring although k' is now smaller than k (for a hardening spring k' will be larger than k). This means the natural frequency of a system with a softening type nonlinearity will be lower

than its natural frequency if the nonlinearity was not present ($\omega_{\emptyset}^2 = k/m$). As the amplitude of vibration (X) increases, the value of k' decreases and for a given amplitude it remains constant. Thus, constant amplitude of vibration tests on any structure with a stiffness type of nonlinearity will effectively linearise the structure and produce data that can be analysed using a linear algorithm but it must be borne in mind that the identified modal properties are amplitude-dependent and are, in turn, dependent on the force and are not the 'true' (linear) values.

4.4.2. TEST WITH CONSTANT AMPLITUDE OF VIBRATION

These tests can only be carried out using sinusoidal excitation because it is not possible to keep the amplitude of vibration constant with any other type of excitation. The amplitude of vibration of point 12 was kept constant and the response was measured at points 12 and 7 first with the input force at point 12 and then with the force at point 7. Figures 4-Ø8 and 4-Ø9 show the mobility modulus and Nyquist plots for mode 3 from $Y_{12,12}$ and $Y_{\emptyset 7,12}$ respectively. By comparing these diagrams with those with constant force (figures 4-Ø2 and 4-Ø3) shows the effect of keeping the amplitude constant. Each plot appears to be linear but differs from the other plots in the sense that the resonance frequency is not the same for any two plots. The Nyquist plots of these data appear to form continuous circles, unlike the constant forcing tests which had large

distortions in the spacing of frequency points. As the amplitude of vibration increases, the modal diameter decreases but still remains circular. The modal properties identified from these plots are given in tables 4-Ø4 and 4-Ø5.

Tables 4-Ø4 and 4-Ø5 show that the RMS error is now very small (less than 2%) and also the modal phase is close to Ø or 18Ø degrees. These results indicate the apparent linearity of the structure for a given value of amplitude. The variation in the natural frequencies and the damping for different mobilities (i.e. $Y_{Ø7,12}$, $Y_{12,12}$ etc.) are more consistent than in the constant force tests.

Some of the 3-D loss factor plots for $Y_{12,12}$ and $Y_{Ø7,12}$ are given in figures 4-1Ø and 4-11 respectively. All these diagrams are flat, without exception, and are similar to those obtained from the analytical linear model (chapter 3). As the amplitude of vibration increases the 3-D plots are shifted (i.e. damping increases) but the plots retain their flatness. These results prove that the structure's main nonlinearity is the stiffness type which we have been able to linearise using constant amplitude of vibration tests.

4.4.3. ASSESSMENT OF RESULTS

The variation of Δ_A as a function of the amplitude of vibration of point 12 of the 'NASTRAN' structure (figure 3-Ø1) is shown in figure 4-12. The deviation of Δ_A from the zero line is much smaller (less than 7%) compared with the values obtained for the constant force cases (figure 4-Ø7).

The values of Δ_A are not zero, as they should be in theory, because;

(i) of the random errors in the measured data;

(ii) the structure is most likely to posess other types of nonlinearities as well as the softening stiffness and dry friction.

4.5. CONCLUDING REMARKS

The constant force results showed that the 'NASTRAN' structure is nonlinear with at least two types of nonlinearity - frictional type (dry friction) and softening stiffness (softening cubic stiffness) - the latter being the dominant.

The effect of cubic stiffness can be reduced by decreasing the excitation force but unfortunately this increases the effect of dry friction (see chapter 3). Since cubic stiffness is the dominant nonlinearity in this case, low levels of excitation force should be used in order to obtain accurate modal properties. The identified modal

parameters have very good consistency at low forcing levels (table 4-Ø2 and 4-Ø3), however, it is not always possible to excite a structure adequately using low excitation force because this usually results in a high level of signal to noise ratio in the measured data, which is just as undesirable as the effect of nonlinearities. Instead, a constant amplitude of vibration should be used as this will give better results than equivalent constant force. However, it is much more difficult in practice to control the amplitude of vibration than the force, especially for a nonlinear structure because the response is not directly proportional to the force (i.e. doubling the force does not necessarily double the response).

In any event, using a constant amplitude of vibration does not solve all the problems because large amplitudes of vibration also give inconsistent modal properties but the inconsistency is smaller than that for the constant force. The main disadvantage of using constant amplitude excitation is that in practice, the amplitude can only be kept constant over a very narrow frequency range, constant force excitation can be used over a much wider frequency range. For example, in this study it was possible to use a constant value of excitation force for the first four modes, but the constant amplitude was applicable for the first two modes only and this value had to be reduced for the higher modes. It appears that each method has its merits; a constant force of excitation helps to identify the type of nonlinearities present in the data and a constant amplitude of vibration

serves to produce an equivalent linear structure in the case of stiffness type of nonlinearities.

$$\begin{bmatrix} Y_{07,07} & Y_{07,12} \\ Y_{12,07} & Y_{12,12} \end{bmatrix}$$

TABLE 4-01 : Measured mobility matrix.

EXCITATION LEVEL (volts)	NATURAL FREQUENCY (Hz)	LOSS FACTOR x1000	RMS ERROR (%)	MODAL CONSTANT x1000 (1/Kg)	MODAL PHASE (Deg)
Ø.Ø5	79.26	6.92	1.13	5.Ø995	26.44
Ø.1Ø	79.14	7.Ø1	2.15	4.994Ø	2Ø.83
Ø.2Ø	78.94	5.52	7.97	3.6666	24.98
Ø.3Ø	78.71	4.83	1Ø.68	3.Ø346	55.45
Ø.4Ø	78.59	6.48	11.43	3.9Ø54	37.14
Ø.6Ø	78.32	5.Ø9	21.88	2.7485	4Ø.24
1.ØØ	77.94	4.37	23.13	1.9256	43.92

TABLE 4-02 : Identified modal properties of mode 3 for measurement $Y_{12,12}$ as function of excitation level.

EXCITATION LEVEL (volts)	NATURAL FREQUENCY (Hz)	LOSS FACTOR x1000	RMS ERROR (%)	MODAL CONSTANT x1000 (1/Kg)	MODAL PHASE (Deg)
Ø.Ø5	79.24	6.96	Ø.29	4.5812	3Ø.32
Ø.1Ø	79.14	7.Ø6	1.89	4.4925	2Ø.23
Ø.2Ø	78.94	5.99	8.66	3.58Ø5	22.26
Ø.3Ø	78.72	5.53	8.59	3.1249	45.25
Ø.4Ø	78.56	5.38	9.19	2.8628	48.21
Ø.6Ø	78.32	5.4Ø	24.25	2.6898	37.28
1.ØØ	77.89	4.67	21.33	1.9Ø32	62.55

TABLE 4-03 : Identified modal properties of mode 3 for measurement $Y_{07,12}$ as function of excitation level.

AMPL. OF VIBRATION OF Pt. 12 (μm)	NATURAL FREQUENCY (Hz)	LOSS FACTOR x1000	RMS ERROR (%)	MODAL CONSTANT x1000 (1/Kg)	MODAL PHASE (Deg)
5	79.35	7.60	0.35	5.3679	-3.39
8	79.20	7.82	1.00	5.4319	-4.26
10	79.09	7.87	0.60	5.1604	-4.47
12	78.96	8.84	0.28	5.4887	-3.39
15	78.84	9.09	0.49	5.3959	-4.07
20	78.65	9.56	1.89	5.1155	-10.53

TABLE 4-04 : Identified modal properties of measurement $Y_{12,12}$ as function of amplitude of vibration of point 12 (mode 3).

AMPL. OF VIBRATION OF Pt. 12 (μm)	NATURAL FREQUENCY (Hz)	LOSS FACTOR x1000	RMS ERROR (%)	MODAL CONSTANT x1000 (1/Kg)	MODAL PHASE (Deg)
5	79.34	7.71	1.02	4.9049	-1.40
8	79.19	7.88	0.79	4.8804	0.06
10	79.08	7.99	0.92	4.6907	-2.09
12	78.95	8.81	0.87	4.8711	-1.80
15	78.84	8.97	0.67	4.7341	-3.77
20	78.62	9.87	0.93	4.7820	-1.43

TABLE 4-05 : Identified modal properties of measurement $Y_{07,12}$ as function of amplitude of vibration of point 12 (mode 3).

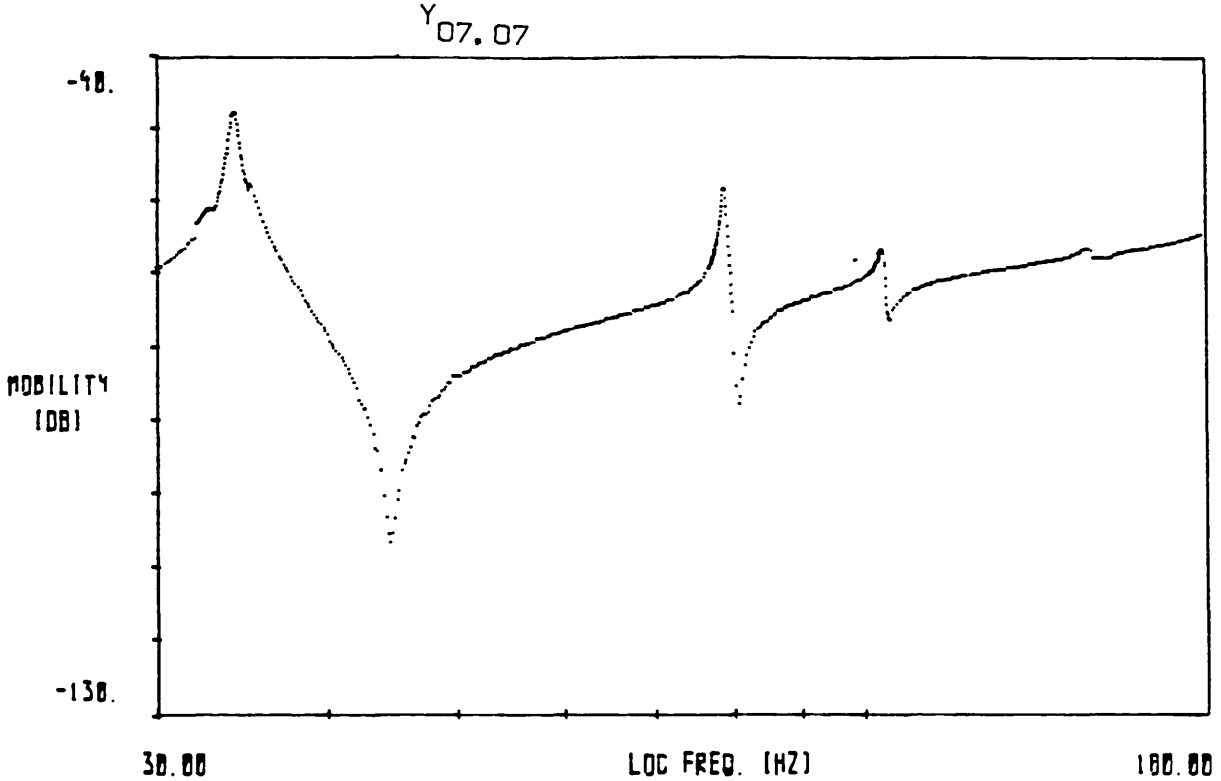

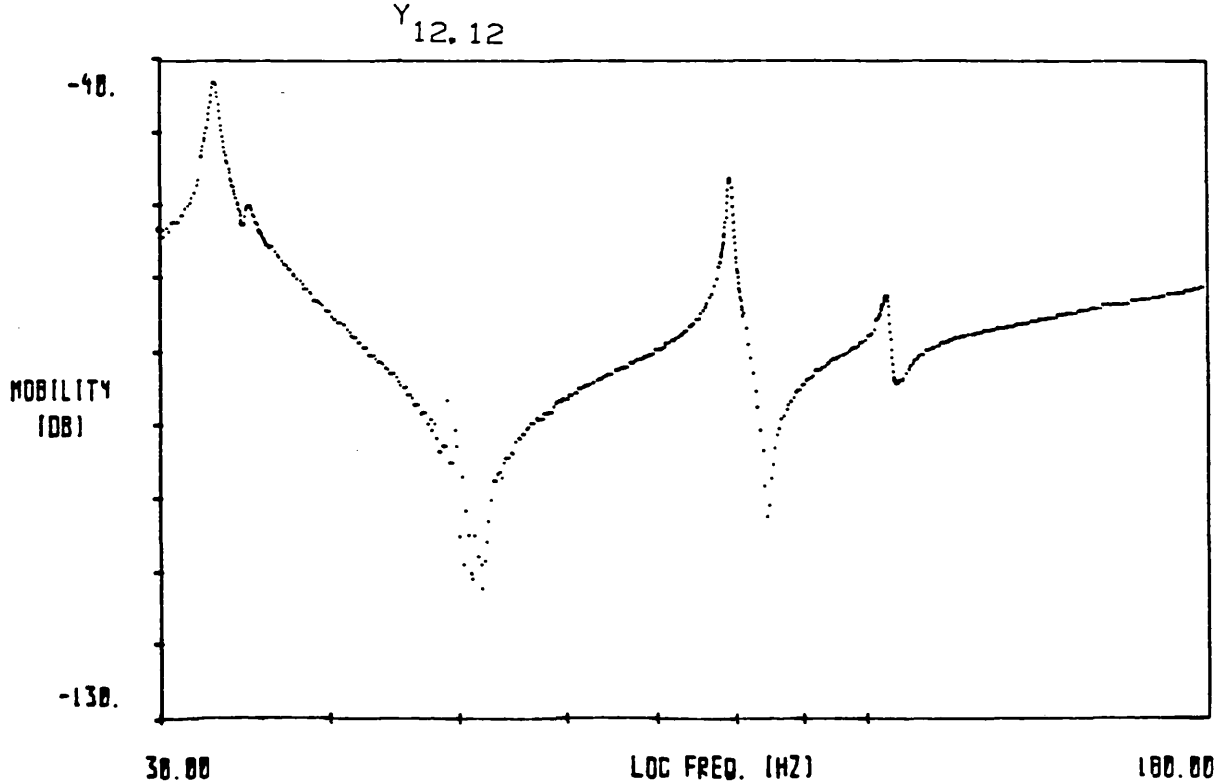

FIGURE 4-01 : Measured point mobility modulus plots of $Y_{07,07}$ and $Y_{12,12}$.

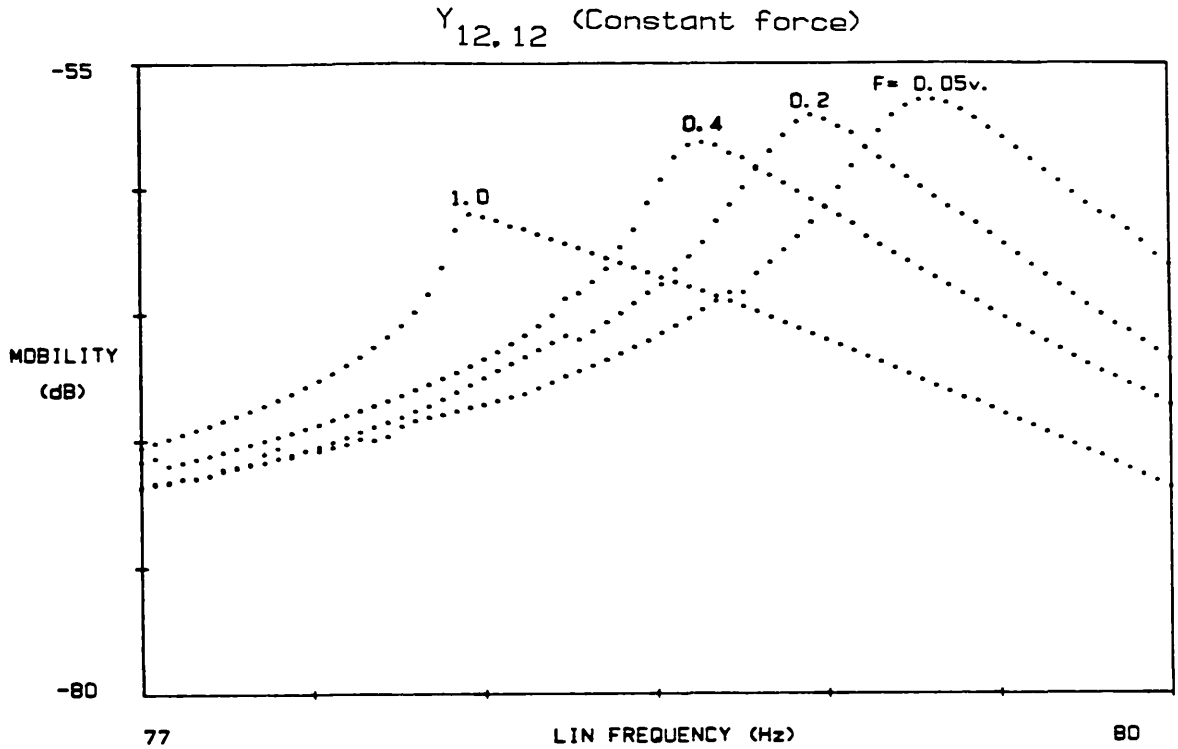

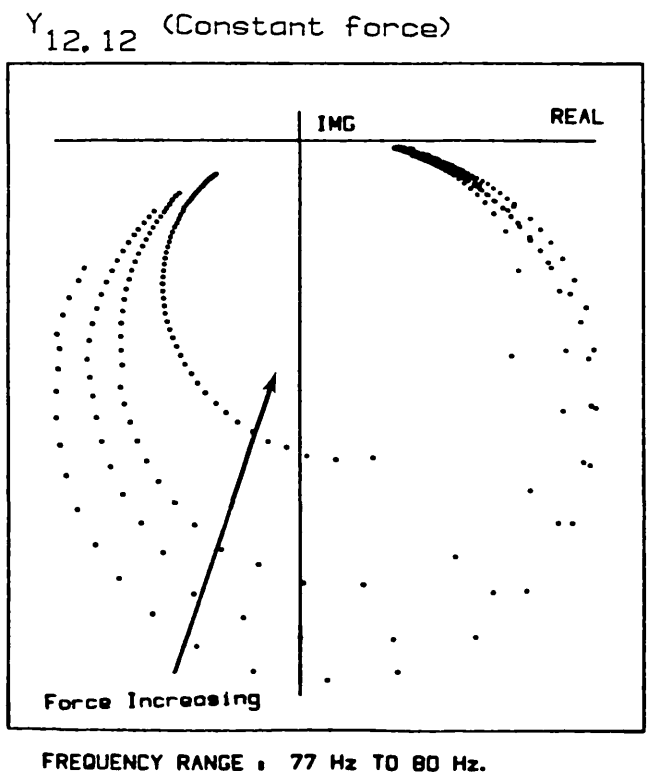

FIGURE 4-02 : Mobility modulus and Nyquist plots of mode 3 for point measurement $Y_{12,12}$ under constant forcing levels.

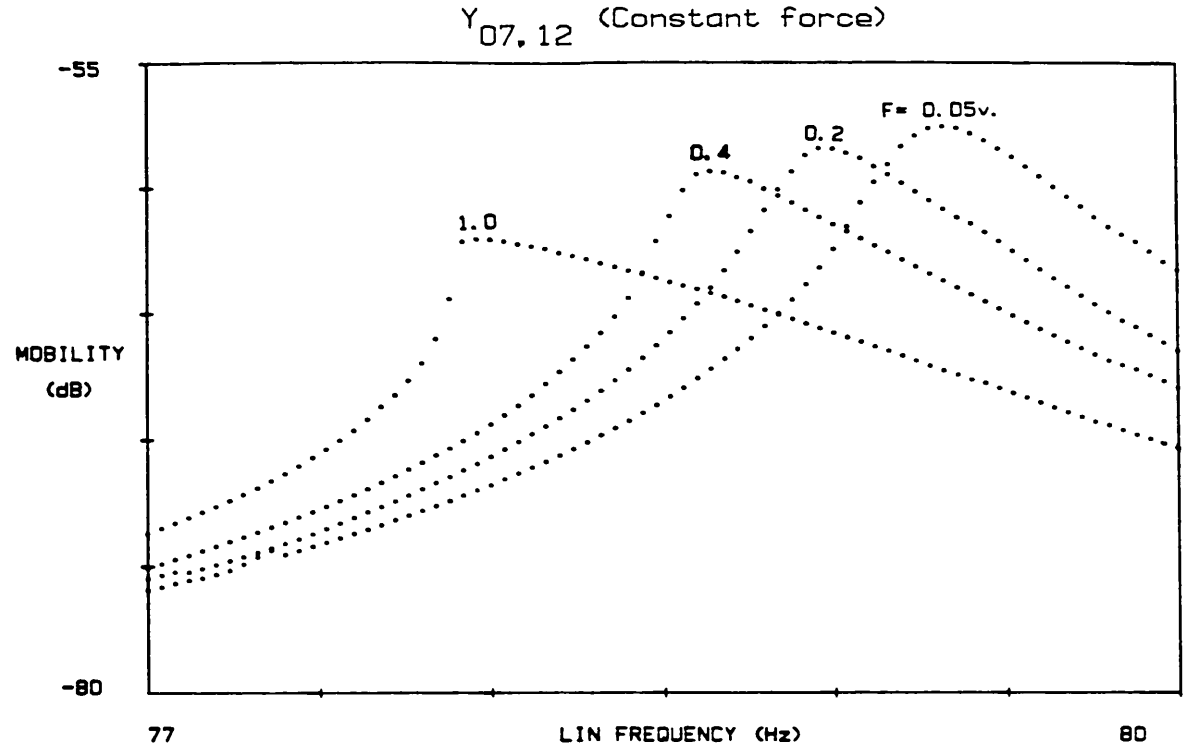

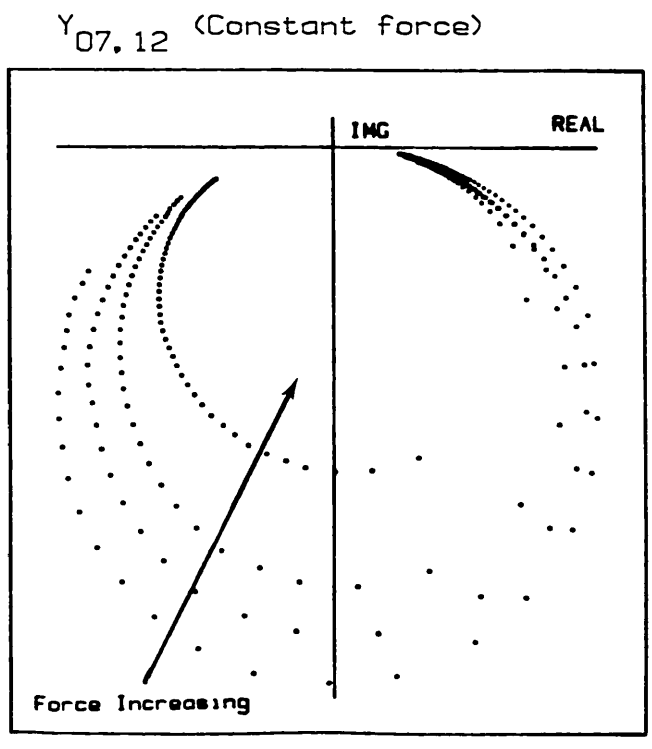

FIGURE 4-03 : Mobility modulus and Nyquist plots of mode 3 for point measurement $Y_{07,12}$ under constant forcing levels.

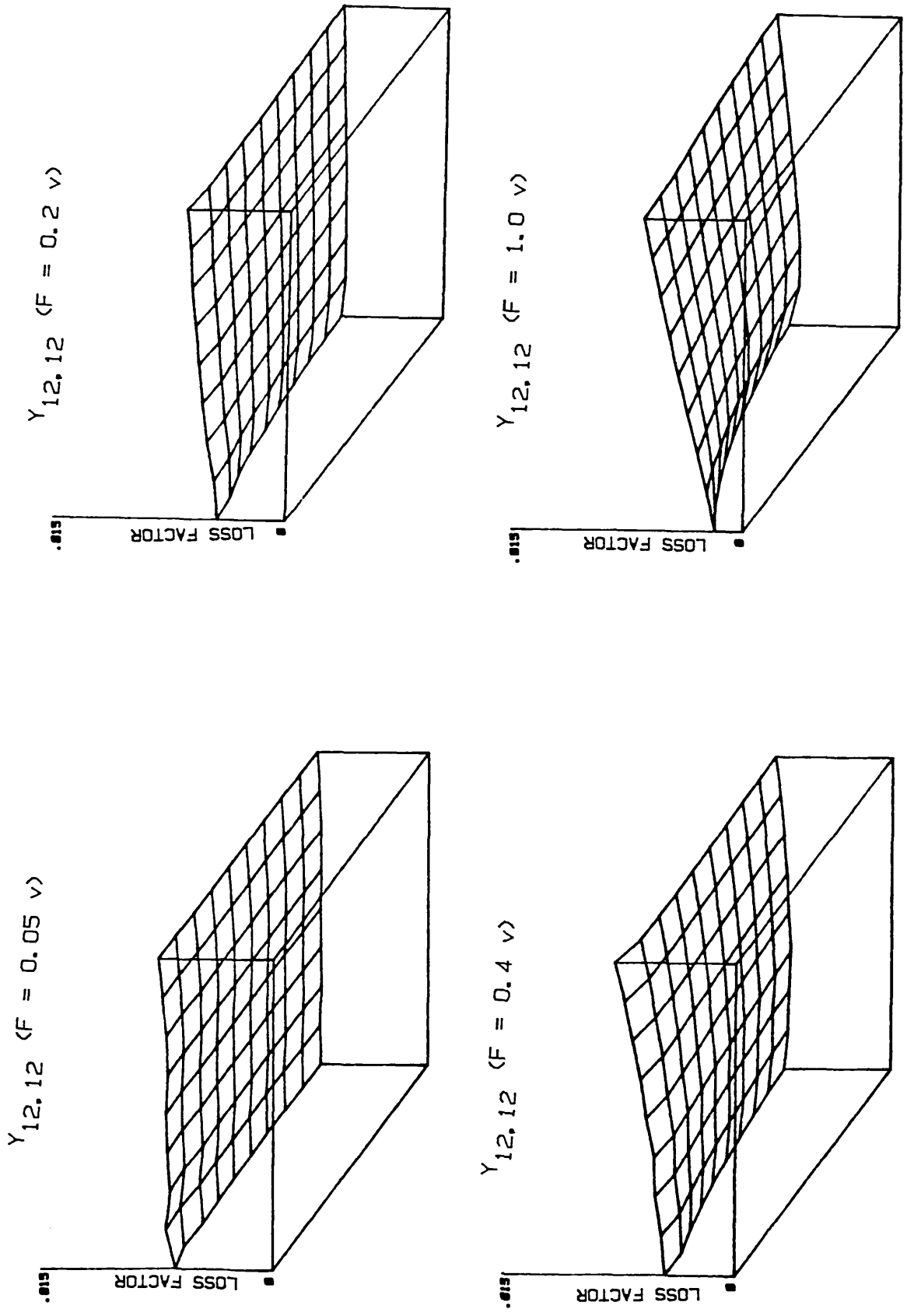

FIGURE 4-04 : Isometric loss factor plots of mode 3 for measurement $Y_{12,12}$ under constant forcing levels.

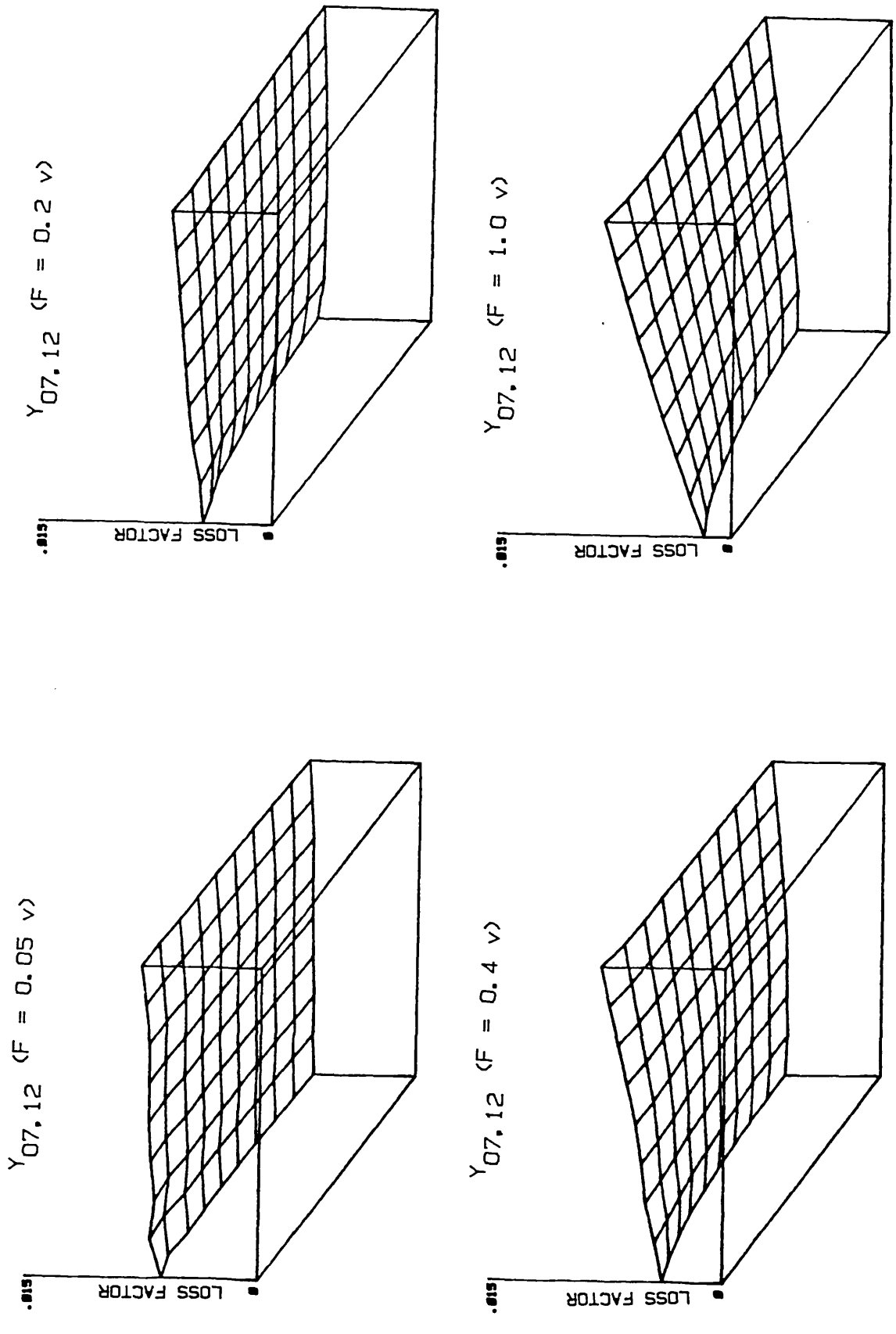

FIGURE 4-05 : Isometric loss factor plots of mode 3 for measurement $Y_{07,12}$ under constant forcing levels.

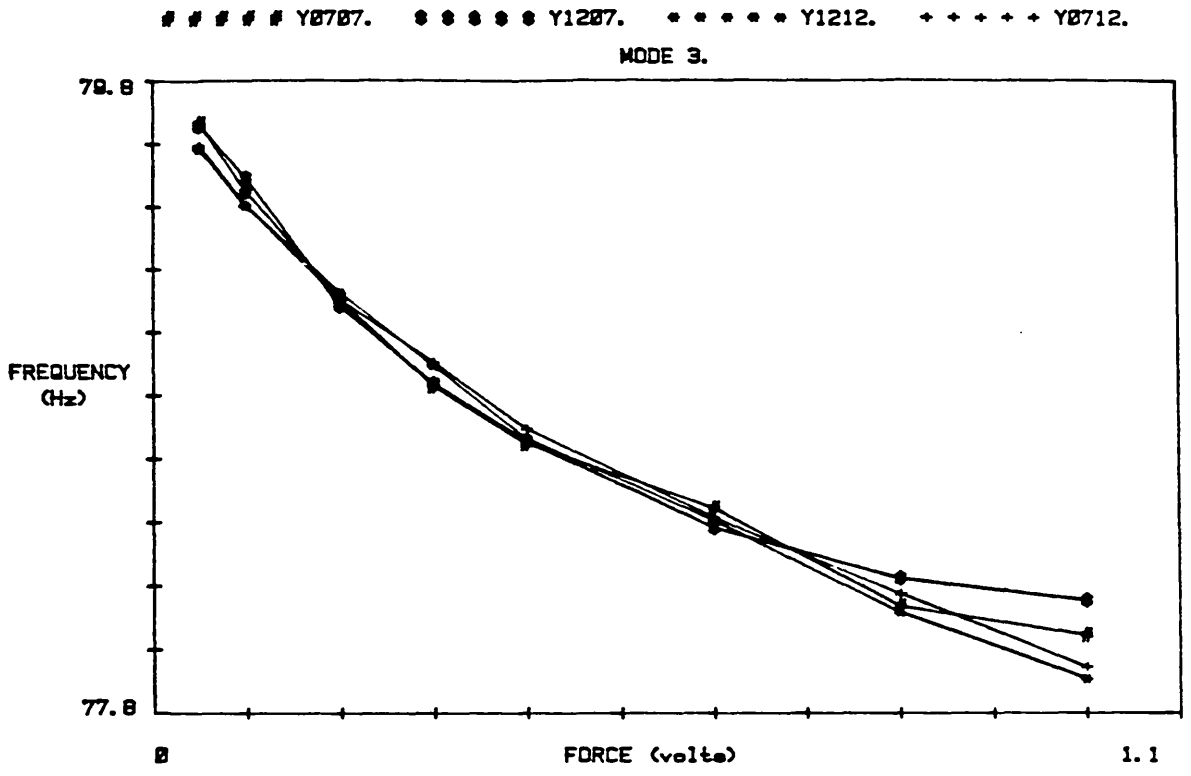

FIGURE 4-06 : Variation of natural frequency as a function of excitation force (mode 3).

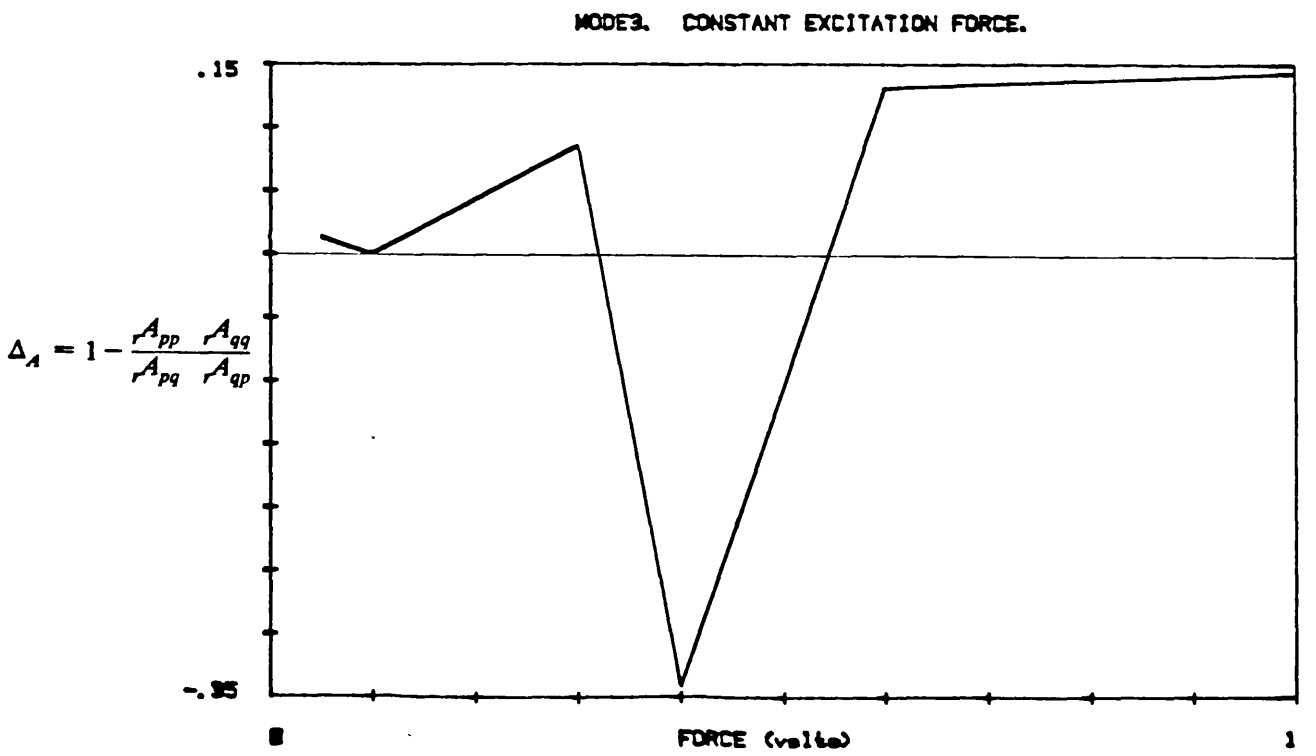

FIGURE 4-07 : Δ_A as function of the excitation level.

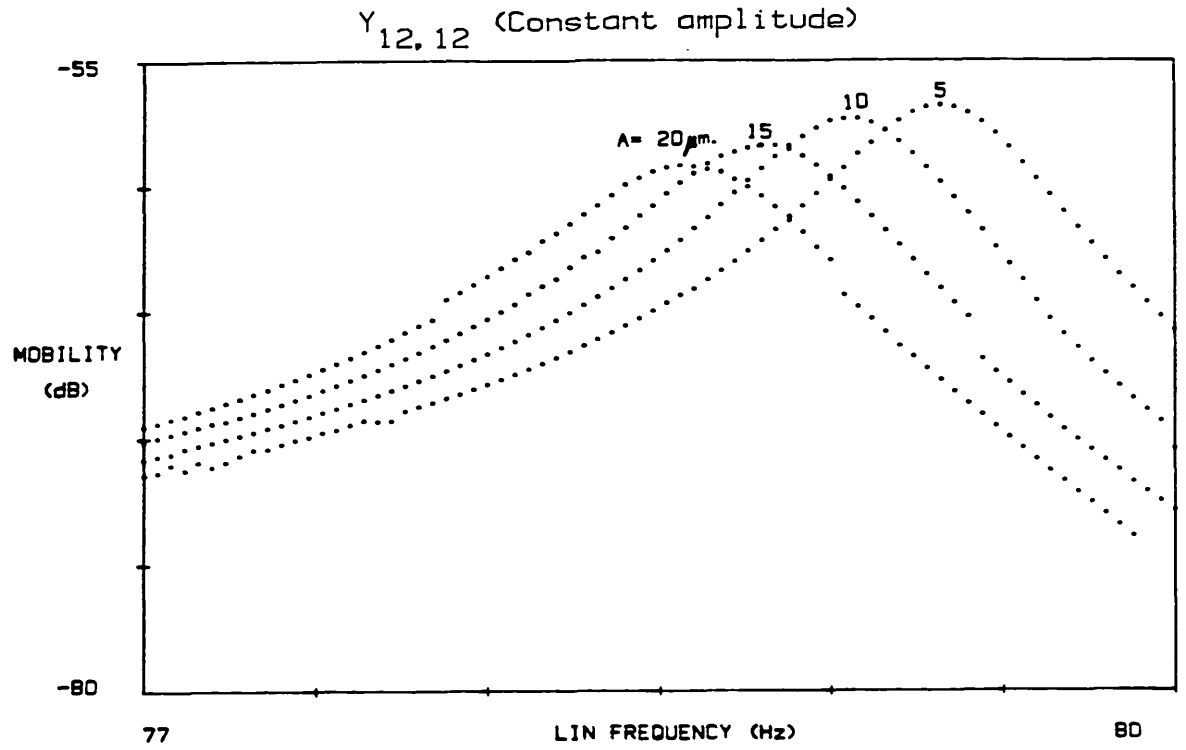

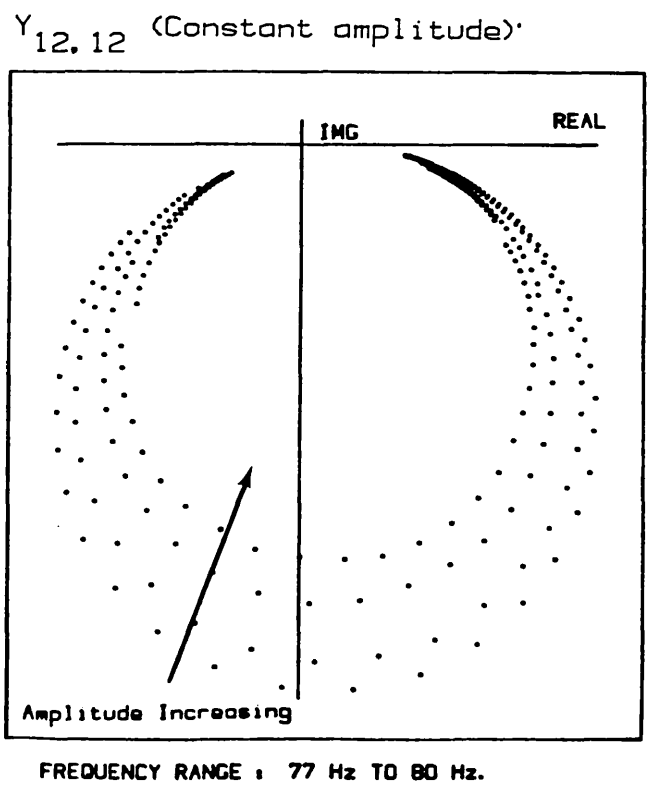

FIGURE 4-08 : Mobility modulus and Nyquist plots for $Y_{12,12}$ under constant amplitude of vibration of point 12 (mode 3).

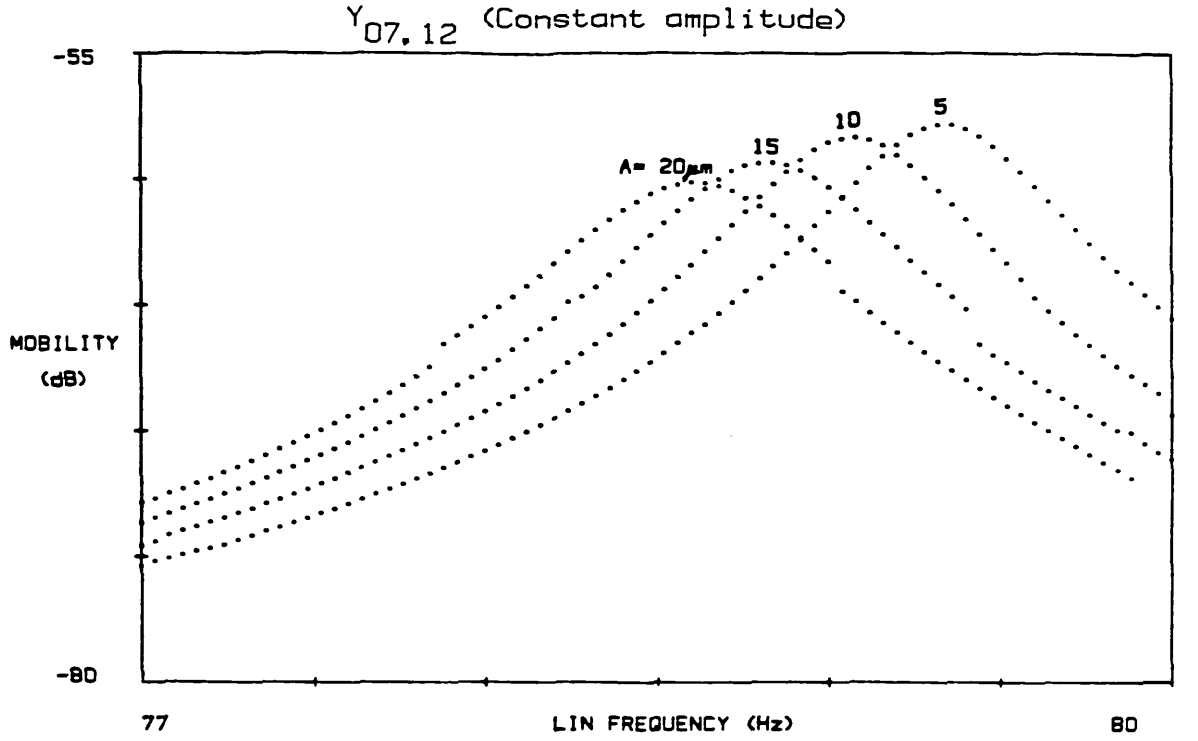

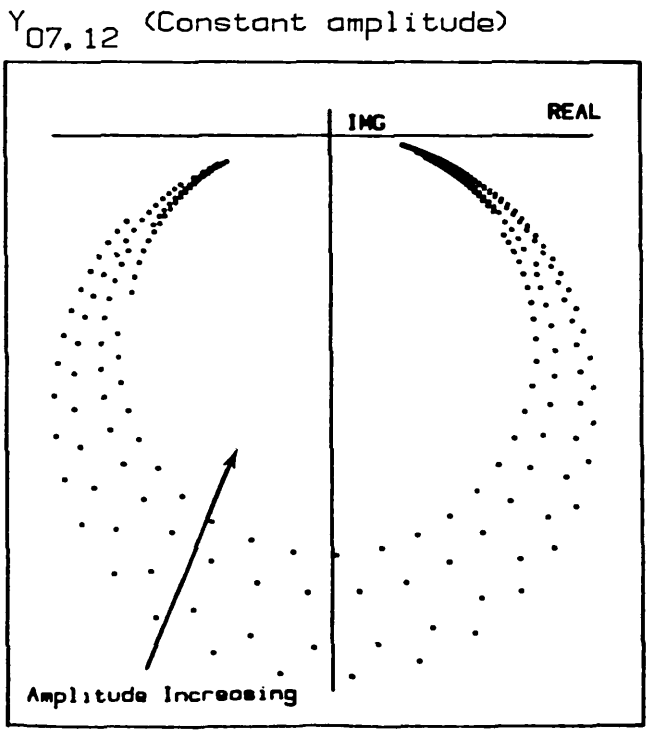

FIGURE 4-09 : Mobility modulus and Nyquist plots for $Y_{07,12}$ under constant amplitude of vibration of point 12 (mode 3).

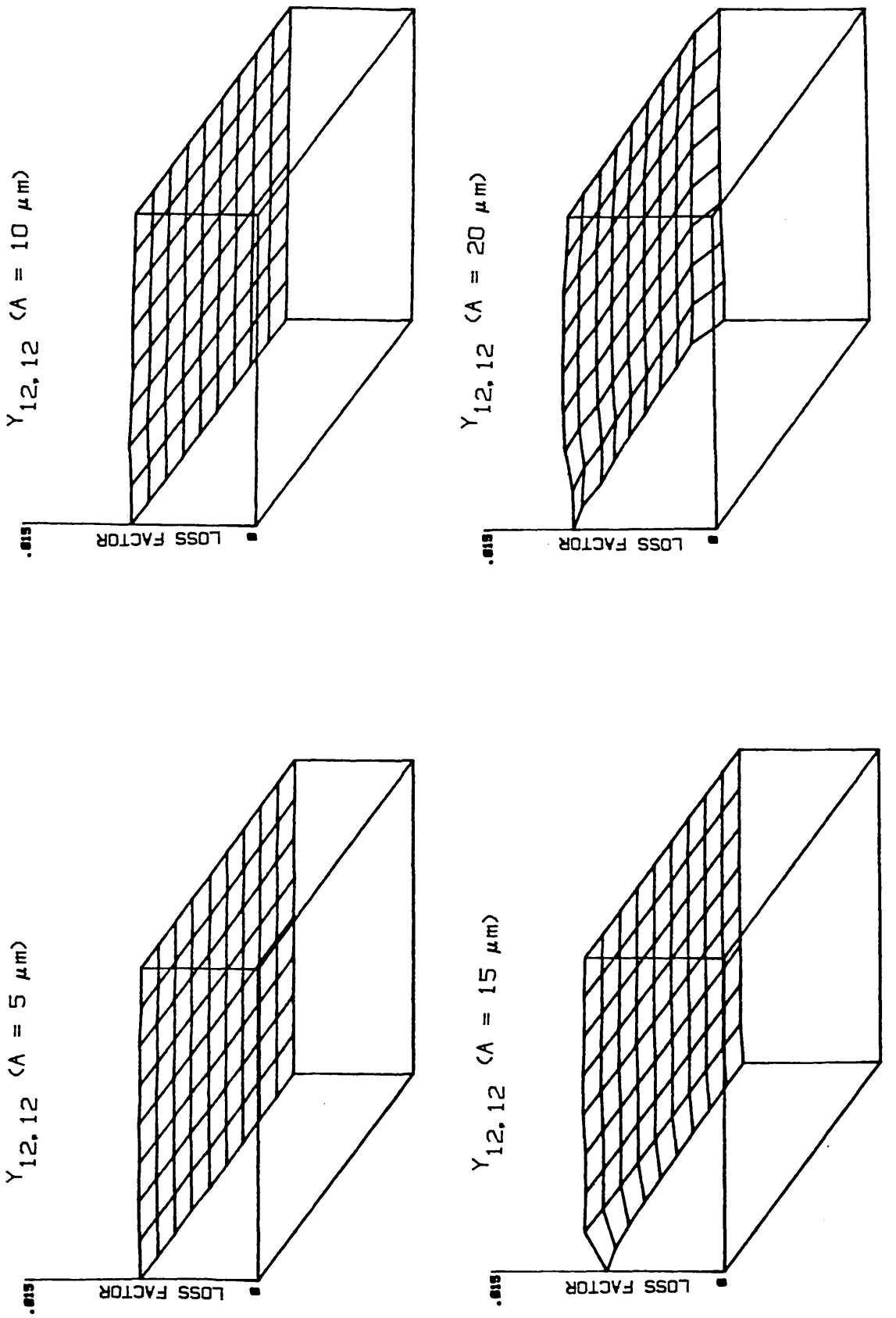

FIGURE 4-10 : Isometric loss factor plots for measurement $Y_{12,12}$ under constant amplitude of vibration of point 12 (mode 3).

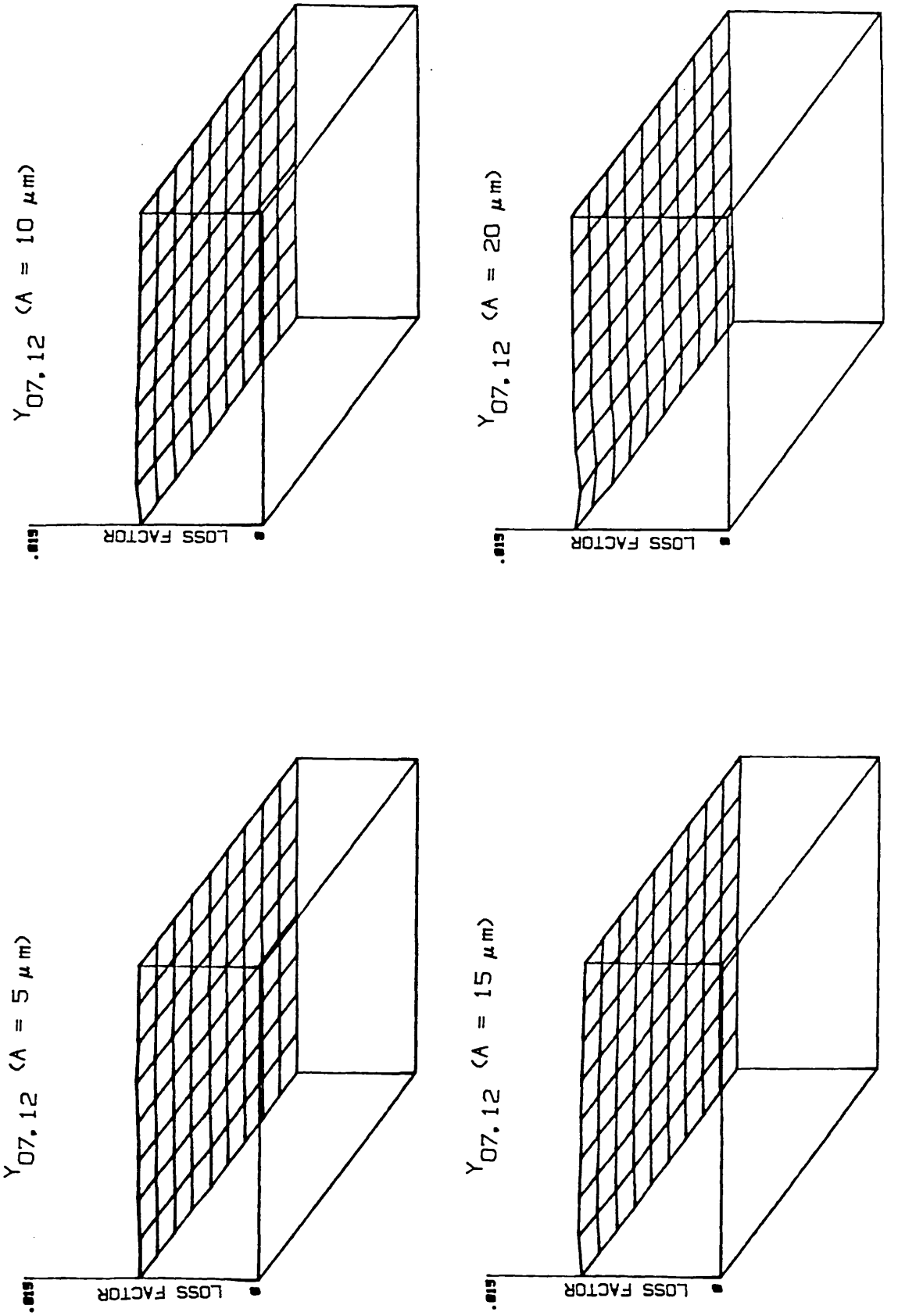

FIGURE 4-11 : Isometric loss factor plots for measurement $Y_{07,12}$ under constant amplitude of vibration of point 12 (mode 3).

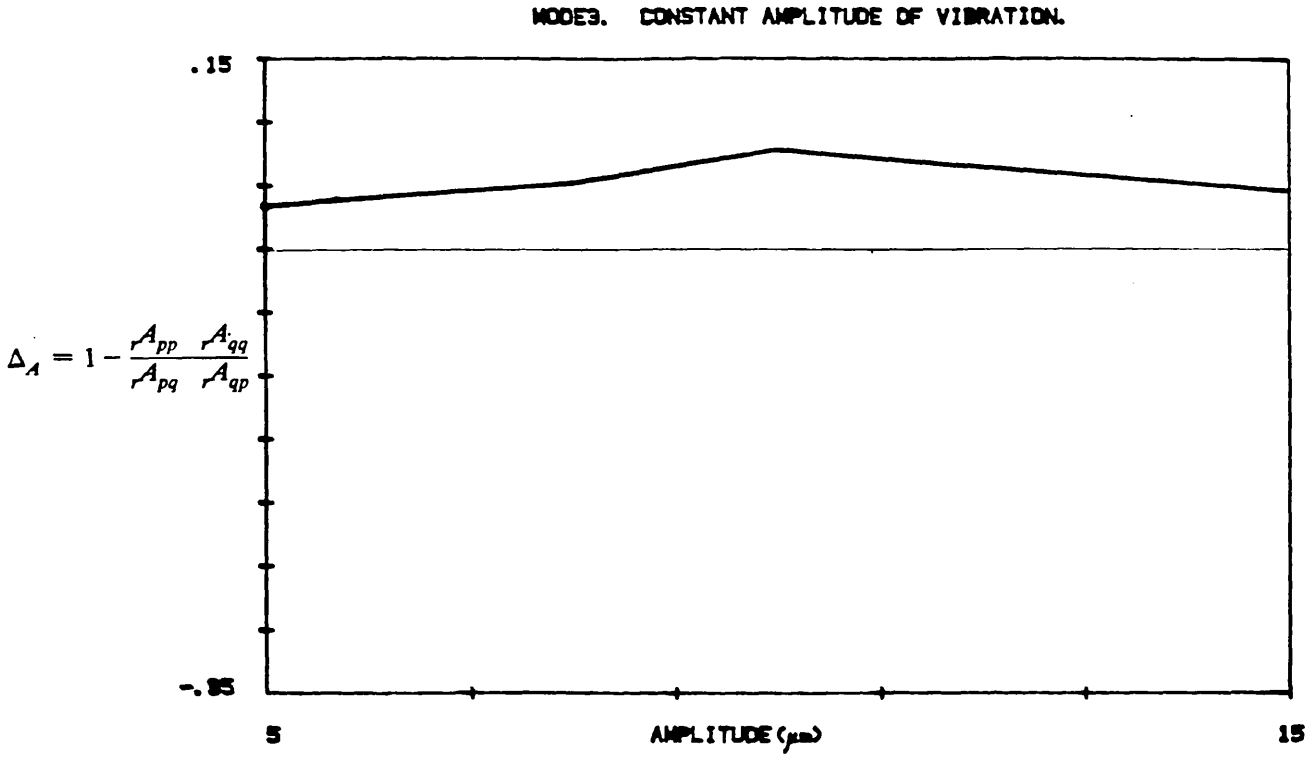

FIGURE 4-12 : Δ_A as function of the amplitude of vibration.

CHAPTER

-5-

5. SIMULATION OF NONLINEAR-SINGLE-DEGREE-OF-FREEDOM SYSTEMS USING AN ANALOGUE COMPUTER

5.1. GENERAL

The recent past has seen many advances in the measurement of frequency response data. The availability of computing power makes it possible to carry out complex operations on the measured data at the same time as they are being measured. Statistical methods based on fast-Fourier-transformation (FFT) are very desirable under certain circumstances. A structure is excited using random or transient input and the response is measured in the time domain and is then transformed from the time domain into the frequency domain. These nonsinusoidal techniques are very useful for testing structures when the environmental input disturbances cannot be controlled, e.g. noise, ground vibrations, wind loading, etc. Another advantage of such methods is the high speed at which they permit us to acquire the test data, compared with the case of sinusoidal excitation.

Fast Fourier Transform machines make use of Duhamel's Integral [47,31], which is linear and therefore the structure's linearity might automatically be assumed. Unfortunately, very few complex structures are linear and hence do not fall into the linear category. Even though FFT machines are intended to test only linear structures, it is quite common practice to make use of them for all sorts of structures and situations. Before using FFT machines on

nonlinear structures, it is essential that the effects of nonlinearities on the test data are investigated. For this study we shall use an analogue computer because it is very difficult to solve nonlinear equations to obtain analytical solutions and the degree of difficulty is increased many fold if the input function (force) is nonsinusoidal.

5.2. ANALOGUE COMPUTER

Analogue simulation can contribute a great deal to the development and utilization of mathematical models in dynamic systems. Multi-degree-of-freedom systems with known modal properties and nonlinearities can easily be simulated. To study the response of these systems to different types of excitation does not present any difficulty as would be the case for a numerical study.

The operation of an analogue computer is very simple because there are only two primary components; integrators and summers [48]. The symbols of these and other components used for this study are given below:

SYMBOL	NAME
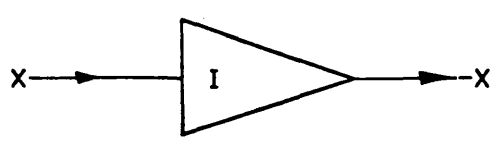	INVERTER
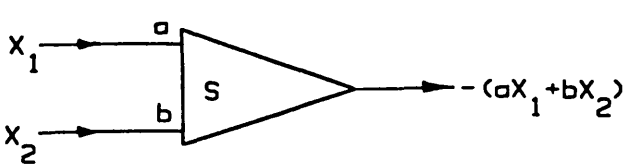	SUMMER

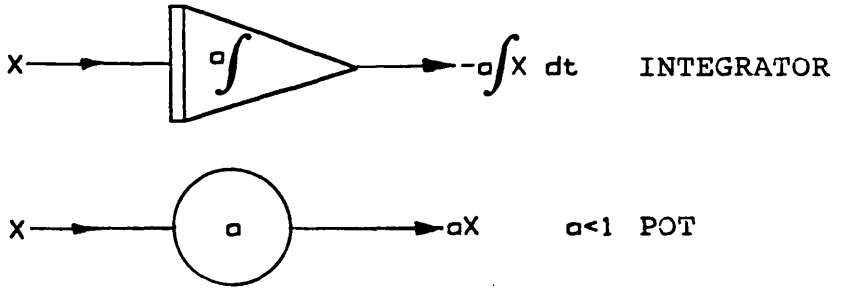

Different combinations of integrators and summers simulate the desired model. Because the analogue computer can only integrate a function and not differentiate it, a differential equation can only be solved for the highest derivative in the equation. However, further integration produces the next derivative down and so on until all the variable are computed [49] (e.g. $\ddot{X}$, $\dot{X}$ and X).

In this study the response of a nonlinear SDOF system will be investigated when excited using sinusoidal, random and transient inputs. Sinusoidal excitation should produce the same results as those obtained from the analytical solutions in chapter 3 and comparison of these data with the analytical values will serve to indicate the accuracy of representing such systems on an analogue computer.

Only two types of nonlinearity are examined: softening cubic stiffness and dry friction.

5.3. SOFTENING CUBIC STIFFNESS SYSTEM

As before, the equation of motion of a SDOF system with viscous damping and softening cubic stiffness is;

$$\ddot{X} + 2\xi\omega_0\dot{X} + \omega_0^2(X - \beta X^3) = F(t) \qquad (5\text{-}\emptyset1)$$

where ξ - viscous damping ratio (Ø.ØØ5);

$\omega_\emptyset$ - natural frequency (1Ø rad/sec);

β - cubic stiffness coefficient (m^{-2});

F(t) - forcing function (N/Kg).

When the above values of coefficients are substituted, equation (5-Ø1) becomes;

$$\ddot{X} + 2\times 0.005\times 10\dot{X} + 10^2(X - \beta X^3) = F(t)$$

$$\ddot{X} + 0.1\dot{X} + 100(X - \beta X^3) = F(t)$$

$$\ddot{X} = F(t) - 0.1\dot{X} - 100X + 100\beta X^3$$

or $$\ddot{X} = -\left\{-F(t) + 0.1\dot{X} + 100X - 100\beta X^3\right\} \qquad (5\text{-}\emptyset2)$$

In the steady-state, the integral of $\ddot{X}$ gives $\dot{X}$ and the integral of $\dot{X}$ is equal to X.

Mathematically;

$$\dot{X} = \int \ddot{X}\,dt \qquad (5\text{-}\emptyset3)$$

$$X = \int \dot{X}\,dt$$

It is necessary to estimate the maximum values of $\ddot{X}$, $\dot{X}$ and X so that the equations can be 'scaled' to prevent the computer from overloading. The analogue computer used for this study (SAE 381) becomes overloaded if the voltage in any part of the circuit exceeds 15 volts. It has been found, by a trial-and-error method, that the maximum values of $\ddot{X}$, $\dot{X}$ and X are likely to be 1 m/sec^2, Ø.1 m/sec and Ø.Ø1 m respectively. If the estimated values are lower than the actual values then the computer will overload, on the other hand, if the maximum values are overestimated then the output signals will be very small and noise is likely to have a large effect on the measured data (signal). Using these values;

$$1\left(\frac{\ddot{X}}{1}\right) = -\left\{-F(t) + 0.1\left(\frac{\dot{X}}{0.1}\right)0.1 + 100\left(\frac{X}{0.01}\right)0.01 - 100\beta\left(\frac{X}{0.01}\right)^3 0.01^3\right\}$$

$$\ddot{X} = -\left\{-F(t) + 0.01\left(\frac{\dot{X}}{10^{-1}}\right) + \left(\frac{X}{10^{-2}}\right) + 10^{-4}\beta\left(\frac{X}{10^{-2}}\right)^3\right\} \qquad (5\text{-}Ø4)$$

and $$\dot{X} = \int \ddot{X}\,dt$$

$$0.1\left(\frac{\dot{X}}{0.1}\right) = \int 1\left(\frac{\ddot{X}}{1}\right)dt$$

or $$\left(\frac{\dot{X}}{0.1}\right) = 10\int \ddot{X}\,dt \qquad (5\text{-}Ø5)$$

and also $$X = \int \dot{X} dt$$

$$0.01\left(\frac{X}{0.01}\right) = \int 0.1\left(\frac{\dot{X}}{0.1}\right) dt$$

or $$\left(\frac{X}{10^{-2}}\right) = 10\int \left(\frac{\dot{X}}{10^{-1}}\right) dt \qquad (5\text{-}\emptyset6)$$

Equations 5-Ø4 through 5-Ø6 can be represented on a circuit diagram as shown in figure 5-Ø1. So far we have not placed any conditions on the forcing function F(t) and so it can be either sinusoidal, random or transient.

Another type of scaling that is often used is the 'time scale' the effect of this is to represent the real time in computer time units i.e. it slows or speeds up simulated process. This is especially useful when the actual process might take too long or the time duration of a process is too short. For example, in order to study the creep properties of a material an actual experiment can take several years, but it can be simulated on an analogue computer and the results obtained in a much shorter time.

In this study, a time scale of Ø.1 seconds was used, the effect of which is to divide any time-dependent function by 1Ø e.g. the natural frequency will be shifted from 1Ø to 1ØØ rad/sec, the force simulated in the circuit will be 1ØØ times the input force and the acceleration signal output will also be 1ØØ times the real value. Since we are interested in the ratio of ($\ddot{X}$/F) and both of these

quantities are multiplied by 1ØØ, the ratio remains unaltered. However, the measured frequency will be 1Ø times the set frequency (i.e. the circuit will resonate at 1ØØ rad/sec rather than at 1Ø rad/sec).

The nonlinearity in the circuit (β) was changed by altering the pot setting K (equation 5-Ø4 and figure 5-Ø1). Below is a table of values of pot setting for different amounts of nonlinearity coefficient (β):

Pot Setting (K)	Nonlinearity (β m^{-2})
Ø.Ø5	5Ø
Ø.2Ø	2ØØ
Ø.4Ø	4ØØ
Ø.6Ø	6ØØ

Three types of input were used; Sinusoidal,Random and Transient.

5.3.1. SINUSOIDAL EXCITATION

A Solartron 1172 Frequency Response Analyser (FRA) was used for these tests. The input force was kept constant as the frequency varied and tests were carried out at different but constant values of nonlinearity coefficient (β).

The mobility modulus and Nyquist plots are presented in figure 5-Ø2 and the modal properties obtained using a linear SDOF algorithm are shown in table 5-Ø1. Isometric loss factor plots were constructed and are displayed in figure 5-Ø3. These results are very similar to those obtained from the analytical study of a system with softening cubic stiffness and so the conclusions drawn from the analytical study apply equally to this case, confirming the correct representation of the system by the analogue circuit (figure 5-Ø1).

5.3.2. RANDOM EXCITATION

For this part of the study, a 2-channel FFT machine (HP542ØA) was used. The forcing function of equation 5-Ø4, F(t), is now random (white noise) and the response of the system was measured and processed by the HP542ØA. The transformation of both signals from the time domain to the frequency domain was carried out and the data displayed in the form of mobility modulus and Nyquist plots (figure 5-Ø4) *for the following conditions*;

Centre frequency = 16.0 Hz ; *Bandwidth* = 2.0 Hz ; *Averages* = 100 ; $H(i\omega) = \frac{S_{fx}(\omega)}{S_{ff}(\omega)}$

These graphs show that as the nonlinearity (β) increases, the natural frequency and the diameter of the

modal circle decrease but the mobility modulus and Nyquist plots remain relatively symmetrical about the frequency of maximum response, similar to the plots obtained from linear data. However, this apparently linear behaviour is unlike that from sinusoidal excitation where the plots lean backwards and, in the extreme case, show a clear jump. With random excitation, there are no jumps or distortion in the spacing of the frequency response points.

Modal properties extracted from these data using a linear SDOF algorithm are shown in table 5-Ø2. The loss factor estimate plots corresponding to these results are shown in figure 5-Ø5 where the plots indicate a drastic change in shape compared with those obtained using sinusoidal excitation. With random excitation the plots have become flat, similar to those obtained from linear system and as the nonlinearity increases the surfaces are generally raised while still retaining their apparently linear characteristics (i.e. the damping appears to be increasing with an increase in nonlinearity).

It is also to be noted that the RMS error and the modal phase are very small compared with those for sinusoidal excitation (table 5-Ø1). In the case of random excitation, the loss factor increases as the amount of nonlinearity is increased whereas sinusoidal excitation gave a decreasing loss factor.

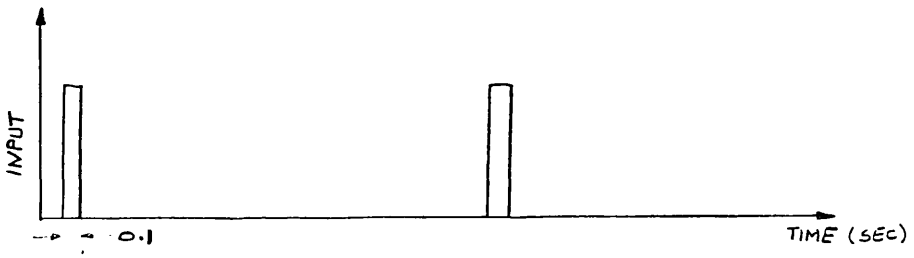
INPUT
0.1
TIME (SEC)

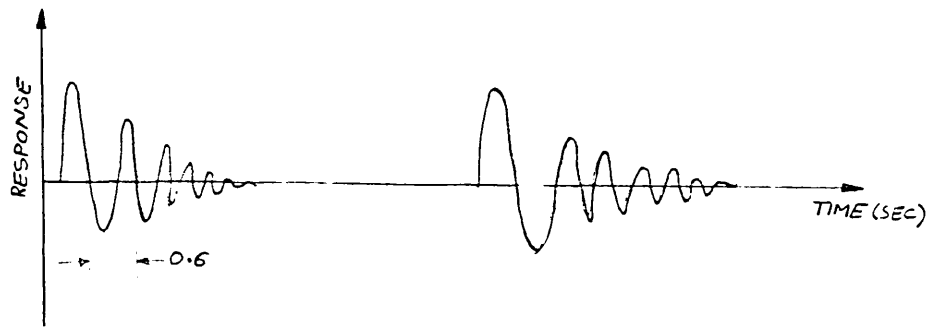
RESPONSE
0.6
TIME (SEC)

5.3.3. TRANSIENT EXCITATION

Again, the FFT analyser (HP542ØA) was used and a transient excitation was simulated using a rectangular voltage pulse input for a short duration. The analyser was set up as in section 5.3.2 and continuously took samples of the signals from the analogue computer. Because of the damping in the simulated system, the response signal became very small after few seconds and at this time another pulse was input and the system was again excited, as shown opposite.

The data obtained from these tests are displayed as mobility modulus and Nyquist plots shown in figure 5-Ø6 and the 3-D loss factor plots are given in figure 5-Ø7. Again, the results indicate an apparently linear behaviour of the system when using transient excitation.

5.4. DRY FRICTION SYSTEM

The equation of motion of a SDOF system with viscous damping and dry friction is;

$$\ddot{X} + 2\xi\omega_0\dot{X} + \omega_0^2 X + R\frac{\dot{X}}{|\dot{X}|} = F(t) \qquad (5\text{-}Ø7)$$

where ξ - viscous damping ratio (Ø.ØØ5);

$\omega_Ø$ - undamped natural frequency (1Ø rad/sec);

R - dry friction coefficient (N/Kg);

F(t) - forcing function (N/Kg).

Substituting these values in equation 5-Ø7 gives;

$$\ddot{X} + 2\times 0.005\times 10\dot{X} + 10^2 X + R\frac{\dot{X}}{|\dot{X}|} = F(t)$$

$$\ddot{X} + 0.1\dot{X} + 100X + R\frac{\dot{X}}{|\dot{X}|} = F(t)$$

$$\ddot{X} = -\left\{-F(t) - 0.1\dot{X} + 100X + R\frac{\dot{X}}{|\dot{X}|}\right\} \qquad (5\text{-}\emptyset8)$$

The integration of equation 5-Ø8 with respect to time gives the velocity ($\dot{X}$) and the integral of velocity gives the displacement (X) i.e.

$$\dot{X} = \int \ddot{X}\,dt$$

(5-Ø9)

$$X = \int \dot{X}\,dt$$

As in the cubic stiffness case, the maximum values of acceleration, velocity and displacement had to be estimated to prevent the computer from overloading or underloading. These values are taken to be the same as those for the previous study, namely, acceleration to be 1 m/sec^2, velocity to be Ø.1 m/sec and displacement Ø.Ø1 m. Equation 5-Ø8 is now scaled with these values as being the maximum. Thus,

$$\ddot{X} = -\left\{-F(t) + 0.01\left(\frac{\dot{X}}{10^{-1}}\right) + \left(\frac{X}{10^{-2}}\right) + R\frac{\dot{X}}{|\dot{X}|}\right\} \qquad (5\text{-}1\emptyset)$$

and

$$\left(\frac{\dot{X}}{10^{-1}}\right) = 10\int \ddot{X}\,dt \qquad (5\text{-}11)$$

also

$$\left(\frac{X}{10^{-2}}\right) = 10\int \left(\frac{\dot{X}}{10^{-1}}\right)dt \qquad (5\text{-}12)$$

The circuit diagram for equations 5-1Ø through 5-12 is shown in figure 5-Ø8. Again, a time scale of Ø.1 seconds is used as described earlier.

The amount of dry friction in the circuit can be altered by changing the voltage as shown in the circuit diagram.

1 volt ≡ Ø.1 N/Kg of dry friction

and tests were carried out for different values of dry friction R.

5.4.1. SINUSOIDAL EXCITATION

As in the case of cubic stiffness, this circuit was also tested using sinusoidal input so that the results from this could be compared with the analytical data (chapter 3) to check the validity of the analogue circuit. The mobility modulus plots, together with the corresponding Nyquist diagrams, are shown in figure 5-Ø9. As usual, these data were analysed using a linear SDOF algorithm and the modal parameters identified are displayed in table 5-Ø3.

The 3-D diagrams are presented in figure 5-1Ø. These results compare very well with those obtained from analytical study, and it is therefore concluded that the circuit indeed represents the desired system.

5.4.2. RANDOM EXCITATION

Again, the FFT Analyser was used for these tests. The mobility modulus and the Nyquist plots obtained are shown in figure 5-11 and the modal properties extracted are given in table 5-Ø4. The loss factor plots for this case (figure 5-12) show no tendency to tilt as the amount of nonlinearity is increased. It is therefore concluded that nonlinearity cannot be detected from a single frequency-response curve when random excitation is used.

5.4.3. TRANSIENT EXCITATION

These tests were carried out in exactly the same manner as those for softening cubic stiffness case for transient excitation. The data from tests are displayed in figure 5-13 in the form of mobility modulus and Nyquist plot and loss factor plots are displayed in figure 5-14. Again, these data do not indicate the presence of any nonlinearities.

5.5. CONCLUSIONS

It is seen from the two types of nonlinearity considered that nonsinusoidal inputs generally produce flat loss factor plots. The small random variation of these surfaces cannot be attributed to the nonlinearities because it is more likely to be due to the small random errors in the measurements. Random and transient excitation appear to linearize the system but this does not mean that the random and transient produce more accurate modal properties than sinusoidal. The identified modal parameters in the tables show that all types of input give inaccurate modal properties when the data acquired from nonlinear systems are analysed using linear SDOF algorithm. A single frequency response curve obtained using nonsinusoidal excitation is not sufficient to identify or even to detect the presence of nonlinearities. Thus, one must be very careful when drawing conclusions from such data as the modal properties are most unlikely to be true representation of the structure.

SOFTENING CUBIC STIFFNESS (m^{-2})	NATURAL FREQUENCY (Hz)	LOSS FACTOR x1000	RMS ERROR (%)	MODAL CONSTANT x1000 (1/Kg)	MODAL PHASE (Deg)
50	15.8820	10.30	3.68	1000.7	17.35
200	15.8220	9.90	13.45	859.4	38.24
400	15.7660	6.70	18.01	644.9	59.00
600	15.7440	6.60	26.41	639.0	49.19
EXACT VALUE	15.9155	10	0	1000	0

TABLE 5-01 : Identified modal parameters as function of softening-cubic stiffness: Sinusoidal excitation.

SOFTENING CUBIC STIFFNESS (m^{-2})	NATURAL FREQUENCY (Hz)	LOSS FACTOR x1000	RMS ERROR (%)	MODAL CONSTANT x1000 (1/Kg)	MODAL PHASE (Deg)
50	15.9125	10.60	0.35	1012.5	-.04
200	15.8781	11.80	3.15	1075.5	.93
400	15.8437	14.60	1.11	1189.7	-2.21
600	15.8156	16.70	4.42	1188.1	-2.32
EXACT VALUE	15.9155	10	0	1000	0

TABLE 5-02 : Identified modal properties as function of softening-cubic stiffness: Random excitation.

DRY FRICTION (N/Kg)	NATURAL FREQUENCY (Hz)	LOSS FACTOR x1000	RMS ERROR (%)	MODAL CONSTANT x1000 (1/Kg)	MODAL PHASE (Deg)
Ø.ØØ	15.916Ø	1Ø.6Ø	1.44	1Ø11.3	1.8Ø
Ø.1Ø	15.914Ø	13.8Ø	Ø.35	1134.Ø	Ø.65
Ø.25	15.816Ø	7.69	Ø.87	2Ø24.6	16.57
EXACT VALUE	15.9155	1Ø	Ø	1ØØØ	Ø

TABLE 5-03 : Identified modal parameters as function of dry friction: Sinusoidal excitation.

DRY FRICTION (N/Kg)	NATURAL FREQUENCY (Hz)	LOSS FACTOR x1000	RMS ERROR (%)	MODAL CONSTANT x1000 (1/Kg)	MODAL PHASE (Deg)
Ø.1Ø	15.9131	11.4Ø	2.27	1ØØ1.4	Ø.25
Ø.15	15.91Ø6	12.3Ø	2.33	989.4	-2.78
Ø.2Ø	15.91Ø6	17.3Ø	2.ØØ	996.5	Ø.Ø8
Ø.25	15.9Ø82	47.9Ø	2.31	9ØØ.Ø	-Ø.Ø5
EXACT VALUE	15.9155	1Ø	Ø	1ØØØ	Ø

TABLE 5-04 : Identified modal parameters as function of dry friction: Random excitation.

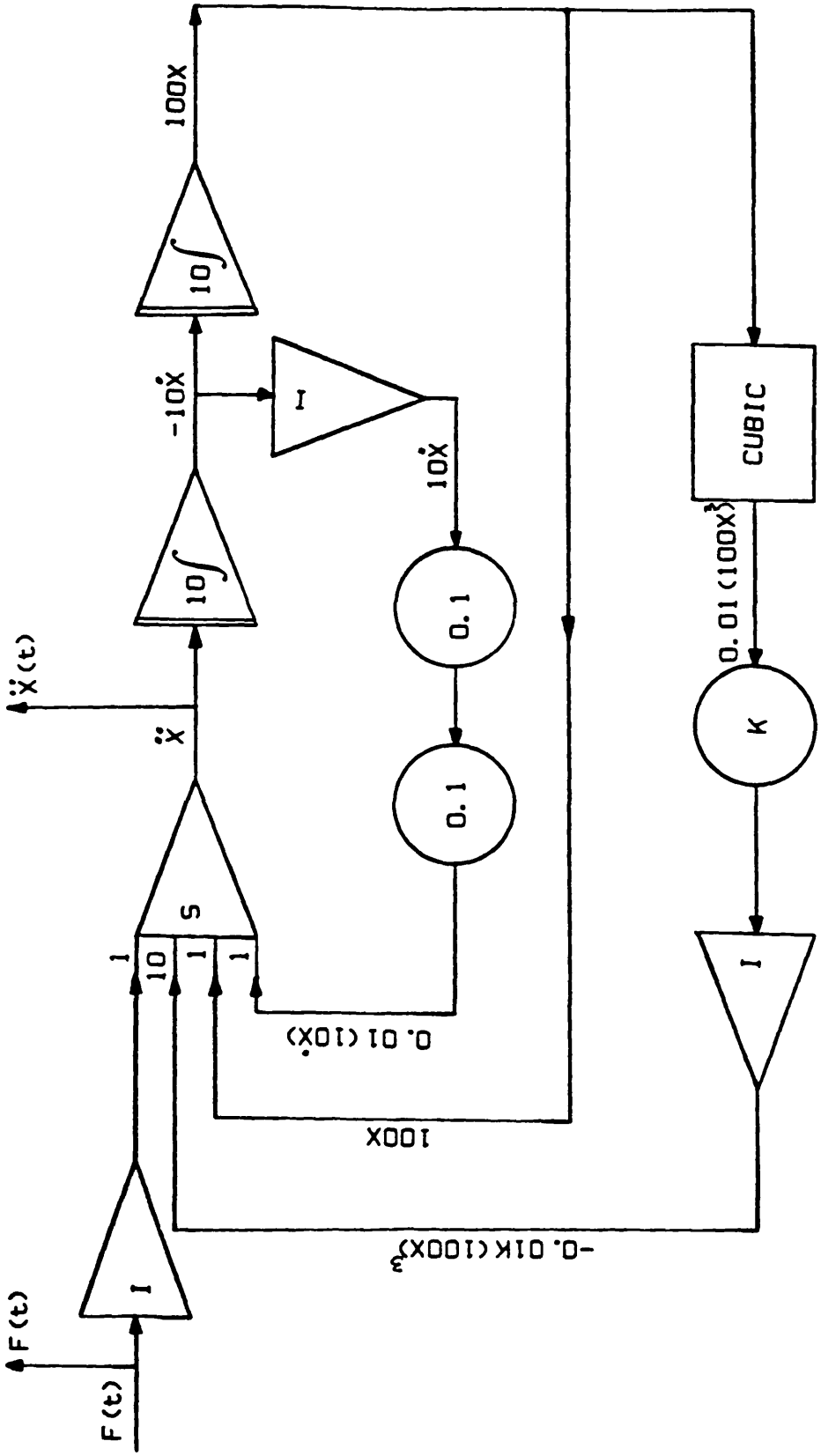

FIGURE 5-01 : Analogue circuit for SDOF system with softening cubic stiffness.

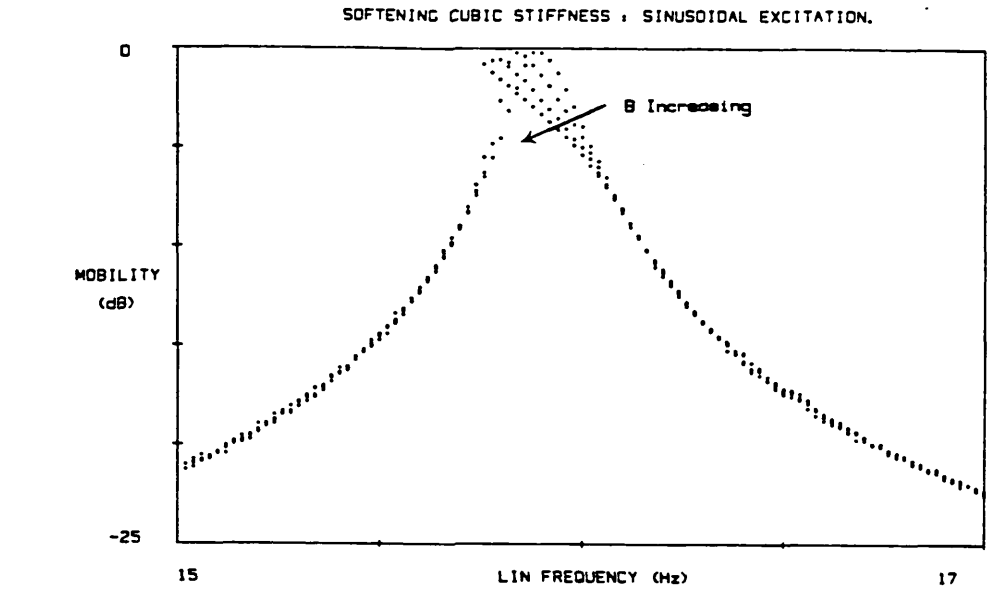

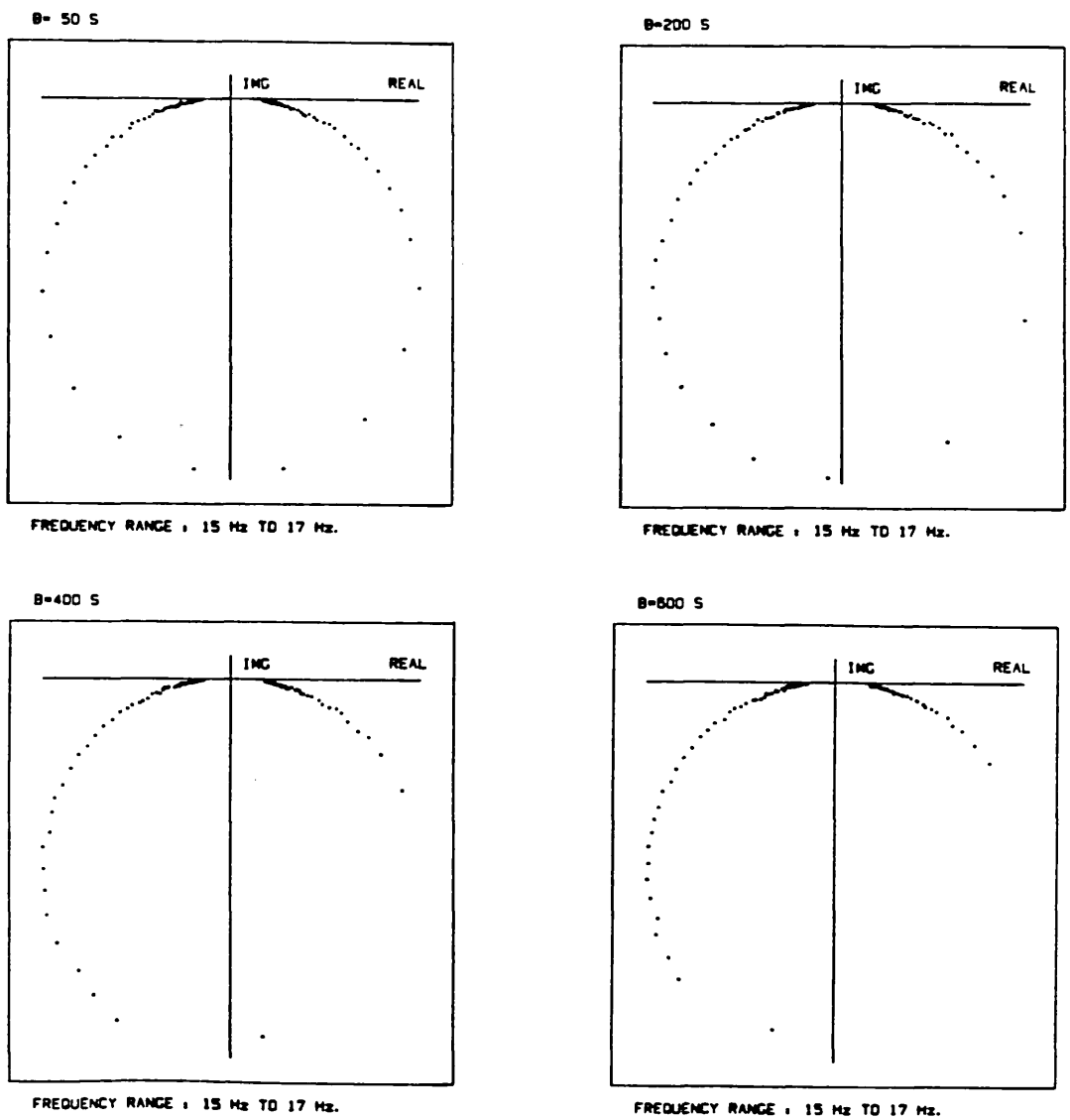

FIGURE 5-02 : Mobility modulus and Nyquist plots for varying levels of softening cubic stiffness: Sinusoidal excitation.

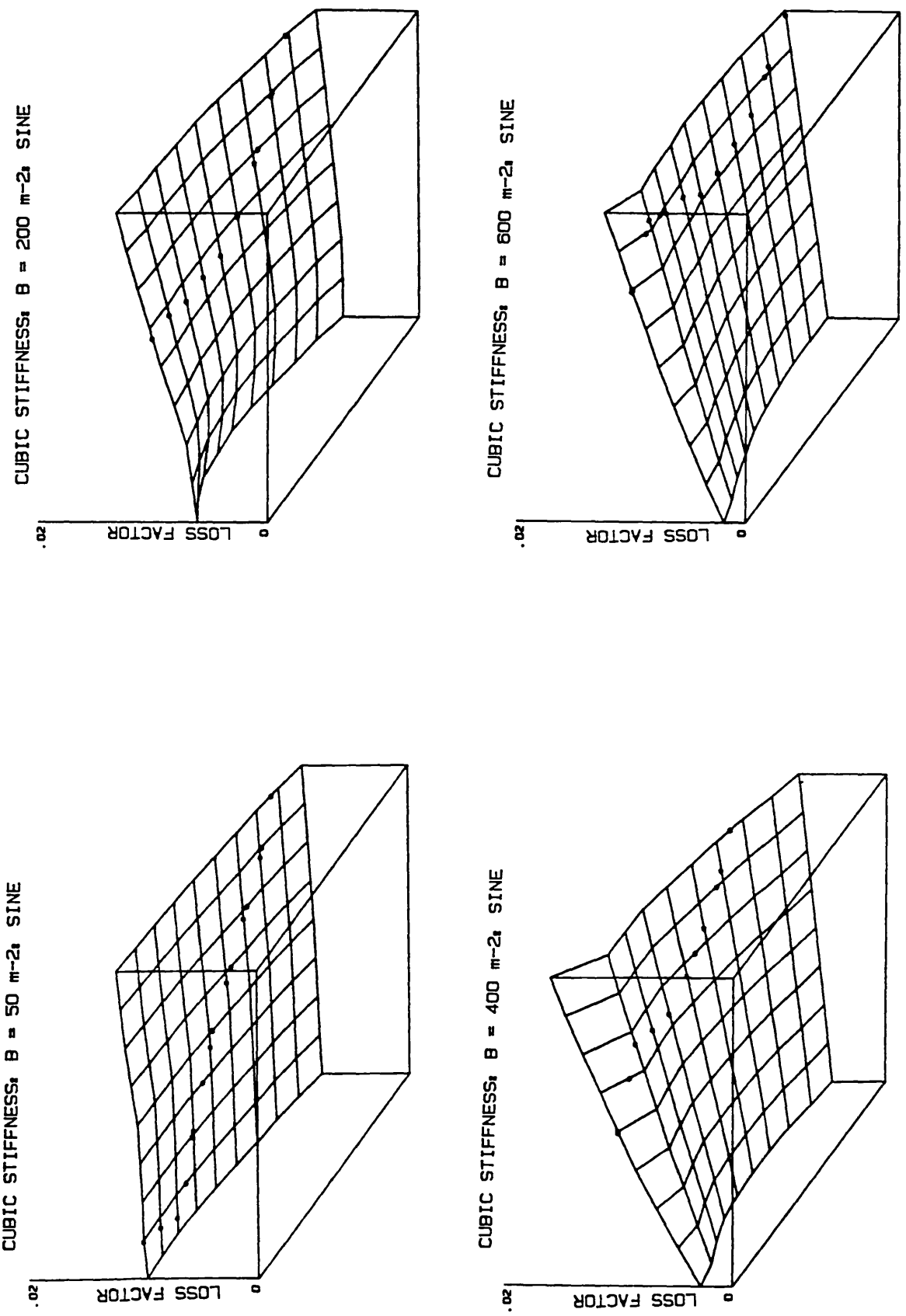

FIGURE 5-03 : Isometric loss factor plots for varying levels of softening cubic stiffness: Sinusoidal excitation.

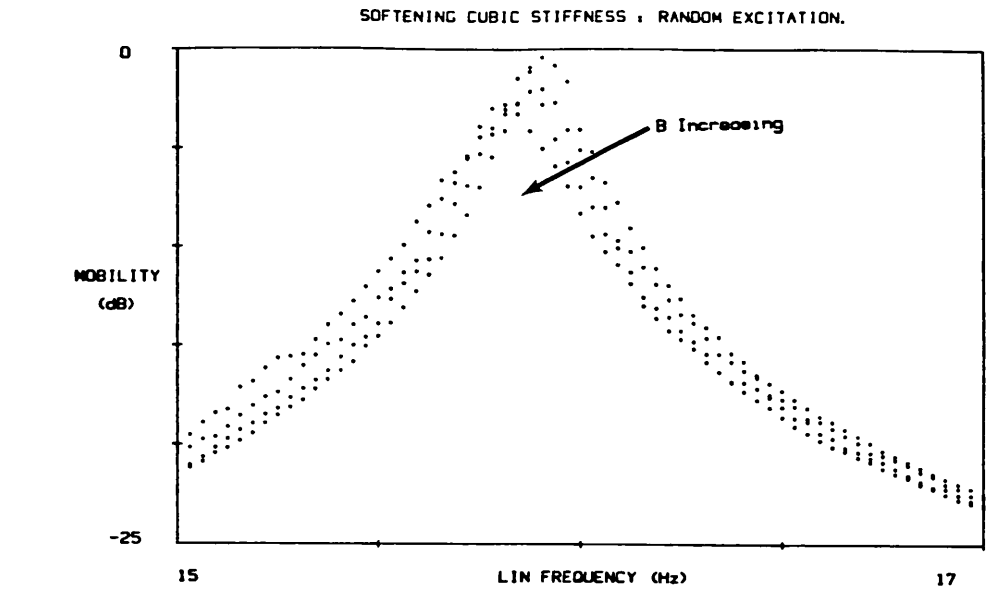

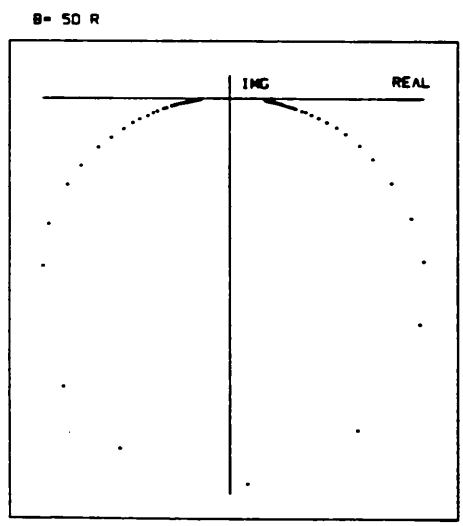

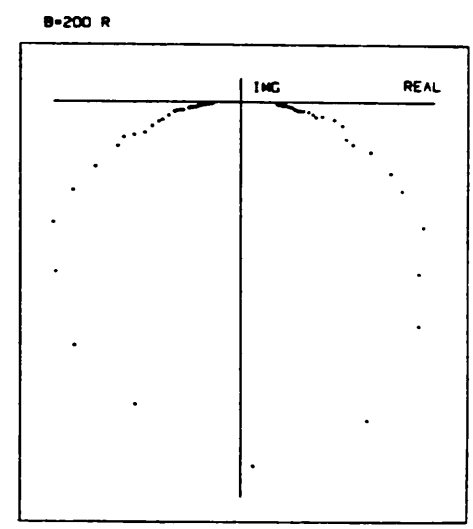

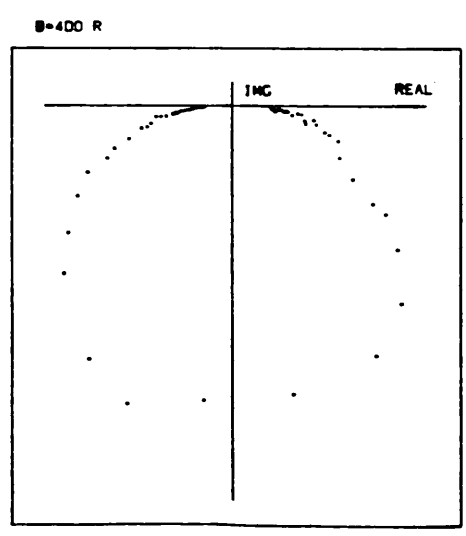

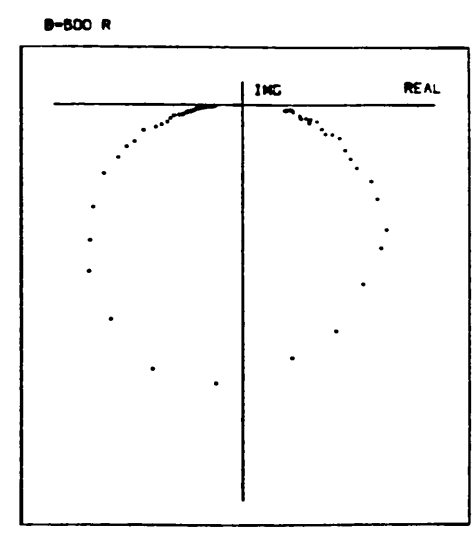

FIGURE 5-04 : Mobility modulus and Nyquist plots for varying levels of softening-cubic stiffness: Random excitation.

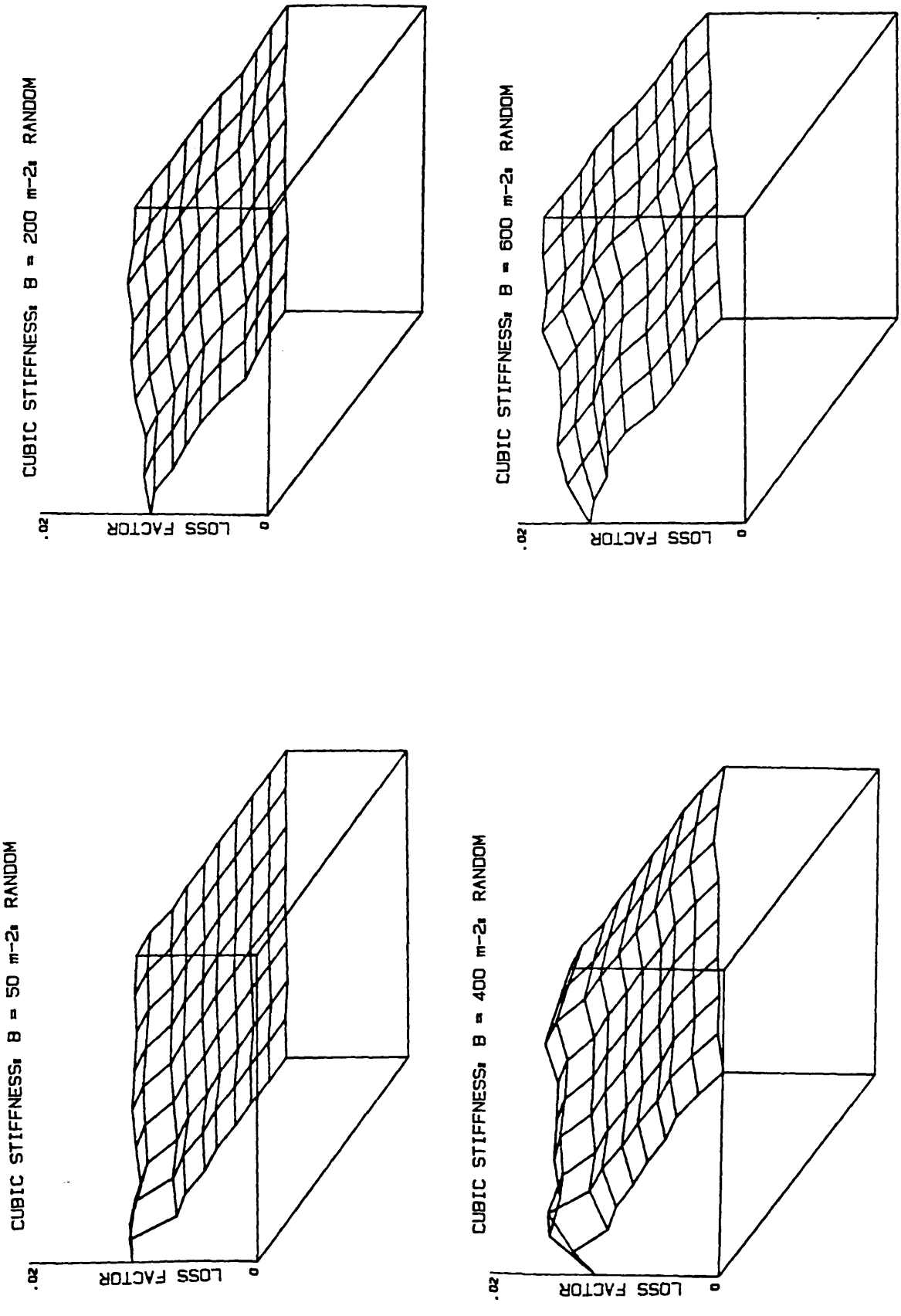

FIGURE 5-05 : Isometric loss factor plots for varying levels of softening cubic stiffness: Random excitation.

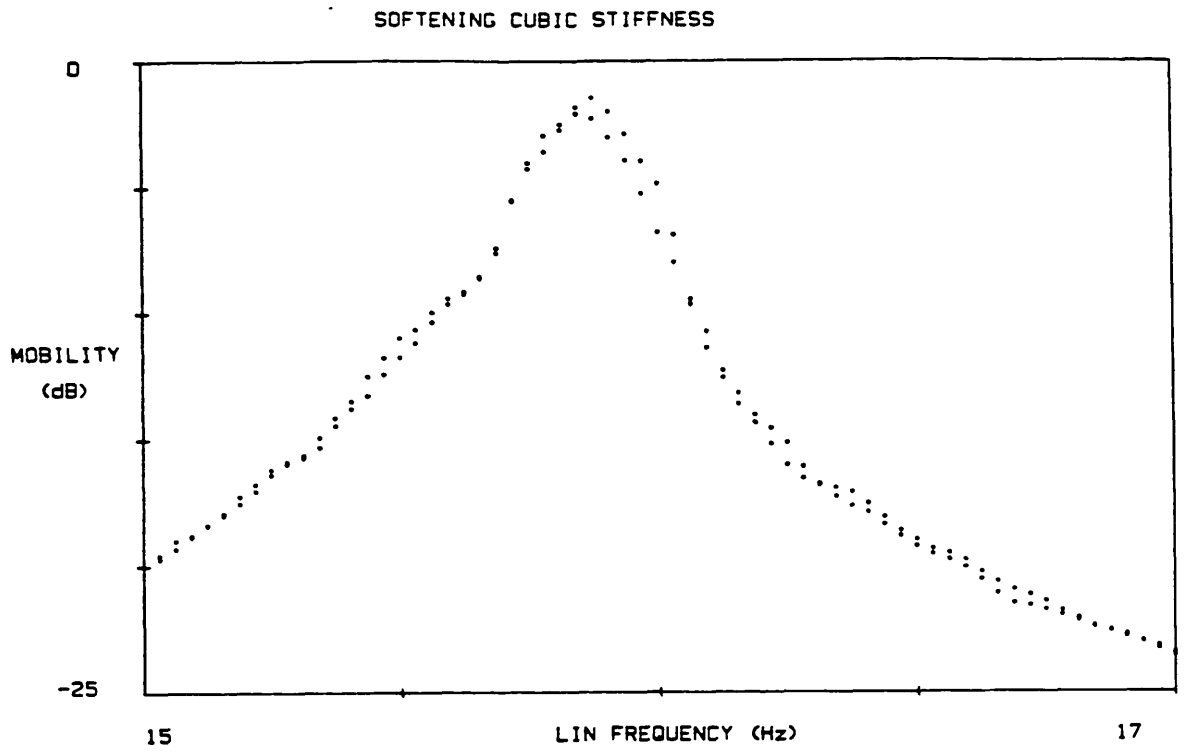

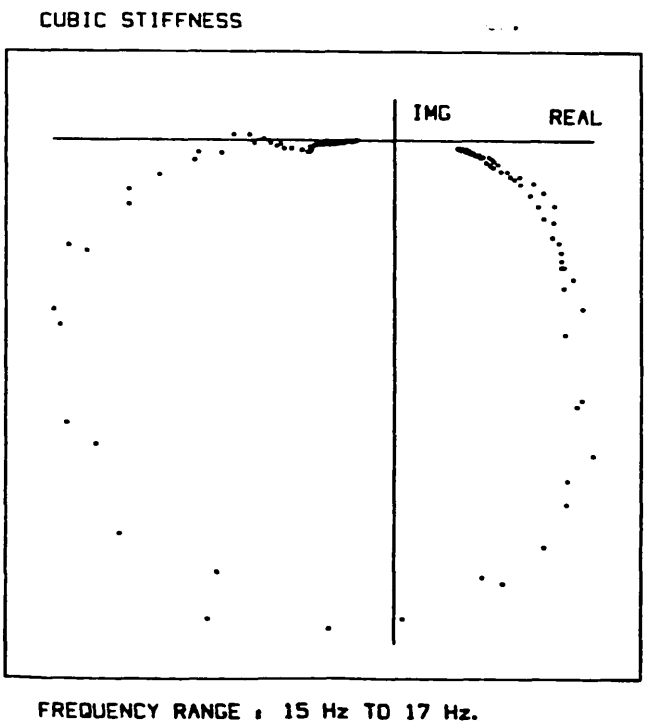

FIGURE 5-06 : Mobility modulus and Nyquist plots for softening cubic stiffness: Transient excitation.

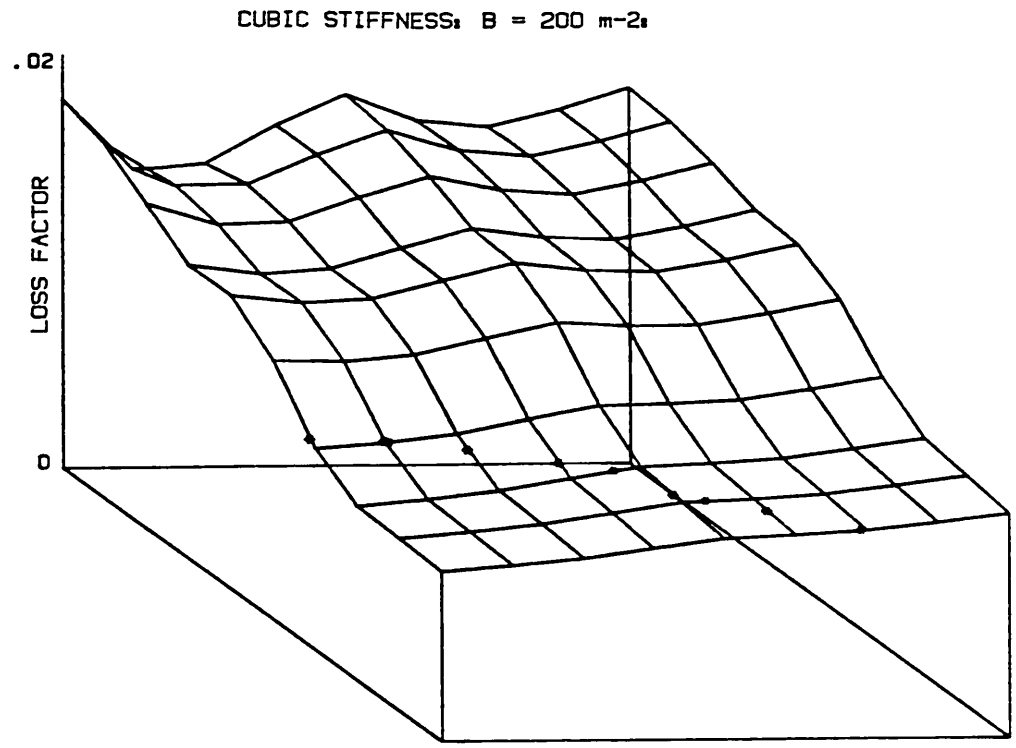

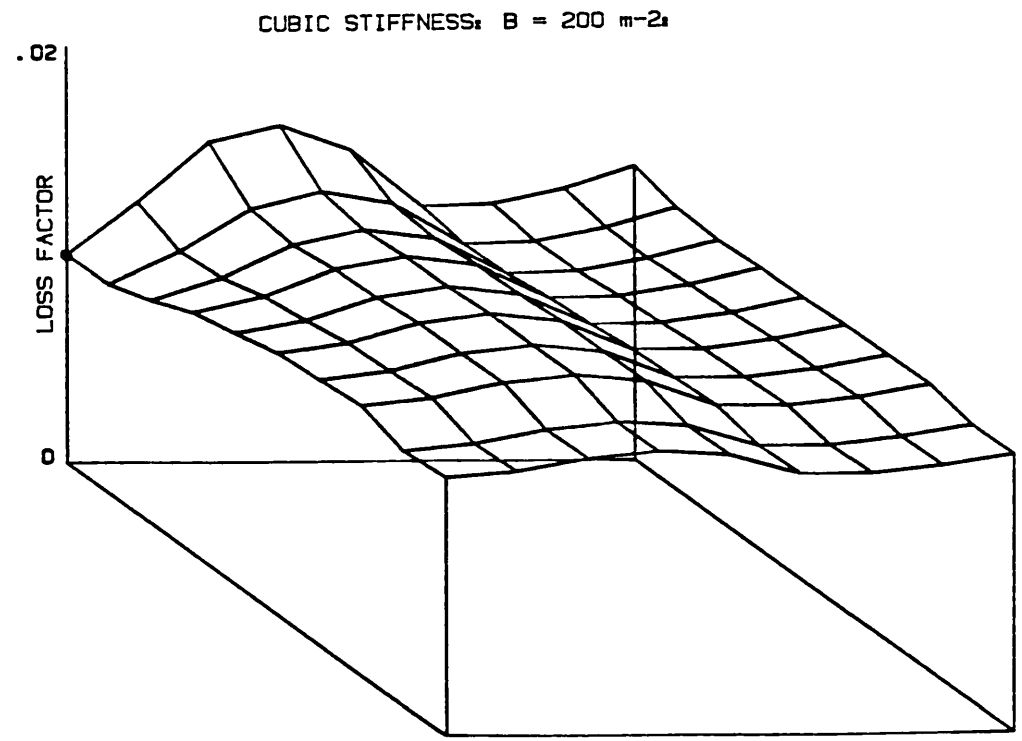

FIGURE 5-07 : Isometric loss factor plots for softening cubic stiffness: Transient excitation.

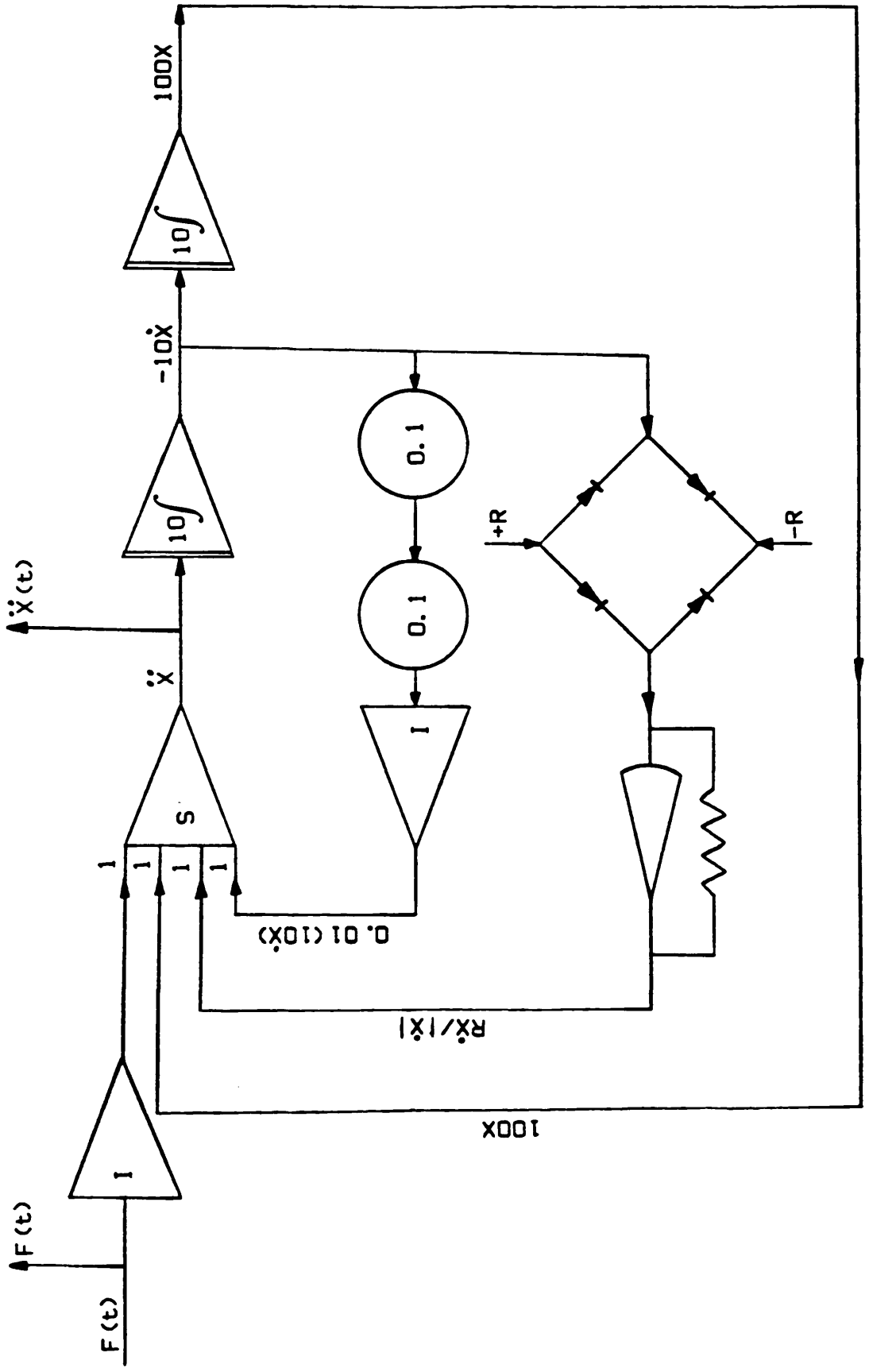

FIGURE 5-08 : Analogue circuit for single- degree-of-freedom system with dry friction.

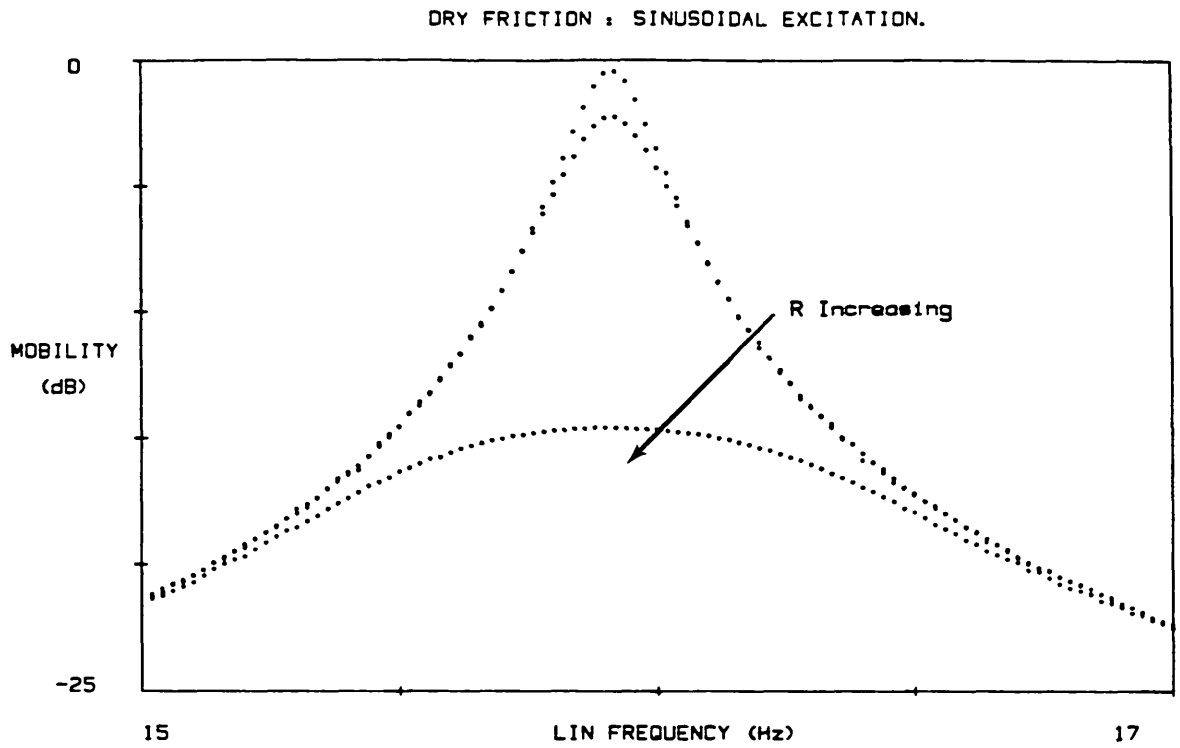

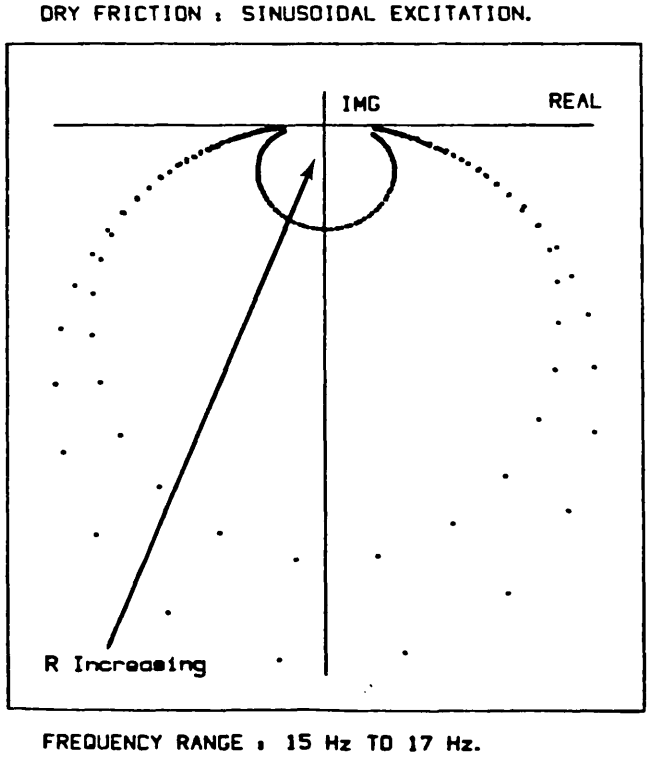

FIGURE 5-09 : Mobility modulus and Nyquist plots for varying levels of dry friction: Sinusoidal excitation.

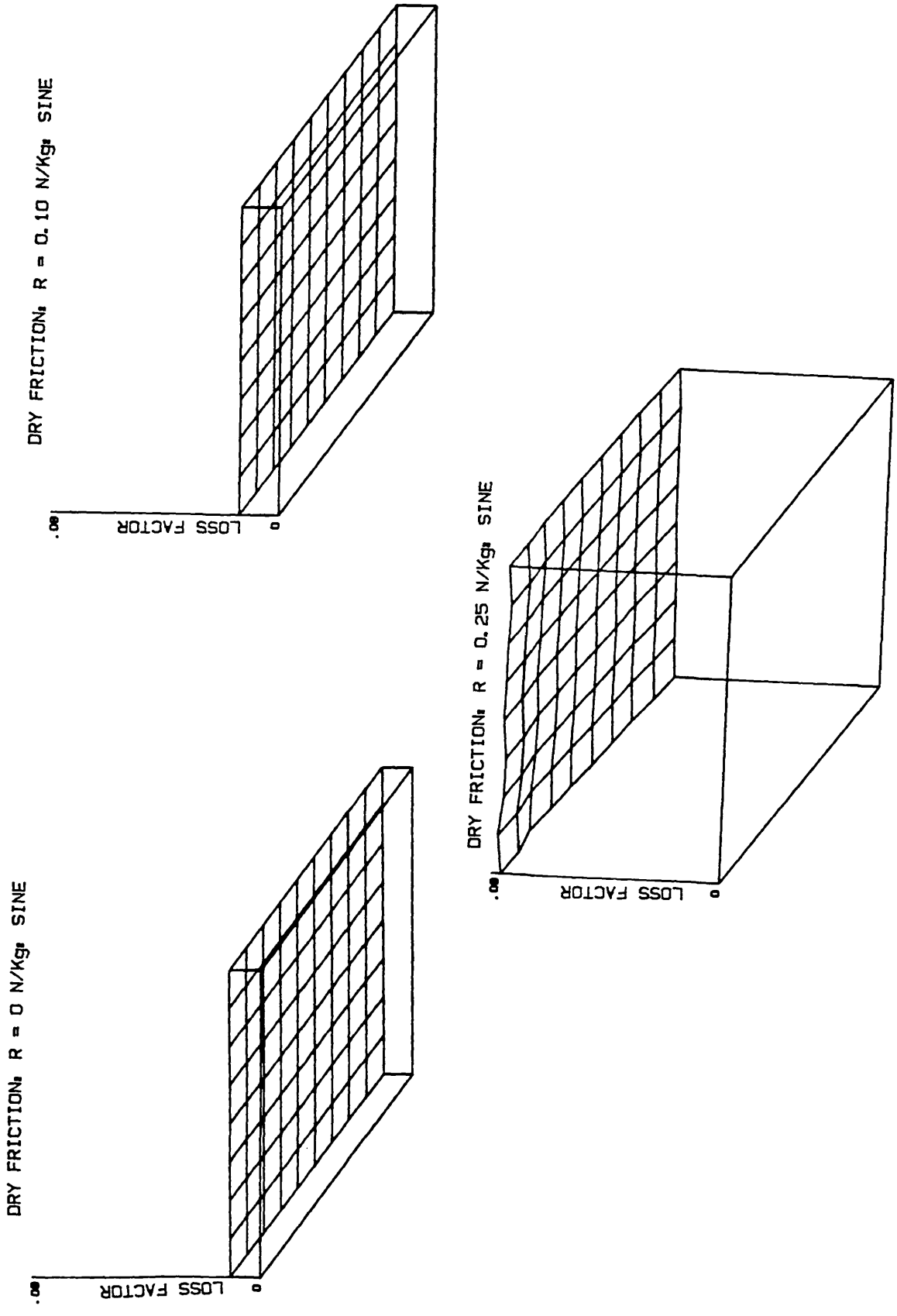

FIGURE 5-10 : Isometric loss factor plots for varying levels of dry friction: Sinusoidal excitation.

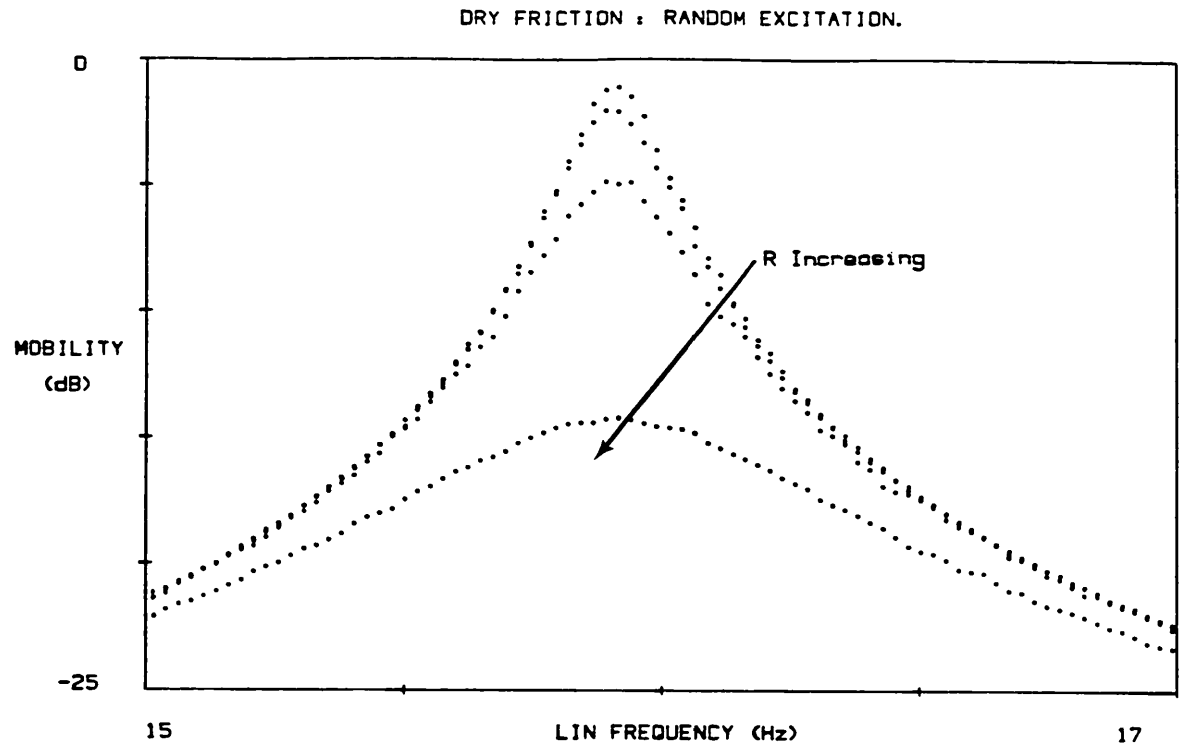

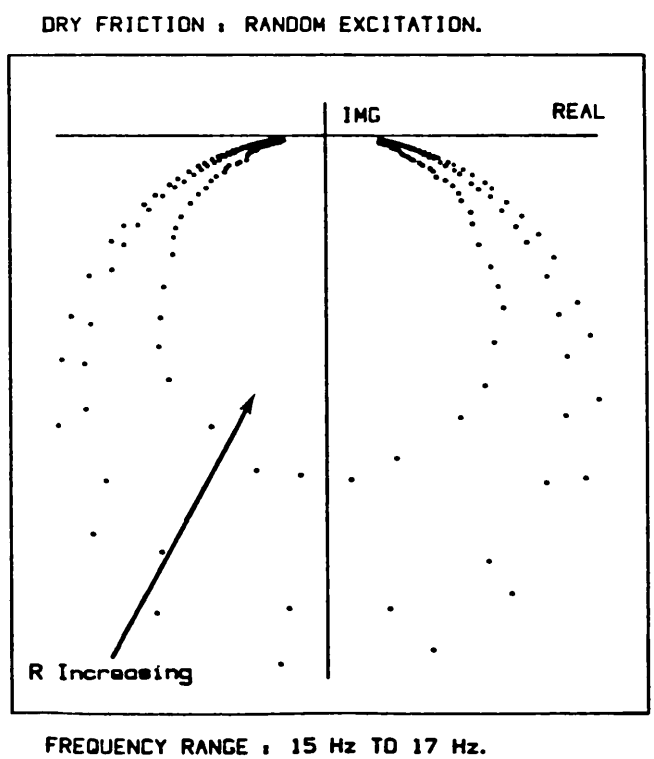

FIGURE 5-11 : Mobility modulus and Nyquist plots for varying levels of dry friction: Random excitation.

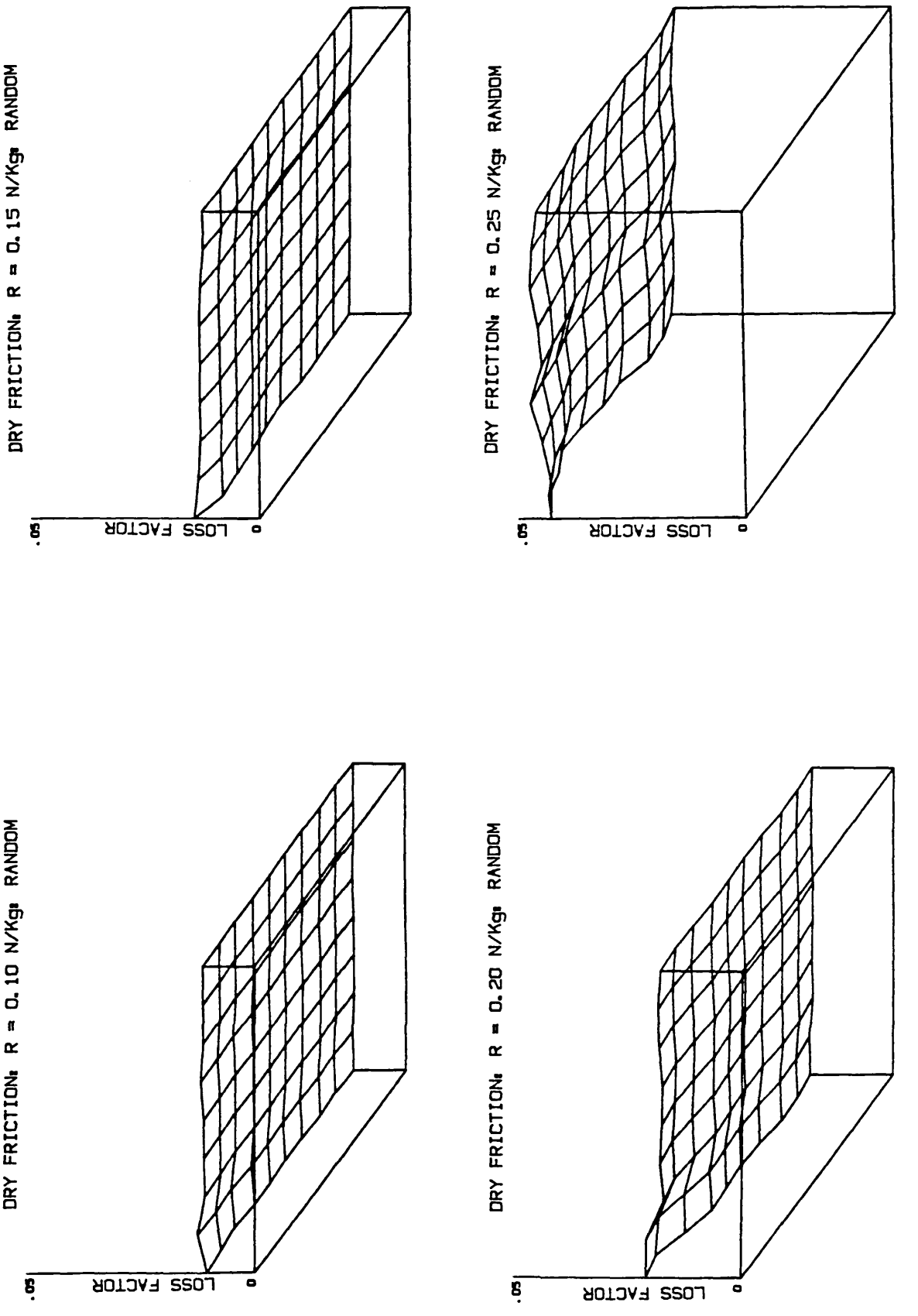

FIGURE 5-12 : Isometric loss factor plots for varying levels of dry friction: Random excitation.

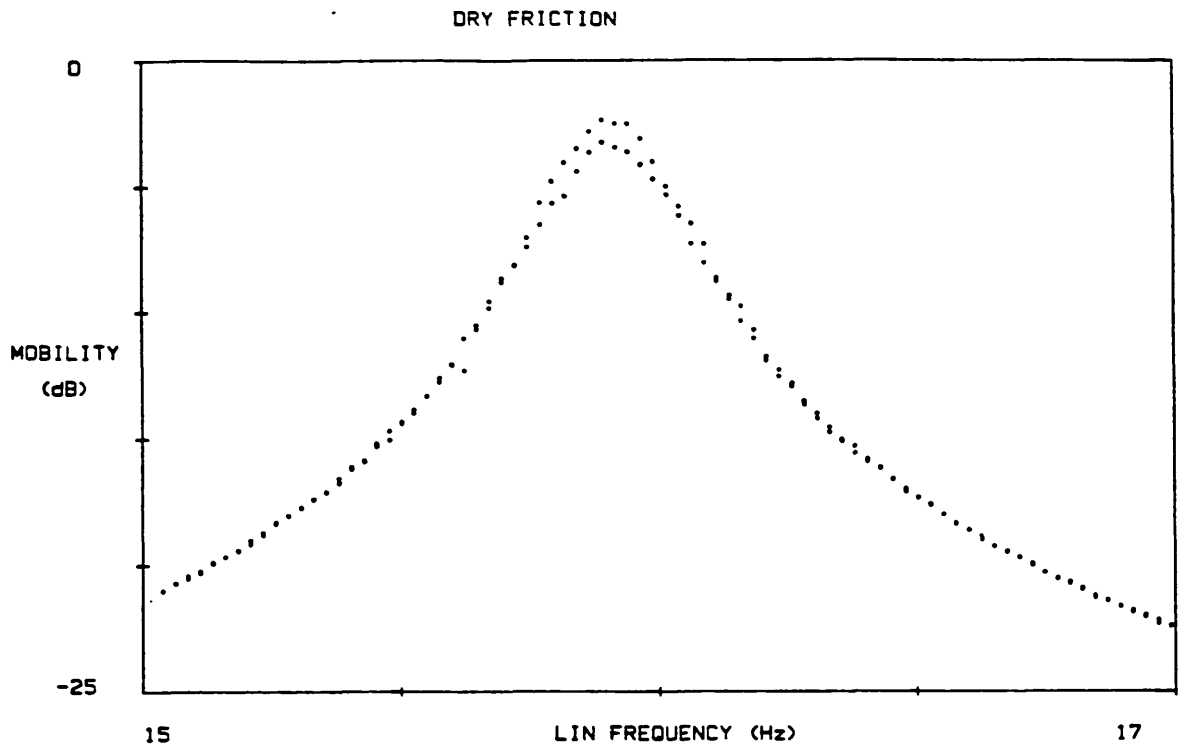

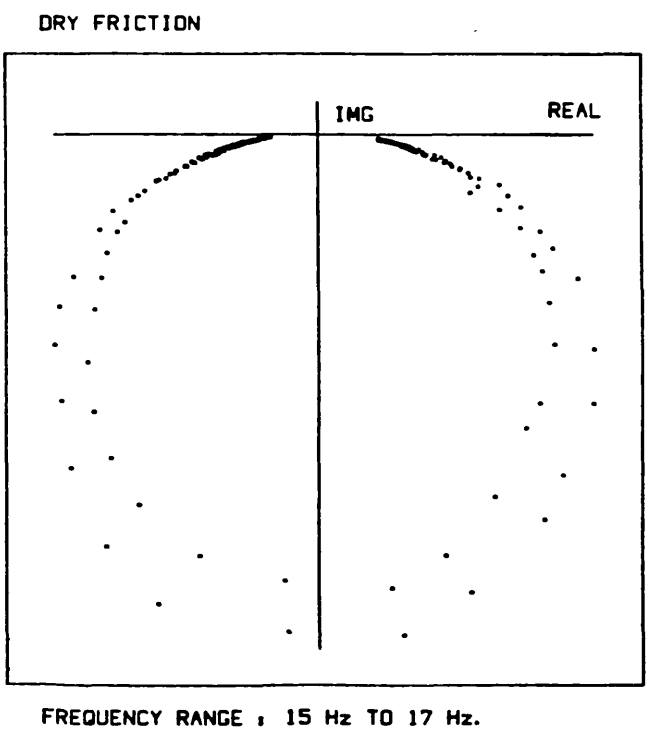

FIGURE 5-13 : Mobility modulus and Nyquist plots for dry friction: Transient excitation.

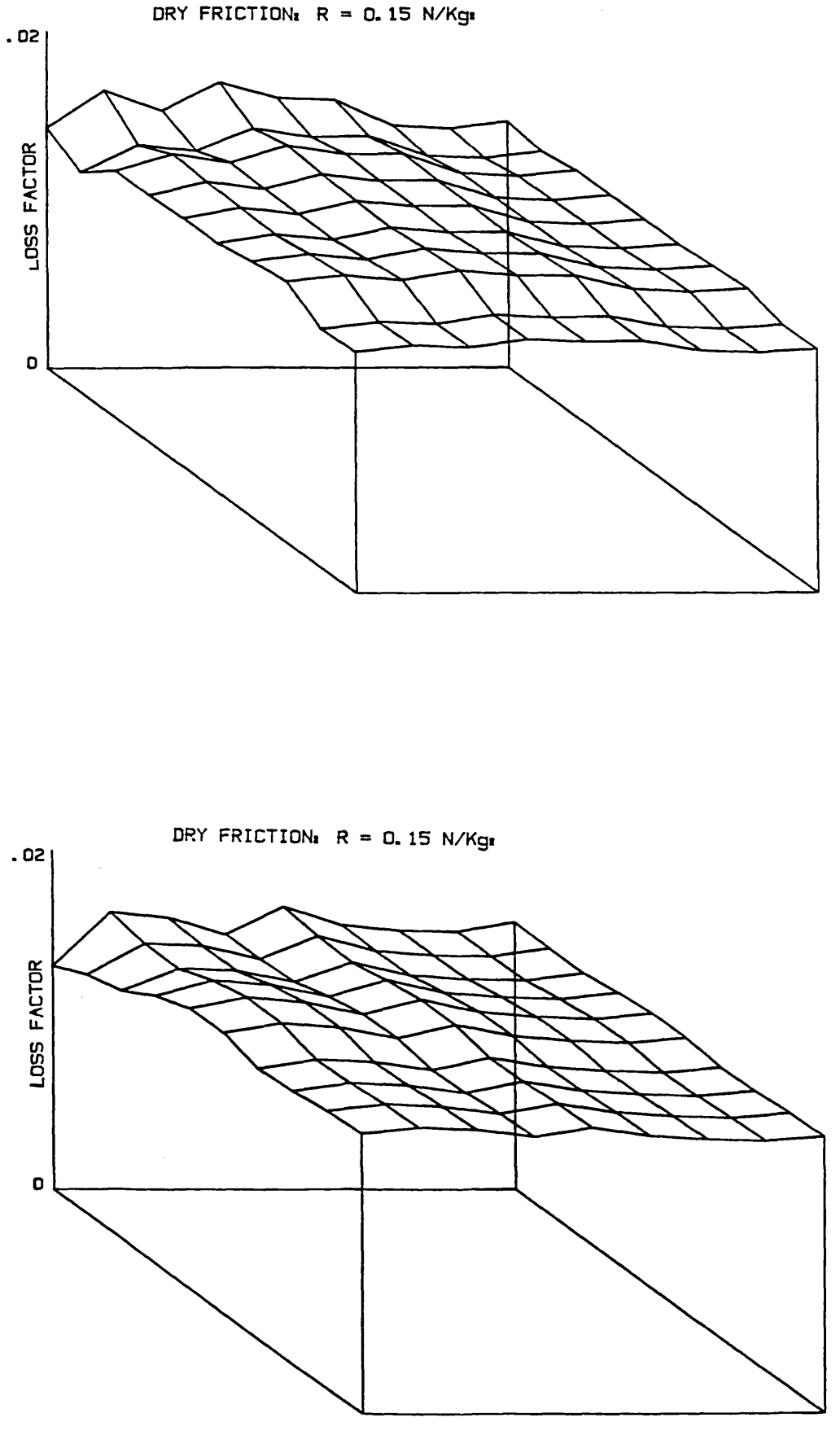

FIGURE 5-14 : Isometric loss factor plots for dry friction: Transient excitation.

CHAPTER

-6-

6. CORRELATION OF ANALYTICAL AND MEASURED MODAL PROPERTIES

6.1. INTRODUCTION

The theoretical study of complex vibrating structures centres around an analytical model and the ultimate test of such a model is how well it performs when it is applied to the problem it was designed to handle. When a model is used, it may lead to inaccurate predictions. The model is then modified, generally relying on 'trial and error' methods, frequently resulting in another equally unsuitable model. In dynamics, such model is often used anyway because it is usually better than nothing.

There is an increasing interest in techniques for improving or refining theoretical models for vibration analysis based on measurements of a structure's response under laboratory testing. Theoretical models which are to be used to predict dynamic response under shock or other complex loading may be validated and refined using measurements made under simpler and lower levels of excitation using the techniques of frequency response measurements. Much of the current activity in this area combines finite element (FE) modelling leading to prediction of undamped natural frequencies and mode shapes with modal testing techniques which permit the estimation of similar modal properties for an actual piece of hardware. All too often, however, the subsequent comparison of the two sets of results is based only on a qualitative correlation of theoretical and measured mode shapes together with a

quantitative comparison of their respective natural frequencies. Relatively few studies have addressed the problem of how to improve one or other set of results by systematic adjustment of the model based on a numerical comparison process between the two sets of modal data.

The objectives of this study are to explore methods of locating weaknesses in a mathematical model and of determining the necessary modifications which will bring the model into closer agreement with the actual (test) structure's vibration characteristics. There are two aspects to this process : that of location and that of correction of the discrepancies. A number of recent studies have dealt with the latter task (see chapter 1), but relatively few have dealt with the former problem of locating the errors or weaknesses which are in the analytical model.

Generally, it is assumed that the experimental set of data are the 'correct' values and that it is the theoretical model which is in error. However, it must always be kept in mind that errors will exist in the experimental results and at all stages in the process the possibility that it is the experimental data, and not the theoretical model, which are in error must be considered.

Having given attention to the quality of frequency response data in chapters 3, 4 and 5, we shall now consider a number of methods which make use of such data to validate the analytical model. In general this means using both the

natural frequencies and the mode shape data in a numerical comparison process. Of particular note is the use of the mass-normalised mode shape properties rather than the arbitrarily-scaled mode shape vectors which are often used.

6.2. COMPARISON OF MODELS

The two types of model can be compared at three stages of the analysis process - frequency response, modal properties or the spatial mass and stiffness matrices stages (figure 6-Ø1). Because of a shortage of experimental data, caused in many cases by a lack of time, it is not always possible to carry out the comparisons at all three stages. The usual practice is to compare the data in the form of frequency response plots and a visual comparison of modal properties. Very little effort has been devoted to the comparison of mass and stiffness matrices. This is mainly due to the fact that to obtain the full mass and stiffness matrices from an experimental approach requires a very large number of measurements.

The theory of comparison of modal properties is still in its infancy and so these methods are best illustrated by application to a case study. In this chapter we shall undertake a numerical study based on the 8 DOF mass-spring system shown in figure 6-Ø2. Two slightly different versions of this system were analysed, the only difference between these being in the stiffness of spring element k_{L3}, which was 1.95 MN/m in the datum case and 1.5Ø MN/m in the

second. The idea of using two models is that one represents the 'true' system - simulating data obtained from tests on an actual structure - while the second one represents a somewhat approximate model of the system - such as would be obtained from an FE analysis of a practical structure. Adjustment of the stiffness parameter k_{L3} represents the real situation where (at least) one of the system properties is slightly inaccurately modelled.

The eigenvalues and eigenvectors for the datum case (where k_{L3} = 1.95 MN/m) are assumed to be equivalent to experimental data and those for k_{L3} = 1.5Ø MN/m are taken as representing an FE model (table 6-Ø1). Thereafter, the two sets of modal properties will be referred to as the experimental and the FE model data.

6.2.1. COMPARISON OF NATURAL FREQUENCIES

Comparison of natural frequencies of the two models considered is a straightforward task. The percentage error in the natural frequencies is calculated for each mode (table 6-Ø2).

The natural frequencies of the FE model (k_{L3} = 1.5Ø MN/m), are lower than in the experimental (k_{L3} = 1.95 MN/m) values for all the modes. This is to be expected as the stiffness of one of the springs in the FE model is lower than the experimental model. A discrepancy of less than 3% in the natural frequency is often considered to be adequate for many practical situations and table 6-Ø2

shows that the natural frequencies (except for mode 4) lie below this value. In practice, an FE model which is so close to the experimental model would be considered to be very good and no further alterations or modifications would be carried out. However, in this case we know that the stiffness of spring k_{L3} was changed by 23% and hence the two stiffness matrices, and therefore the two models, would not be considered to be in good agreement.

The natural frequencies do not indicate the nature or the location of the discrepancy because a change in the natural frequencies can be attributed to a change in the mass, stiffness or both mass and stiffness matrices. Thus it is impossible to say from the comparison of natural frequencies only whether it is the mass or the stiffness matrix that is in error.

6.2.2. COMPARISON OF MODE SHAPES

There are two main techniques that are used to compare the mode shape vectors. First, the experimental and the FE mode shape plots are overlaid (figure 6-Ø3) revealing the nature of any distortion in the mode of vibration of the structure at points of interest. Figure 6-Ø3 indicates that modes 1 and 3 of the 8 DOF system are of the opposite sign (more about this later). There appears to be excellent agreement between the two sets of mode shapes although it is still not possible to locate the specific cause of the discrepancy between the two versions of the 8 DOF system from these mode shape graphs.

The second method [51,52], is a little more quantitative than the first and involves plotting the elements of the mode shape vector from one model against the corresponding elements from that of the other model i.e. experimental against the FE mode shape vector (figure 6-Ø4). Ideally, all points on such a plot should lie along a line of slope ± 1 and deviations from this ideal line can be used to indicate the degree of discrepancy between the two mode shapes. As mentioned earlier, modes 1 and 3 of the 8 DOF system are of the opposite sign and hence lie close to a line of slope -1, while all the other modes lie near a line of slope +1 because in the former case the elements in the measured and predicted mode shape vectors have one-to-one ratio and in the latter case the ratio is minus-one-to-one.

Here again, the correlation is very good but there is no indication of the location or the size of discrepancy between the two models. Nevertheless, this technique is useful in cases of very complex-shaped modes where a mode shape plot may not be immediately recognizable, and the question of whether a particular predicted mode relates to a particular measured mode can be resolved quickly.

6.3. COMPARISON OF 'PSEUDO' INVERSE MASS AND STIFFNESS MATRICES

In the last section the natural frequencies and the mode shapes were compared separately by taking data for one mode at a time. No attempt was made to combine these two sets of properties. Now we shall see how these two parts of the modal model (natural frequencies and mode shapes) may be combined into a single set of data that may be compared taking into account several modes simultaneously. The following theory explains the basis.

For a system that is completely defined by N degrees of freedom, the eigensolution will yield N natural frequencies and associated mode shape vectors. If the mode shapes are mass-normalised, then the following relationship may be established.

$$[\Phi]_{NN}^{T}[M]_{NN}[\Phi]_{NN} = [I]_{NN}$$

$$[\Phi]_{NN}^{T}[K]_{NN}[\Phi]_{NN} = \left[\lambda_r^2\right]_{NN} \qquad (6\text{-}\emptyset 1)$$

where $\left[\lambda_r^2\right]$ - diagonal matrix of eigenvalues;

$[\Phi]$ - mass normalised eigenvectors;

$[M]$ - system mass matrix;

and $[K]$ - system stiffness matrix.

Rearranging equation 6-Ø1 gives;

$$[M]_{NN}^{-1} = [\Phi]_{NN}[\Phi]_{NN}^{T}$$

$$[K]_{NN}^{-1} = [\Phi]_{NN}\left[1/\lambda_r^2\right]_{NN}[\Phi]_{NN}^{T} \qquad (6\text{-}\emptyset 2)$$

where $[M]^{-1}$ - system inverse mass matrix;

$[K]^{-1}$ - system inverse stiffness (flexibility) matrix.

If only m modes are available, but the full (Nx1) eigenvector is obtained at each of the m known natural frequencies, these may be combined to form the reduced modal matrix $[\Phi^R]_{Nxm}$. For only one mode the modal matrix reduces to a vector $\{\Phi^R\}_{Nx1}$.

Equation 6-Ø2 may be used to compute the 'pseudo inverse mass' and 'pseudo inverse stiffness' matrices for a single mode of interest as shown below;

$$[\overset{*}{M}]^{-1}_{NN} = \{\Phi^R\}_{N1}\{\Phi^R\}^T_{1N}$$

$$[\overset{*}{K}]^{-1}_{NN} = \{\Phi^R\}_{N1}\left[1/\lambda_r^2\right]_{1\times1}\{\Phi^R\}^T_{1N} \qquad (6\text{-}Ø3)$$

where $[\overset{*}{M}]^{-1}$ - 'pseudo' inverse mass matrix;

and $[\overset{*}{K}]^{-1}$ - 'pseudo' inverse stiffness matrix.

A 'pseudo' matrix has the same dimensions as the full matrix (i.e. NxN) but the elements in such a matrix are not identical to those in the full (or complete) equivalent (see appendix 1Ø.2). Pseudo matrices will be represented with an asterisk as in equation 6-Ø3.

In the case of a reduced modal matrix $[\Phi^R]_{Nxm}$, equations 6-Ø3 may be modified to give;

$$[\overset{*}{M}]^{-1}_{NN} = [\Phi^R]_{Nm}[\Phi^R]^T_{mN}$$

$$[\overset{*}{K}]^{-1}_{NN} = [\Phi^R]_{Nm}\left[1/\lambda_r^2\right]_{mm}[\Phi^R]^T_{mN} \qquad (6\text{-}\emptyset4)$$

Equation 6-Ø3 is a special case of equation 6-Ø4 for m = 1.

As the number of modes (m) is increased, the elements in the pseudo matrices converge towards the values of the corresponding elements in the full matrix and, of-course, when the number of modes (m) and the number of coordinates (N) are the same, the pseudo matrices are identical to the full (complete) matrices. In mathematical form;

$$\lim_{m \mapsto N}\left[[\overset{*}{M}]^{-1}_{NN}\right] \mapsto [M]^{-1}_{NN}$$

$$\lim_{m \mapsto N}\left[[\overset{*}{K}]^{-1}_{NN}\right] \mapsto [K]^{-1}_{NN} \qquad (6\text{-}\emptyset5)$$

Equation 6-Ø4 offers a method that can be utilized to compare experimental and analytical modal properties. By taking m modes at n points of interest on the structure, the experimental pseudo inverse mass $[\overset{*}{M}_e]^{-1}$ and pseudo inverse stiffness $[\overset{*}{K}_e]^{-1}$ matrices may be computed using equation 6-Ø4 (n < N). The corresponding m modes at the same n points from the analytical model gives the analytical pseudo inverse mass $[\overset{*}{M}_p]^{-1}$ and pseudo inverse stiffness $[\overset{*}{K}_p]^{-1}$ matrices. Because of the discrepancies in the experimental and analytical models, these matrices should

not in general be identical but the elements will be very similar for small differences in the two models. Hence, the difference in the two pseudo inverse mass and two pseudo inverse stiffness matrices can be used as a measure of the discrepancies in the two models i.e.

$$[D_m]_{nn} = [\overset{*}{M}_e]^{-1}_{nn} - [\overset{*}{M}_p]^{-1}_{nn}$$

$$[D_k]_{nn} = [\overset{*}{K}_e]^{-1}_{nn} - [\overset{*}{K}_p]^{-1}_{nn} \qquad (6\text{-}\emptyset6)$$

where $[D_m]$ - difference of pseudo inverse mass matrices;

$[D_k]$ - difference of pseudo inverse stiffness matrices;

$[\overset{*}{M}_e]^{-1}$ - experimental pseudo inverse mass matrix;

$[\overset{*}{M}_p]^{-1}$ - analytical (FE) pseudo inverse mass matrix;

$[\overset{*}{K}_e]^{-1}$ - experimental pseudo inverse stiffness matrix;

$[\overset{*}{K}_p]^{-1}$ - analytical (FE) pseudo inverse stiffness matrix.

In terms of modal properties, the difference matrices $[D_m]$ and $[D_k]$ are given by;

$$[D_m]_{nn} = [\Phi_e^R]_{nm}[\Phi_e^R]^T_{mn} - [\Phi_p^R]_{nm}[\Phi_p^R]^T_{mn}$$

$$[D_k]_{nn} = [\Phi_e^R]_{nm}\left[1/\lambda^2_{re}\right]_{mm}[\Phi_e^R]^T_{mn} - [\Phi_p^R]_{nm}\left[1/\lambda^2_{rp}\right]_{mm}[\Phi_p^R]^T_{mn} \qquad (6\text{-}\emptyset7)$$

where $[\Phi_e^R]$ - experimental eigenvector matrix containing m modes at n coordinates;

$[\Phi_p^R]$ - analytical eigenvector matrix containing m modes at n coordinates corresponding to the

matrix $[\Phi_e^R]$;

$[1/\lambda_{re}^2]$ - diagonal matrix containing the reciprocals of m measured eigenvalues;

$[1/\lambda_{rp}^2]$ - diagonal matrix containing the reciprocals of m analytical eigenvalues corresponding to m measured modes.

Using the modal data of table 6-Ø1 and equation 6-Ø7, we shall compute the pseudo inverse mass and the pseudo inverse stiffness matrices for different combinations of the modes. Figure 6-Ø5 shows some of the difference of pseudo inverse mass matrices plotted on 3-D diagrams while in figure 6-Ø6 the difference of pseudo inverse stiffness matrices are displayed.

Since the aim is to locate the coordinates of the largest elements in the difference matrices, possibly indicating the area of largest discrepancy it was more convenient to plot the absolute values of the elements in the difference matrices. The heading on the plots (MM1, MM1 MM2 MM3 etc.) indicates which modes have been used to compute the difference matrix: e.g. 'MM1' means it was computed from mode 1 and in the case of 'MM1 MM2 MM3', the difference matrix was computed using 3 modes; numbers 1, 2 and 3. (M - mass; S - stiffness). The diagrams shown are those for an increasing number of modes in the calculation of the difference matrices - starting with a single mode and going up to the complete set of 8 modes.

The difference plots of pseudo inverse mass matrices

(figure 6-Ø5) do not show any clear trend in the shape of the surfaces of these diagrams. They vary over a wide range but the plot 'MM1' shows a flat surface with very small (almost zero) values at every point, indicating a good agreement between the two sets of modal properties based just on the first mode. This is also confirmed by the small error in the natural frequency for this mode (Ø.Ø54%) and also the comparison of mode shapes, which showed very little discrepancy (figure 6-Ø3).

The last diagram, calculated using all 8 modes, also has a flat surface with almost zero value at every point. This is to be expected because the mass matrices of the two versions of the 8 DOF system are identical and when all 8 modes are used to calculated the difference matrix it gives the difference of the inverse of two identical mass matrices, which is a null matrix.

Figure 6-Ø6 shows the difference in the experimental (k_{L3} = 1.95 MN/m) and FE (k_{L3} = 1.5Ø MN/m) pseudo inverse stiffness matrices. Again, the plot obtained using just the first mode (SM1) shows very little discrepancy between the two models. There exists no clear indication about the amount or the location of discrepancy which is between the coordinates X_2 and X_3 in this case. As the number of modes is increased, large peaks start to appear on the diagrams but these are not at the coordinates X_2 and X_3. Thus, it appears as though this technique can only be used to compare the modal properties and not to locate the areas of poor modelling.

6.4. COMPARISON OF SPATIAL PROPERTIES

6.4.1. DERIVATION OF ERROR MATRIX EQUATION

The comparison of modal properties and pseudo inverse matrices did not yield the required information about the two models- namely, the area of weak modelling could not be located by these techniques - and we must look further to find another approach. Suppose the full (or complete) stiffness matrices were available for the experimental model as well as for the FE model, then the difference between these two matrices will give not only the amount of any discrepancy in the stiffness matrix but also the coordinates of the largest errors which are directly related to the area of poor modelling. The same process can also be carried out for the mass matrices but in the analysis presented here only stiffness matrices will be considered.

Let $[K_e]$ - be the exact stiffness matrix (experimental model);

$[K_p]$ - be the approximate stiffness matrix (FE model);

and $[E_k]$ - stiffness error matrix such that;

$$[E_k] = [K_e] - [K_p] \qquad (6\text{-}\emptyset 8)$$

For the 8 DOF mass-spring system both the experimental and the FE complete stiffness matrices are known, and hence the EXACT stiffness error matrix $[E_k]$ can be calculated using equation 6-Ø8. Again, this matrix may be examined by representing its elements on an isometric plot

(figure 6-Ø7). The stiffness plot is basically flat with zero values except at the elements (2,2), (2,3), (3,2) and (3,3), indicating an error between coordinates X_2 and X_3 (i.e. spring k_{L3}). The amount of error is given by the height of the peak of the plot. The mass error matrix plot (not shown) has zero elements everywhere because the mass matrices for the two versions of the 8 DOF system are identical.

In practice, the full experimental stiffness matrix $[K_e]$ is not known because to construct such a matrix requires a very large number of measurements to be performed. Even if it were possible to carry out such a large number of measurements, it is not easy to measure the rotational terms and hence the experimental matrix which contains rotational coordinates could not be assumed to be more accurate than the FE matrix. For these reasons the full $[K_e]$ matrix is normally not available and consequently the exact error matrix cannot be calculated using equation 6-Ø8. However, it is possible to compute an approximate error matrix, even with incomplete experimental data, by considering pseudo inverse stiffness matrices. Rearranging equation 6-Ø8;

$$[K_e] = [K_p] + [E_k] \qquad (6\text{-}Ø9)$$

and inverting both sides gives;

$$[K_e]^{-1} = \Big[[K_p] + [E_k] \Big]^{-1}$$

$$= \Big([K_p] \Big[[I] + [K_p]^{-1} [E_k] \Big] \Big)^{-1}$$

$$[K_e]^{-1} = \left[[I] + [K_p]^{-1}[E_k]\right]^{-1}[K_p]^{-1} \qquad (6\text{-}10)$$

Considering the expression in the large square brackets, that is;

$$\left[[I] + [K_p]^{-1}[E_k]\right]^{-1} \qquad (6\text{-}11)$$

and provided that the matrix ($[K_p]^{-1}[E_k]$) is small i.e.

$$\left[[K_p]^{-1}[E_k]\right]^{\infty} = [0] \qquad (6\text{-}12)$$

expression 6-11 can be expanded using the Binomial expansion in the matrix form [53];

$$\left[[I] + [K_p]^{-1}[E_k]\right]^{-1} = [I] - [K_p]^{-1}[E_k] + \left[[K_p]^{-1}[E_k]\right]^2 - \left[[K_p]^{-1}[E_k]\right]^3 + \ldots\ldots \qquad (6\text{-}13)$$

Substituting equation 6-13 into equation 6-10 and post multiplying throughout by $[K_p]^{-1}$ gives;

$$[K_e]^{-1} = [K_p]^{-1} - [K_p]^{-1}[E_k][K_p]^{-1} + \left[[K_p]^{-1}[E_k]\right]^2[K_p]^{-1} - \left[[K_p]^{-1}[E_k]\right]^3[K_p]^{-1} + \ldots\ldots (6\text{-}14)$$

If the matrix product ($[K_p]^{-1}[E_k]$) is such that its square and higher powers are small compared with the matrix $[K_p]$, meaning the FE model closely resembles the experimental model, then equation 6-14 can be approximated by its first two terms i.e.;

$$[K_e]^{-1} \approx [K_p]^{-1} - [K_p]^{-1}[E_k][K_p]^{-1}$$

or $$[K_p]^{-1}[E_k][K_p]^{-1} \approx [K_p]^{-1} - [K_e]^{-1}$$

Pre-and post-multiplying both sides by matrix $[K_p]$ gives;

$$[E_k] \approx [K_p]\left[[K_p]^{-1} - [K_e]^{-1}\right][K_p] \qquad (6\text{-}15)$$

The above equation is a general expression giving the approximate error matrix $[E_k]$ in terms of the matrices $[K_p]^{-1}$, $[K_e]^{-1}$ and matrix $[K_p]$. Before this equation can be applied to the problem of comparing modal properties to locate the weaknesses in the FE model, some modifications have to be made to the equation because of the inevitable incompleteness of the data available to define the matrix $[K_e]^{-1}$.

The only known quantity in equation 6-15 is the matrix $[K_p]$ from the FE model of the structure. It is not always possible to invert this matrix to obtain $[K_p]^{-1}$, for example, for a free-free system at least one eigenvalue (λ) is zero (rigid body mode) and this makes the stiffness matrix singular. However, it is possible to obtain the pseudo matrices of $[K_p]^{-1}$ and $[K_e]^{-1}$ as explained in section 6.3.

In order to use equation 6-15 in practice, it is necessary to assume that in place of the full matrix $[K_e]^{-1}$ we can use the pseudo matrix $[\overset{*}{K}_e]^{-1}$ which may be computed from eigenvalues and eigenvectors (equation 6-Ø3). Now, if the corresponding modes and coordinates are selected from the FE model (as used for $[\overset{*}{K}_e]^{-1}$), then an equivalent pseudo matrix $[\overset{*}{K}_p]^{-1}$ can also be computed. It appears that both $[\overset{*}{K}_p]^{-1}$ and its inverse $[\overset{*}{K}_p]$ are required in the equation 6-15 and, as explained in appendix 1Ø.2, it is not possible to invert pseudo matrices. To avoid this inversion process

it will be further assumed that in equation 6-15 the pre-and post-multiplication may be carried out using the $[K_p]$ matrix which is already known from the FE model.

Equation 6-15 thus becomes;

$$[E_k]_{nn} \approx [K_p]_{nn}\left[[\overset{*}{K}_p]_{nn}^{-1} - [\overset{*}{K}_e]_{nn}^{-1}\right][K_p]_{nn} \qquad (6\text{-}16)$$

where $[\overset{*}{K}_e]^{-1}$ - pseudo inverse stiffness matrix formed by using m modes and n coordinates from the experimental eigenvalues and eigenvectors ($m < n$; equation 6-Ø3);

$[\overset{*}{K}_p]^{-1}$ - pseudo inverse stiffness matrix formed by using m modes and n coordinates (corresponding to the experimental data) from the FE analysis (equation 6-Ø3);

$[K_p]$ - stiffness matrix from the FE analysis.

6.4.2. NUMERICAL STUDY

In the course of deriving equation 6-16, it has been necessary to make several assumptions, namely that the error matrix [E] is small, pseudo matrices can be used in place of the full matrices and the complete $[K_p]$ matrix should be used for pre-and post-multiplication. To lend support to these assumptions, it is appropriate to perform some numerical calculations for which the exact error matrix [E] is known from other sources (figure 6-Ø7) so that comparison of the error matrices obtained using equation 6-16 with the exact error matrix will indicate the validity of this method. We shall use the data of table 6-Ø1 and equation 6-16 to investigate the accuracy of the error matrix equation in the process of locating weaknesses (areas of poor modelling) in the FE model.

The stiffness error matrices were calculated for several combinations of modes using the data of table 6-Ø1 and equation 6-16. It was discovered that the matrices are additive, that is, if $[E_{1,2,3,...}]$ represents the error matrix from modes 1,2,3,... taken together and $[E_1]$, $[E_2]$, $[E_3]$,... are error matrices for mode 1, mode 2, mode 3,... individually, by taking only one mode into account at a time, then;

$$[E_{1,2,3,...}] = [E_1] + [E_2] + [E_3] + ...$$

The order in which the modes are taken in the $[\Phi^R]$ matrix does not effect the error matrix and for 3 modes, for example, we can write;

$$[E_{1,2,3}] = [E_{2,3,1}] = [E_{3,2,1}] = [E_{1,3,2}] \text{ etc.}$$

Some of the error matrix plots are shown in figure 6-Ø8. These diagrams indicate how the stiffness error matrix changes as the number of modes in its calculation are increased from 1 (SM1 plot) to 8 (last plot).

The 'SM1' diagram indicates very small error as the surface of the 3-D plot is close to the zero value. As the number of modes is increased, the error also increases and for four modes, there appears a large error between coordinates X_2 and X_3. These are the coordinates that are directly affected by changes in the stiffness of the spring k_{L3}. As the number of modes is increased from four, the peak at these coordinates becomes more clearly defined with respect to the rest of the matrix. Other coordinates also appear to have small error even though there were no discrepancies at these points, but the reason for this is that the error matrix calculated using equation 6-16 is approximate. The last plot, calculated using all 8 modes, shows no error except between the coordinates X_2 and X_3.

In practice, the number of modes predicted would far exceed the number of measured modes. To simulate a practical situation, we shall only take some of the modes in the calculation of the stiffness error matrix and these are marked with an asterisk in table 6-Ø3 (which is part reproduction of table 6-Ø1). The modes to be included in the calculation of the stiffness error matrix are 2, 3, 4, 6 and 7 from the experimental data (column 2) and the

corresponding modes from the FE model (column 3).

Using equation 6-16 and the modal data from table 6-Ø1, the stiffness error matrix was computed which, when displayed on an isometric plot, clearly shows the maximum error to be between coordinates X_2 and X_3 (figure 6-Ø9). Comparison of this plot with the exact diagram (figure 6-Ø7) indicates the location of the area and the amount of discrepancy to be of the correct order. The mass error matrix for these modes (not shown) indicates a very small error, so it may be assumed that the discrepancy in the complete mass matrices is negligible, which is true because the mass matrices for the two versions of the 8 DOF system are, in fact, identical.

If this error is a true representation of the exact error matrix then it should be possible to calculate a more accurate stiffness matrix than that from the FE model by using equation 6-Ø9. In this equation $[K_p]$ is the stiffness matrix for k_{L3} = 1.5Ø MN/m and error matrix $[E_k]$ has been calculated using equation 6-16, hence $[K_e]$ or a more accurate stiffness matrix can be calculated using equation 6-Ø9. This new matrix $[K_e]$ should give modal properties that are closer to the experimental ones than the FE ones. The eigenvalues computed using the more accurate stiffness matrix and the original mass matrix are given in column 5 of table 6-Ø3. The percentage error between these and the exact (experimental) eigenvalues are displayed in column 6. The percentage error for the modes that were included in the calculation of the error matrix $[E_k]$ have

been considerably reduced (modes 2, 3, 4, 6 and 7) compared with the percentage error of the unmodified FE values (column 4), but the errors in the modes that were excluded from the calculation have increased. This demonstrates that for this case equation 6-16 is an effective error matrix equation, despite all the assumptions made in the process of its derivation.

6.5. CONCLUSIONS

This chapter has concentrated on the comparison of modal properties and spatial properties derived using incomplete modal data. The analytical study made it possible to compare the merits of different techniques, each of which has its own advantages and drawbacks. The first method - comparison of modal properties - is especially useful in deciding which modes are compatible by plotting experimental mode shape against the corresponding analytical mode shape and this informs the analyst whether the correct modes are being compared. The second method, comparison of pseudo inverse matrices, gives an isometric plot of the discrepancies between the two models. The main advantage of this technique is that several modes can be combined into a single matrix but unfortunately this method, like the first, is incapable of precisely locating the areas of any discrepancies. The third and the last method - comparison of spatial model properties - has been found to be the most useful technique. Not only can it be used to compare the properties of several modes at once but it also informs the analyst what action to

take in order to reduce the discrepancies between the two models (i.e. modify mass/stiffness matrix at the coordinates of maximum error).

In the last section 6.4 , it has been demonstrated that it is feasible to locate the areas of poor modelling using incomplete experimental and complete FE modal data. Although the data used in this work were synthesized by analysis and were not actual measured data, the basic concept has been demonstrated. Although only an 8 DOF model was used, it is recognised that most practical structures require many more degrees of freedom for adequate representation. In this study it was also assumed that all the coordinates taken to represent the structure in the analytical model are measurable whereas, in practice, far more coordinates are analysed than measured. Nevertheless, the technique of error matrices appear to work with the data from this simple 8 DOF system.

MODE NO.	kL3 (MN/m)	NATURAL FREQUENCY (Hz)	MASS NORMALISED MODE SHAPE							
			X1	X2	X3	X4	X5	X6	X7	X8
1	1.95	21.3844	.0699	.0728	.0670	.0432	-.0456	-.0628	-.0635	-.0261
	1.50	21.3729	-.0706	-.0737	-.0663	-.0428	.0457	.0626	.0632	.0259
2	1.95	34.4434	.0802	.0028	-.0508	-.0367	-.0533	.0456	.0742	.0340
	1.50	33.8582	.0813	.0105	-.0549	-.0392	-.0507	.0442	.0724	.0332
3	1.95	79.5973	-.0598	-.0437	-.1479	-.2214	-.0502	-.2102	-.1702	.0519
	1.50	78.4522	.0502	-.0027	.1478	.2081	.0340	.2139	.1594	-.0427
4	1.95	93.2860	-.0509	-.2611	-.0276	-.0800	-.0767	.0705	-.1060	.0146
	1.50	89.8641	-.0598	-.2680	-.0357	-.1085	-.0865	.0325	-.1150	.0372
5	1.95	103.4937	-.1241	-.2450	-.2854	-.1061	-.1310	-.2560	-.2616	-.2942
	1.50	103.4225	-.1248	-.2535	-.2855	-.1077	-.1325	-.2489	-.2652	-.2941
6	1.95	213.3259	-.2184	-.2992	-.1388	.3264	-.2211	-.3221	-.1317	.3424
	1.50	212.5663	-.2266	-.3093	-.1324	.3232	-.2293	-.3384	-.1238	.3392
7	1.95	303.8984	-.5623	-.3601	.2594	-.0907	-.5660	-.3951	.2675	-.0914
	1.50	296.4734	-.5202	-.3655	.2647	-.1008	-.5237	-.4089	.2747	-.1019
8	1.95	410.0176	-.7796	.4098	-.0889	.0131	-.7828	.4265	-.0924	.0130
	1.50	406.7665	-.8058	.3894	-.7730	.0117	-.8092	.4076	-.0812	.0116

TABLE 6-01 : Computed eigenvalues and eigenvectors of undamped 8 DOF mass-spring system.

kL3 MODE NO.	1.95 MN/m (≡EXPERIMENTAL) NATURAL FREQUENCY (Hz)	1.5Ø MN/m (≡FE MODEL) NATURAL FREQUENCY (Hz)	 ERROR (%)
1	21.3844	21.3729	Ø.Ø54
2	34.4434	33.8532	1.714
3	79.5973	78.4522	1.439
4	93.286Ø	89.8641	3.668
5	1Ø3.4937	1Ø3.4225	Ø.Ø69
6	213.3259	212.5663	Ø.356
7	3Ø3.8984	296.4734	2.443
8	41Ø.Ø176	4Ø6.7665	Ø.793

TABLE 6-02 : Comparison of natural frequencie of the undamped 8 DOF mass-spring system.

kL3 MODE NO.	1.95 MN/m (≡EXPERIMENTAL) NATURAL FREQUENCY (Hz)	1.5Ø MN/m (≡FE MODEL) NATURAL FREQUENCY (Hz)	 ERROR (%)	1.5Ø MN/m MODIFIED FE MODEL NATURAL FREQUENCY (Hz)	 ERROR (%)
1	21.3844	21.3729	Ø.Ø54	21.3725	Ø.Ø56
2*	34.4434	33.8532	1.714	34.35Ø4	Ø.27Ø
3*	79.5973	78.4522	1.439	79.4316	Ø.2Ø8
4*	93.286Ø	89.8641	3.668	92.286Ø	1.Ø72
5	1Ø3.4937	1Ø3.4225	Ø.Ø69	1Ø3.6894	-Ø.189
6*	213.3259	212.5663	Ø.356	213.1857	Ø.Ø66
7*	3Ø3.8984	296.4734	2.443	3Ø1.859Ø	Ø.671
8	41Ø.Ø176	4Ø6.7665	Ø.793	4Ø6.3512	Ø.894

TABLE 6-03 : Experimental, FE and modified FE eigenvalues of the undamped 8 DOF mass-spring system.

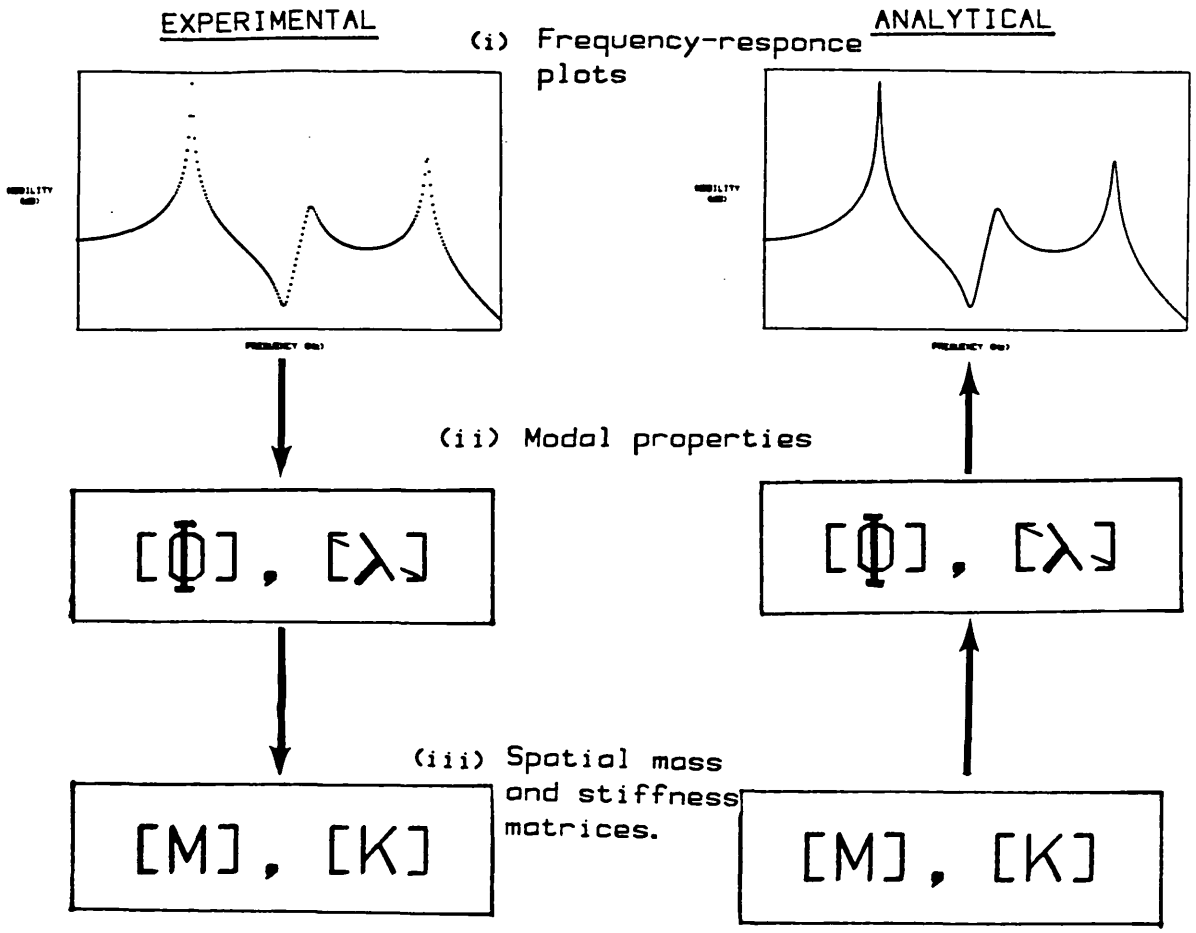

FIGURE 6-01 : Three stages of data comparison.

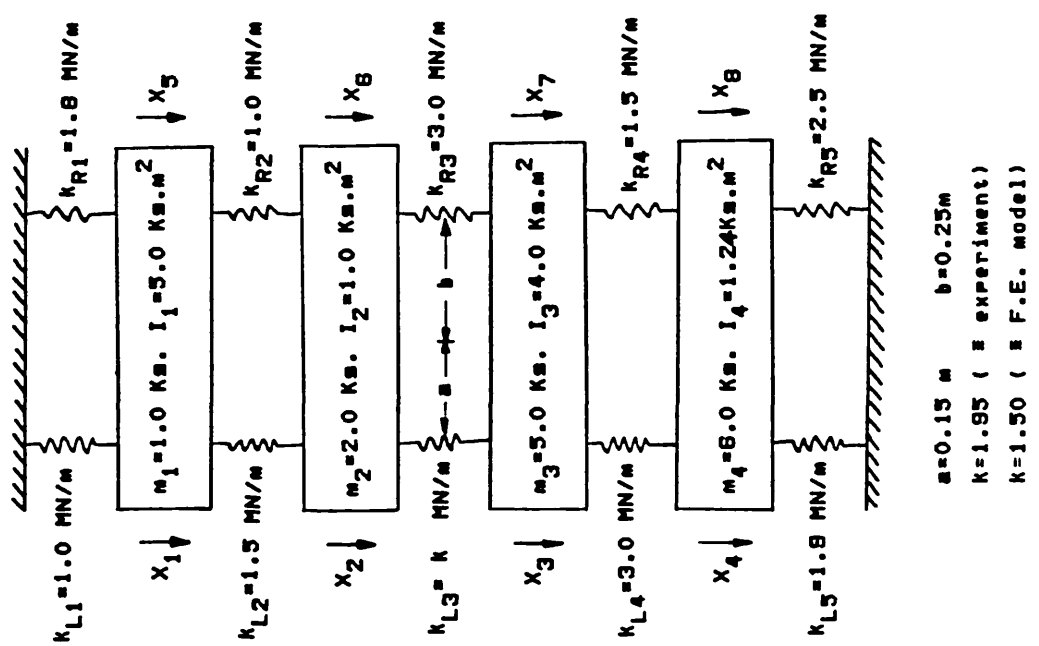

FIGURE 6-02 : Undamped 8 DOF mass-spring system.

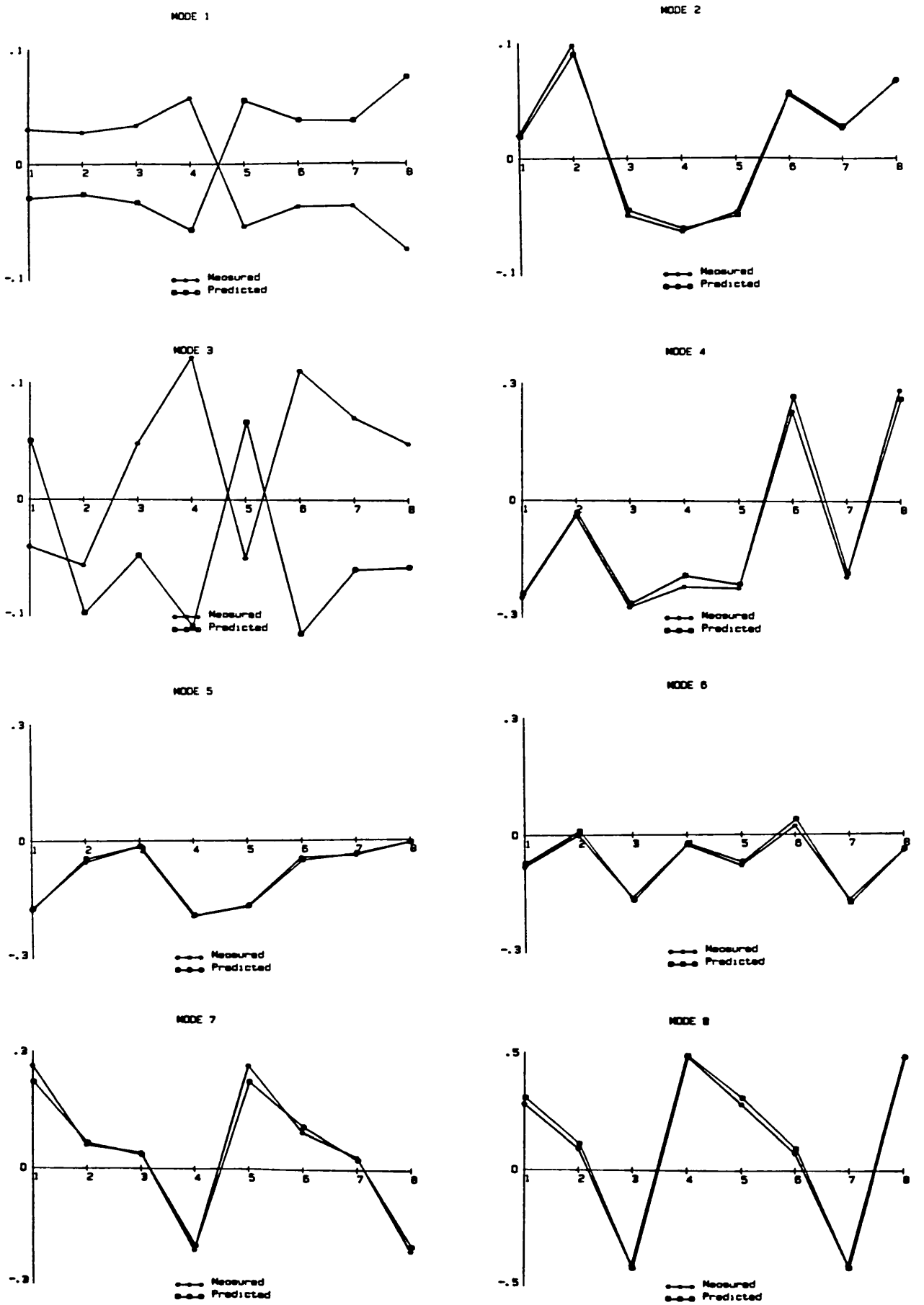

FIGURE 6-03 : Mode shape comparison of the undamped 8 DOF mass-spring system.

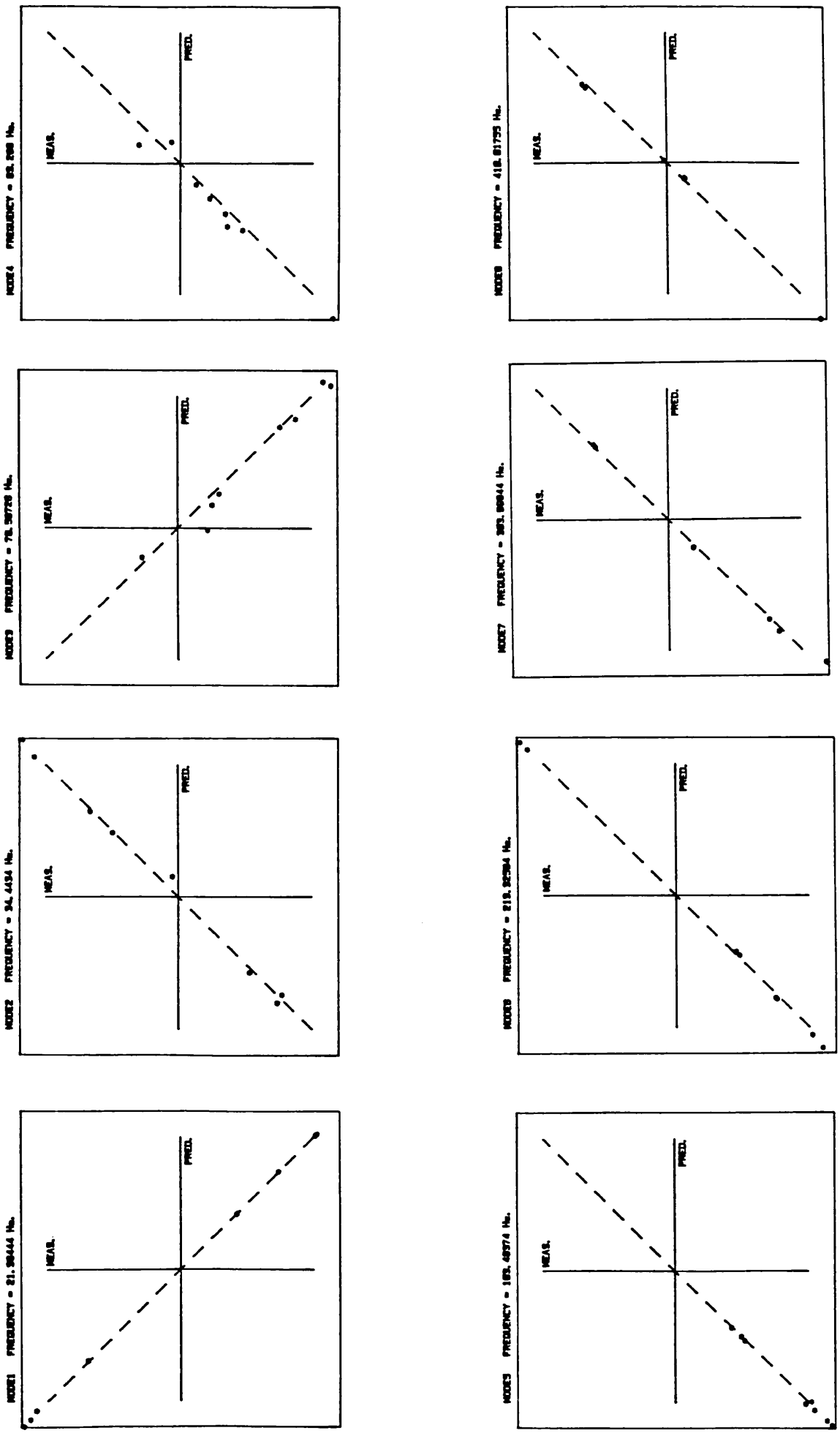

FIGURE 6-04 : Mode shape correlation of the undamped 8 DOF mass-spring system.

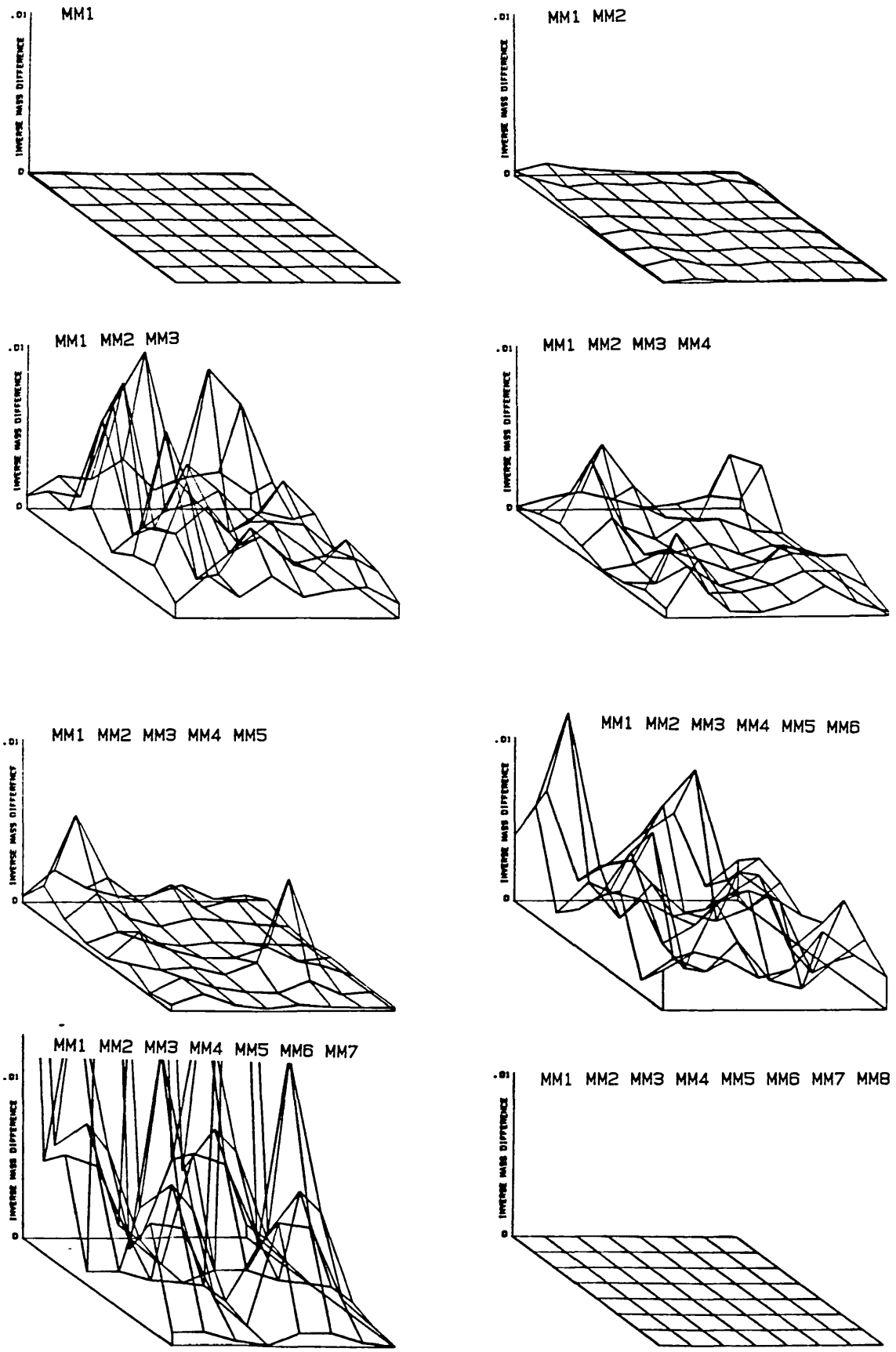

FIGURE 6-05 : Plots of difference of pseudo inverse mass matrices as function of number of modes.

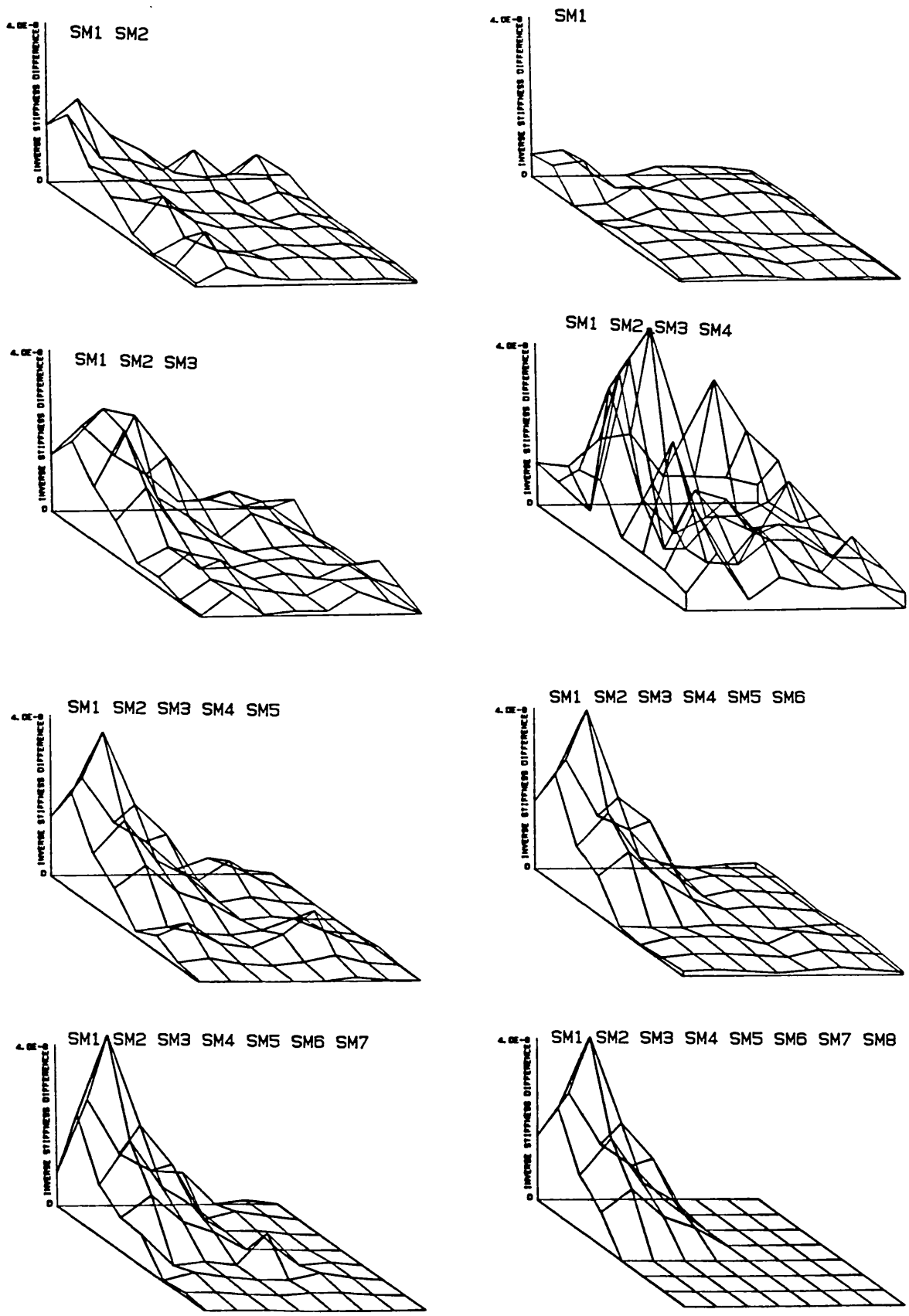

FIGURE 6-06 : Plots for difference of pseudo inverse stiffness matrices as function of number of modes.

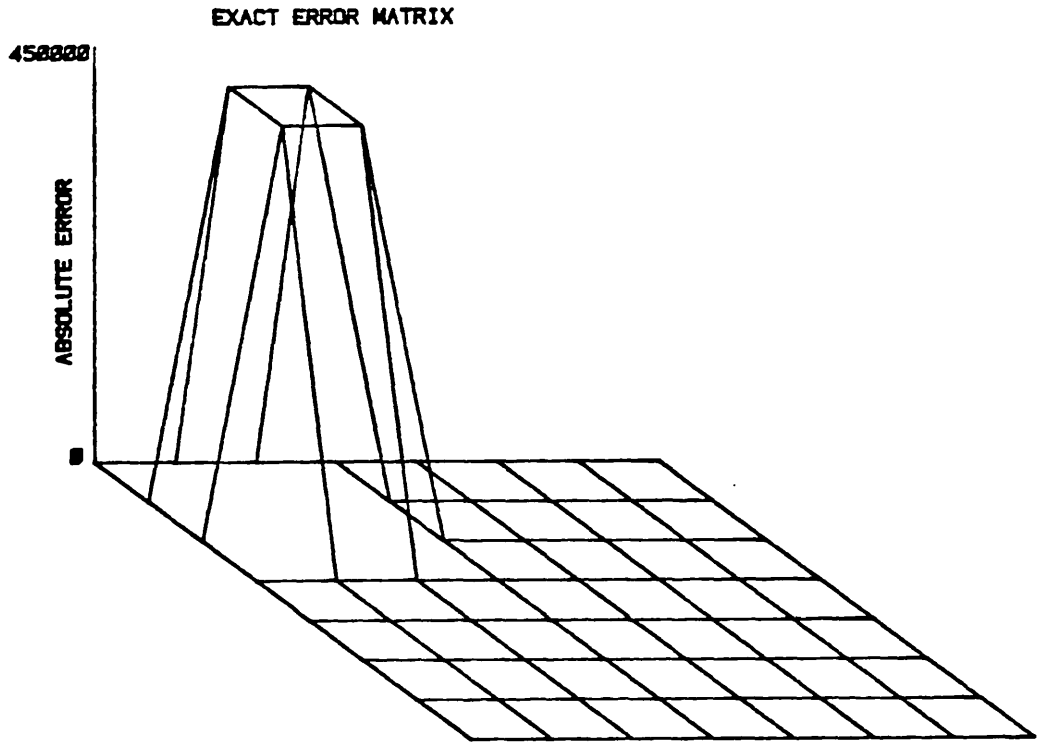

FIGURE 6-07 : Exact stiffness error plot of the undamped 8 DOF mass-spring system.

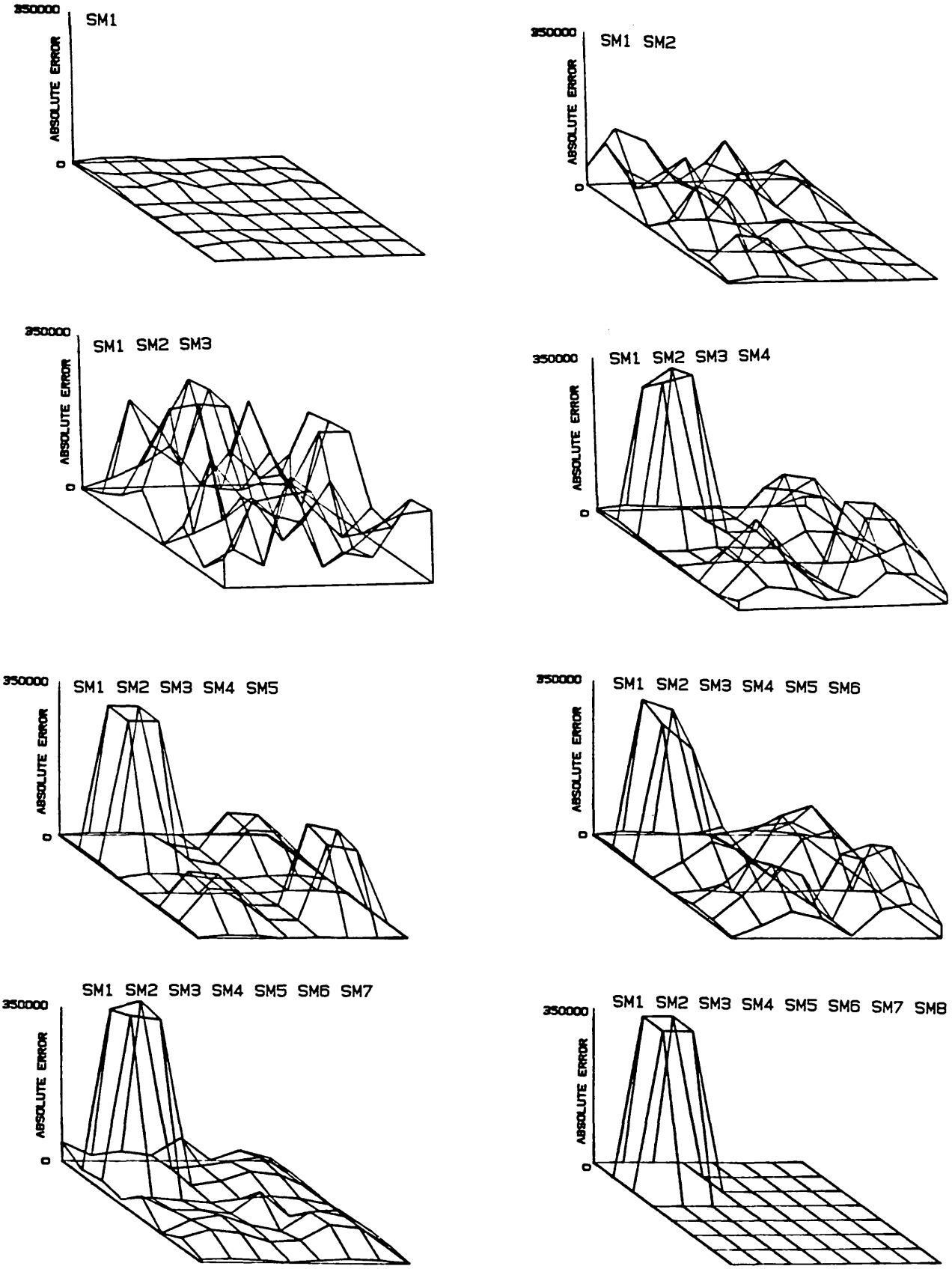

FIGURE 6-08 : Stiffness error plots of the undamped 8 DOF mass-spring system.

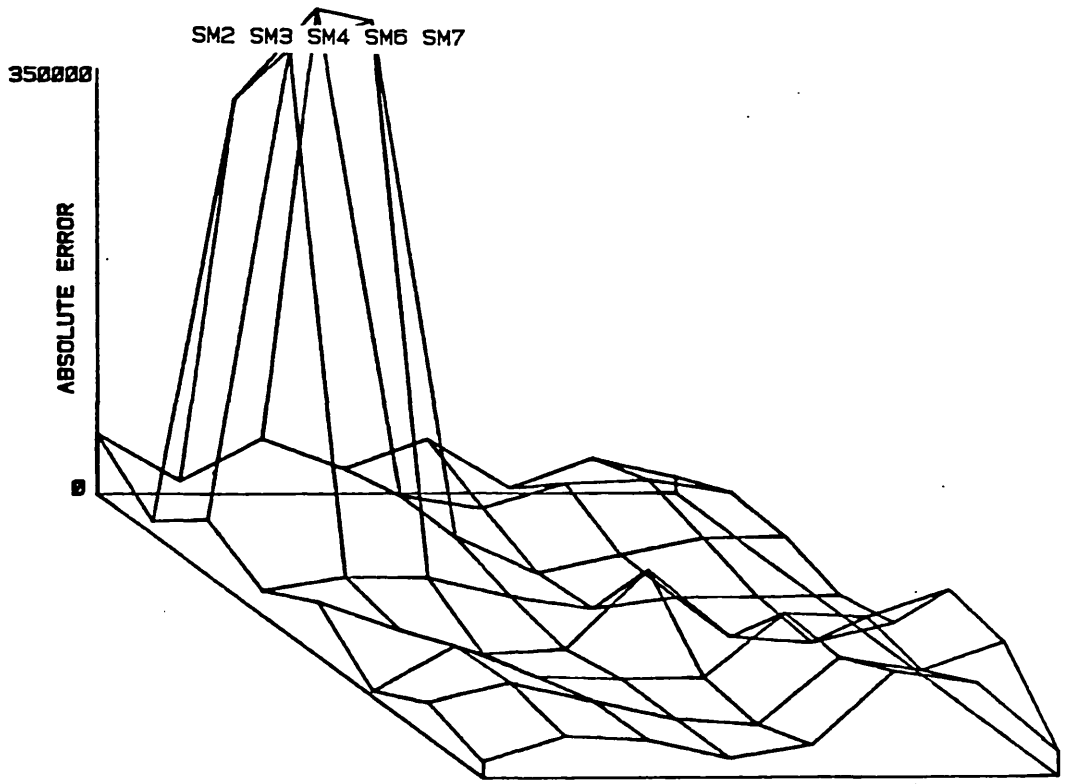

FIGURE 6-09 : Stiffness error matrix plot for modes 2, 3, 4, 6 and 7.

CHAPTER

-7-

7. APPLICATIONS OF THE ERROR MATRIX EQUATION

7.1. INTRODUCTION

The error matrix equation 6-16, developed in chapter 6 was evaluated using an 8 degrees-of-freedom mass-spring system. In that case the number of coordinates measured and the coordinates in the FE model were the same, which means that the dimensions of the matrices were identical. However, in practice the FE model requires many more degrees-of-freedom for accurate modelling than it is possible to measure, and consequently the dimensions of the matrices in the two models are different, i.e. the dimensions of $[K_e]$ are different from those of $[K_p]$. Clearly, the matrix multiplication required by equation 6-16 is not possible because of the incompatibility of the matrices.

Another question that did not arise in the last chapter is that of 'real' and 'complex' mode shapes because the two versions of the 8 DOF mass-spring system were both undamped and hence the mode shapes were all real. The measured modes are usually complex and those from an FE analysis are real.

In this chapter we shall address the above mentioned questions and apply the error matrix equation to two real structures - a small beam (SAMM II B beam) and the NASTRAN structure, first described in chapter 3.

7.2. COMPATIBILITY OF THE MATRICES USED IN THE ERROR MATRIX EQUATION

Because of the different dimensions of the measured and the FE spatial matrices it is not possible to use the error matrix equation 6-16 without modification. Rewriting the stiffness error matrix equation;

$$[E_k] \approx [K_p]\left[[\overset{*}{K}_p]^{-1} - [\overset{*}{K}_e]^{-1}\right][K_p] \qquad (7\text{-}\emptyset 1)$$

where $[K_p]$ - is NxN; N is the number of DOF in the FE model.

$[\overset{*}{K}_e]^{-1}$ - is nxn; n is the number of measured coordinates.

$[\overset{*}{K}_p]^{-1}$ - is also nxn

and N >> n.

Matrices obtained from an FE analysis, such as the $[K_p]$ matrix, are generally very large, while the experimentally derived matrices, such as $[\overset{*}{K}_e]^{-1}$, are relatively much smaller. There are two possible options open to make these matrices conform;

(i) to reduce the $[K_p]$ matrix by ignoring the rows and columns that correspond to the coordinates which are not measured and this will be referred to as the 'elimination method'. The effect of this is to assume that there are no errors at the coordinates that are excluded (see appendix 1Ø.3).

(ii) to use a condensation technique of the type employed in the eigenvalue and eigenvector calculations,

such as the Guyan reduction [54,55]. In this case the full $[K_p]$ matrix can be reduced to one referred just to the measured coordinates so that all the matrices in the calculation of an error matrix then have the same dimensions (nxn), and equation 7-Ø1 thus becomes;

$$[E_k]_{nn} \approx [K_p^R]_{nn}\left[[\dot{K}_p]_{nn}^{-1} - [\dot{K}_e]_{nn}^{-1}\right][K_p^R]_{nn} \qquad (7\text{-}Ø2)$$

where $[K_p^R]$ - is the reduced stiffness matrix.

Before attempting to use these reduction techniques in the calculation of error matrices it is necessary to investigate the accuracy of such procedures.

7.3. GUYAN VERSUS ELIMINATION MATRICES

For this study, the beam shown in figure 7-Ø1 was considered. The beam was divided into 1Ø elements (11 nodes), each node having six DOF; total 66 DOF. The experimental and FE data were simulated by increasing the length of element 2 and decreasing that of element 8 as shown in table 7-Ø1. In this case, the error matrices should show discrepancies between coordinates 2 and 3 (element 2) and between coordinates 8 and 9 (element 8) in all X, Y and Z-directions as well as in the rotational coordinates.

Using the beam element's mass and stiffness matrices (appendix 1Ø.1), spatial mass and stiffness matrices were constructed for both versions of the beam model. It was then a simple task to compute the undamped eigenvalues and

eigenvectors of the beam in the free-free state. The mass and stiffness error matrices were constructed for the first 7 non-rigid body modes using both the Guyan reduction technique and the elimination of rows and columns method. The isometric error matrix plots for the Y-direction are shown in figure 7-Ø2 and those for the Z-direction in figure 7-Ø3.

All the plots indicate errors between coordinates 2 and 3, and between 8 and 9 and so by using either Guyan reduction or by elimination of rows and columns, we have been successful in locating the areas of discrepancies. However, it should be noted that the magnitude of the discrepancies (given by the heights on the 3-D plot) are different in the two cases because the vertical scales are not the same. Comparing these results with the exact error mass and stiffness plots (not shown) indicate that the error matrix calculated using the Guyan reduction method is much closer to the correct values.

Although both reduction methods located the areas containing discrepancies, only one - Guyan reduction - indicated the true nature of the error. In cases where only the areas of discrepancies are required either technique can be used.

7.4. ERROR MATRICES OF THE SAMM II B BEAM

The SAMM II B beam, which consists of welded channel section elements is shown in figure 7-Ø4. Special features of the beam are the welded joints, and the two holes, which are situated near each end of the beam. The joints are welded on only one side and hence are quite flexible.

Frequency response functions for this beam were measured in the free-free state using random excitation. The beam was excited at point 6 in the Y-direction and responses were measured at 11 points in the Y-direction. The excitation was then changed to the Z-direction and again the responses for all 11 points in the Z-direction were measured. Two point mobility plots from these tests, $Y_{yØ6,yØ6}$ and $Y_{zØ6,zØ6}$, are shown in figure 7-Ø5. The measured data were analysed using a linear SDOF algorithm to extract the required modal properties (chapter 2).

A finite element analysis similar to that described in section 7.3, using 1Ø beam elements with 6 DOF at each node, was carried out to predict the dynamic characteristics of the beam. In the FE analysis no allowance was made for the holes and all the joints were assumed to be rigid even though it was clear that the actual welded joints were more flexible. Damping was also ignored and consequently the analysis reduced to that of a free-free undamped beam.

The measured and predicted natural frequencies for the first six non-rigid body modes are shown in table 7-Ø2. The measured mode shapes were only slightly complex (modal phase

close to Ø or 18Ø degrees) and it was assumed that the modulus of each eigenvector element was a true representation of the undamped behaviour of the beam. It was observed that the measured natural frequencies of the modes in the Z-direction were greater than the predicted values and that the reverse was true for those in the Y-direction. This suggests that the FE model give a lower stiffness in the Z-direction and that the predicted stiffness in the Y-direction was greater than the experimental model (assuming the inertia or mass matrix is correct in the FE model).

The correlation between measured and predicted mode shapes (figure 7-Ø6) indicates large discrepancies between the two models, especially for modes 3 and 4, but again does not indicate the area(s) of the discrepancy. Using the error matrix equation 7-Ø1 and these data, stiffness error matrices were computed for both the Y and the Z-directions separately, as described in the last section. In this case, the $[K_p]$ matrix was reduced by ignoring the rows and columns that were not measured (55 rows and 55 columns were ignored out of 66). Again, 3-D plots were constructed and figures 7-Ø7 and 7-Ø8 show the results for the Y and the Z-directions respectively. The notation 'SM2' indicates stiffness matrix calculated using mode 2 and 'SM2 SM5 SM6' implies stiffness error matrix plot from the data of 3 modes numbers 2, 5 and 6 as before.

The stiffness error plot SM2 (figure 7-Ø7) indicates an error at element (5,5) i.e. node 5 on the beam, while

plots SM5 and SM6 show very good correlation between the measured and predicted modal properties for these two modes. The last plot of figure 7-Ø7, diagram SM2 SM5 SM6 which is the overall stiffness matrix for the 3 modes of vibration in the Y-direction, indicates an error at coordinate 5, which is one of welded joints. The plot SM1 in figure 7-Ø8 shows errors in elements (3,3), (1,9) and (1,11), where the offdiagonal terms imply possible errors at both of the coordinates e.g. (1,9) means errors at coordinates 1 and 9. The diagram SM3 shows errors at (9,9) and (11,11) and the overall error plot SM1 SM3 SM4 indicates discrepancies at joints 3 and 9.

The stiffness error plots, figures 7-Ø7 and 7-Ø8 have suggested errors in the FE stiffness matrix at coordinates 3, 5 and 9, all of which are at welded joints. One might expect an error at these points but the plots did not show any error at point 7 which is also a welded joint. A close visual examination of the beam's joints revealed that the welding at joint 7 had penetrated through the joint, making it closer to a rigid joint than was the case for other 3.

Figures 7-Ø9 and 7-1Ø show the mass error plots in the Y and Z-directions respectively. Plot MM2 suggests an error in the mass matrix at point 1Ø. As in the case of the stiffness error matrices, plots MM5 and MM6 demonstrate that there is a reasonable agreement between the measured and the predicted modal properties for modes 5 and 6. The overall mass error plot suggests errors near points 2 and 1Ø, which are coordinates that lie close to the holes. Plot MM2

(figure 7-1Ø) shows an error between points 1 and 2 and plot MM3 points out a very large discrepancy between the measured and the predicted mass matrices at point 11. The error at coordinate 11 is also indicated by the overall error plot. This is probably because one of the holes is close to this point. The other hole is almost midway between coordinates 1 and 2 (element 1) and any error in the mass matrix due to this hole will be shared between them. Consequently, the effect of this hole on the mass error matrix is smaller than that of the hole at point 11, even though both are the same size. The plot MM3 of figure 7-1Ø shows a large error in the mass matrix at coordinate 11 which is close to one of the holes.

We shall now seek to demonstrate that the error at coordinate 11 is probably due to the hole and not to other defects in the beam. Studs were placed in the holes so that they are filled with the same type of material as that of the beam and the beam was retested. All the modes in the Z-direction were remeasured and it was found that only mode 3 was significantly affected, indicating that only this mode out of the 3 modes measured was sensitive to the effect of the hole near point 11. The data from these and the previous tests, together with the FE modal properties for mode 3 are given in table 7-Ø3.

The mass error matrices were computed once again with the remeasured data. These error matrices, together with those obtained with holes in the Z-direction, are displayed on 3-D plots as shown in figures 7-11 and 7-12, with the

negative elements pointing downwards and positive up. Comparing the mass error plots we see that there is a significant change near point 11 for mode 3 but the rest of the plots are very similar in shape. Also, there is a small change in the stiffness error plots near point 11 for this mode but again, the rest of the plots are virtually uneffected by the studs which this suggests that only mode 3 is sensitive to the studs.

It is possible that the error at coordinate 11 may be due to poorly identified modal properties in this region rather than the effect of the hole. To eliminate this possibility the beam was retested, after a time lapse of about 12 months. These tests were carried out for both cases - the holes and the studs - but only mode 3 was remeasured because this was the mode that showed discrepancies due to the holes. Only two coordinates were measured with the studs in place - coordinates 10 and 11 in the Z-direction - and 3 coordinates with holes - numbers 6, 10 and 11. Identified modal properties from these data together with those from the first tests are given in table 7-04. The repeatability appears to be adequate i.e. the identified modal properties of the two tests, 12 months apart are reasonably similar. This indicates that the error at point 11 of plot MM3 (figure 7-10) was probably due to the hole and not due to poorly identified modal properties or other defects in the beam.

We have seen from this study that even a small simple structure, such as the SAMM II B beam, can be very difficult

to model accurately. The two types of discrepancies between the FE and the experimental models were due to the welded joints and the holes. It is possible to include the holes in an FE model using plate elements but this increases the number of DOF significantly. However, the stiffness of the welded joints present in this case cannot be modelled easily. It has been possible to locate the areas of likely errors and visual examination of the beam also points to the same areas as were located by the error matrix equation as being poorly modelled.

7.5. ERROR MATRICES OF THE NASTRAN STRUCTURE

The NASTRAN structure, first described in chapter 4 was slightly modified by removing the heavy mass from the top and installing an empty tank instead and the coordinates of interest were renumbered, as shown in figure 7-13, for the purpose of an experimental study. A finite element model of the structure was constructed, by Westland Helicopters Plc., having about 15ØØ DOF using plate elements and the undamped eigenvalues and eigenvectors extracted and made available for this study.

The first 4 modes of vibration in both the X and the Y-directions were measured at 28 points on the structure. The modes of vibration in the X-direction were excited by forcing point 5X using sinusoidal excitation and those in the Y-direction by forcing point 6Y (figure 7-13). The measured and predicted eigenvalues are shown in table 7-Ø4

The measured and predicted natural frequencies are very close to each other; the maximum error being less than 3%. The correlation of the eigenvectors is also very good but the data for these are too large to be able to include in this study and can be found in reference 56. With such good agreement between the measured and the predicted modal parameters, any discrepancies in the experimental and the FE models are likely to be small.

The $[K_p]$ matrix was reduced to the measured coordinate set using Guyan reduction and mass and stiffness error matrices were computed for the X and the Y-directions separately. The 3-D plots of the error matrices are given in figures 7-14 through 7-17. The code SM1X on the plot denotes: S-stiffness; M1X-first mode in the X-direction; and 'SM1X SM2X SM3X' implies the overall stiffness error in the X-direction calculated using all the modes in that direction.

Figures 7-14 and 7-15 show two main areas of discrepancies between the measured and predicted stiffness matrices; these being at the interface between the tank and the tower and also between the tower and the base, the latter effect being quite small. There appears to be very little discrepancy at other points on the structure. Examination of the mass error matrices (figures 7-16 and 7-17) points to two areas of discrepancies, again at the junction between the tank and the tower but also at the four outer corners of the base, which appear to be areas of poor modelling. The error in the base is much greater than that

at the interface of the tower and the tank although there was no error indicated at the base corners by the stiffness matrices (figures 7-14 and 7-15).

It appears that there were three areas which were inadequately modelled: the junction between the tank and the tower, that between the tower and lastly, the base and the corners of the base.

7.6. CONCLUSIONS

It was necessary to modify the error matrix equation so that the matrices used in its application were compatible and this may be achieved by two techniques - reduction by elimination of rows and columns or Guyan reduction. Although both of these techniques were able to locate the areas of discrepancies, only one - Guyan reduction - actually gave a true indication of the amount of error in the FE model. The main advantage of the reduction method by eliminating rows and columns is that it is very simple to implement whereas a Guyan reduction requires partition of the matrix into 'slave' and 'master' coordinates and further matrix manipulation of these matrices are also necessary [55].

Application of the error matrix equation to an apparently simple beam (SAMM II B) revealed areas of large discrepancy in the mass and stiffness matrices of the FE model. These results were very encouraging because visual examination of the beam pointed to these same areas as being

difficult to model accurately. The tests with studs in the holes demonstrated that the error at point 11 was due to the holes because it disappeared when studs were placed in the holes.

The application of the error matrix equation to the 'NASTRAN' structure was the first real test of this technique because in all the previous applications the structures were small. The fact that this technique pointed to precisely defined areas (around the junction of the tank and the tower), rather than to random points around the structure as being poorly modelled, demonstrates the usefulness of the error matrix equation. No attempt was made to remodel the structures with the knowledge gained from the error matrix plots since the aim was to locate the areas of poor modelling, and once this has been acheived methods in the current literature are capable of making use of this in the remodelling process [22].

ELEMENT NUMBER	(≡EXPERIMENTAL) ELEMENT LENGTH (mm)	INCLINATION TO X-AXIS (deg)	(≡ FE MODEL) CHANGE IN LENGTH (mm)	NEW LENGTH (mm)
1	99.23	Ø.Ø	Ø.ØØ	99.23
2	99.23	Ø.Ø	-19.23	8Ø.ØØ
3	44.Ø1	43.8	Ø.ØØ	44.Ø1
4	44.Ø1	43.8	Ø.ØØ	44.Ø1
5	71.42	Ø.Ø	Ø.ØØ	71.42
6	71.42	Ø.Ø	Ø.ØØ	71.42
7	44.Ø1	-43.8	Ø.ØØ	44.Ø1
8	44.Ø1	-43.8	5.99	5Ø.ØØ
9	67.48	Ø.Ø	Ø.ØØ	67.48
1Ø	67.48	Ø.Ø	Ø.ØØ	67.48

TABLE 7-01 : Geometry of the beam elements used in the two versions of the beam.

MODE NO.	EXPERIMENTAL NATURAL FREQUENCY (Hz)	FE MODEL NATURAL FREQUENCY (Hz)	ERROR (%)	DIRECTION
1	3Ø3.922Ø	245.8Ø22	19.12	Z
2	279.293Ø	33Ø.3359	-18.28	Y
3	423.166Ø	369.Ø759	12.78	Z
4	918.7Ø8Ø	67Ø.4446	27.Ø2	Z
5	753.863Ø	886.Ø863	-17.54	Y
6	1192.87ØØ	14Ø1.1474	-17.46	Y

TABLE 7-02 : Measured and predicted natural frequencies of SAMM II B beam for the first six non-rigid body modes.

	FE (NO HOLES)	EXPERIMENTAL (HOLES)		(STUDS)	
NATURAL FREQUENCY (Hz)	369.Ø76	423.166		422.32Ø	
COORDINATES NUMBER	MODE SHAPE	MODE SHAPE	PHASE (deg)	MODE SHAPE	PHASE (deg)
Z 1	Ø.21Ø4	Ø.ØB2Ø	-2.69	Ø.Ø96Ø	-5.26
Z 2	-Ø.1Ø27	Ø.Ø774	173.87	Ø.Ø998	-16Ø.88
Z 3	-Ø.4123	Ø.2387	178.ØØ	Ø.2237	-161.39
Z 4	-Ø.1687	Ø.Ø575	3.9Ø	Ø.Ø482	2.42
Z 5	Ø.Ø728	Ø.2834	3.86	Ø.26Ø2	-2.57
Z 6	Ø.Ø851	Ø.1364	-1.2Ø	Ø.11Ø1	2.Ø1
Z 7	Ø.Ø856	Ø.11Ø2	-171.92	Ø.Ø667	-173.41
Z 8	Ø.5317	Ø.2759	Ø.42	Ø.262Ø	6.43
Z 9	Ø.974Ø	Ø.6344	5.Ø3	Ø.6Ø35	-Ø.68
Z1Ø	-Ø.173Ø	Ø.423Ø	-175.3Ø	Ø.3822	179.49
Z11	-1.3264	2.2585	176.48	1.3956	173.85

TABLE 7-03 : Mass normalised mode shape vectors of mode of the SAMM II B beam with holes and studs.

COORD. NO.	TEST	NATURAL FREQUENCY (Hz)	LOSS FACTOR	MODAL CONSTANT (1/Kg)
6Z HOLES	FIRST	423.Ø322	Ø.ØØØ4	Ø.Ø145Ø
	SECOND	423.916Ø	Ø.ØØØ6	Ø.Ø1618
1ØZ HOLES	FIRST	421.Ø986	Ø.ØØ12	Ø.Ø5259
	SECOND	422.1288	Ø.ØØ16	Ø.Ø538Ø
11Z HOLES	FIRST	419.3481	Ø.ØØ17	Ø.17699
	SECOND	42Ø.415Ø	Ø.ØØ16	Ø.2Ø73Ø
1ØZ STUDS	FIRST	42Ø.4199	Ø.ØØ13	Ø.Ø4547
	SECOND	42Ø.483Ø	Ø.ØØ13	Ø.Ø41Ø6
11Z STUDS	FIRST	418.8281	Ø.ØØ18	Ø.15818
	SECOND	418.613Ø	Ø.ØØ15	Ø.1499Ø

TABLE 7-04 : Remeasured data for mode 3 of SAMM II B beam.

MODE NO.	EXPERIMENTAL NATURAL FREQUENCY (Hz)	FE MODEL NATURAL FREQUENCY (Hz)	ERROR (%)	DIRECTION
1	48.Ø393	48.977Ø	-1.95	X
1	48.11Ø4	48.977Ø	-1.8Ø	Y
2	83.8234	84.5997	-Ø.93	Y
3	152.586Ø	154.9673	-1.56	X
3	152.881Ø	154.9673	-1.36	Y
4	233.521Ø	239.5457	-2.58	X

TABLE 7-05 : Measured and predicted natural frequencies of the NASTRAN structure for the first 4 modes.

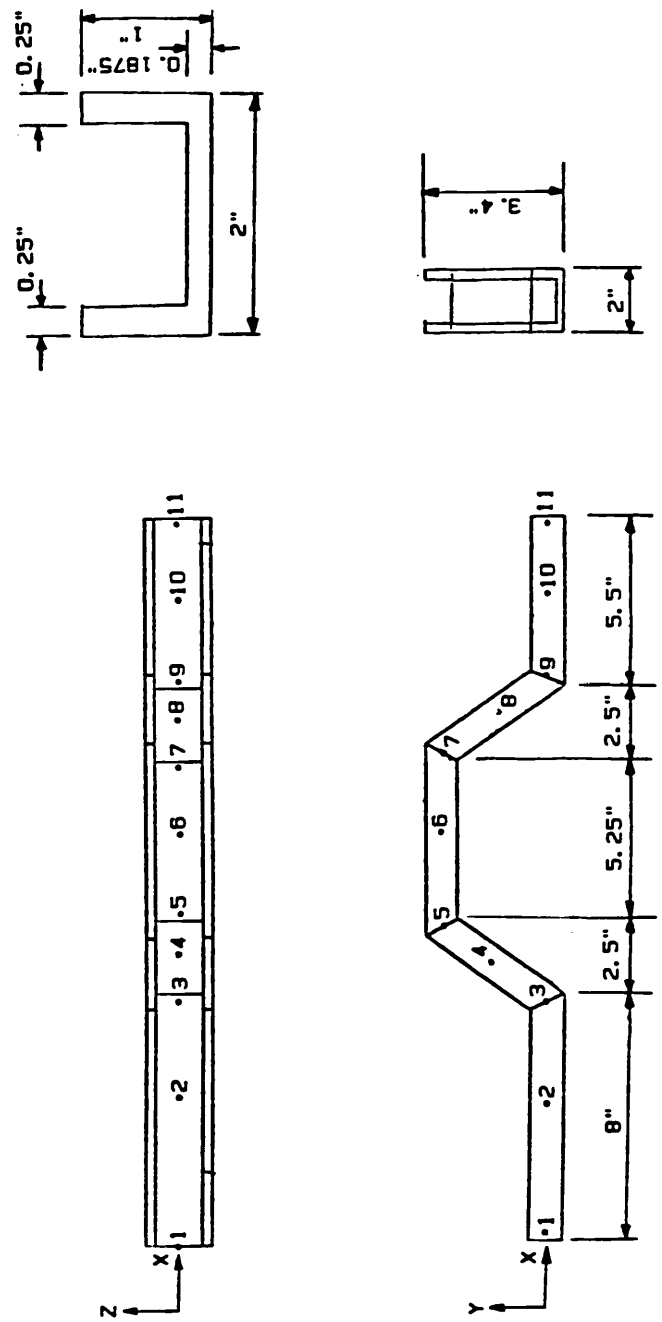

FIGURE 7-01 : Ten beam elements.

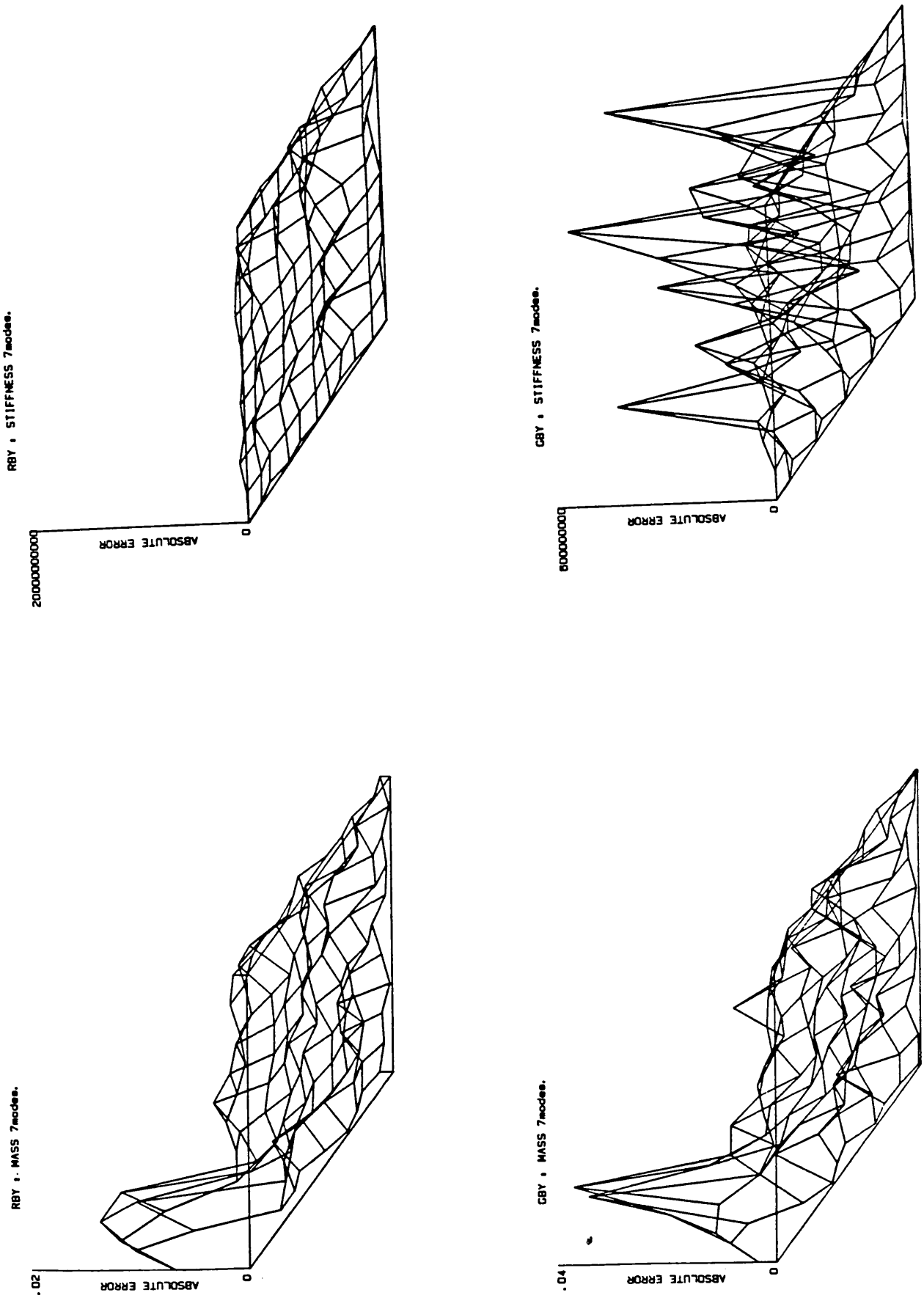

FIGURE 7-02 : Mass and stiffness error matrices for the Y direction of the beam (Guyan v. Elimination).

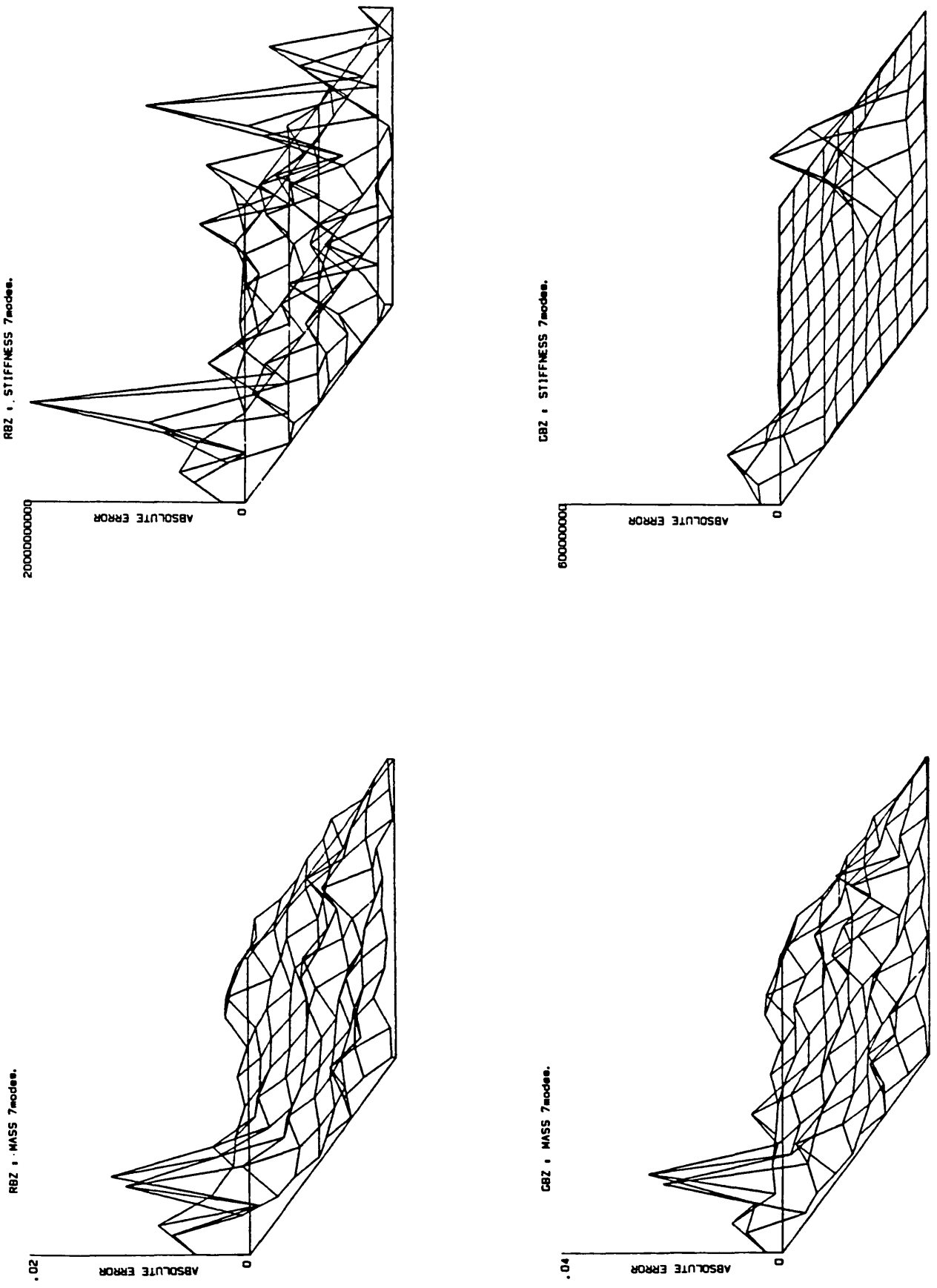

FIGURE 7-03 : Mass and stiffness error matrices for the Z direction of the beam (Guyan v. Elimination).

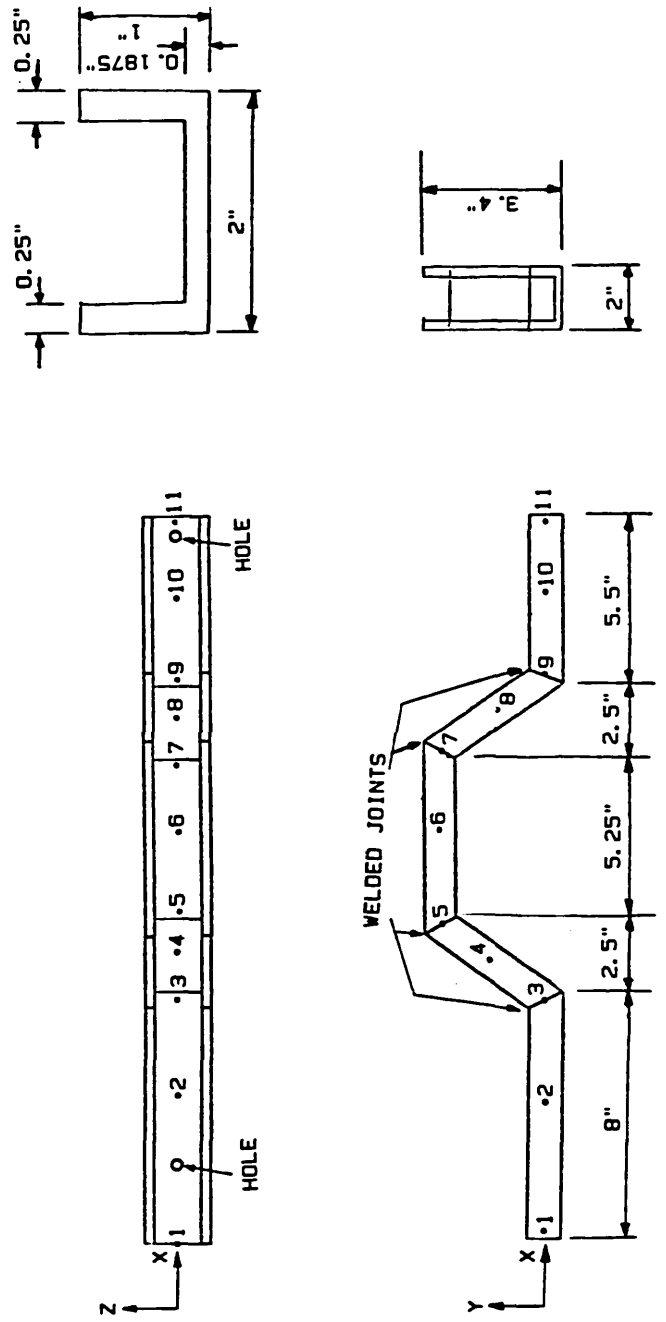

FIGURE 7-04 : The SAMM II B beam.

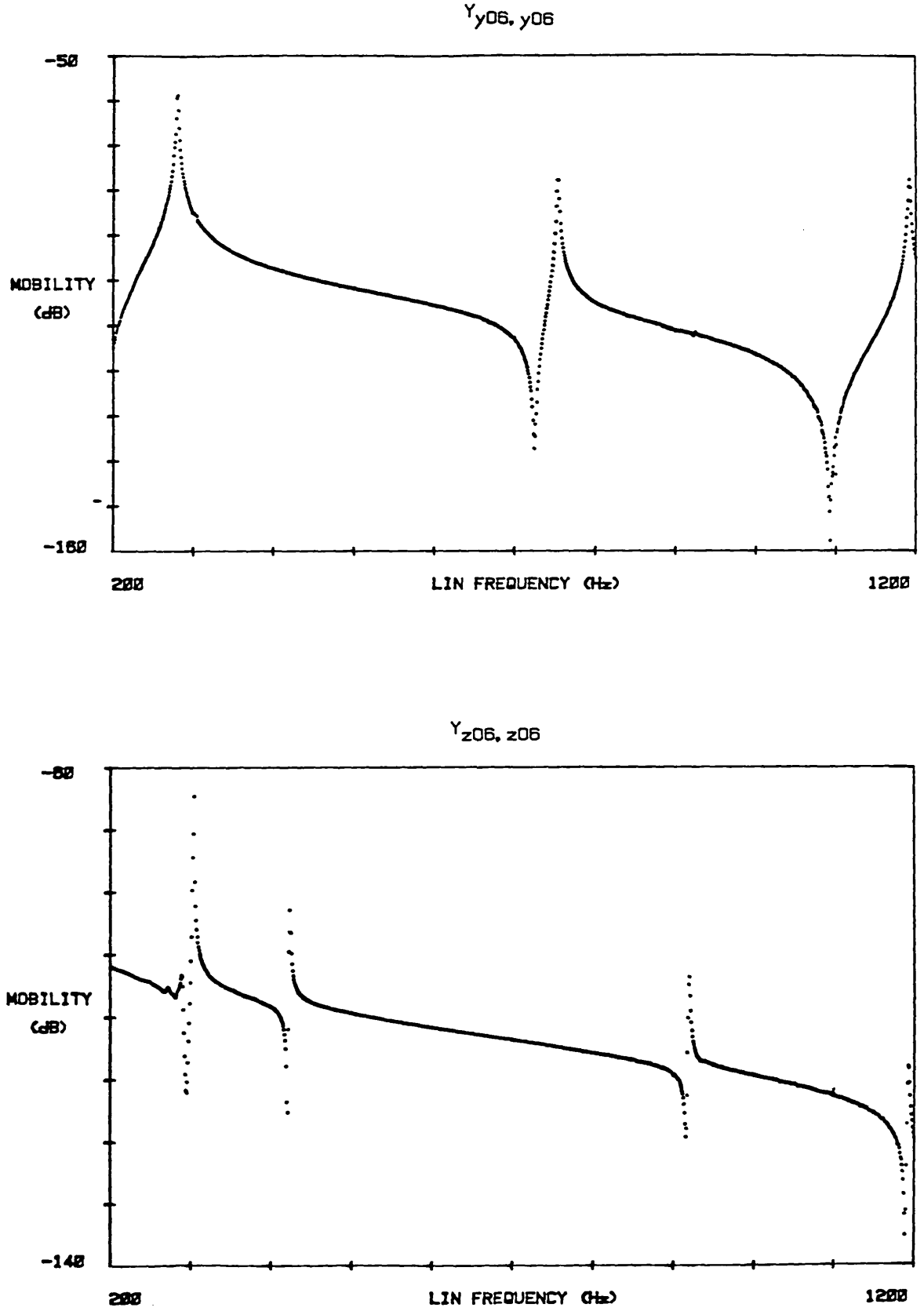

FIGURE 7-05 : Measured mobility modulus plots $Y_{y06,y06}$ and $Y_{z06,z06}$ of SAMM II B beam.

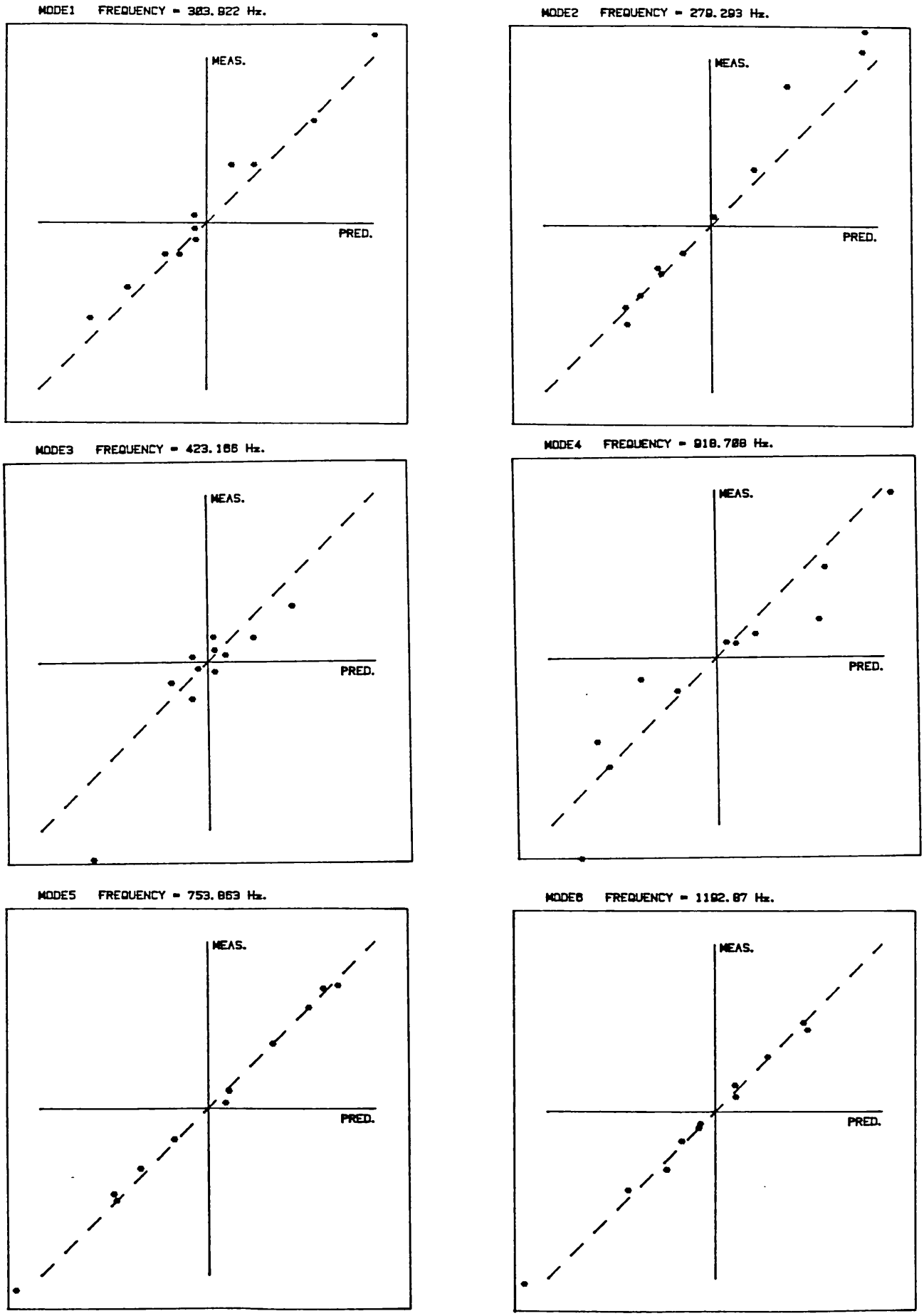

FIGURE 7-06 : Correlation of measured and predicted mode shapes for the SAMM II B beam.

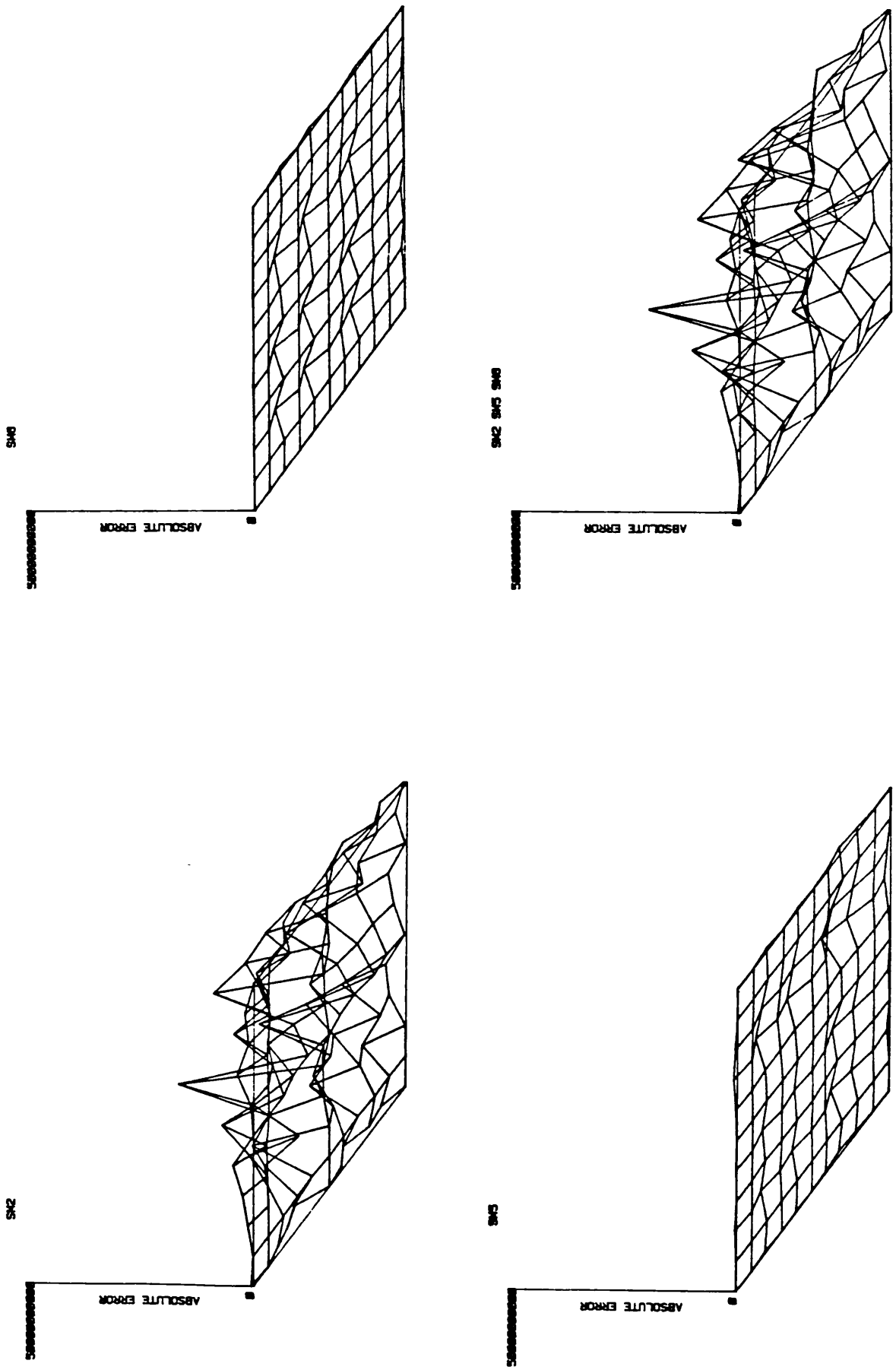

FIGURE 7-07 : Stiffness error matrix plots of SAMM II B beam in the Y direction.

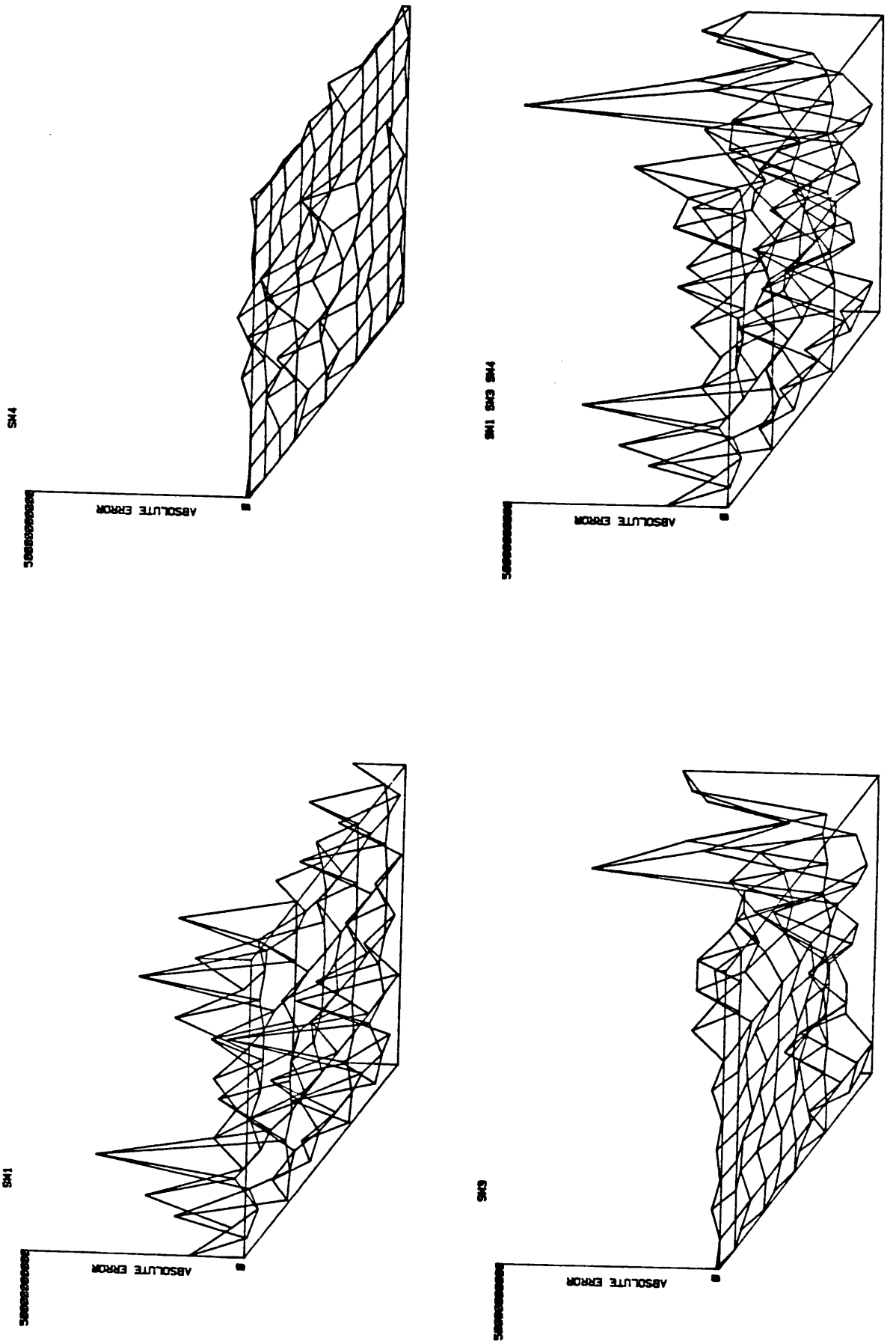

FIGURE 7-08 : Stiffness error matrix plots of SAMM II B beam in the Z direction.

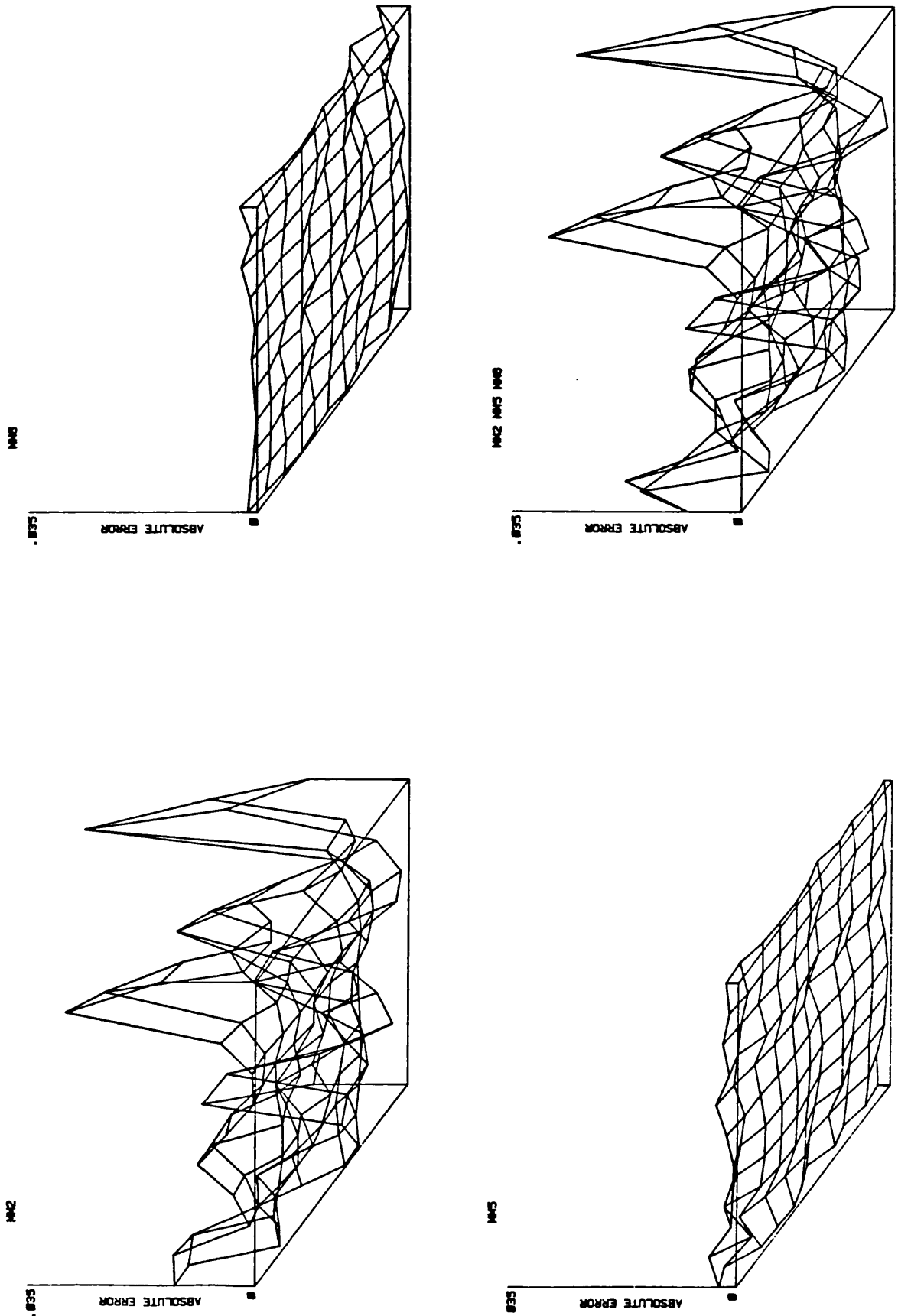

FIGURE 7-09 : Mass error matrix plots of SAMM II B beam in the Y direction.

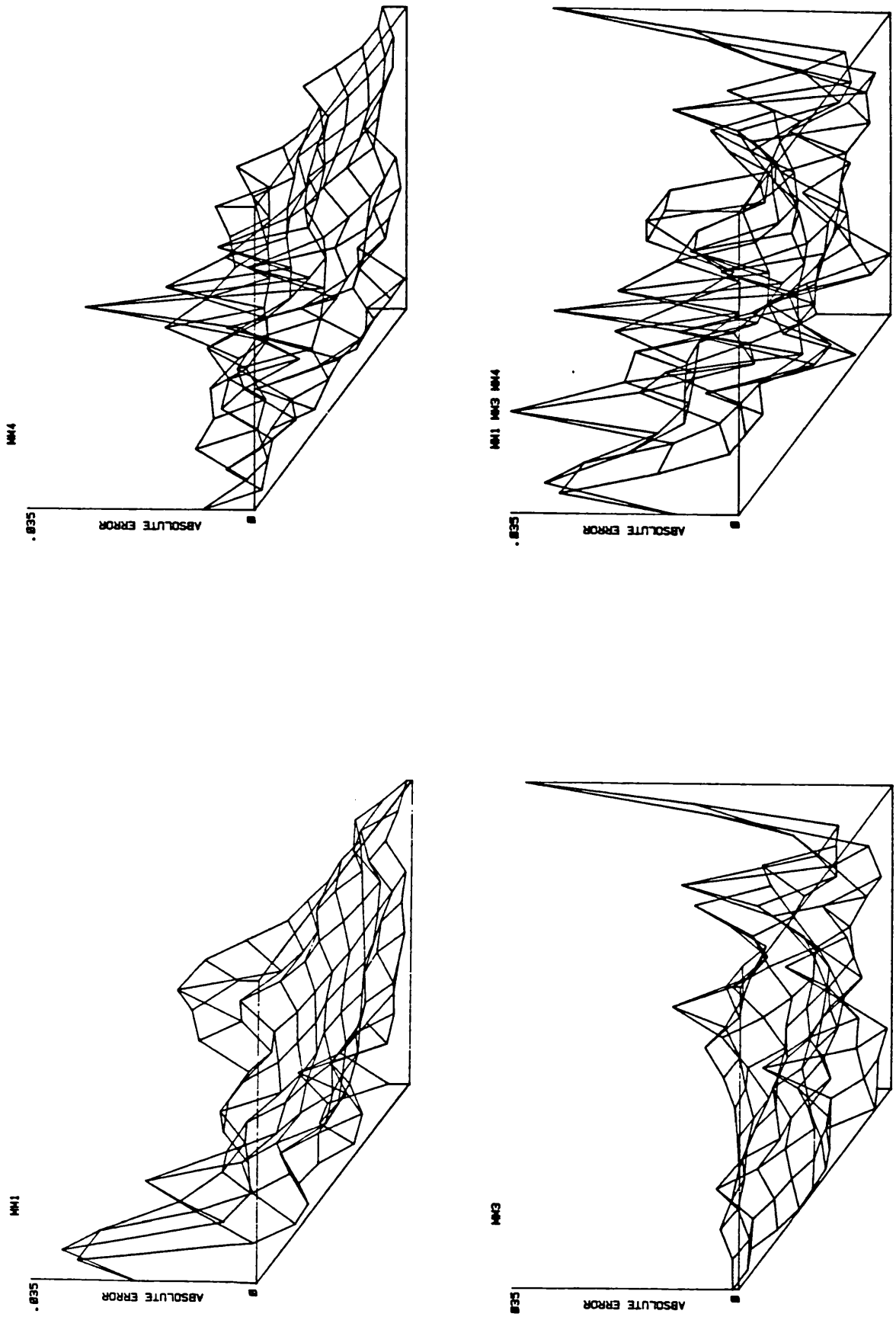

FIGURE 7-10 : Mass error matrix plots of SAMM II B beam in the Z direction.

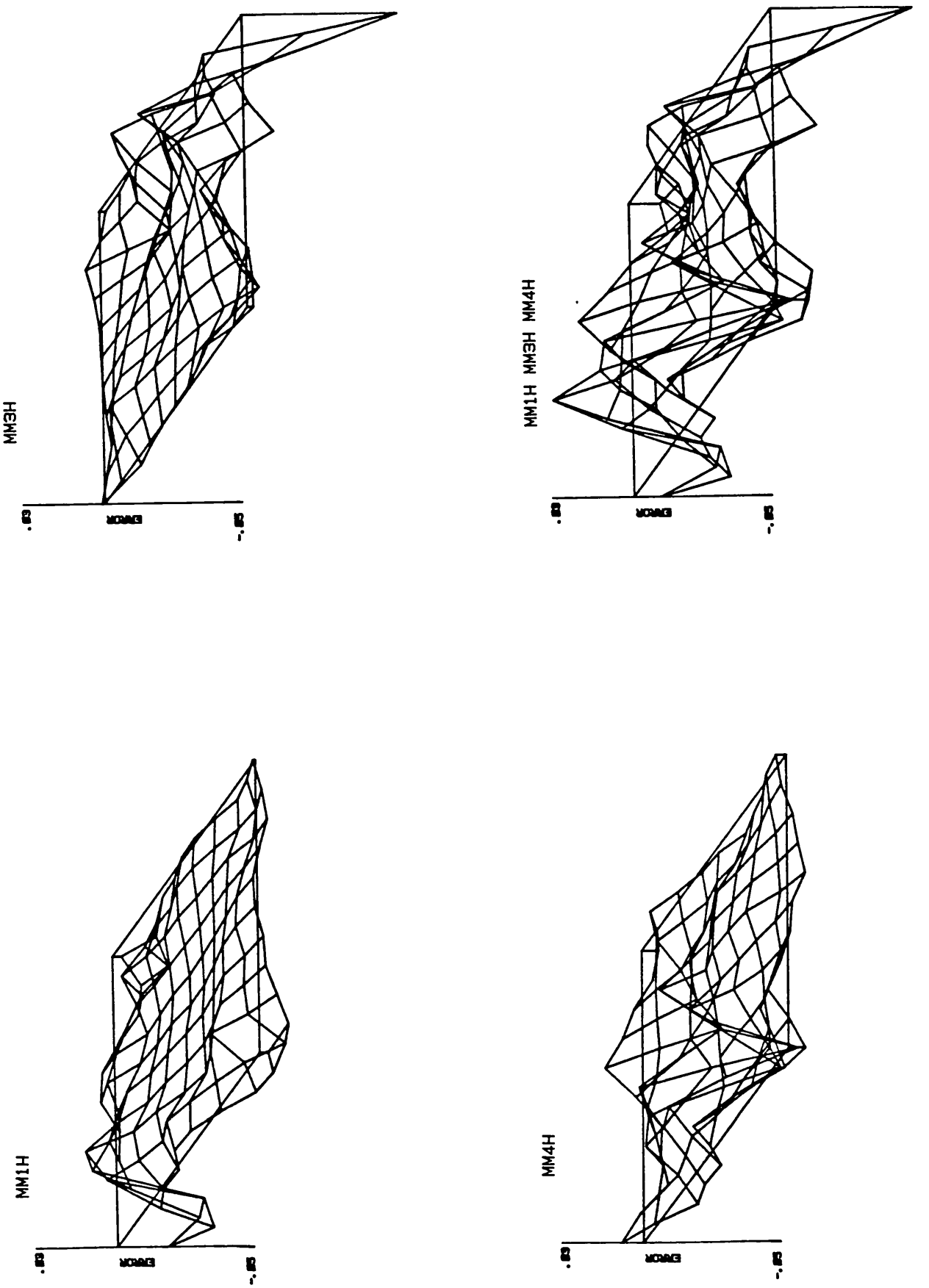

FIGURE 7-11 : Mass error plots of the SAMM II B beam with holes.

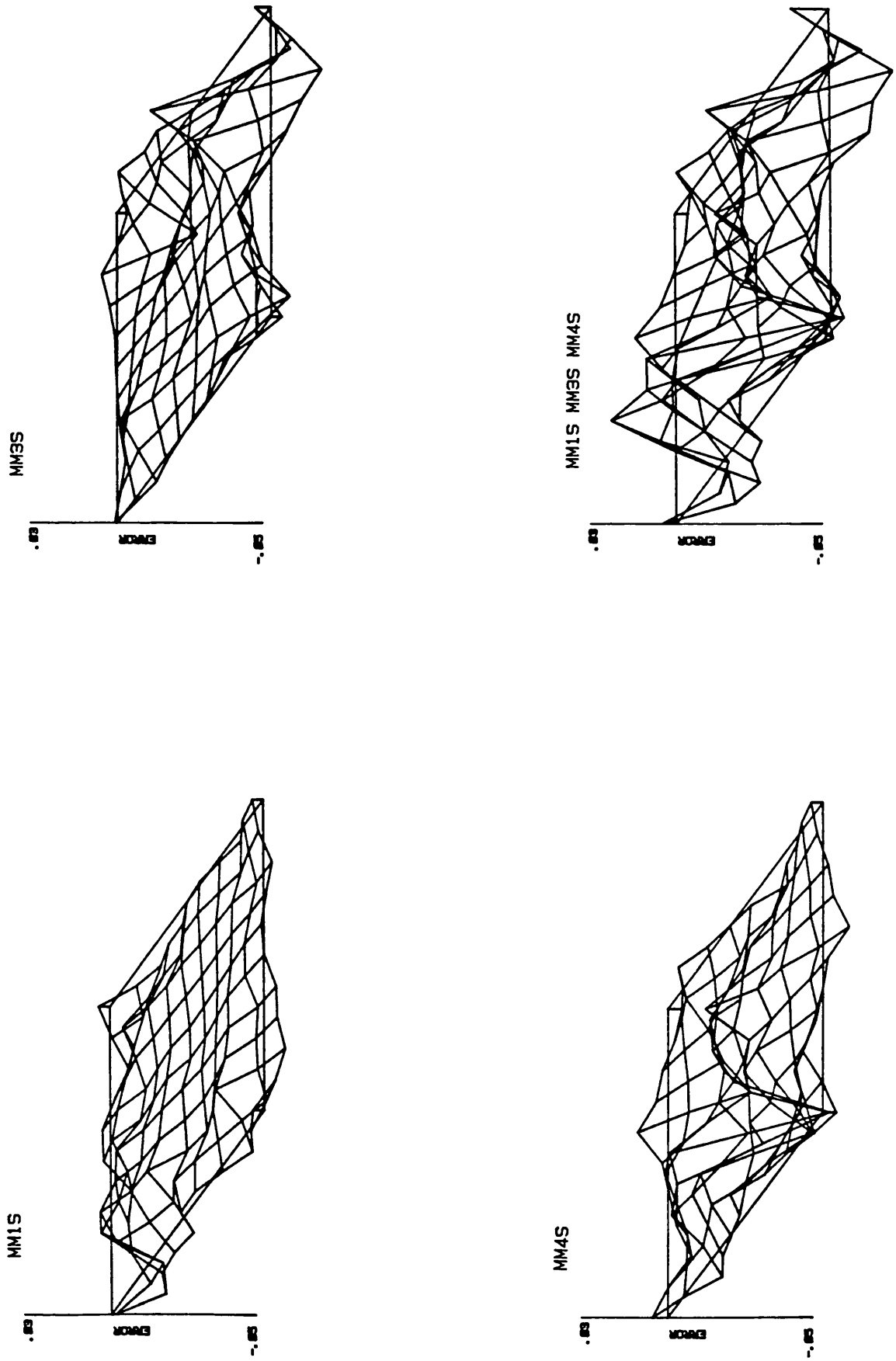

FIGURE 7-12 : Mass error plots of the SAMM II B beam with studs.

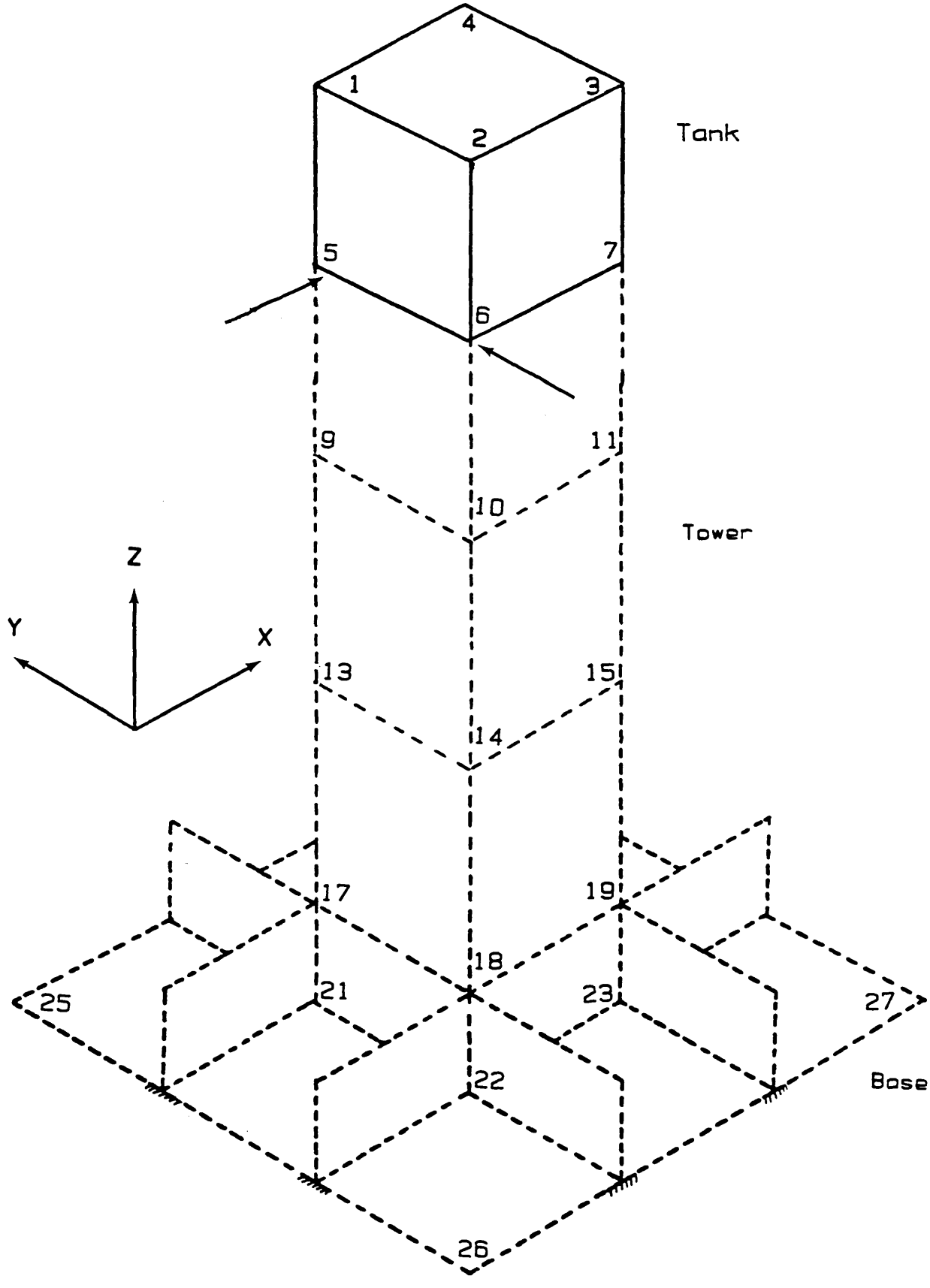

FIGURE 7-13 : NASTRAN tower with tank.

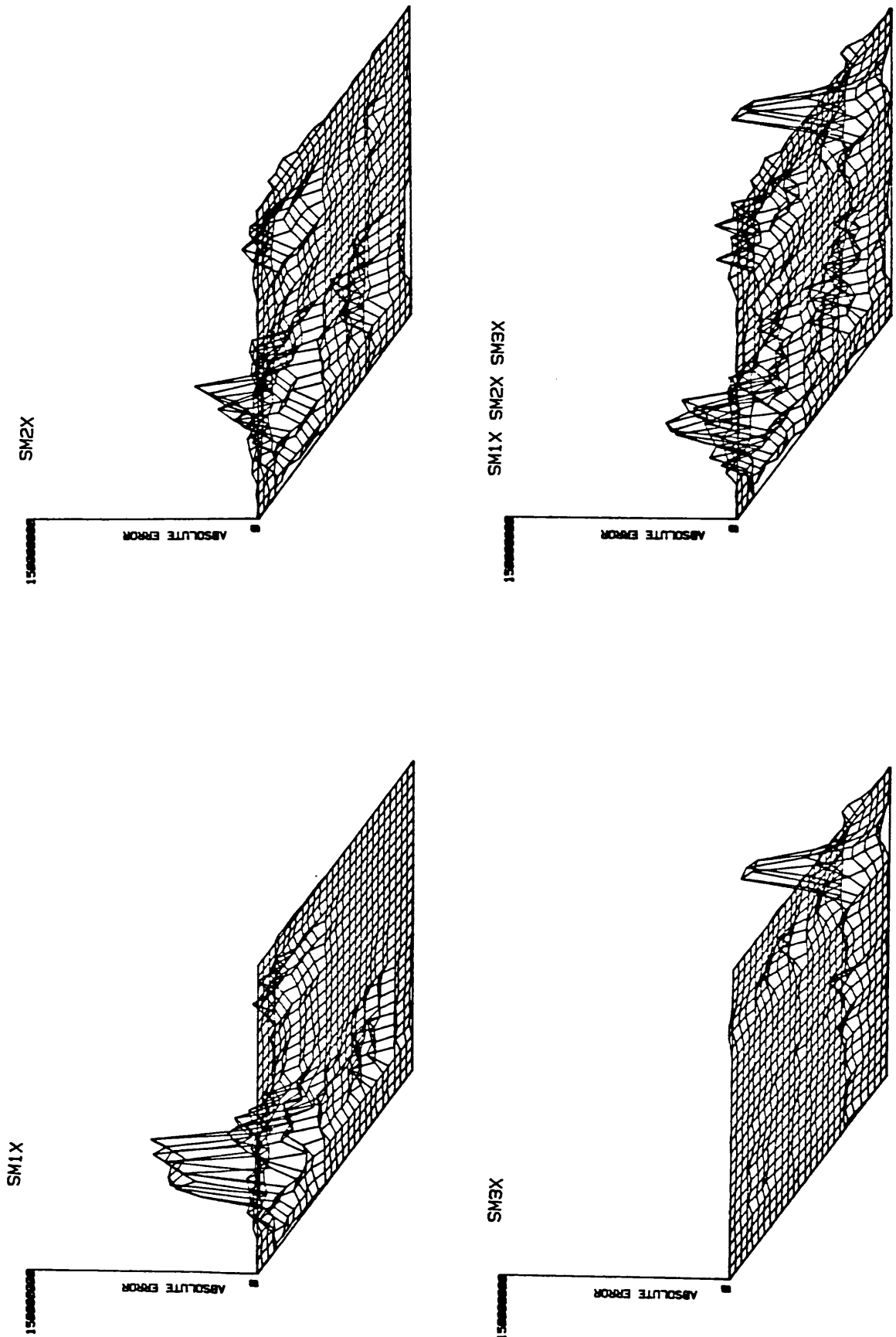

FIGURE 7-14 : Stiffness error plots of the NASTRAN structure in the X direction.

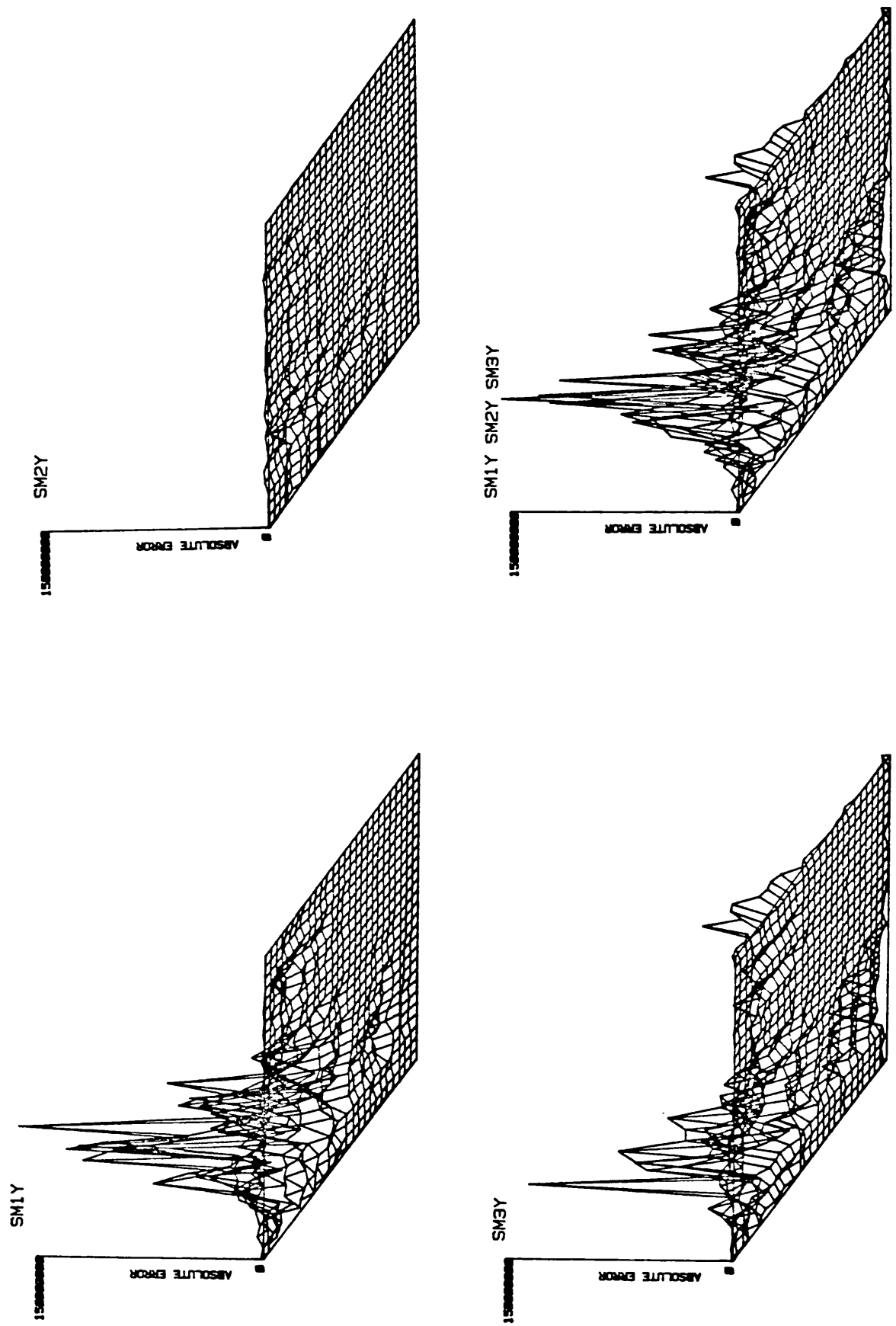

FIGURE 7-15 : Stiffness error plots of the NASTRAN structure in the Y direction.

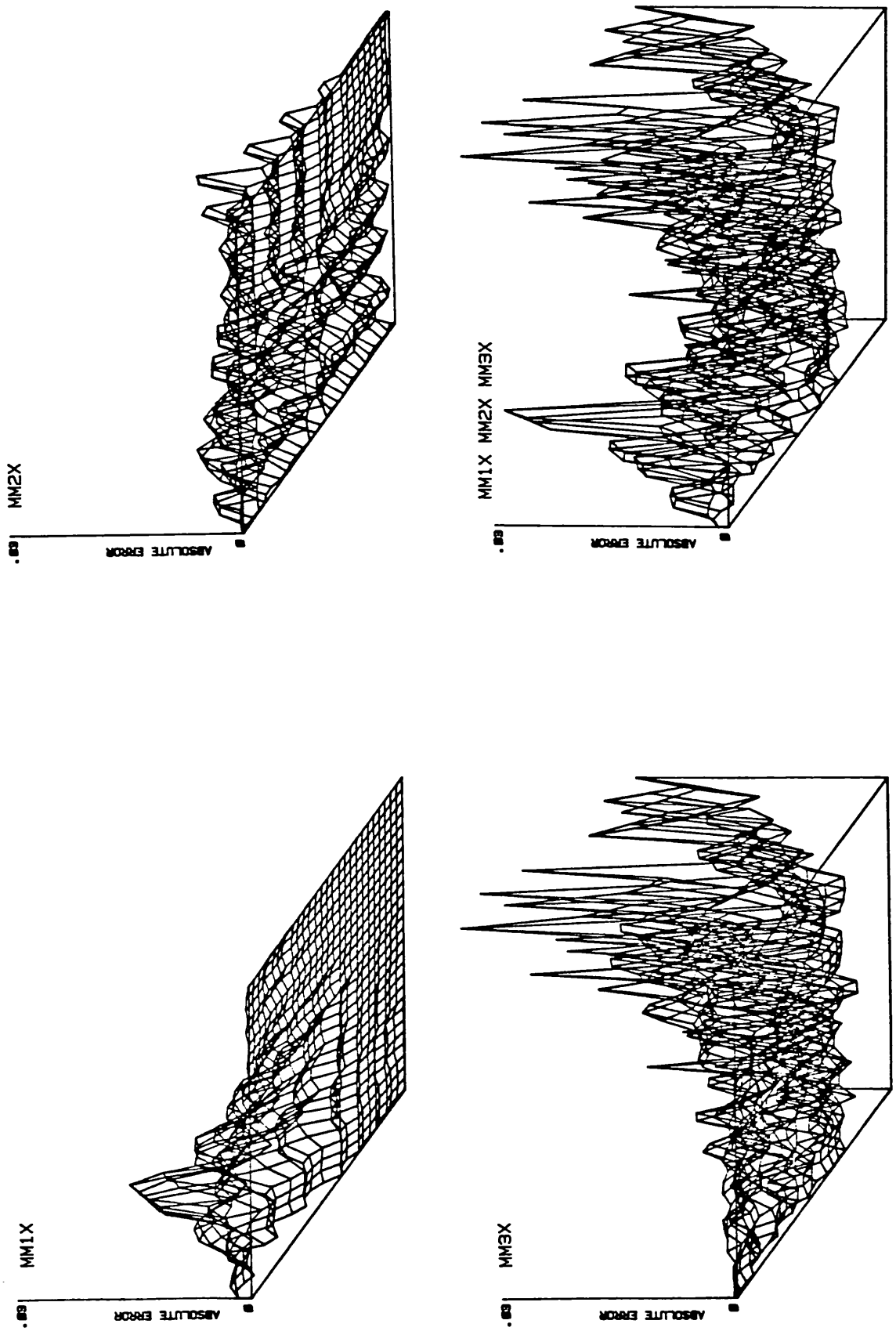

FIGURE 7-16 : Mass error plots of the NASTRAN structure in the X direction.

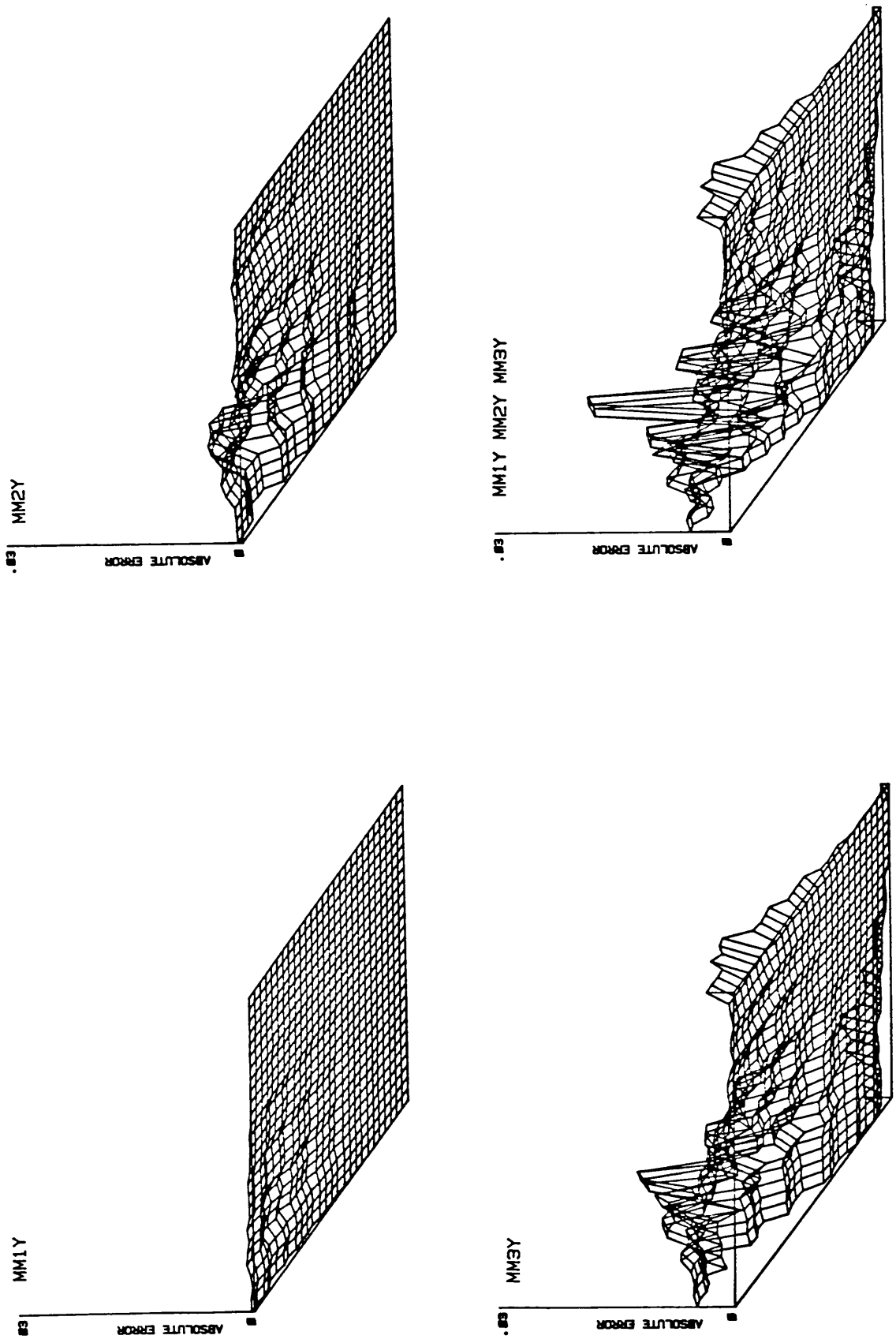

FIGURE 7-17 : Mass error plots of the NASTRAN structure in the Y direction.

CHAPTER

-8-

8. CONCLUDING REMARKS

The results presented in each section were discussed and detailed conclusions were drawn at the end of each chapter. A brief summary of these conclusions is presented here as a review of the entire thesis.

8.1. MODAL TESTING AND NONLINEARITIES

The presence of certain types of nonlinearity may be detected by forcing the structure at constant but different excitation levels thus obtaining several mobility plots. These diagrams should be similar in the sense that the ratio of response to the excitation force should be constant and any significant deviation from this constant ratio for a given frequency which cannot be attributed to experimental errors may be due to nonlinearities. However, such tests are time consuming, and a better method which requires only one set of measured data in the form of a frequency response at constant forcing level, was developed. This method relies on the fact that for any linear system with well-separated modes, the estimated values of damping are independent of the frequency points chosen for the calculation. A damping matrix can be constructed for each mode of interest and it is found that small random errors due to inaccuracies in the measured data usually exist but that these produce random variations in the estimated values of damping while nonlinearities had a markedly systematic effect. The damping matrix thus obtained was examined by

displaying the elements in the matrix on a 3-D plot.

An analytical study, using known types and amounts of nonlinearity, made it possible to calibrate the isometric loss factor plots. Two types of nonlinearity were considered - softening cubic stiffness and dry friction - and these had different effects on the shape of the loss factor diagrams. The cubic stiffness produced a very large variation in the estimated values of damping while that due to the dry friction was much smaller. It was further noted that the effect of cubic stiffness may be reduced by decreasing the input force; but in a practical situation there is a limit beyond which the force cannot be reduced without increasing the noise to signal ratio. On the other hand, to reduce the effect of dry friction, a large input force must be used.

The effect of closely-coupled modes on the isometric loss factor plots was also investigated and in this case the angle PHI plots were useful as well as the loss factor plots in deciding whether the effect of the neighbouring mode was small or not. The closely-coupled modes produced large and sudden changes in the estimated values of damping, unlike the nonlinearities where the variation was gradual.

The NASTRAN structure was shown to be nonlinear by testing it at several different but constant forcing levels and 3-D loss factor plots from the measured data indicated the presence of two types of nonlinearity - frictional and softening stiffness types - the latter having a large effect

on the variation of the estimated damping values. This conclusion was strengthened because it was possible to linearise the structure's data using constant displacement amplitude tests and only a stiffness type of nonlinearity can be linearised by this technique.

The effect of different types of excitation force on the response from a nonlinear system was examined using an analogue computer. In the case of the two nonlinearities investigated - dry friction and softening-cubic stiffness - it was found to be difficult to detect the presence of either type of nonlinearity from a single frequency response curve when the system was excited using random or transient inputs. The effect of such an input was to produce linear data, similar to the constant amplitude tests. A possible explanation for this might be that the structure is being excited at several amplitudes of vibration and at many frequencies within the chosen bandwidth, hence the measured response is the average response due to all of these inputs and may well be linear or very close to it. Although random and transient excitation appear to linearise the measured data, this does not mean that these types of excitation are better than sinusoidal because the analogue study showed that the modal properties extracted from these data using a linear SDOF algorithm were not the actual input values.

It seems that sinusoidal excitation tests, although sometimes slower than the random tests, produce superior frequency response data which may be analysed to identify nonlinearities. Furthermore, sinusoidal excitation is

useful because constant amplitude vibration tests can only be performed using this type of input and structures with stiffness type nonlinearities may be linearised by this method.

8.2. CORRELATION OF MEASURED AND PREDICTED MODAL PROPERTIES

The examination of the current methods available for comparing measured and predicted modal properties showed that it is not possible to use these data in a systematic and quantitative manner to locate the areas of discrepancies between the two models. However, these techniques were useful in deciding which measured mode corresponds to which predicted mode.

The development and application of the error matrix equation made it possible to use the modal data of two models to locate the areas of discrepancies. This technique was applied to an undamped 8 DOF mass-spring system and it was possible to locate exactly the areas of discrepancies. Although the 8 DOF system was far from a realistic situation, it was nevertheless very useful in investigating the accuracy of the error matrix equation.

Before applying the error matrix to real structures it was necessary to make further modifications, especially to the full FE model mass and stiffness matrices, so that these were compatible with the measured pseudo inverse mass and stiffness matrices.

The full spatial mass and stiffness matrices may be

reduced either by eliminating rows and columns that correspond to the unmeasured coordinates or by Guyan reduction. Both of these reduction techniques appeared to be capable of locating the areas of discrepancy between the two models although only the Guyan reduction method gave the true magnitude of the error.

The application of the error matrix equation to the SAMM II B beam showed that 3 out of 4 welded joints were inadequately modelled by the FE analysis and also the comparison for mode 3 located the presence of error in the mass matrix near one of the holes. This error was shown to be due to the hole because it was reduced when studs were inserted in the holes. The possibility of errors being present in the measured data was checked and shown to be negligible by remeasuring the frequency response of the beam.

The NASTRAN structure's FE model appeared to be poorly modelled at 3 distinct locations. This finding was very encouraging because these areas are probably in error due to joints which cannot easily be modelled in the analysis.

8.3. SUGGESTIONS FOR FURTHER RESEARCH

There are two main areas that need further investigation - the analysis of frequency response data and the correlation of measured and predicted modal properties.

In this study we used the simplest of the curve-fitting routine (SDOF) to identify nonlinearities and only certain types of nonlinearities can be detected by this technique i.e. it was difficult to detect small amounts of dry friction while stiffness type nonlinearities appear to be easily detectable. Furthermore, in the nonlinear analytical study, only single degree-of-freedom systems were used while the real structures have infinite degrees-of-freedom and perhaps several types of nonlinearities. A more realistic study would be to simulate multidegree-of-freedom systems with several types of nonlinearities, perhaps using the analogue computer.

The error matrix equation developed in chapter 6 appears to be very useful in locating the areas of weak modelling and hence requires further investigation to clarify few points, especially the following:

(i) the two types of reduction techniques - the Guyan and the elimination of rows and columns - used to reduce the full spatial matrices from the FE analysis appear to give the correct areas of discrepancies between the two models but there was no justification in reducing these matrices by the techniques used and this needs further investigation and perhaps other types of reduction techniques might be more

accurate than the ones considered;

(ii) the error matrix equation is only valid providing the matrix product $[K_p]^{-1}[E]$ is small but it was found that in the 8 DOF system this condition was not satisfied for all the modes yet the correct area of discrepancy between the two models was located using only 4 modes. Not only the area of discrepancy was located but also the amount of discrepancy indicated by the error matrix was of the correct order. This may have something to do with the pseudo matrices being singular;

(iii) it would be ideal if the error matrix can be substituted direct into the spatial matrices to correct the mass and stiffness terms. At the moment it is not possible to do so because the dimensions of the error matrix are different from those of the spatial matrices. This might be overcome by interpolating to estimate the errors at the coordinates that are not measured and hence making the error matrix of the same order as the spatial matrices.

CHAPTER

-9-

9. REFERENCES

1. BROWN D L, CARBON G and RAMSEY K
Survey of excitation techniques applicable to the testing of automotive structures.
SAE Paper No 770029, 1977, 16pp

2. CRAIG RR Jr and SU Y W T
On multiple-shaker resonance testing.
AIAA Journal, Vol 12, No 7, 1974, Pp 924-931

3. De VEUBEKE B F
Comment on multiple-shaker resonance testing.
AIAA Journal, Vol 13, No 5, 1975, Pp 702-704

4. RICHARDSON M and KNISKERN J
Identifying modes of large structures from multiple input and response measurements.
SAE Paper No 760875, 1976, 12pp

5. BENDAT J S
Solutions for the multiple input output problem.
Journal of Sound and Vibration, Vol 44, No 3, 1976, Pp 311-325

6. KENNEDY C C and PANCU C D P
Use of vectors in vibration measurement and analysis.
Journal of the Aeronautical Science, Vol 14, Nov 1947

7. KIRSHENBOIM J

Theory and Practice of Modal Identification Applied to Helicopter Structures.

Imperial College; PhD thesis; Sept 1981.

8. IBRAHIM S R and MIKULCIK E C

The experimental determination of Vibration Parameters from time Response.

The Shock and Vibration Bulletin.

No 46 Part 5 May 1976 Pp 187-196.

9. IBRAHIM S R and MIKULCIK E C

A method for the direct identification of vibration parameters from the free response.

The Shock and Vibration Bulletin

No 47 Part 4 Sept 1977 Pp 183-198.

10. ULM S C and MORSE I E

Recognizing system nonlinearities using modal analysis tests

ASME No 82-DET-138

11. GOYDER H G D

Some theory and applications of the relationship between the real and imaginary parts of a frequency response function provided by Hilbert transforms.

Recent advances in structural dynamics, International conference July 7-11, 1980, University of Southampton.

12. HAOUI A, VINH T, SIMON M and TOMLINSON G R
Some applications of the Hilbert transform to nonlinear systems.
Euromech 168, June 1983, University of Manchester

13. HAOUI A, VINH T and CHEVALIER Y
Applications of Hilbert transform in the analysis of nonlinear structures.
Euromech 168, June 1983, University of Manchester

14. FOX R L and KAPOOR M P
Rate of change of eigenvalues and eigenvectors.
AIAA Journal, Vol 6, Dec 1968, Pp 2426-2429

15. ROGERS I C
Derivatives of eigenvalues and eigenvectors.
AIAA Journal, Vol 8, May 1970, Pp 943-944.

16. PLAUT R H and HUSEYIN K
Derivatives of eigenvalues and eigenvectors in non-self-adjoint systems.
AIAA Journal, Vol 11, Feb 1973, Pp 250-251.

17. RUDISILL C S
Derivatives of eigenvalues and eigenvectors for a general matrix.
AIAA Journal, Vol 12, May 1974, Pp 721-722.

18. NELSON R B

Simplified calculation of eigenvectors derivatives.

AIAA Journal, Vol 14, No 9, Sept 1976, Pp 1201-1205.

19. WEI F S

Stiffness matrix correction from incomplete data.

AIAA Journal, Vol 18, No 10, Oct 1980, Pp 1274-12785

20. BARUCH M

Correction of stiffness matrix using vibration tests.

AIAA Journal, Vol 20, No 3, March 1982, Pp 441-442

21. CHEN J C and WADA B K

Matrix perturbation for structural dynamics analysis.

AIAA Journal, Vol 15, No 8, Aug 1977, Pp 1095-1100

22. GAUKROGER D R

Modification of structural stiffness to obtain specified natural frequencies.

Royal Aircraft Establishment, Technical Memorandum MAT/STR 1001, Aug 1982

23. PRZEMIENIECKI J

Theory of matrix structural analysis.

McGraw Hill, 1968.

Chapter 5.

24. SZILARD R
Theory and analysis of plates.
Chapter 2, Section 10.

25. TIMOSHENKO S
Vibration problem in engineering.
Wiley

26. LIVESLEY R K
The equivalence of continuous and discrete mass distribution in certain vibration problems.
Quarterly Journal of Mechanics and Applied Maths.
Vol 8, 1955, Pp 353-359.

27. GLADWELL G M L
The approximation of uniform beams in transverse vibration by sets of masses elastically connected.
Proceedings of 4th Nat. Congr. App. Mech.
A.S.M.E. 1962, Pp 169-176.

28. FENNER R
Finite Element Methods for Engineers.
The MacMillan Press Ltd., 1975

29. DOBSON B, EWINS D J, PARKES D A C and SIDHU J
Reconciliation of Predicted and Measured Modal Properties.
First Internationl Modal Analysis Conference.
Orlando, Florida, USA, 8-10 Nov 1982.

30. EWINS D J
Whys and wherefores of modal testing.
Journal of SEE Sept 1979.

31. BISHOP R E D and JOHNSON D C
The Mechanics of Vibration.
Cambridge University Press, 1960

32. GLEESON P T
Identification of spatial models.
Imperial College; PhD thesis; 1979.

33. SILVA J M M
Measurement and application of structural mobility data for the vibration analysis of complex structures.
Imperial College; PhD thesis; 1978.

34. SIDHU J
Simulation of non-linear-single-degree-of-freedom system on the analogue computer.
Imperial College Report No 82006

35. SIDHU J

A method for assessing the quality of modal identification from frequency response data.

Imperial College Report No 82ØØ1

36. SIDHU J

A detailed study of some modal properties of the NASTRAN structure.

Imperial College Report No 82Ø3

37. WHITE R G

Use of transient excitation in the measurement of the frequency response of systems with nonlinearities arising from large deflections.

ISVR Technical Report No 27, Feb 197Ø

38. NEWMAN K W

The effect of stiffness nonlinearity on vector response loci.

RAE Technical Report No 71119

39. TOMLINSON G R

An analysis of the distortion effects of coulomb damping on the vector plots of lightly damped systems.

Journal of Sound and Vibration (198Ø) 71(1)

4Ø. TOMLINSON G R and HIBBERT J H
Identification of the dynamics characteristics of a structure with coulomb friction.
Journal of Sound and Vibration (1979) 64(2)

41. EWINS D J and SIDHU J
Modal testing and the linearity of structures.
Mecanique Materiaux Electicite.
No 389-39Ø-391, Mai-Juin-Juillet 1982

42. DINCA F and TEODOSIU C
Non-linear and random vibrations.
Academic Press Inc. New-York, London 1973

43. MINORSKY N
Introduction to non-linear mechanics.
D.W. Taylor Model Basin 1946

44. MINORSKY N
Non-linear oscillations.
Van Nostrand 1962

45. THOMSON W T
Vibration Theory and Applications.
George Allen and Unwin Ltd.

46. STOKER J J
Nonlinear Vibrations.
Interscience Publishers Inc. New-York 195Ø

47. TIMOSHENKO S, YOUNG D H and WEAVER W Jr
Vibration Problems in Engineering
Wiley

48. JAMES M L, SMITH G M and WOLFORD J C
Analog computer simulation of engineering systems.
Intex Education Publications

49. CHARLESWORTH A S and FLETCHER J R
Systematic analogue computer programming.
Pitman Publishing

50. EWINS D J
On predicting point mobility plots from measurements of other mobility parameters.
Journal of Sound and Vibration 70(1), May 1980

51. DOBSON B J, EWINS D J and PARKES D A C
On the comparison of predicted and measured structural vibration characteristics.
1982.

52. BELLAMY R A, BENNETT J C and ELSTON S T
Development of a correlated finite element dynamic model of a complete aero engine.
ASME.

53. KUPERMAN I B

Approximate algebraic equations.

Chapter 8.

Van Nostrand Reinhold Company 1971.

54. GUYAN R J

Reduction of stiffness and mass matrices.

AIAA Journal, Vol 3, No 2, Feb 1965, Pp 38Ø

55. IMREGUN M

Dynamic condensation : theory and application.

MSc thesis, Imperial College, Dynamics Section, Sept 198Ø

56. BOON D J

An investigation into the dynamic analysis of a structure containing fluid using MSC NASTRAN.

Westland Helicopter Ltd., Yeovil, Somerset.

Dynamics department, Note GEN DYN 257N.

CHAPTER

-10-

10. APPENDICES

10.1. MASS AND STIFFNESS MATRICES OF BEAM ELEMENT

The beam element is assumed to be straight bar of uniform cross section area as shown in figure 2-01.

Let {F} be the force and bending moment vector and {V} be the displacement and rotation vector.

From statics and dynamics, it is possible to show that;

$$\{F\} = [K_e]\{V\}$$

and

$$\{F\} = [M_e]\{V\}$$

where $[K_e]$ and $[M_e]$ are the element's mass and stiffness matrices and are given by;

$$k_e = \begin{bmatrix}
\frac{EA}{l} & & & & & & & & & & & \\
0 & \frac{12EI_z}{l^2(1+\Phi_y)} & & & & & & & & & & \\
0 & 0 & \frac{12EI_y}{l^2(1+\Phi_z)} & & & & & & & & & \\
0 & 0 & 0 & \frac{GJ}{l} & & & & & & & & \\
0 & 0 & \frac{-6EI_y}{l^2(1+\Phi_z)} & 0 & \frac{(4+\Phi_z)EI_y}{l(1+\Phi_z)} & & & & & & & \\
0 & \frac{6EI_z}{l^2(1+\Phi_y)} & 0 & 0 & 0 & \frac{(4+\Phi_y)EI_z}{l(1+\Phi_y)} & & & & & & \\
-\frac{EA}{l} & 0 & 0 & 0 & 0 & 0 & \frac{AE}{l} & & & & & \\
0 & \frac{-12EI_z}{l^2(1+\Phi_y)} & 0 & 0 & 0 & \frac{-6EI_z}{l^2(1+\Phi_y)} & 0 & \frac{12EI_z}{l^2(1+\Phi_y)} & & & & \\
0 & 0 & \frac{-12EI_y}{l^2(1+\Phi_z)} & 0 & \frac{6EI_y}{l^2(1+\Phi_z)} & 0 & 0 & 0 & \frac{12EI_y}{l^2(1+\Phi_z)} & & & \\
0 & 0 & 0 & \frac{-GJ}{l} & 0 & 0 & 0 & 0 & 0 & \frac{GJ}{l} & & \\
0 & 0 & \frac{-6EI_y}{l^2(1+\Phi_z)} & 0 & \frac{(2-\Phi_z)EI_y}{l(1+\Phi_z)} & 0 & 0 & 0 & \frac{6EI_y}{l^2(1+\Phi_z)} & 0 & \frac{(4+\Phi_z)EI_y}{l(1+\Phi_z)} & \\
0 & \frac{6EI_z}{l^2(1+\Phi_y)} & 0 & 0 & 0 & \frac{(2-\Phi_y)EI_z}{l(1+\Phi_y)} & 0 & \frac{-6EI_z}{l^2(1+\Phi_y)} & 0 & 0 & 0 & \frac{(4+\Phi_y)EI_z}{l(1+\Phi_y)}
\end{bmatrix}
\begin{bmatrix} u_1 \\ u_2 \\ u_3 \\ u_4 \\ u_5 \\ u_6 \\ u_7 \\ u_8 \\ u_9 \\ u_{10} \\ u_{11} \\ u_{12} \end{bmatrix}$$

Symmetric

where $\Phi_y = \dfrac{12EI_z}{GA_{s_y}l^2} = 24(1+\nu)\dfrac{A}{A_{s_y}}\left(\dfrac{r_z}{l}\right)^2$

and $\Phi_z = \dfrac{12EI_y}{GA_{s_z}l^2} = 24(1+\nu)\dfrac{A}{A_{s_z}}\left(\dfrac{r_y}{l}\right)^2$

$\mathbf{m}_e = \rho Al$

Symmetric

	1	2	3	4	5	6	7	8	9	10	11	12
1	$\frac{1}{3}$											
2	0	$\frac{13}{35}+\frac{6I_z}{5Al^2}$										
3	0	0	$\frac{13}{35}+\frac{6I_y}{5Al^2}$									
4	0	0	0	$\frac{J_x}{3A}$								
5	0	0	$-\frac{11l}{210}-\frac{I_y}{10Al}$	0	$\frac{l^2}{105}+\frac{2I_y}{15A}$							
6	0	$\frac{11l}{210}+\frac{I_z}{10Al}$	0	0	0	$\frac{l^2}{105}+\frac{2I_z}{15A}$						
7	$\frac{1}{6}$	0	0	0	0	0	$\frac{1}{3}$					
8	0	$\frac{9}{70}-\frac{6I_z}{5Al^2}$	0	0	0	$\frac{13l}{420}-\frac{I_z}{10Al}$	0	$\frac{13}{35}+\frac{6I_z}{5Al^2}$				
9	0	0	$\frac{9}{70}-\frac{6I_y}{5Al^2}$	0	$-\frac{13l}{420}+\frac{I_y}{10Al}$	0	0	0	$\frac{13}{35}+\frac{6I_y}{5Al^2}$			
10	0	0	0	$\frac{J_x}{6A}$	0	0	0	0	0	$\frac{J_x}{3A}$		
11	0	0	$\frac{13l}{420}-\frac{I_y}{10Al}$	0	$-\frac{l^2}{140}-\frac{I_y}{30A}$	0	0	0	$\frac{11l}{210}+\frac{I_y}{10Al}$	0	$\frac{l^2}{105}+\frac{2I_y}{15A}$	
12	0	$-\frac{13l}{420}+\frac{I_z}{10Al}$	0	0	0	$-\frac{l^2}{140}-\frac{I_z}{30A}$	0	$-\frac{11l}{210}-\frac{I_z}{10Al}$	0	0	0	$\frac{l^2}{105}+\frac{2I_z}{15A}$

10.2. PSEUDO INVERSE MATRICES

We shall only consider the 'pseudo' inverse stiffness matrices but the same argument may also be applied to the 'pseudo' inverse mass matrices. From equation 6-04 we have;

$$[\overset{*}{K}]^{-1}_{NN} = [\Phi^R]_{Nm}[1/\lambda_r^2]_{mm}[\Phi^R]^T_{mN}$$

The mass-normalised eigenvector matrix $[\Phi^R]$ is a rectangular while the 'pseudo' inverse stiffness matrix is square and symmetrical. In strict mathematical terminology, the word 'pseudo' is applied to a rectangular matrix but in this study we shall apply the term 'pseudo' to a square matrix which is obtained using a rectangular eigenvector matrix.

Numerical calculations show that 'pseudo' matrices are singular. This is because for m < n the rank of the 'pseudo' inverse matrix is m, which is less than the dimensions of this matrix (nxn); consequently, there must be rows and columns that are linear combinations of some or all of the other rows and columns, hence, the 'pseudo' matrix must be singular. For a single mode (m = 1) the above statement may be shown to be true for a general case i.e. for any vector.

Let the elements of a mode shape vector be;

$$\{\Phi\}_{n1} = \begin{Bmatrix} \phi_1 \\ \phi_2 \\ . \\ . \\ . \\ \phi_n \end{Bmatrix}$$

The 'pseudo' stiffness matrix is given by;

$$[\mathring{K}]^{-1}_{nn} = \{\Phi^R\}_{n1} \frac{1}{\lambda_0^2} \{\Phi^R\}^T_{1n}$$

$$= \frac{1}{\lambda_0^2} \begin{Bmatrix} \phi_1 \\ \phi_2 \\ . \\ . \\ . \\ \phi_n \end{Bmatrix} \{\phi_1 \quad \phi_2 \quad \ldots \quad \phi_n\}^T$$

$$= \frac{1}{\lambda_0^2} \begin{bmatrix} \phi_1\phi_1 & \phi_1\phi_2 & \ldots & \phi_1\phi_n \\ \phi_2\phi_1 & \phi_2\phi_2 & \ldots & \phi_2\phi_n \\ . & . & & . \\ . & . & & . \\ . & . & & . \\ \phi_n\phi_1 & \phi_n\phi_2 & \ldots & \phi_n\phi_n \end{bmatrix}$$

Clearly, the rows and columns of the above matrix are related to each other (e.g. common factor in the first column is ϕ_1 and in the second column is ϕ_2 and so on). The rank of the above matrix is one. Because of the dependency of the rows and columns, the determinant of the matrix is zero and hence it cannot be inverted in the usual manner.

1Ø.3. ON THE REDUCTION OF FULL MATRICES BY ELIMINATING ROWS AND COLUMNS

The term reduced means that matrix $[M_p]$ is reduced from NxN to nxn dimensions (N > n) by ignoring rows and columns.

Let us assume that the FE model has a $[M_p]$ matrix which is 4x4 and its coordinates are u's and v's as shown below;

$$[M_p] = \begin{bmatrix} a_{11} & a_{12} & a_{13} & a_{14} \\ a_{21} & a_{22} & a_{23} & a_{24} \\ a_{31} & a_{32} & a_{33} & a_{34} \\ a_{41} & a_{42} & a_{43} & a_{44} \end{bmatrix} \qquad \text{Corresponding coordinate vector} = \begin{Bmatrix} u_1 \\ v_1 \\ u_2 \\ v_2 \end{Bmatrix}$$

Let us further assume that the measured coordinates are u_1 and u_2. In this case the reduced matrix will by 2x2 while the full matrix is 4x4. The matrix $[M_p]$ can be reduced to the same dimensions as the measured $[M_e]$ matrix by ignoring the rows and columns corresponding to v's i.e. rows 2 and 4 and columns 2 and 4). The reduced $[M_p^R]$ thus becomes;

$$[M_p^R] = \begin{bmatrix} a_{11} & a_{13} \\ a_{31} & a_{33} \end{bmatrix}$$

Now we shall examine the effect on the error matrix of omitting these rows and columns. Let us partition the mode shape vector into two sections - measured and unmeasured coordinates, then;

$$[\Phi]_{Nm} = \begin{bmatrix} [\Phi_1]_{nm} \\ [\Phi_2]_{(N-n)\times m} \end{bmatrix}$$

where Φ_1 - the measured coordinates (known);

Φ_2 - the unmeasured coordinates (unknown).

The inverse pseudo mass matrix is given by;

$$[\overset{*}{M}]^{-1} = \begin{bmatrix} \Phi_1 \\ \Phi_2 \end{bmatrix} [\Phi_1 \quad \Phi_2]^T$$

where $[\overset{*}{M}]^{-1}$ - the inverse pseudo mass matrix and

$$[\overset{*}{M}]^{-1} = \begin{bmatrix} \Phi_1\Phi_1 & \Phi_1\Phi_2 \\ \Phi_2\Phi_1 & \Phi_2\Phi_2 \end{bmatrix}$$

$$= \begin{bmatrix} M_1 & M_2 \\ M_3 & M_4 \end{bmatrix}^{-1}$$

The pseudo matrix is also partitioned in four portions - $[M_1]$ is completely known where as $[M_2]$, $[M_3]$ and $[M_4]$ are not known because these depend on the unknown quantity Φ_2.

The error matrix equation requires the difference of the pseudo inverse matrices in the calculation of the error i.e.

$$[D_m] = [\overset{*}{M}_p]^{-1} - [\overset{*}{M}_e]^{-1}$$

$$= \begin{bmatrix} M_{p_1} & M_{p_2} \\ M_{p_3} & M_{p_4} \end{bmatrix}^{-1} - \begin{bmatrix} M_{e_1} & M_{e_2} \\ M_{e_3} & M_{e_4} \end{bmatrix}^{-1}$$

$$= \begin{bmatrix} D_1 & D_2 \\ D_3 & D_4 \end{bmatrix}$$

Again only $[D_1]$ is the known quantity because $[D_2]$, $[D_3]$ and $[D_4]$ depend on $[M_{e2}]$, $[M_{e3}]$ and $[M_{e4}]$ which are unknown. Since the matrix $[D_1]$ is the difference of two similar matrices then its elements will be small hence we shall assume, although it cannot be justified that the unknown quantities - namely $[D_2]$, $[D_3]$ and $[D_4]$ - are small (zero), then matrix $[D_m]$ becomes;

$$[D_m] = \begin{bmatrix} D_1 & 0 \\ 0 & 0 \end{bmatrix}$$

Substituting this in the the error matrix equation gives;

$$[E_m] = [M_p][D_m][M_p]$$

$$= \begin{bmatrix} M_{p_1} & M_{p_2} \\ M_{p_3} & M_{p_4} \end{bmatrix} \begin{bmatrix} D_1 & 0 \\ 0 & 0 \end{bmatrix} \begin{bmatrix} M_{p_1} & M_{p_2} \\ M_{p_3} & M_{p_4} \end{bmatrix}$$

$$= \begin{bmatrix} M_{p_1} D_1 M_{p_1} & M_{p_1} D_1 M_{p_2} \\ M_{p_3} D_1 M_{p_1} & M_{p_3} D_1 M_{p_2} \end{bmatrix}$$

$$= \begin{bmatrix} E_1 & E_2 \\ E_3 & E_4 \end{bmatrix}$$

But when we omit the rows and columns we reduce the $[M_p]$ to just $[M_{p1}]$, in this case the error matrix becomes;

$$[E_m] = [M_{p_1}][D_1][M_{p_1}] = [E_1]$$

which is the known part of the $[E_m]$ matrix.

So the effect of neglecting rows and columns is to assume that the unknown elements in the difference matrix are zero.